Tampere University

MARIA VÄHÄTUPA

Regulation of Angiogenesis

Role of R-Ras, furin and syndecan 4 in retinal angiogenesis

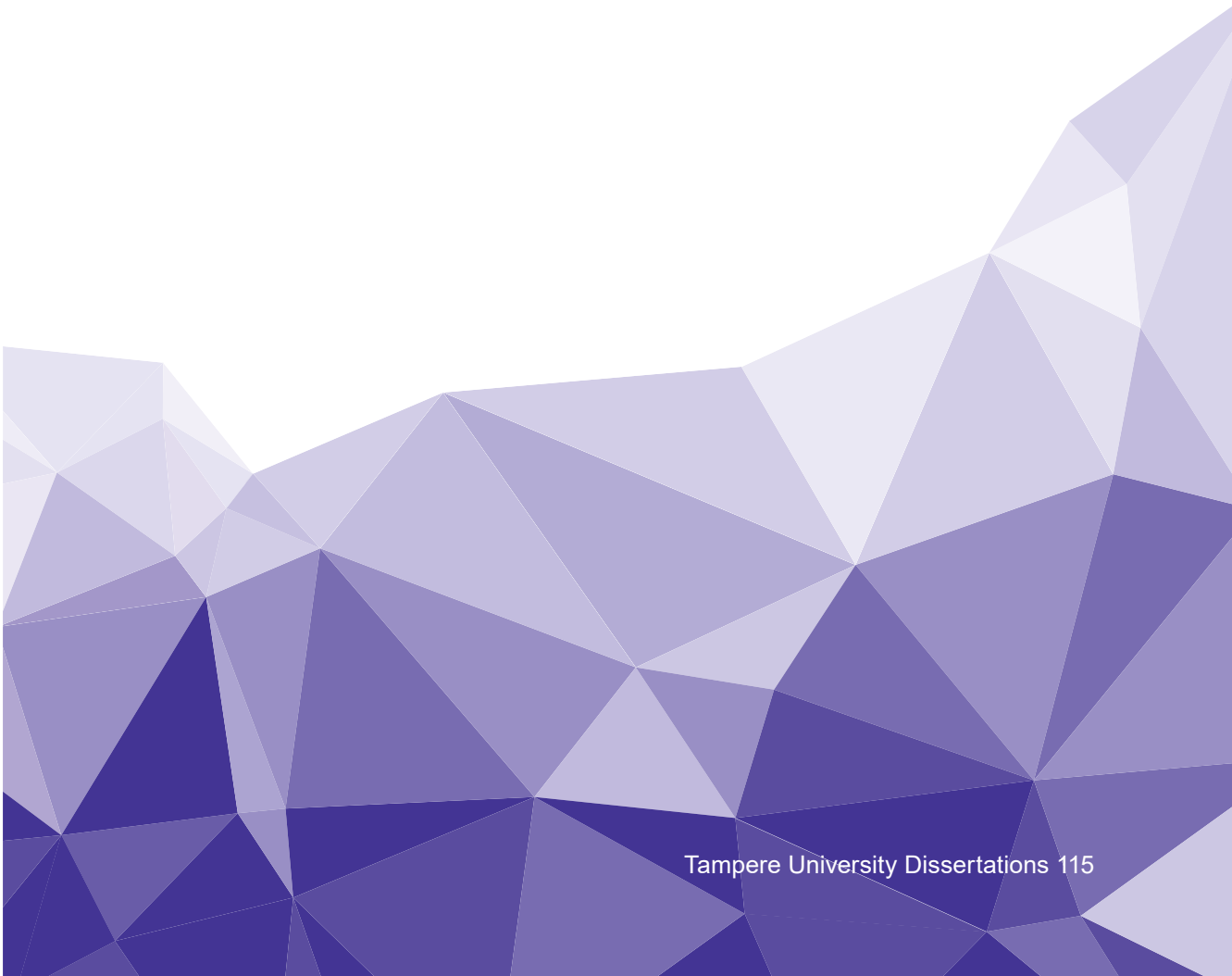

Tampere University Dissertations 115

Tampere University Dissertations 115

MARIA VÄHÄTUPA

Regulation of Angiogenesis

Role of R-Ras, furin and syndecan 4 in retinal angiogenesis

ACADEMIC DISSERTATION
To be presented, with the permission of
the Faculty of Medicine and Health Technology
of Tampere University,
for public discussion in the Yellow Hall F025
of the Arvo building, Arvo Ylpön katu 34, Tampere,
on 20 September 2019, at 12 o'clock.

ACADEMIC DISSERTATION
Tampere University, Faculty of Medicine and Health Technology
Finland

Responsible supervisor and Custos	Professor Tero Järvinen Tampere University Finland	
Supervisor	Docent Hannele Uusitalo-Järvinen Tampere University Finland	
Pre-examiners	Professor Lauri Eklund University of Oulu Finland	Docent Johanna Liinamaa University of Oulu Finland
Opponent(s)	Associate Professor Pipsa Saharinen University of Helsinki Finland	

The originality of this thesis has been checked using the Turnitin OriginalityCheck service.

Cover design: Roihu Inc.

ISBN 978-952-03-1214-5 (print)
ISBN 978-952-03-1215-2 (pdf)
ISSN 2489-9860 (print)
ISSN 2490-0028 (pdf)
http://urn.fi/URN:ISBN:978-952-03-1215-2

PunaMusta Oy – Yliopistopaino
Tampere 2019

ACKNOWLEDGEMENTS

The research of this dissertation was carried out in the Doctoral Programme in Medicine and Life Sciences, at the Faculty of Medicine and Health Technology, Tampere University. I am grateful for the financial support received from the Pirkanmaa Regional Fund/The Finnish Cultural Foundation, Tamperelaisen tutkimustyön tukisäätiö, Sokeain Ystävät ry, Silmä- ja kudospankkisäätiö, Mary and Georg C. Ehrnrooth Foundation, Evald and Hilda Nissi Foundation, Diabetes Research Foundation, Diabetes Wellness Finland, Emil Aaltonen Foundation and the Doctoral Programme in Medicine and Life Sciences, Tampere University. These grants have made it possible to do research full-time and to travel to international conferences.

First and foremost, I would like to thank my supervisors Professor Tero Järvinen (MD, PhD) and Docent Hannele Uusitalo-Järvinen (MD, PhD) for giving me the opportunity to work in their research group and introducing me to the field of academic research. I'm grateful for the guidance and instructive discussions, and the responsibility you have given me allowing me to learn and improve my skills as a researcher. I admire your passion and enthusiasm for science and research.

I would like to thank my opponent, Associate Professor Pipsa Saharinen (PhD) for accepting the invitation for being the official opponent at the thesis defense. I thank the external reviewers of this dissertation, Docent Johanna Liinamaa (MD, PhD) and Professor Lauri Eklund (PhD) for their constructive feedback to improve the quality of the dissertation. I also thank the members of my thesis committee, Professor Hannu Uusitalo (MD, PhD), and Professor Seppo Parkkila (MD, PhD) for the collaboration, feedback about my dissertation and encouragement during these studies.

This research would not have been possible without my co-workers and co-authors who I was happy to be working with. Thanks to our own research group members Ulrike May, Stuart Prince, Toini Pemmari and all the others for creating such a dynamic and an interesting working environment. There was never a boring day at work. My warm thanks for the collaboration during the studies to Marko Pesu, Zuzet Martinez Cordova, Saara Aittomäki, Harlan Barker, Masanobu Komatsu,

James Whiteford and Giulia de Rossi. I'm grateful for the SILK "eye group" members Ulla Aapola, Janika Nättinen, Antti Jylhä and Saara Lähdekorpi and others for their collaboration and delightful company during coffee breaks. I would also like to thank Giedrius Kalesnykas for collaboration during these years.

I would like to express special thanks to our amazing former and current laboratory technicians, Anni Laitinen and Marianne Karlsberg. Anni, thank you for your guidance to basic laboratory work in the beginning of my studies and for helping me with the experiments, even in the middle of the night. I am extremely grateful of having Marianne in our group. You are such a great person to work with and I have learned a lot from you.

I thank the personnel of the Faculty of Medicine and Health Technology who has contributed to this research; my warm thanks to Marja-Leena Koskinen for teaching me techniques in immunohistochemistry in the beginning of my research and providing help with the stainings for this dissertation. I would like to thank the personnel in the Animal Facility for providing great care of the animals and teaching me about animal caretaking while as I was working at the facility before I started my PhD studies. I thank the clinicians from TAYS and KYS; Marko Kataja, Peeter Kööbi and Kati Kinnunen, for providing the valuable patients samples for the research.

Luckily, I have amazing people in my life who have been there during these years to remind me that there is life outside the lab as well. I would like to express my sincere thanks to my dear friends from and outside the university world. Thank you for your support, encouragement and company that you have given me, it means the world to me. Thank you for sharing the happy moments with me and helping me through the tough ones. Finally, I would like to thank my family, my mom and my brother, for encouraging and helping me when needed, and for always being there for me.

Tampere, August 2019

Maria Vähätupa

ABSTRACT

Angiogenesis, the formation of new blood vessels, is important for normal development and the maintenance of tissue homeostasis. However, in many diseases, the events that are normally tightly controlled become disrupted, which can lead to aberrant and extensive growth of the blood vessels. Pathological angiogenesis is a key feature in many vision-threatening eye diseases and in cancers. Vascular endothelial growth factor (VEGF) is the main driver of pathological angiogenesis and VEGF- inhibitors are commonly used as a treatment for neovascular diseases. However, the therapies are not always sufficiently effective, and resistance to them can develop. Thus, more effective and specific therapeutics are needed. For this reason, the better understanding of the molecular mechanisms behind the pathologies is important.

The main aim of this dissertation was to study the effect of different genes on the formation of new blood vessels and to identify new factors that contribute to the regulation of angiogenesis. The dissertation consists of four studies that addressed the role of angiogenesis mainly in eye diseases. These studies made use of experimental models of retinopathies as well as samples from human patients with proliferative diabetic retinopathy and retinal vein occlusion.

The first study investigated the role of R-Ras in the regulation of angiogenesis in ischemic retinopathy. We found that R-Ras was important for the maintenance of vascular stability. The same ischemic retinopathy model was used in the second study, in which we showed that the function of myeloid-specific furin for retinal angiogenesis plays a role in retinal revascularization.

In the third study we performed the most comprehensive proteomic profiling of the oxygen-induced retinopathy model to date. We identified novel proteins that may drive the pathogenesis and neovascularization in the mouse retinopathy model. These proteins may have relevance to human retinopathy as well as new potential drug targets.

The fourth study explored the role of syndecan 4 (SDC4) in angiogenesis using several angiogenesis models. We demonstrated that SDC4 is needed for VEGFA-driven pathological angiogenesis and VE-cadherin trafficking. The therapeutic potential of SDC4 inhibition was tested in an experimental model of wet age-related

macular degeneration (AMD), and we found that it was as effective as a drug commonly used in the clinic for the treatment of wet AMD.

The results of these studies improve the knowledge of the factors that affect angiogenesis. These results could be useful in the future development of new drugs for diseases that involve pathological angiogenesis.

TIIVISTELMÄ

Angiogeneesi, eli verisuonten uudismuodostus on tärkeää normaalin kehityksen ja kudoksen tasapainon kannalta. Useissa sairauksissa muutoin tarkkaan säädellyt mekanismit järkkyvät, mikä voi johtaa verisuonten hallitsemattomaan kasvuun. Patologista uudisverisuonitusta esiintyy useissa näköä heikentävissä ja sokeuttavissa silmänpohjan sairauksissa sekä useissa syövissä. Tiedetään, että verisuonten endoteelikasvutekijä (VEGF) on merkittävässä roolissa edistämässä haitallista verisuonten kasvua, ja sen estäjiä käytetäänkin hoitona useissa neovaskulaarisissa sairauksissa. Nämä hoidot eivät aina kuitenkaan ole tarpeeksi tehokkaita, ja uusia tehokkaampia ja spesifisempiä hoitomuotoja tarvitaan. Tämän takia angiogeneesin liittyvien tapahtumien parempi molekulaarinen tietämys on tarpeen.

Tämän väitöskirjan tavoitteena oli tutkia eri geenien vaikutusta angiogeneesiin ja löytää uusia angiogeneesin säätelyyn osallistuvia tekijöitä. Väitöskirja koostuu neljästä osatyöstä, jotka käsittelevät angiogeneesiä retinan kehityksen aikana sekä osana silmäsairauksia. Osatöissä on suurelta osin käytetty kokeellisia hiirimalleja, jotka mallintavat iskeemisiä retinopatioita. Lisäksi käytössä on ollut lasiaisenpoistoleikkauksen yhteydessä saatuja potilasnäytteitä proliferatiivista diabeettista retinopatiaa ja verkkokalvon verisuonitukosta sairastavailta potilailta.

Ensimmäisessä osatyössä *Rras* geenin roolia tutkittiin iskeemisen retinopatian angiogeneesissä, ja todettiin geenin merkittävä osallisuus verkkokalvon verisuonten läpäisevyyden säätelyssä. Meyloidisolujen furin geenin merkitystä verkkokalvon verisuonten kasvuun tutkittiin toisessa osatyössä ja havaittiin sen edistävän verisuonten kasvua.

Kolmannessa osatyössä kokeellisesta iskeemisestä verkkokalvon angiogeneesimallista tehtiin tähän mennessä laajin hiiren verkkokalvon proteomin kartoittava seulontatutkimus. Tutkimuksessa löydettiin proteiineja, jotka mahdollisesti osallistuvat verkkokalvon haitallisen uudisverisuonitukseen muodostumiseen hiirimallissa sekä ihmisen iskeemisissä retinopatioissa.

Viimeisessä osatyössä tutkittiin syndekaani-4 -geenin (*Sdc4)* merkitystä angiogeneesille useissa eri malleissa ja havaittiin SDC4:n merkittävä rooli VEGFA-välitteisen patologisen verisuonituksen muodostumisessa ja VE-kadheriinin toiminnassa. SDC4 terapeuttista potentiaalia testattiin kokeellisessa silmänpohjan

ikärappeumamallissa, ja todettiin SDC4 toiminnan eston olevan yhtä tehokas kuin ikärappeuman hoidossa kliinisessä käytössä oleva lääke.

Tutkimuksessa saadut tulokset lisäävät tietämystä angiogeneesiin vaikuttavista tekijöistä. Ne voivat olla hyödyllisiä kehitettäessä uusia potentiaalia lääkkeitä sairauksiin, joihin liittyy haitallinen verisuonten uudismuodostus.

CONTENTS

ABBREVIATIONS

AHSG	Fetuin-A
AKT	AKT serine/threonine kinase
AMD	Age-related macular degeneration
ANGPT2	Angiopoietin 2
ANXA	Annexin A
APOA1	Apoliprotein A1
AVA	Avascular area
bFGF	Basic fibroblast growth factor
BRB	Blood-retinal barrier
CNV	Choroidal neovascularization model
DMBA	7,12-Dimethylbenz[a]anthracene
DME	Diabetic macular edema
DR	Diabetic retinopathy
EC	Endothelial cell
ERK	Extracellular signal-regulated kinase
FGF	Fibroblast growth factor
FLNA	Filamin A
$FLNA_{CT}$	C-terminal Filamin A
FLNB	Filamin B
GAP	GTPase-activating protein
GC	Vitamin-D-binding protein
GCL	Ganglion cell layer
GDP	Guanosine diphosphate
GEF	Guanine nucleotide exchange factor
GPX1	Coproporphyrinogen-III oxidase 1
GTP	Guanosine triphosphate
GTPase	Guanosine triphosphatase
HIF	Hypoxia-inducible factor
HRP	Horseradish peroxidase
HSA	Human serum albumin

HSPG	Heparan sulfate proteoglycan
IF	Immunofluorescence
IHC	Immunohistochemistry
INL	Inner nuclear layer
IPA	Ingenuity pathway analysis
IPL	Inner plexiform layer
IS/OS	Inner and outer segments of photoreceptors
KO	Knockout
LysMCre-fur$^{(fl/fl)}$	Myeloid-cell-specific conditional furin knockout
MCAM	Cell surface glycoprotein MUC18
MKNK1	MAP kinase interacting serine/threonine-protein kinase 1
MKL2	MKL/myocardin-like protein 2
MMP	Matrix metalloproteinases
MS	Mass spectrometry
MYH9	Myosin 9
NFL	Nerve fiber layer
NV	Neovascularization
OIR	Oxygen-induced retinopathy
ONL	Outer nuclear layer
OPL	Outer plexiform layer
P	Postnatal day
PCSK	Proprotein convertases subtilisin/kexin
PDGF	Platelet-derived growth factor
PDGFR	Platelet-derived growth factor receptor
PDR	Proliferative diabetic retinopathy
PFA	Paraformaldehyde
PI3K	Phosphatidylinositol-3-kinase
PGF	Placental growth factor
PPIA	Peptidylprolyl isomerase A
PVDF	Polyvinylidene difluoride
qPCR	Quantitative polymerase chain reaction
RIPA	Radioimmunoprecipitation assay
ROP	Retinopathy of prematurity
RPE	Retinal pigment epithelium
RTK	Receptor tyrosine kinase
R-Ras	Ras-related protein R-Ras

RVO	Retinal vein occlusion
SDC4	Syndecan 4
SMC	Smooth muscle cell
SRC	SRC proto-oncogene, non-receptor tyrosine kinase
SWATH	Sequential window acquisition of all theoretical fragment ion spectra
TAGLN2	Transgelin 2
TGF-β	Transforming growth factor β
TPA	12-O-Tetradecanoyl phorbol-13-acetate
VCL	Vinculin
VDR	Vitamin D receptor
VE-cadherin	Vascular endothelial cadherin
VEGF	Vascular endothelial growth factor
VEGFR	Vascular endothelial growth factor receptor
WG	Weeks of gestation
WT	Wild type
WB	Western blot/western blotting

According to the guidelines of the Human Genome Organization Gene Nomenclature Committee (HGNC) and Mouse Genome Informatics (MGI) the following formatting is used for gene and protein names in the text:

Human genes: Italicized, all letters in upper-case (e.g. *VEGF*)
Human proteins: Not italicized, all letters in upper-case (e.g. VEGF)
Mouse genes: Italicized, first letter in upper-case (e.g. *Vegf*)
Mouse proteins: Not italicized, all letters in upper-case (e.g. VEGF)

ORIGINAL PUBLICATIONS

Publication I Maria Vähätupa, Stuart Prince, Suvi Vataja, Teija Mertimo, Marko Kataja, Kati Kinnunen, Varpu Marjomäki, Hannu Uusitalo, Masanobu Komatsu, Tero A.H. Järvinen & Hannele Uusitalo Järvinen. Lack of R-Ras leads to increased vascular permeability in ischemic retinopathy. *Investigative Ophthalmology & Visual Science*. 2016, 57:4898-4909.

Publication II Maria Vähätupa, Zuzet Martinez Cordova, Harlan Barker, Saara Aittomäki, Hannu Uusitalo, Tero A.H. Järvinen, Marko Pesu & Hannele Uusitalo-Järvinen. Furin deficiency in myeloid cells leads to attenuated revascularization in a mouse-model of oxygen-induced retinopathy. *Experimental Eye Research*. 2018, 166:160-167.

Publication III Maria Vähätupa, Janika Nättinen, Antti Jylhä, Ulla Aapola, Marko Kataja, Peeter Kööbi, Tero A.H. Järvinen, Hannu Uusitalo & Hannele Uusitalo-Järvinen. SWATH-MS proteomic analysis of oxygen-induced retinopathy reveals novel potential therapeutic targets. *Investigative Ophthalmology & Visual Science*. 2018, 59:3294-3306.

Publication IV Giulia De Rossi, Maria Vähätupa, Enrico Cristante, Sidath E. Liyanage, Ulrike May, Laura Pellinen, Saara Aittomäki, Zuzet Martinez Cordova, Marko Pesu, Hannele Uusitalo-Järvinen, James W. Bainbridge, Tero A.H. Järvinen & James R. Whiteford. Syndecan-4 is required for efficient VE-Cadherin trafficking during pathological angiogenesis. *Submitted*.

The permission to include the original communications in this dissertation is received from the copyright holders.

Unpublished data included in this dissertation is indicated in the text.

1 INTRODUCTION

Angiogenesis, the formation of new blood vessels, is essential for normal development, and healthy and functional blood vessels are needed for the maintenance of tissue homeostasis. When the balance between pro- and antiangiogenic factors shifts, the formation of pathological neovascularization (NV) can be induced. NV is hallmark of diseases like cancers with solid tumors and many ocular diseases. Ocular neovascular diseases, such as retinopathy of prematurity (ROP), diabetic retinopathy (DR), and the wet form of age-related macular degeneration (AMD), are major causes of severe visual impairment and even blindness in industrial countries. As people live longer, the number of people with diseases involving ocular NV will increase.

In cancers, angiogenesis is needed for the tumor to grow and metastasize. In ocular diseases NV can be either retinal, subretinal, or choroidal. Retinal NV is seen in ischemic retinopathies such as ROP, DR and retinal vein occlusion (RVO). Subretinal and choroidal NV occurs in wet AMD, in which choroidal neovessels grows through Bruch's membrane towards subretinal space and outer retina. Neovessels are fragile and can leak, scarring the retina and leading to photoreceptor damage. This can lead to vision loss and eventually even retinal detachment and blindness.

Vascular endothelial growth factor-A (VEGFA) is a major proangiogenic factor driving angiogenesis and inducing vascular leakage both in both cancers and ocular diseases. The use of VEGF inhibitors as an antiangiogenic treatment for cancers with solid tumors and especially for ocular neovascular diseases has revolutionized the therapies. However, there is nonresponse among patients as well as many off-target effects and systemic adverse effects.

Thus, more effective and specific therapies for neovascular diseases are needed. The aim of this dissertation was to study the regulation of angiogenesis especially in ocular diseases.

2 REVIEW OF THE LITERATURE

2.1 Blood vessel structure and formation

Blood vessels are responsible for delivering oxygen and nutrients to the tissues and disposing waste generated in tissues. Blood vessels are divided into arteries, veins and capillaries, based on their size, structure and function. Veins and arteries consist of three layers; tunica intima, tunica media and tunica adventitia. The inner part of blood vessels has endothelial cells (ECs) in a single layer forming the lumen of the blood vessels. It is surrounded by basement membrane, a thin layer of extracellular matrix tissue (1). The outer layer is connective tissue, attaching the blood vessel to tissue surrounding it. The smallest capillaries consist only of one EC layer and basement membrane.

ECs are surrounded by contractile mural cells, which provide support for and stabilize ECs. Arteries and veins are covered with mural cells referred to as vascular smooth muscle cells (SMCs), whereas smaller capillaries are covered by mural cells called as pericytes (2). The pericyte-to-endothelia ratio varies from 1:1 (or even > 1:1) to 1:100 depending on the tissue and species (3). For example, vascular beds in neural tissue, especially retinal vessels, have the highest pericyte/EC length ratio, ranging from 0.85 to 1.17 in monkey and human retinas (4). ECs and pericytes are wrapped with basement membrane, a thin, fibrous structure of extracellular matrix, which provides structure to blood vessels, but also controls EC growth and is involved in angiogenesis (5). The main structural compartments of capillary blood vessels are presented in Figure 1.

ECs form a tight barrier separating the blood and the surrounding tissue. To be functional, the ECs of the blood vessels need to be in close contact with each other but also able to transport molecules between the blood and tissue. This transport can occur between or through the cells (6). Endothelial junctional proteins play an important role in regulating vascular permeability and angiogenesis. There are three different junction types in ECs: tight, adherens and gap junctions. The junction organization varies depending on the tissue type and its requirements for vascular permeability. Gap junctions are the loosest type of junctions, and they allow small molecules to be transported between cells. Gap junctions are formed from connexin

proteins, which are organized as connexons acting as a channel that allows the passage of small molecules (7).

The majority of EC junctions are tight and adherens junctions (7,8). Tight junctions are composed of both of intracellular and transmembrane proteins, such as occluding and claudins (7). Tight junctions are involved in the control of paracellular signaling pathways in ECs, and they form the barrier in the blood-brain barrier and inner blood-retinal barrier (BRB) (9). Adherens junctions are formed from members of the cadherin family of transmembrane adhesion proteins. The main cadherin types expressed in high levels on ECs are vascular endothelial cadherin (VE-cadherin), which is present only in ECs, and neuronal cadherin, expressed in neuronal cells and SMCs as well (7). Other cadherins expressed in ECs are P-cadherin and T-cadherin, but they are not cell-type-specific (10). Many cadherins, including VE-cadherin, are linked to intracellular adhesion molecules such as β-catenin, plakoglobin and p120, via their cytoplasmic tail. These molecules are further linked to other adhesion proteins, such as α-catenin and vinculin, which are anchored to actin filaments (7). The role of VE-cadherin in angiogenesis and controlling vascular permeability is discussed in more detail in section 2.2.2.

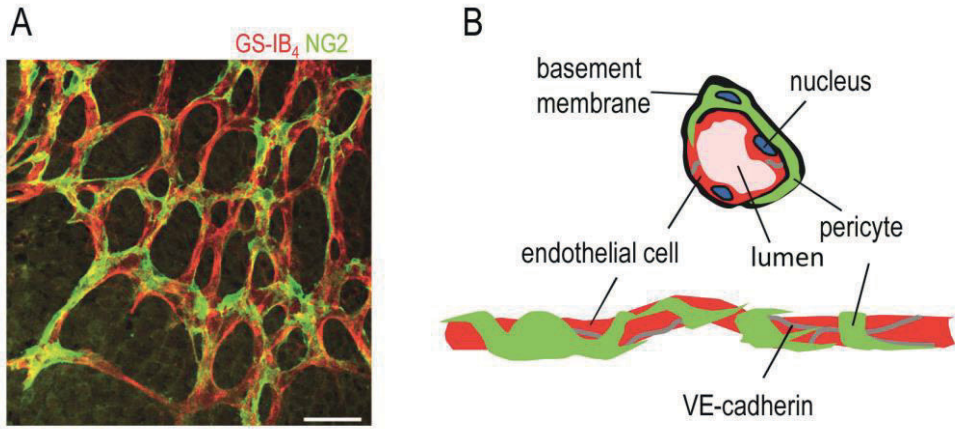

Figure 1. Structure of a capillary blood vessel. (A) Capillary plexus of the mouse retina, where ECs are stained in red, and pericytes are stained in green. Scale bar is 50 μm. (B) Schematic representation of capillary structure.

During early mammalian embryonic development, blood vessels form from angioblasts through vasculogenesis, which gives rise to the primitive vascular plexus (11). As development progresses, new blood vessels start to form from preexisting ones through angiogenesis. Angiogenesis takes place mainly during embryonic

development. In healthy adults angiogenesis occurs in the female reproductive system during the menstrual cycle and pregnancy (12), during physiological tissue or wound healing, when healing tissue requires new blood vessels to form (13) and in skeletal muscle adaptation to stress and exercise (14). Otherwise, the blood vessels in the body are maintained in a quiescent and stable state.

New blood vessels can form through mechanisms other than angiogenesis, such as intussusception, where blood vessels grow via splitting process of an existing blood vessel (15). In tumor environment, new blood vessels can be formed through vessel co-option and vascular mimicry (16,17). Tumor cells essentially grow along existing blood vessels in vessel co-option, whereas tumor cells acquire properties of ECs and establish patterned vascular networks on their own in vascular mimicry. In addition, it has been shown that cancer stem cells can transform into blood vessel ECs (18).

2.2 Angiogenesis

In angiogenesis, blood vessels sprout and grow towards growth the stimulus, which is often caused by tissue hypoxia. New blood vessels are needed to invade the area in order to satisfy the metabolic requirements of the cells in the hypoxic area. Angiogenesis involves EC activation by growth factors, enzymatic degradation of basement membrane in existing blood vessels, EC proliferation, migration of ECs to the interstitial space towards the stimulus, formation of an elongating sprout, EC tube formation, fusion of the vessels, vessel pruning, pericyte stabilization and finally, formation of basement membrane.

Because blood vessels are found in every organ in the body, abnormal angiogenesis is involved in many pathological conditions, including arthritis, stroke, myocardial infarction, cancer and blinding eye diseases (19). Pathological angiogenesis shares many features with physiological angiogenesis. In both cases, the formation of new blood vessels is driven by the increased demand for oxygen and nutrients in the tissue. In physiological conditions, the process is controlled with a balance of pro- and antiangiogenic factors. In pathological conditions, proangiogenic factors are more abundant than antiangiogenic factor, and this imbalance keeps the angiogenic cascade of events going and lead to uncontrolled growth of blood vessels. Many signals can interrupt the balance between pro- and antiangiogenic factors, among them mechanical stress, metabolic stress, genetic mutations, and immune or inflammatory response in the tissue (19,20).

Tumor growth and metastasis are dependent on angiogenesis, because tumors cannot grow beyond a critical size without the formation of new blood vessels into and around the tumor. Tumors can grow approximately 1-2 mm^3 in size before the limitations of oxygen and nutrients requires the tumor to switch to an angiogenic phenotype, in which the balance between pro- and antiangiogenic factors is shifted (19). Vascular density is greatly increased in cancer tissue, and vascular density is a prognostic factor for survival (21). Moreover, the maturation status of the vessels is critical, because stable and mature vessels are needed for efficient delivery of cancer therapeutics into the tumor site (22).

The most prominent proangiogenic stimulus is tissue hypoxia, which is present in many disorders, including ischemic retinopathies and cancer. In growing tumors cancer cells become hypoxic when surrounding blood vessels are too far from them. Hypoxia controls many aspects of angiogenesis, including vessels sprouting, maturation and function. Most transcriptional responses to hypoxia are mediated via hypoxia-inducible factors (HIFs). The stabilization/activation of HIF-1α takes place in hypoxia leading to induction of the expression of angiogenic factors such as vascular endothelial growth factor (VEGFA), erythropoietin, platelet-derived growth factor (PDGF), angiopoietins, basic fibroblast growth factor (bFGF) and many others (23,24). In hypoxia, HIFs accumulate in the cells and translocate into the nucleus, where they form a complex with other factors, bind to hypoxia response elements in the promoter region of target genes and induces gene expression (24,25). HIF-induced angiogenic factors increase EC proliferation, migration and adhesion and increase vascular permeability.

2.2.1 The VEGF family and it's receptors

VEGFs are a family of growth factors that are key regulators of angiogenesis. The VEGF family includes VEGFA, VEGFB, VEGFC, VEGFD and placental growth factor (PGF) (26,27). In addition to these, viral VEGF homolog VEGFE and snake venom homolog VEGFF have been found (28,29). All VEGF family members have distinct functions, and their biological functions are mediated by a type of protein tyrosine kinase receptors, vascular endothelial growth factor receptors (VEGFRs) (30). VEGFA activates VEGFR1 (also known as FLT1) and VEGFR2 (also known as KDR/FLK1); VEGFB and PGF bind to VEGFR1; and VEGFC and -D signal via VEGFR3 (FLT4) (31). In addition, VEGFs can interact with VEGFR co-receptors, such as neuropilins and heparan sulfate proteoglycans (HSPGs) (32).

Among all the angiogenic factors, VEGFA is considered the major factor for both physiological and pathological angiogenesis. By binding to its receptor VEGFR2, VEGFA stimulates multiple signaling pathways in ECs, leading to EC proliferation, migration, and remodeling of the cell-cell junctions between neighboring ECs (33). VEGFA is secreted from multiple cell types, including mural cells, inflammatory cells, and neurons. It and its receptors are highly expressed during embryogenesis and during development in close proximity with vascular networks, suggesting a role in vascular development (34). Threshold levels of VEGFA are needed for proper vascular development. Inactivation of a single *VEGFA* allele led to abnormal blood vessels development and embryonic lethality during early development (34). In the adult body VEGFA is expressed in minimal levels in all vascularized tissues, where it maintains vascular homeostasis (26). Because VEGFA expression is strongly induced under a variety of pathological conditions, the VEGF-VEGFR system is an important target of antiangiogenic therapies for ischemic eye diseases and cancer.

Alternative splicing of *VEGFA* results in different isoforms, that is, $VEGF_{121}$/ $VEGF_{120}$ $VEGF_{165}$/$VEGF_{164}$, $VEGF_{189}$/ $VEGF_{188}$, and $VEGF_{206}$ in humans/mice (35). Different variants have different functions, and $VEGF_{165}$/$VEGF_{164}$ is the predominant isoform in angiogenesis. Moreover, the proteolytic processing of the splice variants affects their ability to interact with VEGF co-receptors, like HSPGs (36,37).

The role of PGF and VEGFB in angiogenesis is elusive and has attracted less research. VEGFB is highly expressed in many tissues, but its exact functions are not fully known (38). Although VEGFB is not needed for blood vessel growth, it is critical for the survival of ECs, pericytes, SMCs and vascular progenitor cells (39), and VEGFB blockage has been shown to inhibit choroidal and retinal neovascularization (NV) (39). Unlike other VEGF family members, VEGFB and PGF do not induce vascular permeability (26,40). PGF is expressed mainly in placenta, and its expression is induced in pathological angiogenic diseases. PGF forms heterodimers with VEGF when they are coexpressed (41). PGF-VEGF heterodimers induce angiogenesis, but PGF alone cannot induce NV (42).

VEGFC and -D and their receptors regulate angiogenesis mainly during embryogenesis, and they mainly regulate lymphangiogenesis in adults (43). However, VEGFC can induce angiogenesis in vivo; for example, it can enhance NV in the mouse cornea (44). In the retina, VEGFC protects ECs from apoptosis and enhances NV (45).

2.2.2 Vascular permeability

One of the phenomena involved in the regulation of angiogenesis is vascular permeability, which is strictly controlled during physiological conditions. However, this control is lost in many diseases and the blood vessels become hyperpermeable. When VEGFA was found, it was first designated as a vascular permeability factor, because it was first described as a protein secreted by tumors that significantly increases vascular permeability (46). It is still understood as the major factor regulating vascular permeability.

There are well-characterized hallmarks of hyperpermeable blood vessels, such as the dropout of pericytes and disorganization of cell-cell junctions. VE-cadherin is needed for the maintenance of a stable vascular system, in which it controls endothelial vascular permeability and prevents excess vascular growth (47). VE-cadherin is a dimeric transmembrane protein that clusters at cell-cell contacts, where it forms complexes with other signaling proteins, such as β-catenin, p120, and plakoglobin. These molecules, in turn, interact further with other signaling proteins, including α-catenin, which connects to actin fibers. In addition, VE-cadherin can interact with proteins that have enzymatic activities, such as tyrosine and serine kinases, tyrosine phosphatases, and guanosine triphosphatases (GTPases) (48). The composition of the VE-cadherin complexes depends on the type and the activation state of the blood vessels (48). The importance of VE-cadherin for blood vessel stability has been shown with administration of VE-cadherin function blocking antibodies on adult mice, which leads to a dramatic increase in vascular permeability and hemorrhages (49). In normal physiological conditions, VE-cadherin clusters at EC junctions in zipper-like structures. The strength of VE-cadherin junctions is reduced by VE-cadherin phosphorylation, which causes the structures to become more loosely attached. During angiogenesis, VE-cadherin needs to be internalized and recycled for proper EC migration to take place. VEGFA induces EC permeability by promoting VE-cadherin endocytosis (50). Many signaling pathways, including the interaction of VE-cadherin and VEGFR2, relate to angiogenesis and vascular permeability (47,51,52).

2.3 R-Ras, furin, and SDC4

The roles of R-Ras, furin, and SDC4 in angiogenesis were studied in this dissertation. Their cellular localizations are illustrated in the Figure 2.

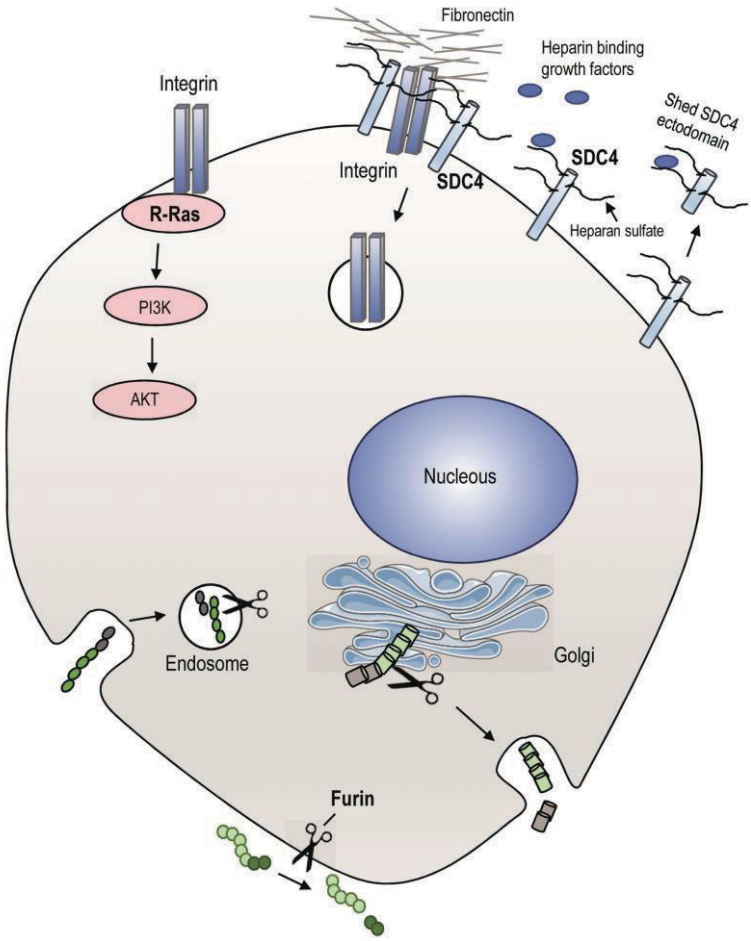

Figure 2. Cellular localization of R-Ras, furin and SDC4 proteins. R-Ras is a cytoplasmic protein that localizes to inner surface of plasma membrane and transduces signals to downstream effectors. R-Ras regulates the activation of the PI3K-AKT signaling, that regulates angiogenic stimulation and barrier function in ECs. Furin (scissors) is principally located in the trans-Golgi network, where it cycles between cell membrane and early endosomes and cleaves proprotein substrates to active proteins. SDC4 is a transmembrane proteoglycan, that has multiple functions related to controlling membrane trafficking and intracellular signaling pathways. It can act independently as a receptor itself, or as a co-receptor with multiple proteins, among them integrins. Extracellular functions of SDC4 are mediated by cleavage and shedding of its ectodomain.

2.3.1 R-Ras

Ras-related protein R-Ras (R-Ras) is a member of the Ras superfamily of small GTPases, which act as molecular switches and transduce signals to their downstream effectors (53). GTPases cycle between an active guanosine triphosphate (GTP)-bound and an inactive guanosine diphosphate (GDP)-bound state. The mechanism controlling the activation state is highly conserved among all GDP/GTP binding proteins. Ras proteins are converted to the inactive form to active form by guanine nucleotide exchange factors (GEFs) and inactivated by GTPase-activating proteins (GAPs) or by intrinsic GTPase activity that hydrolyses GTP to GDP (54) (Figure 3).

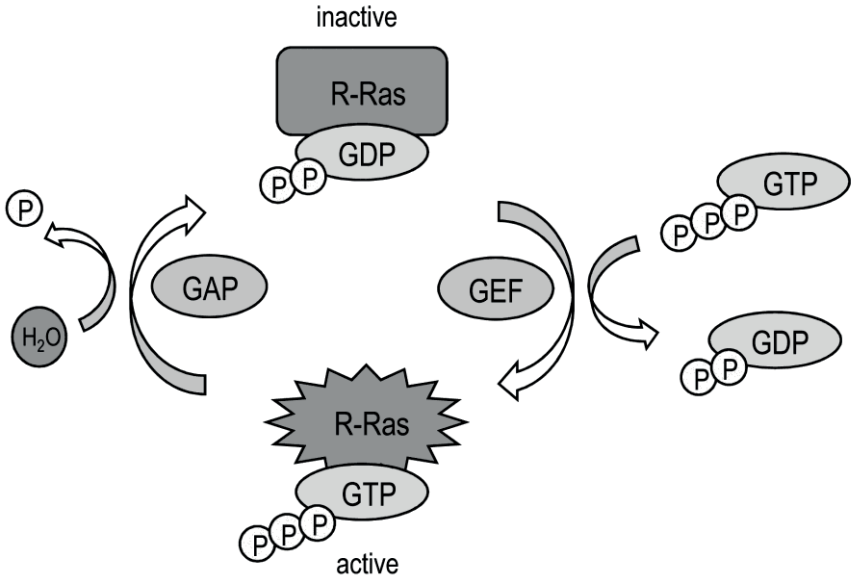

Figure 3. R-Ras GTPase regulatory cycle. R-Ras is cycled between an active GTP-bound state and an inactive GDP-bound state.

The Ras superfamily is divided into five branches based on structure: Ras, Rho, Rab, Ran, and Arf (53). Ras proteins (Ras sarcoma oncoproteins) were the first proteins of the family to be found, and 36 members have now been identified, among them the best-known Ras proteins H-Ras, K-Ras, and N-Ras, along with R-Ras. H-Ras, K-Ras and N-Ras were the first human oncogenes to be described, and their mutations are found in more than 30% of human cancers (55,56). Ras proteins control many downstream effectors that regulate cell proliferation, differentiation and survival (57).

The *RRAS* gene is located on chromosome 19q13.3 (58). Structurally, R-Ras is somewhat similar with other Ras-family members, because it shares approximately 50% amino acid homology with them and an almost identical effector binding region with N-Ras, H-Ras, and K-Ras (57-59). R-Ras has an extra 26 amino acids in the N-terminus, as a result of which R-Ras functions distinctly from the other Ras proteins (58). Although single amino acid mutation converts other family members to proto-oncogenes, this is not the case with *RRAS* (60). Mutations of *HRAS*, *KRAS*, and *NRAS* are frequently seen in cancers (61), whereas *RRAS* shows less or no transformation activity. In contrast to K-Ras, H-Ras, and N-Ras which are well-known activators of the RAF/ERK (or MAPK/ERK) pathway, R-Ras is a poor activator of that pathway (59,62). Instead, R-Ras activates mainly the phosphoinositide 3-kinase (PI3K)/AKT pathway in normal conditions (62) and it has been shown that the activating R-Ras mutations can activate the MAPK signaling pathway only in malignancies (63).

R-Ras is known to regulate many cellular events, including integrin activation, cellular adhesion, migration, and apoptosis. (64,65). Studies have also identified roles of R-Ras in the neural system, such as in migrating axons and the immune system, where R-Ras is needed for immunological synapse formation and T-cell proliferation and trafficking (66,67). Generation of R-Ras deficient mice revealed that R-Ras has previously unknown functions in blood vessels maturation and angiogenesis. For example, a gain-of-function of R-Ras inhibits vessel sprouting and branching, EC migration, and vascular permeability, whereas deletion of R-Ras leads to enhanced vascular permeability in tumors and skin wounds (68-71). As it has been shown that R-Ras maintains cellular quiescence and inhibits cell proliferation, it was surprising that the lack of R-Ras in the chemically induced skin-carcinogenesis model led to protection against tumor formation (72). A potential explanation is that the skin cancer model is dependent on inflammation (73) and that the inflammatory response driving tumorigenesis was significantly attenuated in R-Ras KO mice. Lack of R-Ras has been reported to lead to reduced inflammatory responses in various experimental disease models (66,67,74). The role of R-Ras in the development of allergic inflammation has also been investigated, but R-Ras did not have an effect on the IgE response (75).

The role of R-Ras in retinal vascular development or ischemic retinopathies has not been previously studied, so it was investigated in this dissertation.

2.3.2 Furin

The maturation of many secreted proteins requires enzymatic cleavage as a posttranslational modification step before they become functionally active. There are many types of proteases, and they are classified based on the mechanisms of catalysis as metallo, cysteine, aspartic, serine, and threonine proteases (76). Serine proteases are further divided into trypsin-like, thrombin-like, chymotrypsin-like, elastase-like, and subtilisin-like proteases based on their substrate specificity. The serine proteases include a family of proprotein convertases with nine family members.

The mammalian proprotein convertase subtilisin/kexin (PCSK) family is a group of nine enzymes. The first seven members to be identified, PCSK1-2, furin, and PCSK4-7 are closely related and derived from the bacterial and yeast proteins subtilisin and kexin (77). They cleave basic amino acid motifs, lysine and/or arginine (K/R)-(X)n-(K/R)↓, where X is any amino and n is either 0, 2, 4 or 6 (78). The remaining two members, MBTPS1 and PCSK9, differ in terms of their domain structures and target sites (79).

PCSKs are important for the maintenance of tissue homeostasis, but they also participate in many diseases (80). They activate many proteins that are associated with cancer progression and the promotion of tumor angiogenesis, among them growth factors, including VEGFC and -D, cell-surface receptors, and matrix metalloproteinases (MMPs) (81,82).

Furin is the first-identified member of the PCSK family and is ubiquitously expressed. In cells, furin can be found in the trans-Golgi network, endosomes, and cell membrane (Figure 2). Furin can also be secreted outside the cell. Furin has been associated with biological processes like inflammation and autoimmunity and has been linked to human diseases (78,83-85). Furin expression levels are elevated in many cancers and correlated with tumor progression. These features make it an interesting therapeutic target. We have showed that myeloid-specific furin did not play a role in tumorigenesis in an inflammation-dependent skin-carcinogenesis model, whereas the deletion of furin from T-cells had detrimental effects, leading to enhanced formation of papillomas (85). Because inhibition of PCSKs is a promising therapeutic alternative in cancer treatment (86), these results show that the role of furin is cell specific and that this should be taken into account when planning furin inhibition for therapeutics.

In DR, furin and its target, a (pro)-renin receptor protein are found to be co-localized in PDR fibrovascular membranes. Elevated (pro)-renin receptor protein

levels have been associated with angiogenesis, thus suggesting that furin cleavage plays a role in angiogenic events in DR (87).

Furin expression can be induced in hypoxia by HIF-1α, because furin is one of its target genes (88-90). In addition to the previously mentioned VEGFC and -D, furin activates other angiogenic targets such as PDGF-A and -B, bone-morphogenic protein-4, and transforming growth factor β (TGF-β) (91-94). The exact function of furin in angiogenesis is poorly understood, but blood-vessel-specific functions have been suggested, because complete deletion of furin leads to death during embryonal development due to cardiovascular defects (95,96). Later, Kim et al demonstrated that EC-specific deficiency of furin led to embryonal death due to vascular defects and that the furin deficient ECs were not able to grow ex vivo (97). In vitro, furin inhibition resulted in reduced migration of monocytes and reduced expression of inflammatory and cytokine genes from macrophages and ECs (98). The ability of furin inhibition to protect against vascular remodeling was evidenced by with decreased carotid intimal thickness and a reduction of inflammatory markers in a carotid artery injury model (98).

2.3.3 Syndecan 4

Syndecans are type 1 transmembrane proteins belonging to the HSPG superfamily. There are four syndecan members in vertebrates, and each of them have different functions and are expressed in different cell types and tissues (99). Most cell types express at least one of the syndecans, and some cell types can express all four. Syndecan 1 is expressed mostly by epithelial cells, syndecan 2 by cells of mesenchymal origin, and syndecan 3 mainly by neuronal tissue; syndecan 4 (SDC4), by contrast, is ubiquitously expressed but at lower levels than the others (99,100). More recent studies have shown that the expression of different syndecans is more flexible, depending on the developmental stage and external stimuli (101).

Syndecans are proteoglycans with a core protein to which a variable number of glycosaminoglycan chains are attached. The most commonly attached glycosaminoglycans are heparan sulfates, but chondroitin or dermatan-sulfate chains are sometimes incorporated. The single-pass transmembrane protein core includes a cytoplasmic domain that is highly conserved among all syndecans. The extracellular domain is the most divergent one, and its length varies among the syndecan members. A variety of ligands can interact with syndecans: extracellular matrix molecules, cell-cell adhesion molecules, growth factors, cytokines, and chemokines

and some pathogens. Sometimes, syndecans act as co-receptors with their ligands for other receptors, like integrins or tyrosine kinase growth factor receptors (99,102). A considerable number of angiogenic factors, such as VEGFs, PDGF, FGFs, PGFs and TGF-β have heparin-binding properties (101). VEGFA binds to heparan sulfate with high affinity, and in the absence of heparan sulfate in ECs VEGFA signaling is disturbed, leading to a reduction of VEGFR2 phosphorylation (103,104). VEGFR2 has also been shown to bind to heparan sulfate, suggesting that HSPGs might be needed for the formation of a functional signaling complex as is the case with FGF signaling (105). The interaction between HSPGs and VEGFA is believed to happen mainly through the glycosaminoglycan part of the molecule (103,104), but the specific roles of different HSPG core proteins are not clear. Previous studies have proposed roles for syndecans in angiogenesis. SDC2 has been shown to play a role in VEGFR2 signaling by promoting VEGFA binding and thus promoting NV whereas SDC4 has been shown to have no effect on VEGFA signaling (106). However, previous studies have shown that SDC4 deficiency leads to defects in wound healing and in placental labyrinth formation suggesting some roles for angiogenesis (107,108). The inhibition of SDC4 expression decreased cell motility in HUVECs, resulted in changes in the cell adhesion sites and delayed tube formation (109). We hypothesized that SDC4 plays a role in angiogenesis, and this was investigated in Study IV.

2.4 The retina

The retina is a cup-like structure located in the innermost part of the eye, surrounded by the choroid (outside) and vitreous fluid (inside) (Figure 4A). When light enters the eye, it first passes through the cornea, the pupil, the lens, and the vitreous, until it reaches the photoreceptors of the outer retina. The main function of the retina and its photoreceptors is to sense light and convert it into electrical impulses, which are further transmitted to the brain to create visual perception. A small area in the center of the retina is the called macula, which is responsible for detailed central vision.

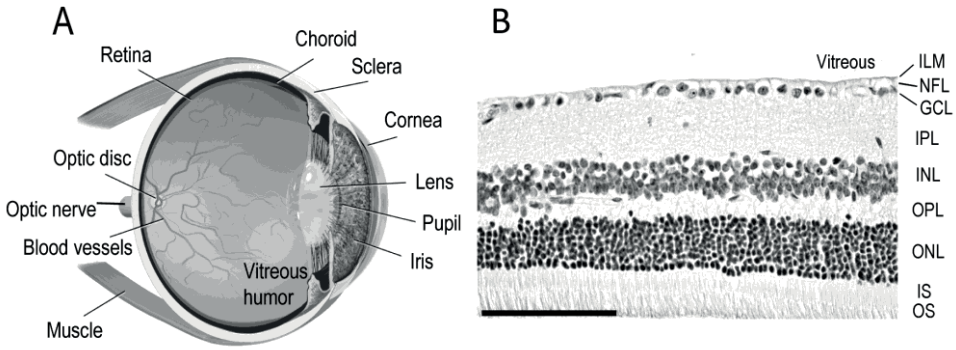

Figure 4. Anatomy of the eye and retina. (A) Cross anatomy of the human eye. The retina is located at the back of the eye, between the choroid and vitreous. (B) The mouse retina is organized into several layers. Scale bar is 100 µm. Image A is modified from Blausen.com staff (2014), Medical gallery of Blausen Medical (2014).

Retinal cells are well organized in several layers, as follows: the retinal pigment epithelium (RPE), inner and outer segments of photoreceptors (IS/OS), outer nuclear layer (ONL), outer plexiform layer (OPL), inner nuclear layer (INL), inner plexiform layer (IPL), ganglion cell layer (GCL), nerve fiber layer (NFL), and inner limiting membrane (ILM) (Figure 4B).

The retina consists of five major neuronal types: photoreceptors, bipolar cells, horizontal cells, amacrine cells, and retinal ganglion cells in all vertebrates (110,111). Retinal photoreceptors are the main cell type responsible for phototransduction. There are two types of photoreceptors, rod and cone photoreceptors. Rods are extremely sensitive to light and responsible for dim-light vision. Rods are 20-times more numerous than cones in humans, and over 30 times more numerous in mice (112,113). Cones are 100 times less sensitive to light than rods, but they are sensitive to a specific wavelength of light and thus involved in bright-light color vision phototransduction (114). Synaptic transmission of neural impulses takes place through retinal layers, that is, from photoreceptors to bipolar and horizontal cells and subsequently to amacrine and ganglion cells which conduct action potentials to the brain (111).

Retinal neurons are surrounded and supported by two types of retinal macroglial cells: Müller cells and astrocytes. Müller cells span the entire thickness of the neural retina, provide metabolic and homeostatic support to retinal neural cells and can become activated by pathogenic stimuli (115,116). An important function of Müller cells is the uptake of glutamate and gamma-aminobutyric acid, the main retinal

neurotransmitter. Thus, Müller cells regulate the synaptic activity and participate in neurotransmission in the retina (117). They also mediate the transcellular transport of water, iron, and bicarbonate, protect the photoreceptors from oxidative stress, and participate in the regulation of the tightness of the BRB and angiogenesis (118). Retinal blood vessels are surrounded by Müller cells' endfeet, forming a link through which molecules can be changed (116). Müller cells can also regulate blood flow in the vessels (115). The other retinal macroglial cells, astrocytes, are found mainly in the NFL and in close proximity to blood vessels in the INL, because they play a critical role in retinal angiogenesis (119,120).

Beneath the neural retina lies the RPE and Bruch's membrane, which is the RPE's basement membrane. The RPE is a thin layer of pigmented cells between the photoreceptors and Bruch's membrane and the choroid. The RPE transfers nutrients and oxygen from the choroid to the photoreceptor cells. It also carries waste products away from photoreceptor cells to the choroid (121). In addition, RPE cells phagocytose the ends of photoreceptor outer segments to prevent damage from built-up waste products, recycle proteins and other components involved in the phototransduction process, and provide other survival proteins to the retina (122). Bruch's membrane serves as a barrier between the RPE and the capillaries in the choroid and forms the BRB, which separates the RPE from the choroid (123).

The retina receives its blood supply from two sources. The outermost part of the neural retina is avascular, and it receives its nutrients from choroidal vasculature through the RPE and Bruch's membrane. The inner retina is vascular, and the main function of this vascular network is to sustain the inner part of the retina by delivering nutrients and oxygen to retinal neurons and their support cells.

The biggest difference between the retina in mice and humans is that the mouse retina lacks macula, an area near the central retina that is responsible for high-resolution color vision. In the center of the macula is the fovea, a region specialized for maximum visual acuity and full of cone photoreceptors. The fovea is located in an avascular region, and it receives oxygen by diffusion from choroidal vessels.

2.4.1 Retinal vascular development

During early embryonic development, the retina receives its nutrient supply from hyaloid vasculature, which begins to regress as soon as retinal vasculature starts to develop. The existence of the hyaloid vasculature is a relic from lower vertebrates, in which vitreous vessels provide nutrients to the retina (124). Human retinal

vasculature starts to develop at approximately at 15 weeks of gestation (WG) from an existing capillary ring at the optic nerve head, from which it sprouts across the inner surface of retina (125). The vasculature reaches the periphery at 36-40 WG, first nasally and then temporally forming the superficial vascular plexus. The vasculature of the deeper plexus starts to develop at 25-26 WG by angiogenic sprouting from the existing primary plexus (125,126). The sprouts penetrate into the retina, and form two vascular networks on both sides on the INL. The foveal zone remains avascular during development (127). If a baby is born full-term, the growth of vasculature has been completed and the vessels in the vitreous, called hyaloid vasculature, have regressed (128).

The development of the retinal vasculature is similar in mice, except that the vasculature starts to develop postnatally. Vessels start to grow to the retina from the optic nerve head, from which the vessels sprout and form flat plexus to the NFL. This most superficial vascular plexus develops first during the first week of development and will reach periphery around postnatal day 7 (P7) (Figure 5). The EC tip cells start to sprout downwards, deeper into the retina, from the veins of the primary plexus (129). The deeper vascular plexus will develop around the INL and complete its development in the third postnatal week. Vascular sprouts from the superficial and deep vascular plexus form an intermediate vascular plexus. The hyaloid vasculature regresses after the vascular plexuses have formed, that is, by the third postnatal week (128).

The developing retinal vasculature of mice is an ideal model for examining the interactions between different cell types in the retina, due to its developmental similarity to the retinal vasculature in humans, its easy accessibility, and possibility to genetic manipulations. Mouse retinal vasculature provides a tool for investigating both physiological and pathological angiogenesis. Models of pathological angiogenesis in the mouse retina will be discussed in section 2.4.3.

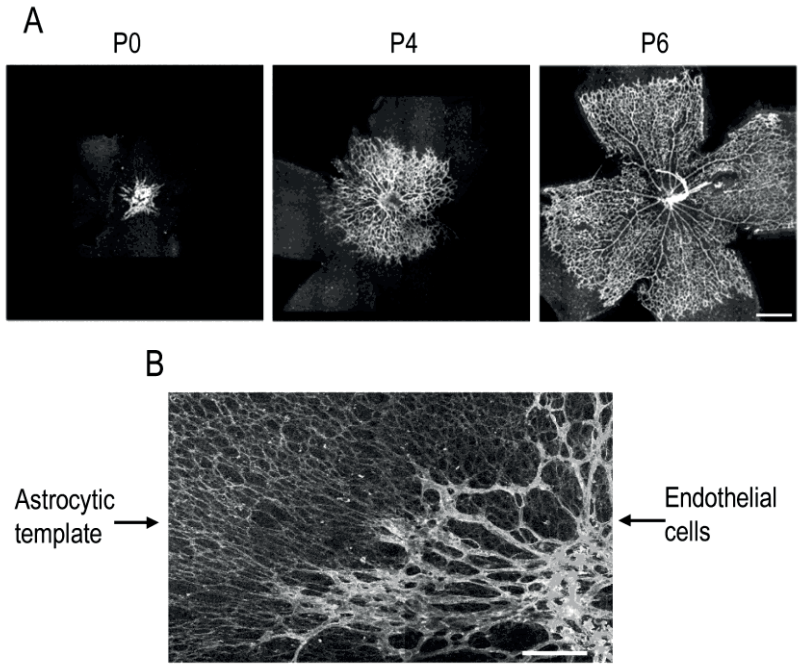

Figure 5. Development of mouse superficial retinal vascular plexus. (A) Blood vessels sprout from the optic nerve towards the periphery of the retina during the first week of development. (B) The sprouting of the vascular plexus is guided by an astrocytic template.

Vascular network remodeling occurs after the formation of the vascular plexuses. Some of the major veins in the primary plexus relocate into the deeper plexus. In contrast, all arteries remain in the primary plexus. Thus, these two plexuses differ in terms of venous drainage but share arterial supply (130). After the vascular plexuses have been established, the blood vessels are either differentiated into mature vessels or they are pruned. This occurs via EC migration, in which some ECs migrate to neighboring vessels, leading to the pruning of some capillaries and the firming of the others (131).

The development of retinal vasculature is highly dependent on retinal astrocytes, because the vascular plexus develops on top of the astrocytic template (Figure 5B). Immature astrocytes invade the retina and start to express platelet-derived growth factor receptor A (PDGFRA), which is a protein specific to retinal astrocytes (120). Interactions between neuroretina and astrocytes are needed for astrocyte maturation, especially from retinal ganglion cells, which secrete the ligand PDGFA for the astrocytic PDGFRA. These interactions guide astrocytes to proliferate and migrate towards the retinal periphery, creating a mesh-like network (132). The network of

retinal astrocytes on the ILM and NFL provides a template for the developing retinal superficial vascular plexus, and these cell types engage in interaction with each other. Astrocytes also express VEGFA due to physiological hypoxia in the avascular retina, and this is one of the growth factors that stimulates blood vessels to grow (133). In addition to astrocytes, other retinal neuronal cells influence the growth of retinal vasculature by sensing hypoxia and expressing angiogenic growth factors. VEGFA can also be produced by Müller cells, retinal ganglion cells, and photoreceptors (130,134,135). Retinal ganglion cells also produce antiangiogenic factors, controlling the vascular development and limiting the growth of the blood vessels to the NFL (136).

During angiogenesis, the sprouting front of the EC plexus consists of different kind of ECs. The ECs in the very front of the sprout are called tip cells, and they are more motile and less proliferative than the ECs located further back, called stalk cells. Tip cells are responsible for guiding the direction of growth by sensing growth factors, whereas stalk cells proliferate and thus supply ECs to form the vessel lumen (137,138). The selection of tip or stalks cells is regulated by Notch-Delta-like 4 signaling (139). After the formation of the vascular network, newly formed blood vessels mature to become stable blood vessels. This maturation process involves interactions between ECs and mural cells (SMCs and pericytes) (140). Mural cells are recruited by PDGFB, which acts as a chemoattractant expressed by ECs. Mural cells, on the other hand, express its receptor, PDGFRB (141). There are other factors that promote the EC coverage by mural cells, such as Jagged1/Notch3 signaling. The BRB controls the entry of the fluids and electrolytes into the extracellular space in the brain. The BRB consists of two parts: the inner BRB, which is made up of the retinal vascular endothelium, pericytes, and Müller glial cells and the outer part of the BRB, which consists of pigment epithelial cells in the RPE layer (9). In the inner BRB, ECs are connected to each other with tight junctions. Disruption of the BRB is common pathological condition in many human diseases. For example, DR is associated with alterations of inner BRB, whereas AMD is associated with alteration in the outer BRB.

2.4.1.1 Retinal glial cells in the retina and angiogenesis

Retinal glial cells can be divided into macroglia and microglia. Retinal macroglia are Müller cells and astrocytes, whereas retinal microglia are specialized macrophages of the central nervous system. Both Müller cells and astrocytes play an important role in the regulation of retinal angiogenesis (142,143). Müller cells enhance the EC

barrier function, by secreting various factors, such as thrombospondin-1 and pigment epithelium-derived factor (144). However, under hypoxia or inflammation, Müller cells start to express factors that enhance vascular permeability, such as VEGFA, tumor necrosis factor and MMPs (145,146). The ablation of Müller cells leads to the breakdown of the BRB and intraretinal NV (147).

Retinal microglia are immunocompetent cells of the central nervous system, and they constitute 5%–20% of the glial cell population (148). Retinal microglia regulate neuronal survival and maintain neuronal connections and functions. Microglia can be found in all layers of the developing retina, whereas in adults they are absent from the nuclear layers (149,150). Microglia play a role in retinal angiogenesis; they guide the growth of retinal vessels growth during development (125). Microglia activation is a hallmark of many pathological conditions, in which they can participate in neurodegeneration via their ability to produce proinflammatory cytokines and phagocytose neuronal cells (151). Both resident microglia and invading macrophages contribute to the pathogenesis of retinal diseases. Retinal microglia and invading macrophages can produce angiogenic factors, such as TGF-β, bFGF, MMPs, and cytokines (152). However, the mechanisms underlying the contribution of retinal microglia to retinal pathology and pathological angiogenesis need further clarification.

2.4.2 Neovascular eye diseases

Ocular NV contributes to vision loss in many ocular diseases, of which DR, wet AMD, RVO and ROP are the most prevalent among different age groups. These diseases can affect people of different age and they are the main cause of severe vision loss and legal blindness in developed countries.

2.4.2.1 Diabetic retinopathy

The prevalence of diabetes mellitus is 1 in 11 adults (425 million in the year 2017), and one of its complication is DR. DR remains a leading cause of vision loss among the working-age population in developed countries (153-155). It has been estimated that about a third of diabetic patients have signs of DR, a third of whom may have vision-threatening retinopathy (156). The incidence and severity of DR increases with time and the duration of diabetes. It is estimated that nearly all patients with type 1 diabetes have DR after 20 years of diabetes and that > 60% of patients with

type 2 diabetes have signs of retinopathy (154,157). Of type 1 diabetics, 15%-50% develop PDR and 10%-20% have diabetic macular edema (DME) (158).

The primary cause of DR is high glucose levels, which causes damage to the retinal capillaries and thereby disrupts blood flow in the capillaries. In addition to problems in carbohydrate metabolism, aberrant fat and protein metabolism contribute to DR. Among the indirect causes of causing DR are oxidative stress, formation of advanced glycation products and their receptors, and activation of protein kinase C (159-161). Early signs of DR include basement membrane thickening, pericyte loss, microaneurysm, and capillary drop out, which lead to increased vascular permeability and retinal ischemia (162). As retinal ischemia increases, DR progresses to proliferative diabetic retinopathy (PDR) (154) (Figure 6C), in which hypoxia induces retinal NV. PDR is a condition characterized by NV of the retina and vitreous. Vascular leakage in the macula causes diabetic macular edema (DME) and impairment and ultimately loss of central vision. DME can develop at any stage of DR. Central vision can also be impaired due to capillary nonperfusion. During NV, retinal vessels sprout form pre-existing ones, first within the retina (intraretinal microvascular abnormalities) but eventually towards the retinal surface and to the vitreous, becoming new abnormal blood vessels. Neovascular blood vessels leak plasma into surrounding tissue and the vitreous, causing the vitreous fluid to contract and collapse, which pulls on the retina. Because NV is attached to both the vitreous and retina, the pulling and vitreous contraction can either lead to hemorrhage, when NV shears, or if NV remains intact, can pull on the retina, leading to tractional retinal detachment, a dreaded complication of PDR (163). This can lead to severe vision loss if the macula is detached. Another cause of tractional retinal detachment is fibrosis, that is the most severe clinical feature of late-stage neovascular diseases. Fibrosis occurs when a reparative process in response to injury is not successful and fibrotic connective tissue is formed during the process. Sometimes a fibrous scar restores the functionality of the tissue, but at other times scar tissue leads to severe problems, as in ocular diseases in which scar tissue compromises vision and ultimately lead to blindness. In PDR, fibrosis results from gliosis, that is, activation and proliferation of glial cells (164). Retinal glial cells are the main participants in retinal fibrosis, because they are the equivalent of peripheral fibroblasts in the central nervous system (165).

Even though vascular changes are the main pathology observed in the disease, DR is defined as a neurovascular disorder (166). Several studies have suggested that diabetes adversely affects the entire neurosensory retina, causing neuronal apoptosis and changes in the metabolism of the supporting cells (167,168).

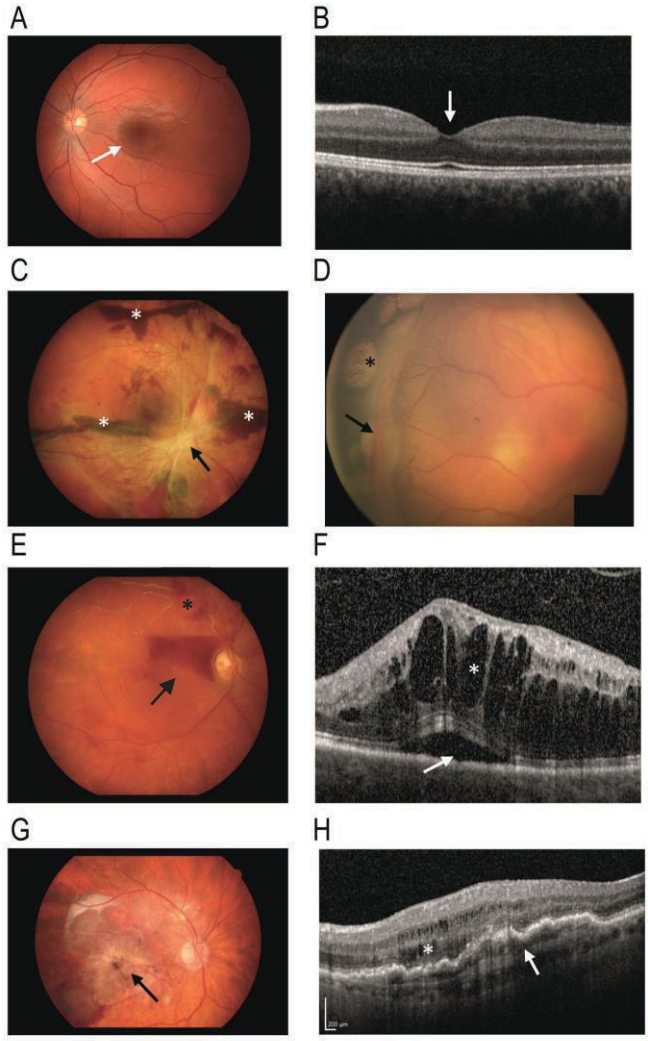

Figure 6. Fundus photographs and optical coherence tomography (OCT) images of patients with neovascular eye diseases. (A) Fundus photography of a normal eye. Arrow is pointing to the macula. (B). OCT image of normal macula. Arrow is pointing to the foveal pit in the macula. (C) Patient with severe PDR, in which NV is associated with hemorrhages (asterisks), fibrovascular proliferation (arrow), and tractional retinal detachment. (D) Fundus photography of ROP patient. Elevated ridge of fibrovascular proliferation is seen (arrow). Patient was treated with cryotherapy, and cryo scars are seen anterior to the vascularized retina (asterisk). (E) Patient with BRVO and retinal NV associated with vitreous hemorrhages (arrow). (F) OCT image of macular edema with intraretinal fluid (asterisk) and subretinal fluid (arrow) accumulation secondary to CRVO**.** (G) End-stage wet AMD with disciform scar in the macula (arrow). (H) OCT image of a wet AMD patient shows pigment epithelial detachment (arrow) and intraretinal fluid accumulation (asterisk).

2.4.2.2 Retinopathy of prematurity

ROP is a vasoproliferative retinal disorder primarily affecting prematurely born infants. It is among the leading causes of childhood blindness in Western countries (169). Between 2000 and 2012 in the United States, ROP affected 2.4% of prematurely born infants weighing over 2,500 grams and 30% of newborns with birth weight under 1,000 grams (170). Due to improved intensive care, even very small infants survive, but the most preterm infants or infants associated with neonatal morbidity (such as respiratory distress syndrome, infection, hyperglycemia etc.) with very low birth weights are at the highest risk for ROP (170,171). ROP was first described in the 1940s as a disorder in which fibrous tissue forms behind the lens, causing severe visual impairment and blindness (172).

In ROP, the pathology develops in two stages. First, the primary stage or vasoconstrictive phase occurs after preterm birth, when retinal vascular maturation slows as intravitreal VEGF levels decrease in the presence of the relatively hyperoxic ex utero environment. This is followed by the secondary stage or vasoproliferative phase, when increasing metabolic demand causes ischemia and the production of proangiogenic factors in the avascular retina. Due to increased hypoxia in the avascular retina and induction in VEGFA levels, there is dilation and tortuosity of the existing vessels and NV in the retina, which then grow towards the vitreous (173) (Figure 6D). The stages of ROP involved different degrees of vascular changes, ranging from stage 1 (a demarcation line seen between the avascular and vascular retina) to stage 5, which is full retinal detachment. The intervening stages involve NV, fibrosis, and partial retinal detachment (174).

2.4.2.3 Retinal vein occlusion

RVO represent a group of disorders that involve impaired venous return from retinal circulation. RVOs can be divided into different classes, depending on the site of the obstruction: branch retinal vein occlusion (BRVO), hemiretinal vein occlusion (HRVO), and central retinal vein occlusion (CRVO) (Figure 6E-F). Of the retinal vascular diseases causing blindness, RVO comes second after DR. The worldwide prevalence of BRVO is estimated at 0.4% and that of CRVO at 0.08%, and it was estimated that 16 million people had this condition in 2010 (175). Older age is a factor of increased risk for RVO, and individuals with RVO are at increased risk for RVO in the contralateral eye (176,177). Risk factors for RVO include hypertension, diabetes, arteriosclerosis, and glaucoma (178). The clinical features of RVO can

range from mild to severe vision-threatening complications, including macular edema, macular ischemia, NV, vitreous hemorrhage, optic neuropathy, or even retinal detachment (179).

2.4.2.4 Age-related macular degeneration

AMD is a neurodegenerative disease that affects the macula. There, dysfunction of the photoreceptor-RPE complex leads to visual impairment. AMD is the main cause of central vision loss in the developed world, affecting 10% of people over 65 years of age and more than 25% of people over 75. As life expectancy increases, the number of AMD patients rises accordingly (180).

There are two different forms of AMD: dry or nonexudative AMD and wet AMD, also called exudative or neovascular AMD (181) (Figure 6G-H). The majority of AMD patients (80%-90%) suffer from the dry form, which usually progresses slowly. However, it can also progress to a severe form of dry AMD, called geographic atrophy. In this condition, the RPE slowly degenerates, which leads to secondary photoreceptor loss.

The cause of early AMD is still largely unknown, but several risk factors, such as aging, smoking and genetic predisposition, have been identified (180,182). With aging, RPE cells' capacity to remove waste material, such as lipid deposits, is reduced. When RPE dysfunction progresses, it leads to alterations in Bruch's membrane, and the extruded materials start to accumulate between the RPE and Bruch's membrane. The hallmark of AMD is the presence of these yellow accumulations of extracellular material, called drusens, within the macula, where they disturb vision. Drusen formation can lead to various pathologies such as focal detachment of the RPE, outer retinal atrophy, and new blood vessels growing between Bruch's membrane and the retina.

The wet form of AMD affects only 10%-20% of AMD patients, but it is associated with more rapid progression, and it causes 90% of all the cases of severe vision loss related to AMD (181). In this disease, the choroidal blood vessels start to grow towards the retina and into the subretinal space, causing leakage and fibrosis. Due to the leakiness of the vessels, it causes fluid accumulation within and underneath the retina in the macula, as well as retinal hemorrhages and, ultimately, macular fibrosis and blindness.

2.4.2.5 Common pathophysiology

Common to the above-mentioned retinal diseases is excessive ocular NV caused by tissue hypoxia. Hypoxia activates the expression of HIF-1, which in turns leads to the expression of angiogenic factors like VEGFA, PDGFB, Angiopoietin 2 (ANGPT2), PGF etc. (163,183).

Retinal hypoxia upregulates many inflammatory cytokines, including VEGFA, which is the main promoter of NV and increased vascular permeability. Upregulated VEGFA levels have been reported in many diseases, such as DR, ROP, RVO and wet AMD (183-185). Other common factors that may drive angiogenesis in these diseases are ANGPT2, PGF, TGF-β and fibroblast growth factors (FGFs) (184,186-189).

A proangiogenic cytokine, ANGPT2 acts as a ligand in the ANGPT-TIE receptor system, which is a signaling system specific to ECs in blood vessels as well as lymphatic vessels (190). ANGPT2 binds to its receptor TIE2 in ECs. Increased ANGPT2 expression decreases vascular stability, leading to EC activation, vascular leakage and NV (191,192). Elevated ANGPT2 levels have been reported in wet AMD, PDR and ROP (186,193,194).

Many studies have suggested that retinal inflammation plays a role in the pathogenesis of ocular neovascular diseases, such as wet AMD. Activated microglia are present even at early stages of the disease in DR, where they cluster in the microvasculature (195,196). Hypoxia-induced upregulation of VEGFA and other factors stimulates recruitment of bone-marrow-derived cells into ischemic tissue, including monocytes/macrophages where they can contribute to NV through paracrine stimulation (197). The role of macrophages in ocular diseases is complex, because depending on macrophage phenotype, they can either stimulate or suppress NV (198-200).

In addition to angiogenic factors, other factors participate in the pathogenesis of retinal neovascular diseases. Oxidative stress due to mitochondrial dysfunction is known to exacerbate NV (201).

2.4.2.6 Therapeutic aspects

The use of anti-VEGF agents has revolutionized the treatment of neovascular eye diseases, and it has become a standard treatment for AMD, DME, and cystoid macular edema related to RVO (202). They are also commonly used in the treatment of PDR and ROP (202-205).

Currently, four VEGF inhibitors are in clinical use: aflibercept, bevacizumab, pegaptanib, and ranibizumad. The first drug to use the anti-VEGF strategy in cancer treatment was bevacizumab (Avastin), which is a humanized VEGF antibody that blocks all VEGF isoforms (202). It is also currently used in ophthalmology as an off-label drug due to its affordability (206). The first VEGF inhibitor approved for ophthalmic use was pegaptanib (Macugen), an RNA aptamer that neutralizes $VEGF_{165}$ (207). Later, a truncated variant of bevacizumab, called ranibizumab (Lucentis), entered the market. Ranibizumab is the Fab fragment of anti-VEGF antibody containing the complementary domain region of bevacizumab, followed by affinity selection using phage display (202,208).

Whereas bevacizumab and ranibizumab are anti-VEGF antibodies, aflibercept is a recombinant fusion protein consisting of portions of VEGFR1 and VEGFR2 fused to an Fc domain of human IgG, so it works as a soluble VEGF-trap (209,210). Aflibercept has a longer intravitreal half-life than conventional soluble VEGF receptors/inhibitors. In addition to VEGFA, aflibercept binds to VEGFB, PGF, and non-VEGF family member galectin-1 (211,212).

Even though the use of anti-VEGFs has represented a great breakthrough in the treatment of the neovascular eye diseases, it still has some drawbacks. Some patients treated with anti-VEGF's are nonresponders, some have poor response, and some develop loss of efficacy over time (213). The proportion of poor responders and nonresponders to anti-VEGFs varies from 7% to 50% (214,215).

The most common side effects of the ocular injection itself are intraocular inflammation (1.4% to 2.9% incidence) (uveitis) and endophthalmitis (0.016% to 0.026% incidence) (216). In rare cases, intravitreal injection can cause rhegmatogenous retinal detachment (0% to 0.67% incidence) (217). There are also potential systemic side effects, because intraocularly administered VEGF inhibitors have been found from the circulation, and systemic VEGF levels are reduced after intravitreal anti-VEGFs in patients with AMD, DME, and ROP (218-220).

There are also safety concerns associated with VEGFA/VEGFR2 targeting drugs (221,222), because cell types other than ECs are also VEGF-dependent. The usage of anti-VEGF agents has been shown to have off-target effects on retinal neurons and glial cells and in the RPE. VEGFA is expressed in several cell types in the eye, including astrocytes, ganglion cells, microglia, and RPE cells (133,223). Moreover, VEGFR2 is expressed in ganglion cells, photoreceptors, Müller cells, and the RPE (224-226).

In addition to pathological angiogenesis, VEGFA plays a major role in vascular homeostasis in normal physiological conditions. The VEGF/VEGFR2 axis

mediates the activation of several pathways, resulting in regulation of, for example, EC survival and proliferation and junctional stability (227). For this reason, therapeutics targeting only pathological angiogenesis instead of physiological angiogenesis are needed.

In addition to the above-mentioned risk factors, patients and the healthcare system still bear the burden of monthly visits when anti-VEGF injections are given as a treatment. For this reason, new, more specific, and more effective treatments with sustained effect are needed.

2.4.3 Models of retinal angiogenesis

Because mouse and human retinal vasculature resemble each other (with vascular plexuses developing in the same manner), mouse models have been used to understand human retinal vascular development. The fact that the mouse retina is avascular at the time of birth and that its vasculature starts to develop after birth provides an effective tool for investigating retinal vascular development. Animal models also provide genetic uniformity and opportunities for transgenic technology. The use of rodent models has contributed knowledge of the molecular mechanisms behind the pathologies and enabled the preclinical assessment of new potential drugs (159).

Commonly used rodent models of obesity-induced type 2 diabetes mellitus and DR are leptin receptor deficient mice (dp/dp mice) and experimentally induced diabetes through administration of β-cytotoxic drugs, such as streptozotocin (228,229). However, these models do not develop NV, which is the hallmark of PDR.

2.4.3.1 Oxygen-induced retinopathy model

The observation that exposure to high oxygen levels suppresses vascular development and causes nonperfused areas and subsequent NV in the retina led to better understanding of the development of ROP (230-232). The most common in vivo model for studying retinal NV is the oxygen-induced retinopathy (OIR) model (233). This model is widely used to study retinal neovascular diseases, because it shares many hallmarks with human ischemic retinopathies (129,234). However, the rodent models do not develop the preretinal fibrosis that is associated with the human disease. The OIR model has been widely used to test new potential

antiangiogenic factors. There are both mouse and rat OIR models. In the mouse model, the vaso-obliteration occurs in the central retina, while in the rat vaso-obliteration is peripheral, as seen in human ROP (235). The mouse model is more commonly used than the rat one, because there are more transgenic mouse than rat strains with which to study different genotypes.

In the mouse OIR model, the blood vessels in the developing mouse retina are plastic, and for this reason they undergo regression during hyperoxia stimulus (236). In the OIR model, P7 mouse pups with their nursing mothers are exposed to 75% oxygen for five days, until P12, after which they are returned to normoxic conditions (233). The model can be divided into two phases, the vessel regression phase and the proliferative/neovascular phase. In the hyperoxic first phase (P7-P12), the retinal vasculature regresses, leaving only the peripheral retina vascularized (Figure 7). Upon return to normoxia, the avascular retina becomes hypoxic, which triggers revascularization of the retina from the periphery towards the central retina. Due to excessive hypoxic stimuli, some of the retinal blood vessels start to sprout towards the vitreous, forming preretinal NV, called preretinal tufts. These neovascular tufts are immature and hyperpermeable. The NV reaches its highest point at P17 (Figure 7). In the OIR model, the pathological changes are transient. By P21-P25, the retina is fully revascularized, and preretinal NV is fully regressed. Using the OIR model, both the state of revascularization and pathological NV can be measured from retinal flat mounts (129,237). Traditionally, retinal cross sections have been used for the quantification of the amount of vascular cell nuclei extending the INL of the retinal surface to the vitreous. However, using this method, the quantification of physiological revascularization was not possible, and thereafter the use of retinal flat mounts became the most commonly used method (234).

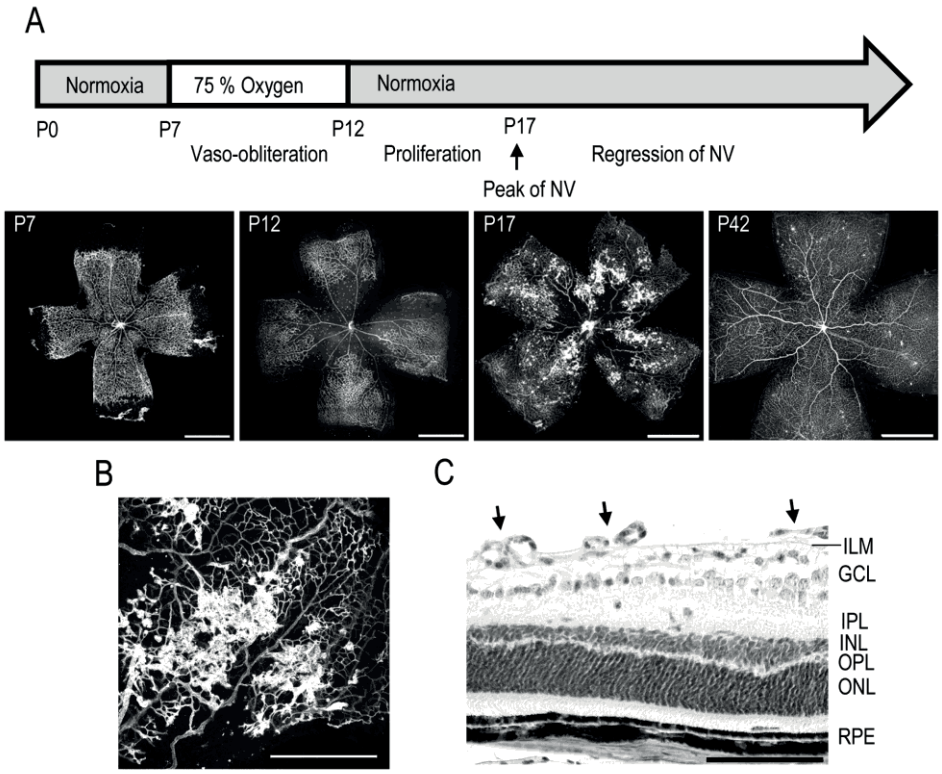

Figure 7. Mouse oxygen-induced retinopathy model. (A) Timeline of the OIR model. Induction; mice are exposed to 75% oxygen from P7 to P12 and returned to normal room air. Avascular area in the central retina (at P12) induces revascularization, and peak of preretinal NV is seen at P17. (B) Preretinal neovascular tufts form at the border between the vascular and avascular retina. (C) Retinal cross section of OIR retina at P17, where preretinal tufts are sprouting towards the vitreous. Moreover, thinning of INL and OPL layers is seen. Scale bars are 1 mm in A, 500 µm in B, and 100 µm in C.

In both mouse and rat OIR models, the severity of the disease phenotype is dependent on the strain and even vendor, suggesting that there is wide genotypic variation in the development of the pathology (238). In general, albino rodents do not develop as severe phenotype as pigmented ones. Albino BALB/c mice retinas revascularize rapidly and do not develop NV at all (239). C3H/HeJ mice that have a mutation in the retinal degeneration 1(*Rd1*) gene have thin retinas and do not develop NV (240). For these reasons, pigmented inbred C57BL/6J mice are most commonly used for OIR studies, because they develop abundant NV.

2.4.3.2 Laser-induced choroidal neovascularization model

The mouse laser-induced choroidal neovascularization (CNV) model is commonly used model to study wet AMD, and its implementation has led to a better understanding of AMD pathogenesis and has contributed to the development of many current therapies. First introduced in the late 90s using krypton laser photocoagulation, it has become the main model for studying CNV (241). This model recapitulates biological processes, such as inflammation and angiogenesis, that are involved in AMD. Main factors reported to have a key role in CNV development include VEGFA, PGF, and many proteases (242,243). Inflammatory cells, such as macrophages and neutrophils, also have a substantial impact on CNV development (199,244). In the model, the RPE and Bruch's membrane are subjected to targeted laser injury, and the defect in Bruch's membrane allows NV to grow. After a follow-up period, usually between 5 and 14 days, areas of CNV can be measured using fluorescein angiography or from choroidal flat mounts (245,246).

3 AIMS OF THE STUDY

The aim of this dissertation was to investigate the regulation of angiogenesis during retinal development and neovascular diseases and provide new information about the mechanisms of angiogenesis.

The main aims of this study were as follows:

- Investigate the role of R-Ras in the regulation of developmental and pathological angiogenesis in the mouse retina and in human PDR (Study I).
- Investigate the role of myeloid-specific furin in a mouse model of oxygen-induced retinopathy (Study II).
- Characterize factors in the development of a mouse oxygen-induced retinopathy model and human PDR using a proteomics-based approach (Study III).
- Investigate the role of SDC4 in the regulation of developmental and pathological angiogenesis (Study IV).

4 MATERIALS AND METHODS

4.1 Experimental animals and human patient samples

Three different transgenic mouse strains, R-Ras KO, myeloid-specific furin KO, SDC4 KO, and their WT control strains were used in the studies. Mice were housed at Tampere University and at the Queen Mary University of London and fed with standard laboratory pellets and water ad libitum. The genotype was determined in each animal used in the studies by PCR and the lack of the protein (R-Ras or SDC4) was confirmed by either immunoblotting or immunohistochemistry (IHC). All of these transgenic knockout mice lines reproduced normally, and no obvious abnormalities were detected in physiological conditions.

4.1.1 R-Ras knockout mice

Conventional homozygous knockout (-/-) mice deficient for R-Ras expression (R-Ras KO mice) were generated previously by an insertion of the gene-trap vector VICTR20 between exons 4 and 5 on chromosome 7 in the *Rras* gene region (OST24882) (69,247). Mice were obtained from the laboratory of Masanobu Komatsu (Sanford-Burnham Medical Research Institute at Lake Nona, Orlando, FL, USA). *Rras* heterozygous mice were backcrossed with C57BL/6 strain (Harlan Laboratories, Indianapolis, IN, USA) to obtain the R-Ras KO and WT strains in the same genetic background.

4.1.2 Myeloid-cell-specific conditional furin knockout mice

Conditional knockout mice for myeloid-cell (monocyte/macrophage)-specific deletion of furin (LysMCre-fur$^{(fl/fl)}$) were generated as described previously (249,250). To obtain the inactivation of the furin in myeloid cells, the Cre-lox recombination system was used (251). In brief, mice bearing floxed fur alleles (fur$^{fl/fl}$) were six times backcrossed with C57BL/6 mice and then bred with LysMCre mice

(on C57BL/6 background, purchased from Taconic Biosciences, Rensselaer, NY, USA) to generate myeloid-specific furin knockout mice, referred as LysMCre-fur$^{(fl/fl)}$ (Figure 8). These mice have insertion of the cre cDNA in the endogenous M lysozyme locus, creating myeloid-cell-specific gene deletion.

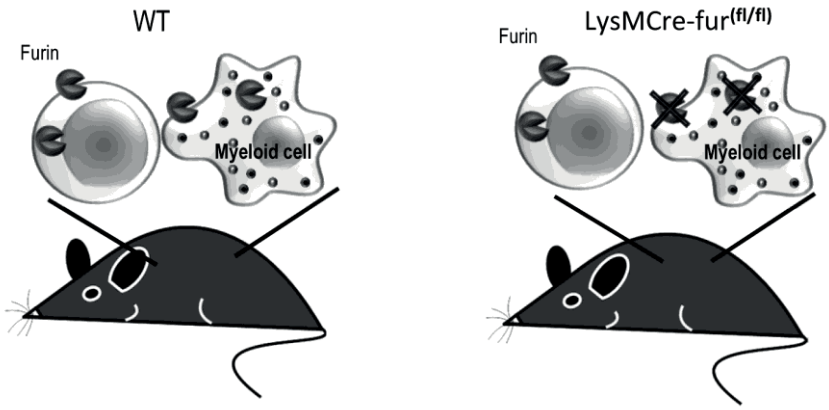

Figure 8. Myeloid-cell-specific furin knockout mouse strain. Furin is deleted from the myeloid cells, generating a conditional knockout mouse strain, LysMCre-fur$^{(fl/fl)}$. Figure is modified from Vähätupa et al. (85).

4.1.3 SDC4 knockout mice

A conventional homozygous knockout (-/-) mouse line deficient for *Sdc4* expression (*Sdc4* -/-, referred as SDC4 KO) was generated as previously described (248). Briefly, exons 2 and 3 and part of exon 4 were deleted and replaced by the neomycin resistance (*Neo*) gene. Heterozygous *Sdc4* mice were crossed to yield the knockout mice (in C57BL/6 genetic background). WT, SDC4 KO, and *Sdc4* heterozygous (+/-) mice were used in the studies.

4.1.4 Human patient samples

Preretinal fibroneovascular membranes were obtained from seven PDR patients and one RVO patient who were undergoing pars plana vitrectomy for the treatment. Altogether, eight patients (four females and four males, all Caucasians) were included in the studies (I, III, IV). At the time of pars plana, the mean age was 34 years (range,

27-56 years), and the mean duration of diabetes was 26 years (range, 21-32 years). During vitrectomy, fibrovascular membranes were isolated, grasped with vitreous forceps, and pulled out through a sclerotomy, where after samples were fixed with 10% formalin for three hours, transferred to 70% ethanol and embedded in paraffin. In Study I, control retinal tissue was obtained from eyes enucleated due to choroidal melanoma.

4.1.5 Ethical considerations

Permissions to breed the transgenic animals (R-Ras KO, LysMCre-fur$^{(fl/fl)}$), and SDC4 KO) were granted by the Laboratory Animal Centre of Tampere University. All animal experiments were performed in accordance with the protocols approved by the National Animal Ethics Committee of Finland (ESAVI/92/04.10.07/2014 and ESAVI/6421/04.10.07/2017) for ophthalmic studies in I-IV. All the animal experiments were conducted under ARVO Statement for the Use of Animals in Ophthalmic and Vision Research guidelines. The animal experiments conducted in the United Kingdom for Study IV, were approved by the UK Home Office according to the Animals Scientific Procedures Act 1986 (ASPA).

The permission to collect human samples was granted by the Pirkanmaa Hospital District review board and the Kuopio University Hospital (license number R08037). Studies involving patient samples were conducted in accordance with the Declaration of Helsinki and all patients gave written informed consent.

4.2 In vivo models

4.2.1 Two-stage skin carcinogenesis model

One commonly used model to study skin cancer development is chemically induced two-stage skin carcinogenesis model. This model provides a tool to study epithelial carcinogenesis and factors modulating it (252,253). In this model, first stage is the initiation of papilloma formation done with a low dose of a known mutagen, such as 7,12-Dimethylbenz[a]anthracene (DMBA) followed by prolonged exposure to the tumor promoter, 12-O-Tetradecanoyl phorbol-13-acetate (TPA) (254). The model provides a tool to study tumor initiation, promotion and progression as well as

specific cell biological phenomena such as angiogenesis and immune cell infiltration that contribute to tumor progression.

The two-stage skin carcinogenesis model was used in the study IV. Briefly, SDC4 KO and their WT controls were anesthetized, and the back skin of the mice was shaved. 24 h later, 50 μg carcinogen DMBA (Sigma-Aldrich, Dorset, UK) was applied in 200 μl acetone on dorsal skin. A week later, the application of 5 μg of TPA (Sigma-Aldrich) in 200 μl acetone was started and repeated twice a week for total of 19 weeks. Fur from the back skin was carefully shaved every two weeks. During the study period, papilloma formation was carefully tracked, and new papillomas (>1 mm) were calculated. The location of the papillomas was marked down to track down a specific papilloma for its size. At the end of the study trial, tissues were collected and processed for further analysis as described later.

4.2.2 Oxygen-induced retinopathy model

As described above (section 2.4.3.1), the mouse OIR model is commonly used to study ischemic proliferative retinopathies. In this dissertation, the OIR model (Figure 7) was used in Studies I-IV. Because postnatal weight gain has been shown to have an effect on the outcome of the OIR pathology (255), mice used in the study were weighed, and the similarity of pups' weights between different groups (WT and KO) was ensured. Moreover, at least three individual chamber runs with individual litters of pups were performed in each study. Briefly, mice pups and their nursing mothers were placed in 75% oxygen for five days and returned to normal room air. After the induction, retinal tissue was collected at different time points (P12, P13, P17 or P42) and processed further for either immunohistochemical, mRNA, or immunoblotting analysis.

4.2.3 Laser-induced choroidal neovascularization model

The laser-induced CNV model was used in Study IV to investigate whether SDC4 deficiency affects the formation of neovascular lesions in the model. The CNV model was also used to test the therapeutic effect of the soluble glycanated form of SDC4 (SolS4). Briefly, six week-old WT and SDC4 KO mice were anesthetized, and their pupils were dilated with 1% tropicamide and 2.5% phenylephrine. Three burns per eye were made by laser photocoagulation (680 nm; 100 μm spot diameter; 100 ms duration; 210 mW). The success of the burns was checked, and only burns that

ruptured the Bruch's membrane were included in the study. Seven days after the injury the choroidal NV areas were imaged by fundus fluorescein angiography, and the lesions were quantified using Imaris Software (Bitplane, Belfast, UK). The mice were sacrificed, and choroidal flat mounts were made, stained with lectin GS-II (Thermo Fisher Scientific, MA, USA), and imaged via confocal microscope for volumetric analysis of the lesions with Imaris Software (Bitplane). The effect of soluble SDC4 ectodomain (solS4) on the inhibition of lesion formation was tested in the CNV model. SolS4 or aflibercept (Eylea®, Regeneron Pharmaceuticals, NY, USA) was administered intravitreally after laser photocoagulation. Seven days later the size of NV lesions was measured as described above.

4.2.4 Matrigel plug assay

Matrigel plug assay is an in vivo technique to explore new blood vessel growth to a transparent gel in different conditions. Matrigel mimics the physiological matrix containing ECM proteins and growth factors and it is widely used matrix substrate to study angiogenesis in vivo and in vitro (256).

We used the Matrigel plug assay in the Study IV. Matrigel was mixed with PBS containing angiogenic growth factors (100 ng/ml VEGFA, 100 ng/ml bFGF either in combination or separately) and 20 U/ml of Heparin (Sigma-Aldrich). The gel was injected subcutaneously on the side of 6-week-old mice and 5 days later the mice were sacrificed, and the plugs were collected and imaged. Plugs were weighed and incubated overnight 4 °C with 500 µl of dH2O. For the analysis of the plug vascularity the amount of hemoglobin in the plugs was measured using Drabkin reagent kit (Sigma-Aldrich) and by spectrophotometer at 540 nm. The results were expressed by the concentration of hemoglobin/gram of plug.

4.3 Ex vivo models of angiogenesis

4.3.1 Aortic and choroid sprouting assay

The aortic ring model and choroid sprouting assay were used as an ex vivo models of angiogenesis in Study IV. The choroid sprouting assay is an ex vivo model of CNV, where explants of choroid/RPE tissue are used. In both models, the explants

are embedded in biomatrix gel like collagen I matrix and incubated with proangiogenic factors such as VEGFA (257,258).

In our study, the aortas from 6-8-week-old mice were dissected and sliced into rings of 1 mm in diameter and incubated overnight in serum-free medium (OptiMEM) at 37 °C. For choroid sprouting assay, choroids were dissected and cut into pieces (1 mm^2) and incubated with serum-free medium as described above. Both aortic ring and choroid explants were embedded in type I collagen matrix in E4 media (Invitrogen, Carlsbad, CA, USA) in a well plate. Plates were incubated 37 °C for 30 min, where after 200 µl OptiMEM with 1% FBS and VEGFA (30 ng/ml) or FGF (10 ng/ml) or both were added. Explants were incubated at 37 °C, 10% CO2 and after 1 week the angiogenic sprouts from the aortic rings and choroidal explants were counted.

4.4 In vitro methods

4.4.1 Retinal flat mounts and immunohistochemistry

To visualize retinal vasculature during development and OIR, retinal flat mounts were prepared (Studies I-IV). The mice were euthanized, and their eyes were enucleated and fixed with 4% paraformaldehyde (PFA), and the retinas were dissected under a stereomicroscope. Retinal blood vessels were labeled with Isolectin GS B4 (Thermo Fisher Scientific), and the retinas were then flat mounted and imaged via confocal microscopy (LSM 700, Carl Zeiss, Oberkochen, Germany). Additional primary antibodies were used when mural cells were visualized on the retinal flat mounts (Studies I, IV). To examine the angiogenic responses in the OIR model, avascular areas (AVAs) and the amount of NV were manually quantified using Adobe Photoshop CS (Adobe Systems, Inc., San Jose, CA, USA). For developmental angiogenesis the length of superficial vascular plexus (Studies I, II, IV) and the number of branching points and filopodia (Study III) were measured in Adobe Photoshop CS.

4.4.2 Immunohistochemistry and quantification

Retinal and skin cross sections were obtained to investigate the localization of proteins of interest. For paraffin-embedded samples, tissues were fixed with 4% PFA

and then transferred to 70% ethanol and processed with tissue processing (Tissue-Tek VIP, Sakura Finetek, Torrance, CA, USA) and paraffin embedding. Samples were cut to 4-6-µm-thick sections, and antigen retrieval was performed with either trypsin, citrate buffer (pH6), or Tris-EDTA (pH9), depending on the following primary antibodies. A list of the antibodies and detection methods used in Studies I-IV is presented in Table 1. For traditional IHC horseradish peroxidase (HRP) conjugated secondary antibody reagents were used. Hematoxylin was used as a counterstain. For frozen sections, tissues were collected and freshly embedded in ornithine carbamoyltransferase embedding compound and frozen with liquid nitrogen cooled isopentane and stored at -80 °C prior to being cut into 4-6-µm-thick sections. Sections were fixed with methanol and blocked prior to being stained with primary antibodies (Table 1). As a negative control, tissue sections from KO animals were used to check that there was no signal from KO tissue with the antibody. To check for unspecific binding of the secondary antibody, sections without the primary antibody were included.

IHC stainings with visible chromogen (3,3'-Diaminobenzidine DAB or Vina Green) were visualized via light microscope and quantifications of mouse retina and human PDR fibrovascular membranes were performed using the IHC Profiler plugin in ImageJ software (National Institutes of Health, Bethesda, MD, USA). Skin tissue sections were scanned via Aperio ScanScope CS and XT systems (Aperio Technologies Inc., CA, USA and then quantified using algorithms in ImageScope viewer (Study IV). Immunofluorescence (IF) stainings were visualized via confocal microscopy (LSM 700 or LSM 780, Carl Zeiss) (Studies I-IV). Pericyte coverage and VE-cadherin expression in retinal vasculature was quantified using BioImageXD (provided in the public domain at http://www.bioimagexd.org) (Study I).

Table 1. List of primary antibodies used in the studies. IHC-P, immunohistochemistry-paraffin section; IF-F, immunofluorescence-frozen section; IF-FM, immunofluorescence-flat mount; WB, western blot.

Antibody	Host	Clone	Manufacturer	Application	Tissue	Study
α-SMA	Mouse	1A4	Sigma-Aldrich	IF	Mouse choroid/RPE, aorta, retina, skin, muscle	IV
β-tubulin	Mouse	TUB 2.1	Sigma-Aldrich	WB	Cells	IV
CD138	Rabbit	EPR6454	Abcam	IHC-P	Mouse retina, rat gut	I
CD3	Rabbit	Polyclonal	Dako	IHC-P	Mouse skin	IV
CD31	Rat	MEC 13.3	BD Pharmingen	IHC-P, IF-F	Mouse skin, mouse retina, human PDR membrane	I- IV
CD31	Mouse	JC70A	Dako	IHC-P	Human PDR membrane	I, III, IV
F4/80	Rat	BM8	Life Technologies	IHC-P, IF-F	Mouse skin, mouse retina	II, IV
FLNA	Rabbit	EP2405Y	Abcam	IHC-P, WB	Mouse retina	III
Furin	Rabbit	Polyclonal	Santa Cruz Biotechnology	IHC-P, IF-F	Mouse retina	II
GAPDH	Goat	Polyclonal	Abcam	WB	Mouse retina,	I, III
HSA	Rabbit	Polyclonal	Lifespan Biosciences	IHC-P	Human PDR membrane	I, III
IgG	Horse	Polyclonal	Cell Signaling Technology	WB	Mouse retina	I
MYH9	Rabbit	Polyclonal	Proteintech	IHC-P, IF-F, WB	Mouse retina, human PDR membrane	III
Neutrophil elastase	Rabbit	Polyclonal	Abcam	IHC-P	Mouse skin	IV
NG2	Rabbit	Polyclonal	Millipore	IF-FM	Mouse retina	I
NG2	Guinea pig	Polyclonal	William Stallcup	IF-F	Mouse retina	I, III
R-Ras	Rabbit	Polyclonal	Cell Signaling Technology	WB, IHC-P, IF-F	Mouse retina, human PDR membrane	I
R-Ras	Rabbit	Polyclonal	Santa Cruz Biotechnology	IF-F	Mouse retina, human PDR membrane	I
SDC4	Rat	KY/8.2	BD Biosciences	IHC-P	Human PDR membrane	IV
VE-cadherin	Rabbit	Polyclonal	Abcam	IF-F	Mouse retina	I, IV
VE-cadherin	Rat	BV13	eBioscience	IF, WB	Mouse cells, skin, muscle, choroid, human cells	IV
VEGFR2	Rabbit	55B11	Cell Signaling Technology	IHC-P	Human PDR membrane	I, IV
VEGFR2	Rabbit	D5B1	Cell Signaling Technology	IF, WB	Human cells	IV
VEGFR2-p(Tyr1175)	Rabbit	D5B11	Cell Signaling Technology	WB	Cells	IV

4.4.3 Immunoblotting and densitometry

To detect the protein expression levels for R-Ras in retina (Study I) and to validate the chosen proteins from the mass spectrometry (MS) OIR study (III) and SDC4 (Study IV), western blotting (WB) was used. Retinal tissues were lysed in radioimmunoprecipitation assay (RIPA) buffer and proteins were extracted and run on 4%-12% gradient gels (NuPage, Invitrogen) and electroblotted on polyvinylidene difluoride (PVDF) membranes (Studies I, III, IV). Membranes were blocked and immunoblotted with the desired primary antibodies (Table 1) and subsequent HRP coupled secondary antibodies. Immunoblotted membranes were imaged using enhanced chemiluminescence and the ImageQuant system (GE Lifesciences, Amersham, UK). Densitometric analysis to quantify the amount of protein of interest normalized against endogenous loading control (glyceraldehyde 3-phosphate dehydrogenase, GAPDH in studies I and III) was performed using Adobe Photoshop CS (Adobe Photoshop).

4.4.4 Quantitative PCR

Quantitative polymerase chain reaction (qPCR) was used to investigate changes in *Rras* and *Sdc4* gene expression during retinal development and in the OIR model (Studies I, IV). Total RNA was extracted using an RNA isolation kit (RNeasy, Qiagen, Hilden, Germany) as described in the original publications and RNA was converted to cDNA by reverse transcription using the Thermo Maxima First Strand cDNA Synthesis Kit for RT-qPCR (Life Technologies, Ltd., Paisley, UK) according to the manufacturer's instructions. Real-time qPCR was performed using SYBR Green (Thermo Fisher Scientific) as a PCR dye and the signal was detected using a sequence detection system (ABI Prism 7000 Sequence Detection System 1.2; Applied Biosystems, Carlsbad, CA, USA) (Study I) and ABI7900HT (Applied Biosystems) (Study IV). Peptidylprolyl isomerase A (*Ppia*) was used as an endogenous reference gene in Study I, and *Gapdh* was used in Study IV. As negative controls, no-template and no-reverse transcriptase controls were included in every qPCR run. Reaction efficiencies for all the primers were tested and due to similar efficiencies, the differences in gene expression levels were quantified using the comparative Ct method (ΔΔCt method) (259).

4.4.5 Vascular permeability assay

Vascular permeability in WT and R-Ras KO retinas in healthy and OIR model animals were quantified using the Miles assay as described previously (260). In this method, Evans Blue dye (2% in PBS, 7.5 µl/g; Sigma-Aldrich) was injected intraperitoneally and allowed to circulate (1h or 24h), enabling Evans Blue to bind to plasma albumin. Mice were sacrificed at P17, and blood samples and retinas were collected. Samples were incubated in N, N-dimethylformamide (Sigma-Aldrich) overnight at 78 °C and centrifuged, and the absorbance for Evans Blue was measured from the supernatants at 620 nm as described previously (Study I). The concentration of Evans Blue in the retina was normalized by weight of the tissue and Evans Blue concentration in the plasma (261). Miles assay were also used to measure leakage in WT and SDC4 KO animals by injecting Evans Blue dye (0.5% in PBS, 5 µl/g) intravitreally, and the dorsal skin of the mice was then injected with either PBS, PBS containing VEGFA (100 ng) or Bradykinin (100 µg), which is a known vasodilator and inflammatory mediator (262). After 90 minutes, mice were sacrificed, patches of dorsal skin were collected and incubated in formamide at 56 °C for 24 hours, and the amount of accumulated Evans Blue was quantified from the supernatants by spectrometry at 620 nm as described previously (Study IV).

4.4.6 Mass spectrometry and proteomic analysis

In recent years, MS has been widely used to study different biological samples, because it can be used to detect and quantify the majority of the proteins in a given sample, and changes in cellular functions and metabolism can therefore be detected more reliably. Proteomics and MS is a widely used method for gaining unbiased information about the changes in protein expression during development and disease (263). A recently developed MS method, sequential window acquisition of all theoretical fragment ion spectra (SWATH), combines data-independent acquisition (DIA) with targeted data extraction (264,265). For biomarker studies, SWATH-MS has been shown to be more sensitive, reliable, and repeatable compared to other MS methods such as isobaric tags for relative and absolute quantification (iTRAG) (266,267).

The retina is a complex tissue with several cell types and besides angiogenic changes, damage in other retinal cell types has also been reported in OIR (268,269). For this reason, it is important to study the OIR pathogenesis from the whole retina simultaneously. In recent years, studies have utilized different MS methods (iTRAG

and the ion-current-based MS1 quantification approach) in the study of OIR pathogenesis (270,271). In this dissertation, MS-based proteomic profiling was conducted to gain more information about OIR pathogenesis (Study III). Proteomic profiling of the OIR model and normoxic control retinas was performed with SWATH-MS proteomics, extending the throughput of proteins that can be targeted and data completeness compared to other proteomic methods (267). For the study retinas from OIR and normoxic control mice were collected at P13 (early hypoxic phase), P17 (late hypoxic phase and peak of NV) and P42 (after vascular recovery) as indicated in the study outline (Study III/Figure 1). Sample preparation, including protein extraction, reduction, alkylation, and tryptic digestion, is described in the article (III, supplementary methods). For the MS analysis, a 4-μg sample (two replicates) was analyzed by Nano-RPLC- TripleTOF instrumentation using Eksigent 425 NanoLC coupled to a high speed TripleTOF™ 5600+ mass spectometer (Sciex, Concord, Canada). 30 kDa molecular weight cut-off (MWCO) centrifugal devices were used. From the retinal samples, a relative protein quantification library for SWATH analysis was created by the information dependent-acquisition (IDA) method, consisting of > 3,500 retinal proteins. Protein identification and relative quantification were performed using the SWATH method (272). Proteins with significant or interesting findings in the data analysis were subjected to manual inspection of peptides. Quantified protein levels were log2 transformed, and the geometric means of replicate MS analyses were taken, and the quality was analyzed.

4.4.7 FANTOM and microarray analysis of furin expression

Published data from genome-wide expression studies were used to evaluate the expression of furin in the retina using the wide-searching FANTOM project and the retinal-cell-specific E-GEOD-33089 experiment. The FANTOM project has performed genome wide gene expression analysis of human samples, 1,839 samples from 573 primary cells, 250 cell lines and 152 tissues. Briefly, the data come from cap analysis gene expression sequencing of cDNA (273). The expression values for furin in relevant cell types were extracted, including ECs, pericytes, astrocytes, RPE cells, neurons, neutrophils, endothelial progenitor cells, corneal epithelial cells and monocyte derived macrophages (Study II). Mouse retinal-cell-specific microarray analysis (E-GEOD-33089) was performed previously (274) and stored on the ArrayExpress database (https://www.ebi.ac.uk/arrayexpress/experiments/E-GEOD-33089). From this data, the expression values for furin were extracted for

155 samples across seven cell-type groups: amacrine, cone, rod, bipolar, horizontal, ganglion, and microglia (274). For our study (II) supercomputer resources provided by the CSC-IT Center for Science of the Finnish Ministry of Education and Culture was used to process the raw data from the FANTOM and the microarray analyses as described previously (275).

4.4.8 Statistical analyses

The normality of the data was checked using the D'Agostino-Pearson omnibus test or the Shapiro-Wilk normality test. Levene's test was used to check the equality of variances. Based on this, the difference between two groups was determined using a two-tailed Student's *t-test* for normally distributed data and the Mann-Whitney U test for nonparametric data. Parametric one- or two-way ANOVA, followed by the Tukey/Bonferroni post hoc-test, was used to compare the average of three or more groups. Survival plot data were analyzed by a log-rank (Mantel-Cox) test, and non-normally distributed time course data were analyzed by nonlinear regression (negative binominal regression analysis, Study IV). To test the correlation between variables, either Spearman's rank correlation test (Study I) or multiple linear regression analysis, was conducted (Study IV). The significance threshold (α) was set to 0.05; thus $p < 0.05$ was considered statistically significant. *$p < 0.05$; **$p < 0.01$; ***$p < 0.001$.

To analyze differences between control and OIR retinas in the proteomics study (III), a two-sample t-test was used, and Levene's test was performed for the statistically significant proteins. If the Levene's test was significant, the nonparametric Mann-Whitney U test/Wilcoxon rank sum test was used to check the statistical significance. To account for multiple testing, the Benjamini-Hochberg adjustment was used. Principal component analysis (PCA) was used to cluster the samples based on the proteomic profiles. Statistical analysis was conducted using R software version 3.2.3 (R Core Team, Foundation for Statistical Computing, Vienna, Austria) and IPA software (IPA; QIAGEN, Redwood City, CA, USA). The majority of the statistical analysis was conducted using IBM SPSS Statistics (IBM, Amonk, NY, USA) and GraphPad Prism 6.01 (GraphPad Software, San Diego, CA, USA). STATA 13 (StataCorp LP, College Station, Texas, USA) software was used for nonlinear regression analysis.

5 SUMMARY OF THE RESULTS

5.1 R-Ras regulates vascular permeability in retinopathy

R-Ras is a known regulator of vascular permeability in several in vivo models, and it has been shown to inhibit EC sprouting in tumors. We examined the role of R-Ras in mouse retinal angiogenesis and human PDR.

First, the R-Ras expression pattern during retinal development and in the OIR model was determined. The expression of *Rras* peaked during developmental angiogenesis at P17 in both mRNA and protein level (Study I/Suppl. Figure 1). In the OIR model, the expression of R-Ras was first reduced during the hyperoxic phase at P12 and then induced during the hypoxic phase at P17. This indicated that R-Ras could play a role in the OIR model pathogenesis.

Using immunohistochemistry, we showed that R-Ras is expressed in the blood vessels of the normal mouse retina and in the blood vessels in the inner retina in OIR. However, its expression was reduced in the preretinal neovascular tufts in the OIR model (Study I/Figure 2) and in the vasculature of human PDR patients (Study I/Figure 6).

Using R-Ras KO mice, the effect of R-Ras on normal retinal developmental angiogenesis and on revascularization and NV in the OIR model was determined. R-Ras deficiency did not affect the formation of the superficial vascular plexus during early retinal development (Study I/Suppl. Figure 3). WT and R-Ras KO mice were subjected to the OIR model, and retinal revascularization and preretinal NV was quantified. R-Ras deficiency did not have an effect on either of these parameters (Study I/Figure 3). However, there was threefold increase in the leakage of OIR model retinas in the R-Ras KO compared to WT (Study I/Figure 4). Because pericyte coverage around the ECs is important for vascular integrity, especially in retinal blood vessels, we investigated the pericyte coverage in OIR in WT and R-Ras KO retinas. The pericyte coverage was found to be reduced in R-Ras KO blood vessels by 40% compared to WT animals (Study I/Figure 5). Because it is known that R-Ras stabilizes adherens junctions by modulating VE-cadherin dynamics, we quantified VE-cadherin expression in OIR model blood vessels. Both the intensity of VE-cadherin expression and co-localization with CD31 positive ECs were

reduced in R-Ras KO mice (Study I/Figure 5), which can result in increased leakiness.

Because VE-cadherin is important for vascular permeability, we stained human PDR samples for VE-cadherin and determined that the leakiest samples exhibited the most aberrant pattern of VE-cadherin expression (Figure 9). Double-staining of the human PDR samples with CD31/VEGFR2 and R-Ras and staining of adjacent section with human serum albumin (HSA) revealed that there is a negative correlation between R-Ras and VEGFR2 expression (Study I/Figure 6). The leakiest samples (based on HSA staining) had more R-Ras negative blood vessels, indicating that the blood vessels are leaky due to the lack of R-Ras.

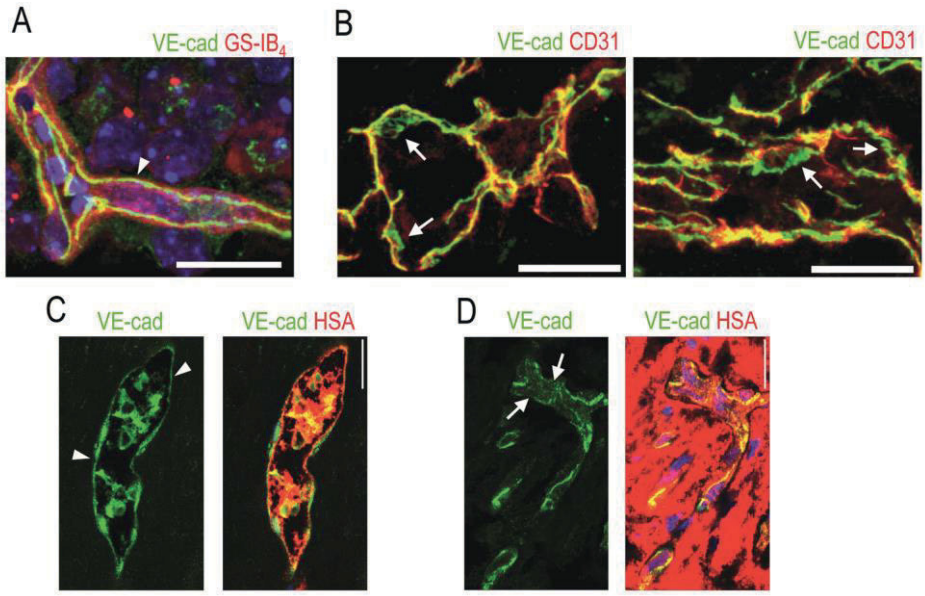

Figure 9. VE-cadherin expression in human PDR. (A) VE-cadherin (arrowhead, green) exhibits uniform expression in healthy mouse retina ECs (red). (B) VE-cadherin expression is aberrant in the vasculature of human PDR samples, (arrow). (C) In blood vessels where normal or continuous (arrowhead) VE-cadherin expression is seen, human serum albumin (HSA, red) is seen inside the blood vessels. (D) In the areas of discontinuous or absent VE-cadherin (arrows), HSA is seen around the blood vessels, indicating leakage. Unpublished data. Scale bar is 200 µm.

5.2 Furin deficiency leads to attenuated revascularization

The role of myeloid-cell-derived furin on retinal angiogenesis was examined using myeloid-cell-specific furin KO mice (LysMCre-fur$^{(fl/fl)}$) during developmental angiogenesis and in the OIR model. Using the FANTOM analysis of furin expression, we showed that furin is most abundantly expressed in monocyte-derived macrophages (Study II/Figure 1A), and using the retinal-cell-specific microarray, the highest expression was found in the microglia (Study II/Figure 1B). Furin expression in the mouse retina during development and in the OIR model was investigated using IHC.

IHC stainings from the mouse retina during development and in OIR showed that furin is weakly expressed during early development (P4) but that its expression increases when the retina matures (Study II/Figure 1). We did not detect any effect of myeloid-specific furin on early developmental retinal angiogenesis, because the length of the vascular plexus, amount of branching points, and filopodia counts were similar between WT and LysMCre-fur$^{(fl/fl)}$ mice (Study II/Figure 2A-E).

Furin expression was detected in OIR model retinas, and with double IF its expression was localized to retinal ECs and macrophages/microglia surrounding the blood vessels (Study II/Figure 1E-H). Furin deficiency from myeloid cells led to attenuated retinal revascularization without an increase in retinal NV in the OIR model (Study II/Figure 2H-K). These results indicate that myeloid-cell-derived furin has an effect on pathological angiogenesis, but not on physiological angiogenesis.

5.3 Proteomics-based approach reveals potential therapeutic targets

Using the SWATH-MS full proteome-based approach, we investigated the pathogenesis of the mouse OIR model (Study III). Three time points in OIR were chosen: P13 as an early hypoxic phase, P17 as a late hypoxic phase and peak of the NV, and P42, a time point when retinal vasculature has recovered on a microscopic level from the hypoxic insult.

Overall, we were able to quantify almost 3000 unique proteins and their expression levels during the OIR pathogenesis and in normal controls. First, we examined the overall distribution of the proteins in the samples with PCA. This analysis revealed that the strongest cause for the differences in the protein expression levels appears to be the developmental stage of the retina (Figure 10A). Volcano plot

analysis showed that there is a group of proteins that is most upregulated at P13 OIR compared to their controls. This outstanding group of proteins are crystallins, including members from all three families: α, β, and γ crystallins (Figure 10B).

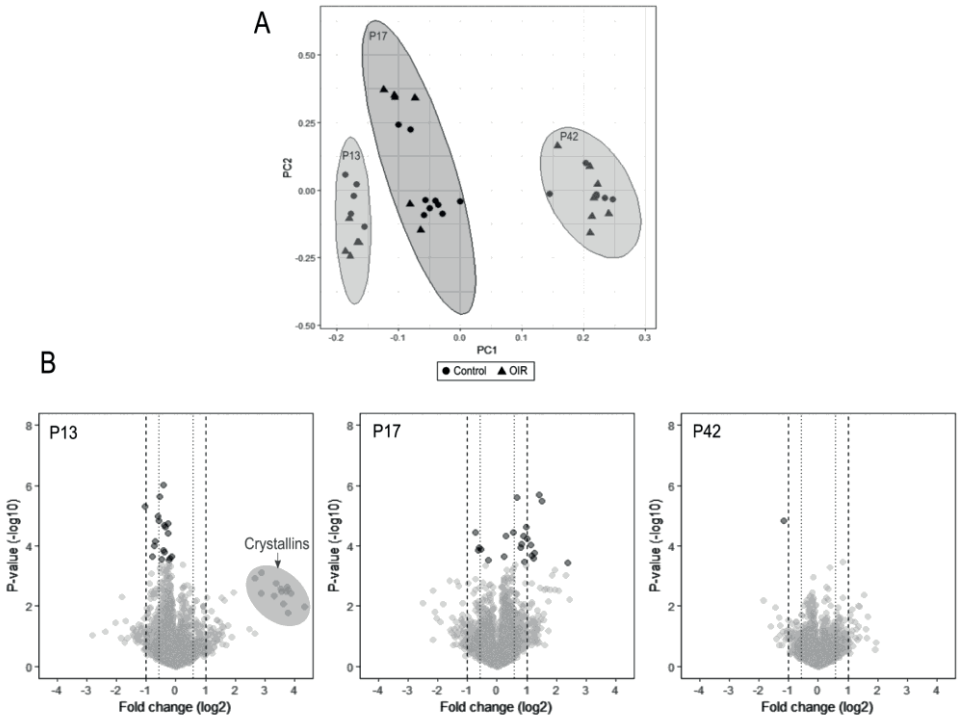

Figure 10. Visualization of protein expression during retinal development and in the OIR model. (A) Principal component analysis shows that retinal proteins cluster based on the developmental stage of the retina. (B) Volcano plots of the differential expression analysis in each time point. Log2 fold change is on the x-axis and *p*-value is on the y-axis. Most down- or upregulated proteins in OIR are separated in the top-left and -right corners. A group of proteins, crystallins, separate at P13. Figure is modified from Study III, Figures 2 and 3.

When comparing OIR-induced retinas to their controls at each time point, there were 364 differently expressed proteins at P13, 387 at P17, and 104 at P42, prior *p*-value adjustment. When the error resulting from multiple testing was taken into consideration and the *p*-value adjustment was completed, the number of statistically significant (adjusted *p*-value <0.05) proteins reduced to 17 at P13, 22 at P17, and none at P42. Based on the fold change alone, the most upregulated proteins at P17 were vitamin-D-binding protein (GC), Fetuin-A (AHSG), and α-1-antitrypsin 1-4 (SERPINA1D), from which AHSG reached statistical significance after *p*-value

adjustment as well. (Study III/Figure 4). At the peak of angiogenesis (at P17), after *p*-value adjustment, the most upregulated proteins in OIR compared to normoxic controls were AHSG, annexin A2 (ANXA2), transgelin-2 (TAGLN2), cell surface glycoprotein MUC18 (MCAM), tropomyosin a-4 chain, filamin-B (FLNB), protein SON, coproporphyrinogen-III oxidase 1 (GPX1), vinculin (VCL), myosin 9 (MYH9), serpin H1, filamin-A (FLNA), moesin, and annexin A6 (ANXA6) (Study III/Figures 4B, 5).

To validate the results obtained using with the MS proteomics, we chose FLNA and MYH9 (upregulated at P17 OIR) for immunoblotting. Densitometric analysis and using antibody against C-terminal FLNA showed a 4.6-fold increase in total FLNA at P17 OIR compared to P17. In hypoxia, FLNA is cleaved, and approximately 90 kDa C-terminal fragment is created (276). The increase in C-terminal FLNA ($FLNA_{CT}$) was 14-fold. (Figure 11). Another protein we validated by immunoblotting was MYH9, which exhibited a 9.6-fold increase in its protein level at P17 OIR compared to the controls. To further determine the localization of FLNA and MYH9 in the retina, we performed IHC and IF stainings, showing that both are strongly expressed in the retinal vasculature and that the expression is increased at P17 OIR (Figure 11A and 12A).

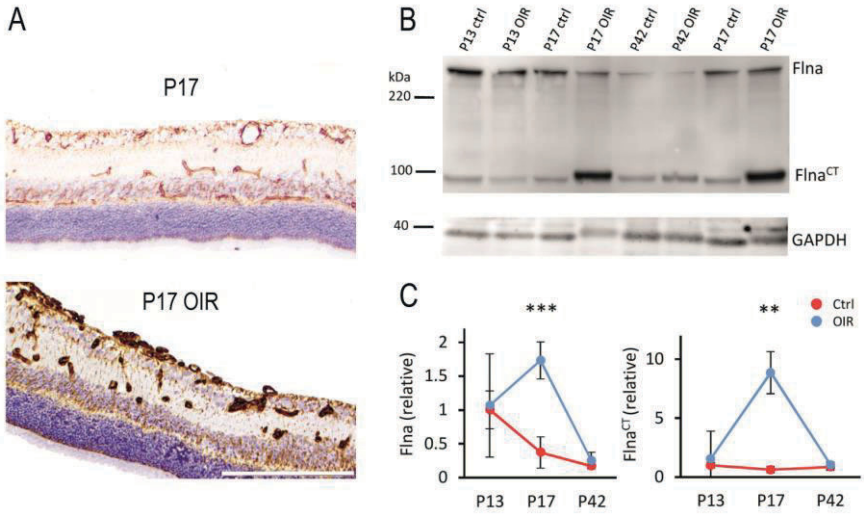

Figure 11. Filamin A upregulation in OIR retinal blood vessels. (A) Retinal sections stained for FLNA (brown) show induction of FLNA in retinal blood vessels in OIR. (B) Western blot of control and OIR retinas at different time points shows increase of cleaved FLNA fragment, $FLNA_{CT}$ in OIR at P17. (C) Quantification of total FLNA and $FLNA_{CT}$ in control and OIR retinas. Scale bar is 200 µm. Figure modified from Study III Figure 5.

To determine whether these results are relevant in the case of human disease, fibrovascular membranes obtained from patients with PDR and RVO were obtained and stained for CD31, MYH9, and HSA. These IHC stainings showed that strong MYH9 staining in and outside the blood vessels correlated with HSA leakage to the surrounding tissue (Figure 12B and Study III/Figure 7A). Some samples also exhibited regional correlation with the MYH9 and HSA expression, indicating that strong MYH9 expression in the tissue could lead to increased vascular leakage, shown by HSA accumulation in the tissue (Study III/Figure 7B).

To determine which pathways or biological functions are potentially upregulated in the OIR model, ingenuity pathway analysis (IPA) was conducted with the differentially expressed proteins. The top canonical pathways linked to differentially expressed proteins at P13 OIR proteins were phototransduction pathway, protein kinase A signaling and glutamine biosynthesis. At P17, the top pathways were actin cytoskeleton signaling (activation score 2.1), ILK signaling (activation score -1) and glutamine biosynthesis. Necrosis and cell death were reduced while angiogenesis was increased, based on the disease and biological function enrichments. Proteins linked to increased angiogenesis at P17 were ANXA2, FLNA, FLNB, GPX1, MCAM, MYH9, and serpin H1. Upregulation of TAGLN2, VCL, MCAM, FLNB, PFKP, MYH9 and FLNA was linked to cell-cell adhesion (Amigo2).

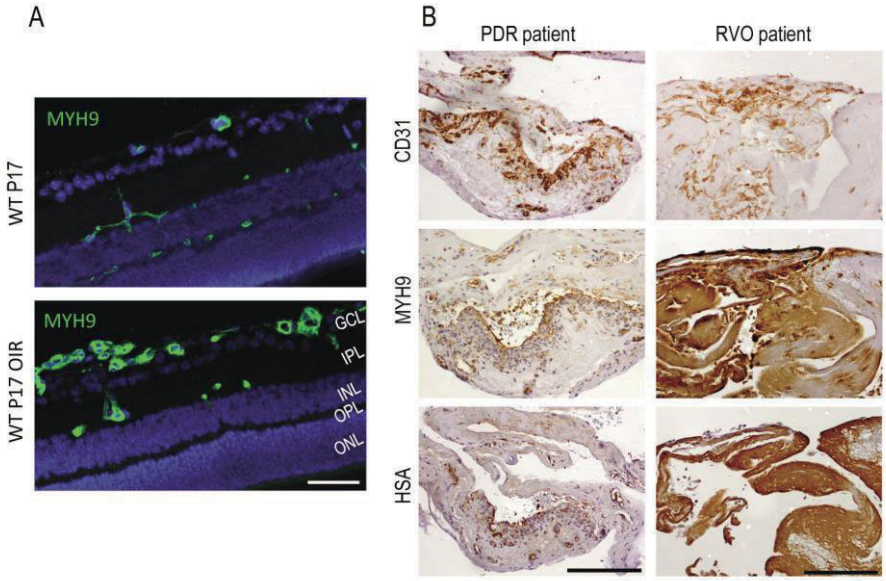

Figure 12. Myosin 9 is expressed in OIR retinas and human PDR and RVO fibrovascular membranes. (A) Mouse retinal sections stained for MYH9 (green) exhibit increased expression in the blood vessels in OIR retinas. (B) The blood vessels (CD31) had HSA restricted inside the blood vessels when MYH9 expression was low. Strong MYH9 expression is associated with strong HSA accumulation throughout the sample in fibrotic RVO sample. In PDR samples with low MYH9 expression in the blood vessels (CD31) had HSA restricted inside the blood vessels. In fibrotic RVO sample strong MYH9 expression together with strong HSA accumulation throughout the sample was seen. Scale bar is 50 µm in A and 200 µm in B. Figure modified from Study III, Figures 6 and 7.

Upstream regulator analysis suggested TGF-β1, MAP kinase interacting serine/threonine-protein kinase 1 (MKNK1), and MKL/myocardin-like protein 2 (MKL2) as potential angiogenic enhancers in the OIR model (Study III, Supplementary Table 4).

Because there were no statistically significant proteins between control and OIR at P42 after p-value adjustment, IPA analysis was performed with proteins (p <0.05 before p-value adjustment. Neurotransmission was decreased at P42 OIR, and KEGG pathway analysis specified the changes in the synaptic vesicle cycle (Study III/Supplementary Figure 4).

5.4 SDC4 deficiency leads to impaired tumor angiogenesis

The role of SDC4 in tumor incidence and size were studied using the two-stage skin carcinogenesis model (DMBA-TPA model). WT animals had on average 2.4 times more tumors than SDC4 KO mice and their tumors were larger (Study IV/ Figure 1A-D). Staining of the papilloma sections with an EC marker CD31 revealed that the blood vessels were narrower in SDC4 KO in the papillomas (Study IV/Figure 1E-F), which suggests that the tumor vessel formation is affected by SDC4 deficiency. Tumor cell implantation model was used to study the phenotype further. B16F1 melanoma cells expressing SDC4 were injected into WT and SDC4 KO mice. After two weeks both tumor volume and weight were reduced in SDC4 KO mice (Study IV/Figures 1G-H and Suppl. Figure 1B). Immunohistochemical analysis of the tumors showed well-defined lumens in the WT tumor vasculature, the ECs failed to form tubules in the SDC4 KO mice (Study IV/Figure 1I-J).

Since the DMBA-TPA model is an inflammation driven model, the infiltration of inflammatory cells (macrophages, T cells and neutrophils) were analyzed from skin sections of WT and SDC4 KO animals and no differences were seen (Suppl. Figure 3A-F). No differences between WT and SDC4 KO mice were seen in the number of natural killer cells, B cells, T cells, monocytes or neutrophils in the immune infiltrates from B16F1 tumors (Study IV/Figures 1K-L and Suppl. Figure 2A-B). These results suggest that that reduced tumor growth is primarily due to defective tumor vascularization in SDC4 KO mice.

5.5 SDC4 is needed for ocular neovascularization

The role of SDC4 in developmental and pathological angiogenesis was examined using several in vivo and ex vivo models, including mouse OIR and CNV models, the Matrigel plug assay, the aortic ring model, and the choroid explant assay (Study IV). The levels of syndecan family members during retinal vascular development and in the OIR model were measured. The qPCR results showed that the levels of *Sdc1* and *Sdc3* were altered during retinal development, whereas *Sdc4* and *Sdc2* levels remained constant from P0 to P7 (Study IV/Figure 2G). However, *Sdc4* levels peaked (2 times compared to normoxic controls) in the OIR model at P17, while the levels of other syndecans remained constant, indicating that SDC4 could play a role in pathological retinal NV. In line with this finding, SDC4 is also the predominant syndecan expressed by lymphatic ECs in pathological lymphangiogenesis (277).

SDC4 did not play a role in developmental angiogenesis quantified by the extension of retinal vasculature at P6 (Study IV/Suppl. Figure 5). Only minor reduction in the vascular density and vascular area coverage was observed in the SDC4 KO retinal superficial vascular plexus, but no other vascular abnormalities were seen in SDC4 during development.

In the OIR model, SDC4 KO mice exhibited significantly less NV (~40% reduction) and slightly enhanced retinal revascularization (~22% smaller AVAs) compared to WT (Figure 13A and Study IV/Figures 2A-B, Suppl. Figure 6). Similar results of reduced angiogenesis were evident in the mouse CNV model, which is a model mimicking many features of wet AMD. In this model, the volume of laser-induced choroidal NV lesions was greatly reduced in SDC4 KO mice (~80%) compared to WT controls (Figure 13B, Study IV/Figure 2C-F). Overall, these results indicate that SDC4 plays a critical role in pathological ocular angiogenesis but not in developmental angiogenesis.

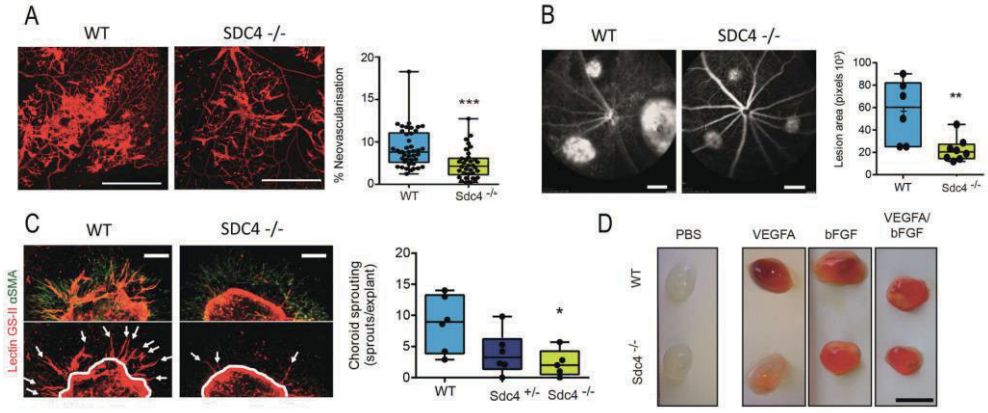

Figure 13. SDC4 deficiency leads to reduced VEGFA induced pathological angiogenesis. (A) Preretinal NV was decreased in SDC4 KO (*Sdc4 -/-*) retinas in the OIR model at P17. (B). Lesions at day 7 post laser-induced CNV model are significantly smaller in SDC4 KO than in WT mice, as seen in fundus fluorescein angiogram images. (C) VEGFA-induced angiogenic sprouting in the choroid explant model exhibits reduced sprouting in SDC4 KO explants. (D) Matrigel plugs supplemented with PBS or VEGFA were injected in WT and SDC4 KO mice. Plug vascularity was significantly impaired in SDC4 KO plugs in the VEGFA environment. Scale bar is 500 µm in A, 2.4 mm in B, 10 µm in C and 1 cm in D. Figure modified from Study IV, Figures 2 and 3.

In addition, we showed that SDC4 was expressed in the blood vessels of fibroneovascular membranes collected from PDR patients. More importantly, SDC4 expression levels correlated with the levels of VEGFR2 (a marked for immature

pathological neovessels); areas with strong VEGFR2 expression level had strong SDC4 expression, whereas areas with low VEGFR2 levels showed low levels of SDC4 (Study IV/Figures 3A-C).

Because VEGFA is a major angiogenic driver in the studied in vivo models, we investigated if responsiveness for VEGFA is SDC4 dependent. Ex vivo model of CNV and an aortic ring model of angiogenesis were used, and similar results with limited angiogenic sprouting in SDC4 KO tissues were seen (Figure 13C, Study IV/Figure 3F-H). Matrigel containing VEGFA was injected to WT and SDC4 KO mice and this triggered angiogenic response in WT but not in SDC4 KO mice (Figure 13D & Study IV/Figure 3D-E). These data suggest that the responsiveness to VEGFA is abrogated in SDC4 KO mice.

5.6 SDC4 plays a role in VEGFA induced VE-cadherin trafficking

We hypothesized that endothelial SDC4 could regulate VEGFA-dependent EC migration, so EC migration was analyzed with a scratch assay. The migratory response of SDC4 KO lung EC was disturbed in VEGFA supplied environment, whereas it was normal in growth factor rich environment (Study IV, Figure 4A-B).

To investigate changes in the endothelium and the integrity of the EC junctions we measured vascular permeability induced by VEGFA or Bradykinin (a known vasodilator) using the Miles assay in WT and SDC4 KO mice. VEGFA-mediated vascular permeability was reduced in SDC4 KO animals compared to WT, whereas Bradykinin had a similar effect on both groups (Study IV/Figure 4C-D). The hypothesis that SDC4 might regulate VEGFA induced VE-cadherin trafficking was tested in an antibody-feeding experiment, where ECs from SDC4 KO mice showed reduced VE-cadherin internalization after VEGFA exposure (Study IV, Figure 4E-F). Similarly, neovascular blood vessels in the OIR model in SDC4 KO animals showed more continuous VE-cadherin staining, whereas in the blood vessels of WT animals, the staining pattern of VE-cadherin was more discontinuous and exhibited abundant intracellular VE-cadherin vesicles (Study IV, Figure 4G).

To test the diminished responsiveness to VEGFA in SDC4 KO we looked at the phosphorylation status of VEGFR2, its downstream kinases (SRC and ERK) and VE-cadherin. No differences were detected in their phosphorylation status after VEGFA stimulation of WT and SDC4 KO primary lung ECs (Study IV, Figure 4H).

There was no difference in the cell-surface levels of VEGFR2 between the ECs of WT and SDC4 KO animals (Study IV, Figure 4I).

Due to these results, we examined the pathways downstream of VEGFA/VEGFR2. Fluorescence recovery after photo-bleaching technique was used to measure the kinetics of diffusion of a junctional SDC-4-eGFP. Recovery of eGFP-SDC4 fluorescence was enhanced after addition of VEGFA, supporting the hypothesis that SDC4 is acting downstream of VEGFA and possibly involved in trafficking (Study IV/Figure 5E-F). Previously reported SDC4 phosphorylation at Y^{180} regulating integrin recycling in fibroblasts (278) led us to test whether phosphorylation of this residue is important for the VEGFA stimulated response observed with SDC4-eGFP. We used a mutant non-phosphorylatable form of eGFP-SDC4 (SDC4(Y/A)-eGFP) and showed that the fluorescence recovery of this form was more rabid in basal conditions and VEGFA stimulation had no effect on this (Study IV/Figure 5D-F). This suggests that the non-phosphorytable form of SDC4 is not complexed with any other molecule as it recovers more rapidly, indicating that the complex involving SDC4 requires phosphorylation of SDC4 at Y^{180}.

To identify potential binding partners with SDC4, we first studied if there is an interaction between SDC4 and VE-cadherin. Interaction with these molecules was detected under basal conditions using proximity ligation assay, but the interaction declined after VEGFA stimulation and recovered later (Study IV/Figure 6A-C). Further analysis using HUVECs expressing SDC4 conjugated to eGFP or a mutated non-phosphorylatable form of SDC4 (SDC4(Y/A)-eGFP), we saw a marked decrease in cell surface VE-cadherin after VEGFA treatment in SDC4-eGFP but not in cells transfected with the non-phosphorylatable form of SDC4 (Study IV/Figure 6D). In addition, we saw an increase in intracellular VE-cadherin positive vesicles after VEGFA stimulation in SDC4-eGFP transfected cells but not with SDC4(Y/A)-eGFP transfected cells (Study IV/Figure 6E-G).

5.7 Soluble SDC4 reduces VE-cadherin internalization and NV

Finally, the therapeutic potential of soluble glycanated form of SDC4 (solS4) to act as competitive inhibitor towards endogenous membrane-bound SDC4 was studied. We hypothesized that solS4 would interfere the proangiogenic role of SDC4 by disrupting the SDC4/VE-cadherin interaction. We found that VEGFA-driven VE-cadherin internalization was prevented by solS4 (Study IV/Figure 7A-B) and that it

also prevented VEGFA-induced cell migration (Study IV/Figure 7D). Notably, and in contrast, the cells treated with soluble SDC2 (solS2) maintained the responsiveness to VEGFA (Study IV/Figure 7D). Importantly, solS4 treatment bypassed early VEGFA-driven events, since the signaling kinases immediately downstream to VEGFR2 activation (SRC, ERK and AKT) were not impacted (Study IV, Figures 7E and Suppl. Figure 10), suggesting that solS4 interferes directly with VE-cadherin internalization.

We treated ex vivo aortic explants with solS4 and saw reduced sprouting (Study IV/Figure 7F-G). Lastly, the efficacy of solS4 was tested in the CNV model in comparison with aflibercept (Eylea®, Regeneron), and we found that single injection of 100 ng of solS4 reduced NV by 50% compared to PBS control and was similar in efficacy than aflibercept (Study IV/Figure 7H-I). To conclude, solS4 inhibits VE-cadherin internalization, EC migration and NV in the mouse CNV model.

6 DISCUSSION

6.1 R-Ras, furin and SDC4 in developmental retinal angiogenesis

Because the developing mouse retina provides a great tool for studying developmental angiogenesis, the roles of R-Ras, myeloid-specific furin and SDC4 in physiological angiogenesis were investigated. We showed that there is a peak in R-Ras expression in normal retina at P17, which is the time point at which vascular plexuses have formed. This is in line with previous studies showing that R-Ras expression is the strongest in quiescent, mature blood vessels during cell differentiation (69). Consistent with this presumption, there were no differences in the rate of early retinal vascular development between WT and R-Ras KO animals.

The impact of myeloid-specific furin on developmental retinal angiogenesis was examined, because it was previously reported that total depletion of resident retinal macrophages slows down the development of the superficial vascular plexus (152). However, the depletion of furin in myeloid cells did not have an effect on neonatal retinal vascular development. This is reasonable, because only faint furin expression was detected in the early developing retina.

In Study IV, the expression profiles of all syndecan family members were investigated during developmental angiogenesis, and no peak in the expression levels of SDC4 was detected. Using homologous WT and SDC4 KO and heterozygous mice, the rate of superficial vascular development was examined, and no differences in the length of the plexus nor in the number of arteries and veins were detected. However, a small decrease in the density of the vascular plexus was seen in the SDC4 KO animals. Further studies of other vascular beds (skin, connective tissue, and muscle) confirmed the finding that SDC4 does not participate in developmental angiogenesis. Alternatively, if SDC4 plays a role in developmental angiogenesis, its deficiency could be compensated for by other structurally similar members of the syndecan family (1 and 3, and 2 and 4). For example, SDC2 is upregulated in the developing cartilage in the absence of SDC4 (279). Interestingly, in a recently published study showed that SDC4 does not affect developmental retinal

angiogenesis, whereas SDC2 deletions delays it. These results confirm our findings that SDC4 does not participate in developmental retinal angiogenesis (106).

6.2 R-Ras and SDC4 in angiogenesis

6.2.1 The role of R-Ras in ocular vascular permeability

We showed that R-Ras is crucial for blood vessel integrity and stabilization in the mouse OIR model and that the lack of R-Ras therefore leads to increased vascular permeability (Study I). Our data showed that the expression of R-Ras is reduced in the vasculature of human PDR patients and correlates with vascular leakage, suggesting that R-Ras might be a crucial regulator of vascular permeability in human retinal vasculature. These results are in line with previously published results regarding the role of R-Ras in controlling vascular permeability in tumor vasculature and its role in physiological tissue repair, that is, in skin wounds (68,71,280). The blood vessels of R-Ras KO mice in the OIR model lacked pericytes and had reduced expression of VE-cadherin, whose role in EC barrier function is further discussed in section 6.2.3. Interaction between pericytes and endothelium is crucial for the stability of vessels (281,282). Pathological blood vessels, like tumor vessels and blood vessels in neovascular eye diseases, are known to have reduced pericyte coverage that leads to leakage of the vessels (162,283). A similar decrease of pericytes in the tumor vasculature of R-Ras KO animals has previously been reported in a tumor implant model. In that model, both the pericyte coverage and vascular maturation were enhanced after increased R-Ras signaling induced with lentivirus carrying activated R-Ras (R-Ras 38V) (68).

In addition to the OIR model, R-Ras may also play a prominent role in the control of vascular integrity in human PDR patients, in whom its expression exhibited an association with VEGFR2 expression and vascular leakage (Study I). VEGFR2 is highly expressed in the ECs of immature vessels. VEGFR2 and R-Ras have opposite temporal expression patterns during development, and findings similar to those obtained in our study have been reported in the tumor vasculature, where the vasculature of R-Ras KO mice exhibits strong expression of VEGFR2 (68).

One of the known roles of R-Ras is its contribution to integrin activation (64). For example, R-Ras binds to FLNA, which is an actin binding scaffold protein that interacts with β1, β2, and β7 integrin tails, and thus regulates integrin dependent cell

migration (284). In addition, a mechanism for R-Ras involving interaction with FLNA has been reported in the regulation of vascular permeability (285); R-Ras interacts with FLNA and co-localizes into plasma membrane. Disrupting this interaction promotes disorganization of VE-cadherin at adherens junctions and leads to leaky vessels. Interestingly, we also showed that FLNA is one of the most strongly upregulated proteins in the neovascular phase in OIR, i.e. shows similar expression pattern as R-Ras in OIR. The role of FLNA in angiogenesis is further discussed in section 6.3.2.

The key roles of R-Ras is in the stabilization and proper lumenogenesis of vasculature via AKT signaling (286). Based on our results and the possible relevance of R-Ras in DR, R-Ras could potentially be used as an agonistic therapy in the treatment of vascular leakage in the retina. As the gain of function of R-Ras inhibits EC migration, vessel sprouting and branching (68,70), it could be that enhanced R-Ras expression, for example via gene therapy, might be beneficial for the treatment of retinal vascular diseases. The mechanism of R-Ras might be different from that of other antiangiogenic therapies, because R-Ras is functionally different form classic antiangiogenic agents. R-Ras does not induce EC death as other antiangiogenic molecules do, which can thus affect also normal retinal blood vessels. Instead, R-Ras promotes EC survival and their maturation and enhances proper vessel lumenization (68).

6.2.2 The role of SDC4 in pathological angiogenesis

The effect of SDC4 on angiogenesis was seen only in pathological scenarios, in which SDC4 deficiency led to reduced pathological NV in several VEGF-dependent models. Our results show that SDC4 localizes to EC-cell contacts where it colocalizes with VE-cadherin. We also showed that vascular leakage was greatly reduced in SDC4 deficient mice after NV formation induced by VEGFA.

In a very recent study, it was shown that deletion of SDC2 led to defects in angiogenesis and impaired $VEGF_{165}$ signaling (106). However, the deletion of SDC4 did not exhibit a similar effect. This difference was explained by increased binding of $VEGF_{165}$ to SDC2 HS chains, which was driven by unique protein sequence in the *Sdc2* gene.

While they show that SDC2 is required for VEGFR2 activation, our data show that SDC4 functions downstream of VEGFR2. The role of SDC4 for VEGF-induced VE-cadherin internalization is further discussed in the section 6.2.3. Overall,

our data suggest that VEGFA-driven pathological angiogenesis is SDC4 dependent, and thus SDC4 KO mice have a specific defect in the responsiveness to VEGFA-driven pathological angiogenesis in ocular and tumor models but not in developmental angiogenesis. This is in line with previous finding that SDC4 plays a role in pathological lymphangiogenesis (277).

6.2.3 VE-cadherin in the regulation of vascular permeability

Adherens junctions and VE-cadherin in particular play an important role in controlling vascular permeability and integrity. VE-cadherin was found to be important in both R-Ras, and SDC4-mediated regulation of vascular permeability and angiogenesis.

VE-cadherin tyrosine phosphorylation or the phosphorylation of other members of the complex can be caused by several factors, including histamine and TNF-α (48). Tyrosine phosphorylation can also be induced by leukocyte adhesion via intercellular adhesion molecule 1 (ICAM1) (287). The exact mechanism of VE-cadherin phosphorylation has not been fully clarified, but it is speculated that tyrosine kinase SRC is involved in the mechanism (288). The site of phosphorylation determines the effect on the junctions. For example, VE-cadherin phosphorylation at Ser665 mediates internalization of VE-cadherin and thus increases vascular permeability (50). SRC, in turn, is activated by VEGF and phosphorylates only tyrosine 685 in ECs (289). The increase in vascular permeability can also occur without VE-cadherin phosphorylation, when intercellular gaps are caused by cytokines at inflammatory conditions or by permeability-increasing agents (290). Furthermore, instability of VE-cadherin junctions in ECs can also be caused by VE-cadherin internalization, which is regulated by clathrin dependent manner, where p120 catenin controls the endocytosis of VE-cadherin (291).

In Study I, we showed that in the R-Ras KO vasculature, the expression of VE-cadherin is decreased, measured both by the intensity of staining and the amount of co-localization with CD31. These results were expected, because R-Ras is known to inhibit VEGF induced VE-cadherin internalization (68). Previous experiments on tumor vasculature have had similar findings: reduced VE-cadherin expression was seen in R-Ras KO animals, and VE-cadherin accumulation in cell-cell junctions was increased with constitutively active mutant R-Ras, R-Ras 38V (68). A possible mechanism of R-Ras -mediated VE-cadherin trafficking is the actin-binding protein Girdin. R-Ras controls the subcellular localization of Girdin and also regulates the

interaction between Girdin and VE-cadherin containing vesicles after VEGF stimulation, suggesting that the R-Ras/Girdin complex promotes VE-cadherin recycling to the plasma membrane (292). Our results suggest that the increased vessel leakiness of R-Ras deficient mice in OIR could be due to the disorganization of VE-cadherin and hence the disruption of the adherens junctions.

The role of VE-cadherin in controlling vascular permeability was also investigated in our SDC4 study. SDC4 was not involved in the interaction between VEGFA and VEGFR2, but our data indicates that it acts downstream of VEGFR2. SDC4 is a known component of focal adhesion complex (293) and the disruption of the cell adhesions are crucial for angiogenesis. We showed that the VE-cadherin trafficking away from the junctions were diminished in the SDC4 deficient ECs. We propose that phosphorylated SDC4 forms a complex with VE-cadherin and is needed for proper VE-cadherin internalization.

Increasing endogenous VE-cadherin expression and thus normalizing the vasculature has been proposed as a therapeutic approach to the treatment of DR (294). It is known that in the diabetic retina, the expression of VE-cadherin is reduced, and the expression pattern is aberrant (Figure 9) (295). Blocking the pathological angiogenic effect of SDC4 could serve as a potential way to prevent VE-cadherin internalization and hence vascular instability.

6.2.4 Therapeutic potential of SDC4

Because VEGF signaling is needed for vascular homeostasis under normal conditions and because many cell types in the eye are dependent on VEGF signaling, alternative or more specific therapeutic approaches to ocular eye diseases are needed. VE-cadherin internalization and subsequent junctional disassembly are VEGFA induced but are EC specific. Hence, they provide a selective target with less off-target effects on other retinal cell types.

We showed that by blocking the proangiogenic effect of membrane-bound SDC4 with a soluble and glycanated form of SDC4 (solS4), VE-cadherin internalization can be blocked without affecting the up-stream VEGF signaling events immediately after VEGFR2 binding. Importantly, ECs pretreated with soluble syndecan 2 (solS2), the syndecan most structurally similar to SDC4, maintained responsiveness to VEGF, highlighting the specific role of SDC4 in VEGF-driven angiogenesis. The antiangiogenic effect of solS4 was confirmed using the CNV model, in which solS4 achieved an effect similar to that of aflibercept. Therapies targeting SDC4 could have

potential to block tumor angiogenesis but also stabilize the vessels to improve delivery of chemotherapy. Since SDC4 acts downstream of VEGF/VEGFR2 complex, it could possibly have less side effects than anti-VEGF therapies.

6.3 Proteomic analysis of the OIR model

In Study III, we carried out the most extensive proteomic profiling of the OIR model to date. As expected, we found changes in the expression of proteins related to angiogenesis as well as in proteins involved in neuronal functions. We detected a group of proteins, crystallins, that were greatly upregulated in OIR at the early hypoxic time point. Crystallins are small heat-shock proteins that play roles in neuroprotection, because they protect cells from hypoxia and maintain mitochondrial homeostasis (296,297). It has been found that crystallins are expressed in the retina, where they participate in the development of retinal vasculature (298,299). Studies have shown that α-crystallins have therapeutic value in the retina. The administration of α-crystallins inhibited retinal degeneration, protected retinal ganglion cells from apoptosis, and promoted axonal regeneration in experimental animal models (300). αA-crystallin might be useful in the treatment of early DR, because adenovirus-mediated delivery reduced apoptosis of pericytes and vascular leakage (301).

In addition to their neuroprotective and developmental roles, some of the crystallins have been reported to play a role in pathological conditions. For example, αB-crystallin is a modulator of angiogenesis because it functions as a chaperone for VEGF and is needed for its adequate folding and secretion (302,303). In the OIR model, mice deficient for αB-crystallin had less VEGF and NV compared to WT. αB-crystallins have been reported to participate in the epithelial-mesenchymal transition (EMT), leading to TGF-β driven subretinal fibrosis in AMD (304). In addition, αB-Crystallin is overexpressed in many cancers, such as basal-like breast cancer, non small cell lung cancer, colorectal cancer, and retinoblastoma, and it promotes tumor angiogenesis (300,305). Another proteomics-based study reported that its overexpression might be linked to CNV pathology (306). An experimental diabetes study reported overexpression of α, β and γ-crystallins in the diabetic retina, but they had lost their neuroprotective functions due to diabetes (307).

The expression of crystallins is greatly increased in many human retinal diseases, such as AMD, DR and uveoretinitis, as well as after mechanical injury or ischemic insult (297,308,309). αB-crystallin is expressed in PDR epiretinal membranes from

pathological blood vessels and is also found in vitreous fluid, and its levels correlate with VEGF levels (201,310). In view of the results of previous animal studies and previous clinical data and the opposite functions of different crystallins, the therapeutic potential of crystallins needs to be investigated further.

6.3.1 Angiogenic proteins in OIR

Among the most upregulated proteins at the peak of angiogenesis (at P17) were plasma proteins such as GC, Albumin, and Apoliprotein A1 (APOA1). This is most likely due to increased plasma leakage from abnormal blood vessels. However, these proteins might also have biological functions in the OIR pathogenesis. The most upregulated protein based on fold change at P17 was GC, a vitamin-D-binding protein. It was substantially more upregulated than serum albumin, the most abundant blood protein in mammals. GC is a multifunctional glycoprotein and a member of the albumin superfamily of binding proteins. It is an important carrier of vitamin D metabolites, such as calcitriol, the active form of vitamin D (311). Interestingly, calcitriol has been reported to be antiangiogenic in a dose dependent manner in the OIR model (312). In addition to calcitriol, other vitamin D receptor agonists attenuated ocular angiogenesis in a zebrafish larvae model (313). GC can also modulate inflammatory functions. It can be converted to a vitamin-D-binding protein-macrophage activating factor (DBP-MAF), which has been suggested to have antitumorigenic and antiangiogenic effects (314,315). The antiangiogenic functions of DBP-MAF are based on its ability to inhibit VEGF signaling by decreasing the phosphorylation of VEGFR2 and ERK1/2 (316). Low serum levels of vitamin D represent a risk factor for AMD, DR, and glaucoma (317,318), and vitamin D metabolism has been linked to ocular disease pathology (319). Vitamin D receptor (VDR) is expressed in neurons, in retinal and choroidal ECs, and especially strongly in pericytes (317,320). Mice deficient for VDR had an increased number of pericytes and impaired NV and were resistant to the antiangiogenic functions of calcitriol in OIR (320). It has been suggested that vitamin D protects against oxidation and inflammation and consequently prevents angiogenesis and thus vitamin D supplementation might prevent ocular inflammation and NV in these diseases (317,318).

It could be that the upregulation of GC in OIR at P17 could be an endogenous signal to suppress angiogenesis or a response to low levels of vitamin D metabolites in the retina. A proteomic study of ROP showed that GC was one of the proteins

found in the vitreous of ROP patients but not in the healthy controls (321). On the other hand, the ECs release GC under stress, but not during normal growth. GC works as a growth factor in blood vessels and induces cell migration and proliferation of vascular SMCs at the site of vascular injury (322). The role of GC in ocular angiogenesis and OIR has not been investigated. Thus, further studies are needed to clarify its role in neovascular ocular diseases.

AHSG is an adhesive glycoprotein in serum that induces cell proliferation in the target cells. AHSG binds to its receptors ANXA2 and ANXA6, which were also highly upregulated in OIR samples in our study. Interestingly, it has been shown that ANXA2 drives angiogenesis in OIR (323). The upregulation of both the ligand and receptor in OIR, indicates that the AHSG/ANXA2-pathway plays a role in OIR pathogenesis.

Among the seven proteins that IPA analysis found linked to increased angiogenesis at P17 OIR was the melanoma cell adhesion molecule, MCAM (CD146). MCAM is a cell surface glycoprotein that displays different isoforms and is found in the junctions of vascular endothelium. It is also expressed by other cell types, such as pericytes, SMCs, and cancer cells (324). It was originally described as a marker of tumor blood vessels (325-328), but the most recent studies have suggested that it plays roles in angiogenesis, vascular permeability, and tumorigenesis. Its expression is upregulated by VEGF, and it is localized to tumor blood vessels but not to the healthy vasculature, theoretically providing a new molecular target for cancer treatment (328). In addition, MCAM interacts with VEGFR2 on tumor ECs, and it is required for VEGF-induced VEGFR2 phosphorylation that promotes EC migration and tumor angiogenesis (329). A soluble form of MCAM promoted NV in an experimental hind-limb ischemia model (330). Blocking of MCAM could provide a new therapeutic target in ischemic ocular neovascular diseases. The therapy could be specific for pathological blood vessels, leaving the healthy vasculature intact.

According to IPA analysis, MYH9 was among the proteins responsible for angiogenesis. MYH9 encodes for a myosin IIA heavy chain, a cytoskeletal contractile protein, which is involved in several functions such as generation of intracellular chemomechanical force and translocation of the actin cytoskeleton (331). Its expression levels are considered to reflect the stiffness of the tissue, such that the stiffest tissues express high levels of MYH9 (332). When cells are migrating, they adhere to the extracellular matrix, which transmits forces inside the cell, and the nonmuscle myosins balance the mechanical forces. The stiffer the tissue, the more contractility the migrating cells need, which destabilizes endothelial cell-cell junctions

and increases vascular permeability (333-335). MYH9 is overexpressed in many cancers and its high expression is associated with poor prognosis (336). In addition to regulating the endothelial cell-cell junctions, MYH9 regulates cell migration (337). The activation of MYH9 led to elevated VEGF expression and induction of arteriogenesis in the ischemia-driven arteriogenesis (338). MYH9 has also been shown to control the translocalization of nucleolin, which is primarily a nuclear protein but translocates to the EC surface in angiogenesis (339-341). Therapies that antagonize nucleolin or block MYH9 inhibit angiogenesis by causing EC apoptosis and normalizing the vasculature (341). In our proteomic study, we observed only a modest increase in the nucleolin expression. However, the gene expression levels are not relevant to nucleolin, because its function in angiogenesis is in translocation to cell surface. It was recently shown that nucleolin is translocated to the EC surface in neovascular blood vessels in OIR, whereas it stayed nuclear in the normoxic conditions (342).

Strong MYH9 expression correlated with HSA staining in PDR and RVO membranes. This indicates increased EC contractility, which in turn, results in increased vascular permeability. MYH9 is also expressed in fibroblast like cells that have undergone endothelial to mesenchymal transition (EndMT) (343). In EndMT, cells start to express mesenchymal markers, gain increased motility, and begin the secretion of extracellular matrix proteins. This phenomenon is involved in a variety of disease processes, such as vascular or tissue fibrosis, and in the tumor environment (344). Our upstream regulator analysis in the proteomic study identified TGF-β, MKL2, and MKNK1 as potential enhancers of increased angiogenesis in OIR. MKL2 is a transcriptional coactivator that actually regulates the conserved TGF- signaling pathway in developing vasculature and is required for maturation and stabilization of embryonic vasculature (345-347). In addition, TGF-β is known for its roles in the induction of EMT and myofibroblast transformation. MKL2 (and MKL1) are key regulators in these cellular processes (348,349). Increased TGF-β signaling leads to EndMT in the vasculature, which shares many features with EMT (350,351). Enhanced vascular TGF-β signaling may also induce fibrosis to surrounding tissue. EndMT takes place in glucose-treated retinal ECs, where EC damage leads to a decrease in endothelial markers and an increase in mesenchymal markers, which is induced by TGF-β (352,353). EndMT was prevented by inhibiting TGF-β by overexpression of one long noncoding RNA H19, which is involved also in TGF-β-induced EMT during tumor metastasis. Deletion of H19 in mice led to EndMT in the retina. Furthermore, H19 was found to be downregulated in the vitreous humor in PDR patients (353). Our results suggest that upregulation of the

crystallins MYH9 and MKL2/TGF-β enhances angiogenesis in OIR. In light of the recent finding that TGF-β together with αb-crystallin is associated with EMT and with subretinal scarring, this could provide hints about the potential events that ultimately lead to fibrosis in angiogenic retinal diseases.

The third potential upstream regulator driving angiogenesis in OIR was MKNK1/MNK1. MNK1 is a kinase that plays a role in environmental stress, and it phosphorylates a cap-binding subunit of the eIF4F translation initiation complex, eIF4E. eIF4E is overexpressed in many human malignancies, in which it is thought to drive tumorigenesis by inducing translation of proliferation and survival promoting mRNAs, one of which is VEGFA (354). Inhibiton of eIF4E phosphorylation via inhibition of MNK suppressed tumor angiogenesis and tumor growth (355). In the retina, eIF4E is known to interact with 4E-bp1, and this interaction is enhanced in the diabetic rat retina and leads to the induction of VEGF expression (356-359). Our finding that MKNK1/MNK1 is a potential driver of angiogenesis in OIR suggests that targeting the MNK-eIF4E pathway could be a potential target for blocking pathogenesis in ischemic eye diseases as well.

6.3.2 Filamin A in angiogenesis

One of the proteins predicted to be causing enhanced angiogenesis in the OIR model was FLNA, which is the most abundant member of the filamins. Filamins act as binding proteins that maintain extracellular matrix connections. We showed that FLNA was expressed in the retinal blood vessels that the expression was increased in OIR. The increased FLNA expression in OIR was also validated with immunoblotting, which detected C-terminal FLNA ($FLNA_{CT}$). In addition to the increase in the levels of total FLNA, a substantial induction of $FLNA_{CT}$ was detected. In hypoxia, FLNA is rapidly upregulated and then interacts with HIF-1α and promotes angiogenesis (276,360). In hypoxia, FLNA undergoes calpain dependent cleavage, and its 90 kDa C-terminal fragment ($FLNA_{CT}$) accumulates into the nucleus, where it enhances HIF-1α (but not HIF-2α) accumulation and interacts with HIF-1α to localize it to the promoter regions of HIF-1α target genes. This causes the enhanced expression of these genes (276). Upregulation of FLNA has been found in many cancers, and tumor cells lacking FLNA exhibits impaired growth and angiogenesis as well as the reduced expression of HIF target genes (276,361). Targeting FLNA has been proposed as a target for cancer therapy (361).

Taking into account that N-terminal FLNA is needed for the stability of the EC barrier, specific inhibition of $FLNA_{CT}$ could provide a more potent antiangiogenic therapeutic effect than general FLNA inhibition. Indeed, it was recently shown that blocking the calpain-dependent cleavage of FLNA hinders the growth of tumor cells (362). Our results showed that R-Ras regulates vascular permeability in OIR, and that lack of R-Ras is associated with enhanced leakage in human PDR (Study I). Interestingly, as previously discussed, FLNA A interacts with R-Ras to control cell migration and maintain vascular barrier function (285). Loss of FLNA, in turn, leads to increased vascular permeability and even embryonic lethality due to cardiac defects and aberrant vascular patterning (285,363). R-Ras binds to FLNA in its N-terminus (285), thus selective blocking of the cleaved FLNA C-terminus could be a potential therapeutic target in ischemic retinopathies involving NV.

However, another hypothesis has been presented regarding the role of FLNA in tumor metastasis. First, it was shown that $FLNA_{CT}$ co-localized to the nucleus with androgen receptor, a nuclear transcription factor that is associated with the promotion of prostate cancer. There, $FLNA_{CT}$ repressed androgen receptor transactivation and its interactions, suggesting that nuclear FLNA may act as an inhibitor of tumorigenesis (364). Thus, one hypothesis is that FLNA has a tumor-promoting effect only when FLNA is found in the cytoplasm, whereas if FLNA is cleaved and $FLNA_{CT}$ translocates to the nucleus, it prevents tumor growth and metastasis (365). In the end, the function of FLNA in the cell, or as a nuclear transcriptional modulator, is dependent on its binding partners. Due to this controversy over the role of FLNA and its cellular localization, further studies are needed to elucidate the potential role of FLNA as a therapeutic target in neovascular ocular diseases.

Similarly to FLNA, the expression of Filamin-B (FLNB) was increased at P17 OIR. It has been shown that whereas FLNA is more ubiquitously expressed in vascular mural and ECs, the expression of FLNB is restricted to ECs (366). Disruption of FLNB, but not FLNA, leads to inhibition of EC migration after VEGF induction (366). FLNB deficiency led to an impaired microvascular network in the central nervous system (367), whereas gain of function of FLNB is proposed to modulate the interaction between FLNA and FLNB and impair FLNAs function in the regulation of angiogenesis, which could lead to abnormal angiogenesis. Another link between FLNB and angiogenesis is that VEGF and protein kinase C promote the ubiquitination of FLNB, which leads to angiogenic-promoting HDAC7 phosphorylation (368). Taking together, these results suggest, that the increased expression of FLNA may play a role in the regulation of vascular permeability via

N-terminal FLNA, whereas $FLNA_{CT}$ and FLNB may drive angiogenesis and the migration of ECs in OIR.

6.3.3 Proteins involved in neurotransmission in OIR

To study whether retinal hypoxia and NV leaves persistent changes in the retinal proteome, a late time point, P42, was included in the study. The IPA analysis of our study revealed that those proteins that showed marginal changes in OIR at P42 compared to normoxic controls were proteins involved in neurotransmission; specifically, they are involved in the synaptic vesicle cycle pathway. Previously, it was reported that in the OIR model some morphological changes persist in the retina and there is a decrease in neuronal function (369). It is important to better understand the long-term changes in OIR, because they could provide relevant information about the prognosis of ROP.

6.4 Role of myeloid-specific furin in angiogenesis

Our expression analysis of furin revealed the highest expression of furin in monocyte-derived macrophages and retinal microglia, highlighting the importance of furin in retinal myeloid cells. Both recruited macrophages and retinal microglia participate in the regulation of angiogenesis in the OIR model (152,370-372). Thus, the effect of myeloid-specific furin in the OIR model was investigated. Our results show that myeloid-specific furin plays a role in the retinal revascularization process in ischemic retinopathy but that does not contribute to pathological NV. In the OIR model, retinal revascularization and NV processes are usually inversely correlated, such that attenuated retinal revascularization is accompanied by increased NV. However, this was not the case with the LysMCre-$fur^{(fl/fl)}$ mice, in which AVAs were bigger than in WT mice, without a subsequent increase of NV. During the hyperoxic period in OIR, microglia persist in the retina, although the central retinal becomes avascular (373). In response to hypoxia, the microglia start to secrete proangiogenic growth factors directing revascularization in the retina. In LysMCre-$fur^{(fl/fl)}$ mice, the revascularization is reduced, and possibly due to the lack of activation of proangiogenic growth factors, the blood vessels do not start to sprout towards the vitreous neither.

Our results confirmed the importance of furin for angiogenesis, because it was previously shown that EC-specific furin deficiency is lethal (95). Furin has many proangiogenic targets, one of which, VEGFC (81), is expressed in macrophages and it is involved in the control of vascular branching in the retina (374). Interestingly, furin cleavage is not required for the activation of VEGFA, and myeloid-cell specific VEGFA expression does not have an effect on angiogenesis in the OIR model (375,376). Expression of furin in myeloid cells could be involved in the activation of proangiogenic factors, such as VEGFC. This hypothesis is in line with previous studies, in which both furin and VEGFC expression have been involved in the same disease models, among them several cancers, and the synergy has been linked to increased angiogenesis (81,377-379).

Anti-inflammatory TGF-β1 is another major angiogenic factor that requires cleavage and activation by furin convertase (84,94,380). Furin is the main proprotein convertase of pro-TGF-β1, and the inhibition of furin has impaired the production of mature and functional TGF-β1 (94). Furthermore, furin activates other TGF-β family members, such as bone morphogenetic protein-4 (93). The interplay between furin and TGF-β family members is complex; TGF-β2 induces furin expression, and together they form a positive feedback loop for high TGF-β activity (381). However, when the cleavage of TGF-β1 and -β2 was addressed, it was determined that even though TGF-β2 has a consensus cleavage site for furin, one that is found in other proteins efficiently cleaved by furin, TGF-β2 is insensitive to furin due its structure. (382). This may help to explain why TGF-β isoforms have different functions despite being expressed at the same site, because they are activated via different processes (382).

Furin plays an important role in myeloid cells, where furin deficiency led to reduced TGF-β1 bioactivity (250). TGF-β signaling has been associated with NV in many diseases, including ocular diseases such as AMD (188,383,384). Our results showing induction in TGF-β1 targets in the OIR model (Study III) are in line with a previous study showing elevated TGF-β1 signaling in the OIR model (385). Thus, the attenuation in revascularization in the OIR model in LysMCre-fur$^{(fl/fl)}$ mice could be due to the reduced bioavailability of TGF-β1. However, the role of TGF-β family members in angiogenesis is controversial. Both pro- and antiangiogenic roles for TGF-β have been described. In the OIR model, intraperitoneally injected mesenchymal stem cell invaded to the retina and secreted TGF-β1, which suppressed NV. This effect was blocked by the treatment with TGF-β1 siRNA (386).

Very recently, the effect of TGF-β for a hypoxia-mediated blood-brain barrier function was investigated (387). Interestingly, TGF-β exposure increased furin

expression via TGF-β type I receptor activin-like kinase 5. Furin inhibition, in turn, prevented TGF-β induced EC migration, suggesting that there is a feedback loop between furin and TGF-β. In addition, both furin and TGF-β were important for the regulation the blood-brain barrier function, since either furin or TGF-β receptor (activin-like kinase 5) blockage protected from the barrier disruption. (387). These results suggest that furin or TGF-β inhibition might be a novel therapeutic target for the treatment of diseases where blood-brain barrier or BRB function is compromised.

Because the role of TGF-β remains unclear in the OIR model and ischemic eye diseases, there is a need for the full characterization of TGF-β family members and their receptors in OIR. However, the results of our OIR proteomics study indicate that one of the upstream regulators driving angiogenesis is TGF-β1 (Study III). In addition to TGF-β and VEGFC, other proangiogenic factors activated by furin are VEGFD, PDGF-A and -B, and bone morphogenetic protein-4 (91-93,388). These factors can be produced by macrophages, but because furin can also be secreted outside the cell, the effect of myeloid-specific expression of furin can extend outside the cell. More studies are needed to clarify the mechanism underlying myeloid-specific furin's control of retinal revascularization in OIR.

7 CONCLUSIONS

The aim of this thesis was to investigate the role of R-Ras, furin, and SDC4 in developmental and pathological angiogenesis. In addition, protein expression levels and molecular pathways driving angiogenesis in the mouse OIR model were examined using the full proteome-based approach. Based on the results of these studies, the following conclusions can be made:

- R-Ras plays a major role in the regulation of vascular permeability in the OIR model and in the proliferative retinopathy in human (Study I).
- Furin is expressed in retinal myeloid cells, and myeloid-cell-specific furin enhances revascularization in the mouse OIR model (Study II).
- Mass-spectrometry and proteomics-based characterization of protein levels in the mouse OIR model reveals novel potential drivers of angiogenesis and potential therapeutic targets for the treatment of ischemic eye diseases (Study III).
- SDC4 is needed for VEGFA-driven angiogenic responses in pathological setting and SDC4 deficiency protects from ocular NV and impairs tumor angiogenesis and growth (Study IV).
- SDC4 is needed for VEGFA induced VE-cadherin trafficking and internalization (Study IV).
- Targeting SDC4 using soluble SDC4 reduces VE-cadherin internalization and NV in a laser-induced CNV model (Study IV).

The main results of this thesis are presented in Table 2.

These results provide more knowledge about the regulation of angiogenesis, and vascular permeability and can thus be useful for the future development of novel therapeutics. However, further studies are needed to evaluate the true relevance of these results to human diseases.

Table 2. Main results of the dissertation.

Protein	Expression in the mouse retina	Role in developmental angiogenesis	Role in pathological angiogenesis	Role for vascular permeability	Relevance to human disease
R-Ras	ECs and pericytes. Upregulated in the OIR model.	No effect for developmental retinal angiogenesis.	No effect for revascularization nor the amount of NV in the OIR model.	Deficiency leads to increased permeability, impairs pericyte coverage and reduces VE-cadherin expression in OIR.	Reduced expression correlates with leakage and VEGFR2 expression in PDR membranes.
Furin	Monocyte derived macrophages, microglia and ECs. Weak expression during development, increased in OIR.	No effect for developmental retinal angiogenesis.	Deficiency leads to attenuated revascularization in OIR.	N/A	Colocalized with its proangiogenic target, a (pro)-renin receptor protein in PDR membranes (87).
SDC4	Expression increased at P17 in the OIR model (unlike SDC1-3). Expression remains unaltered during retinal vascular development.	No effect for vascular extension or number of arteries and veins in retina. Small reduction in retinal vascular density. No effect for normal vascular development in skin, muscle and connective tissue.	Deficiency leads to reduced NV in ocular models and impaired tumor angiogenesis. Needed for VEGFA induced angiogenic response in aortic ring model and Matrigel plug assay. Required for VEGFA dependent EC migration.	Deficiency leads to reduction of VEGF mediated hyperpermeability. VE-cadherin trafficking and internalization is SDC4 dependent.	Correlates with VEGFR2 in human PDR membranes. Soluble SDC4 reduces NV and VE-cadherin internalization in a mouse model of wet AMD.

N/A = information not available/ was not studied.

REFERENCES

1. Pugsley MK, Tabrizchi R. The vascular system. An overview of structure and function. J Pharmacol Toxicol Methods. 2000;44(2):333-340.

2. Gerhardt H, Betsholtz C. Endothelial-pericyte interactions in angiogenesis. Cell Tissue Res. 2003;314(1):15-23.

3. Sa-Pereira I, Brites D, Brito MA. Neurovascular unit: A focus on pericytes. Mol Neurobiol. 2012;45(2):327-347.

4. Frank RN, Turczyn TJ, Das A. Pericyte coverage of retinal and cerebral capillaries. Invest Ophthalmol Vis Sci. 1990;31(6):999-1007.

5. Grant DS, Kibbey MC, Kinsella JL, Cid MC, Kleinman HK. The role of basement membrane in angiogenesis and tumor growth. Pathol Res Pract. 1994;190(9-10):854-863.

6. Stevens T, Garcia JG, Shasby DM, Bhattacharya J, Malik AB. Mechanisms regulating endothelial cell barrier function. Am J Physiol Lung Cell Mol Physiol. 2000;279(3):L419-22.

7. Bazzoni G, Dejana E. Endothelial cell-to-cell junctions: Molecular organization and role in vascular homeostasis. Physiol Rev. 2004;84(3):869-901.

8. Dejana E. Endothelial cell-cell junctions: Happy together. Nat Rev Mol Cell Biol. 2004;5(4):261-270.

9. Cunha-Vaz J, Bernardes R, Lobo C. Blood-retinal barrier. Eur J Ophthalmol. 2011;21 Suppl 6:S3-9.

10. Ivanov D, Philippova M, Antropova J, et al. Expression of cell adhesion molecule T-cadherin in the human vasculature. Histochem Cell Biol. 2001;115(3):231-242.

11. Goldie LC, Nix MK, Hirschi KK. Embryonic vasculogenesis and hematopoietic specification. Organogenesis. 2008;4(4):257-263.

12. Demir R, Yaba A, Huppertz B. Vasculogenesis and angiogenesis in the endometrium during menstrual cycle and implantation. Acta Histochem. 2010;112(3):203-214.

13. Tonnesen MG, Feng X, Clark RA. Angiogenesis in wound healing. J Investig Dermatol Symp Proc. 2000;5(1):40-46.

14. Olfert IM, Baum O, Hellsten Y, Egginton S. Advances and challenges in skeletal muscle angiogenesis. Am J Physiol Heart Circ Physiol. 2016;310(3):H326-36.

15. Burri PH, Djonov V. Intussusceptive angiogenesis - the alternative to capillary sprouting. Mol Aspects Med. 2002;23(6S):S1-27.

16. Qian CN, Tan MH, Yang JP, Cao Y. Revisiting tumor angiogenesis: Vessel co-option, vessel remodeling, and cancer cell-derived vasculature formation. Chin J Cancer. 2016;35:10-015-0070-2.

17. Hillen F, Griffioen AW. Tumour vascularization: Sprouting angiogenesis and beyond. Cancer Metastasis Rev. 2007;26(3-4):489-502.

18. Wang R, Chadalavada K, Wilshire J, et al. Glioblastoma stem-like cells give rise to tumour endothelium. Nature. 2010;468(7325):829-833.

19. Carmeliet P, Jain RK. Angiogenesis in cancer and other diseases. Nature. 2000;407(6801):249-257.

20. Noonan DM, De Lerma Barbaro A, Vannini N, Mortara L, Albini A. Inflammation, inflammatory cells and angiogenesis: Decisions and indecisions. Cancer Metastasis Rev. 2008;27(1):31-40.

21. Lissbrant IF, Stattin P, Damber JE, Bergh A. Vascular density is a predictor of cancer-specific survival in prostatic carcinoma. Prostate. 1997;33(1):38-45.

22. Goel S, Duda DG, Xu L, et al. Normalization of the vasculature for treatment of cancer and other diseases. Physiol Rev. 2011;91(3):1071-1121.

23. Forsythe JA, Jiang BH, Iyer NV, et al. Activation of vascular endothelial growth factor gene transcription by hypoxia-inducible factor 1. Mol Cell Biol. 1996;16(9):4604-4613.

24. Krock BL, Skuli N, Simon MC. Hypoxia-induced angiogenesis: Good and evil. Genes Cancer. 2011;2(12):1117-1133.

25. Depping R, Steinhoff A, Schindler SG, et al. Nuclear translocation of hypoxia-inducible factors (HIFs): Involvement of the classical importin α/β pathway. Biochim Biophys Acta. 2008;1783(3):394-404.

26. Ylä-Herttuala S, Rissanen TT, Vajanto I, Hartikainen J. Vascular endothelial growth factors: Biology and current status of clinical applications in cardiovascular medicine. J Am Coll Cardiol. 2007;49(10):1015-1026.

27. Holmes DI, Zachary I. The vascular endothelial growth factor (VEGF) family: Angiogenic factors in health and disease. Genome Biol. 2005;6(2):209

28. Ogawa S, Oku A, Sawano A, Yamaguchi S, Yazaki Y, Shibuya M. A novel type of vascular endothelial growth factor, VEGF-E (NZ-7 VEGF), preferentially utilizes KDR/flk-1 receptor and carries a potent mitotic activity without heparin-binding domain. J Biol Chem. 1998;273(47):31273-31282.

29. Yamazaki Y, Takani K, Atoda H, Morita T. Snake venom vascular endothelial growth factors (VEGFs) exhibit potent activity through their specific recognition of KDR (VEGF receptor 2). J Biol Chem. 2003;278(52):51985-51988.

30. Shibuya M. Vascular endothelial growth factor (VEGF) and its receptor (VEGFR) signaling in angiogenesis: A crucial target for anti- and pro-angiogenic therapies. Genes Cancer. 2011;2(12):1097-1105.

31. Ferrara N, Gerber HP, LeCouter J. The biology of VEGF and its receptors. Nat Med. 2003;9(6):669-676.

32. Olsson AK, Dimberg A, Kreuger J, Claesson-Welsh L. VEGF receptor signalling - in control of vascular function. Nat Rev Mol Cell Biol. 2006;7(5):359-371.

33. Miller JW, Le Couter J, Strauss EC, Ferrara N. Vascular endothelial growth factor a in intraocular vascular disease. Ophthalmology. 2013;120(1):106-114.

34. Carmeliet P, Ferreira V, Breier G, et al. Abnormal blood vessel development and lethality in embryos lacking a single VEGF allele. Nature. 1996;380(6573):435-439.

35. Vempati P, Popel AS, Mac Gabhann F. Extracellular regulation of VEGF: Isoforms, proteolysis, and vascular patterning. Cytokine Growth Factor Rev. 2014;25(1):1-19.

36. Lee S, Jilani SM, Nikolova GV, Carpizo D, Iruela-Arispe ML. Processing of VEGF-A by matrix metalloproteinases regulates bioavailability and vascular patterning in tumors. J Cell Biol. 2005;169(4):681-691.

37. Cebe Suarez S, Pieren M, Cariolato L, et al. A VEGF-A splice variant defective for heparan sulfate and neuropilin-1 binding shows attenuated signaling through VEGFR-2. Cell Mol Life Sci. 2006;63(17):2067-2077.

38. Li X, Aase K, Li H, von Euler G, Eriksson U. Isoform-specific expression of VEGF-B in normal tissues and tumors. Growth Factors. 2001;19(1):49-59.

39. Zhang F, Tang Z, Hou X, et al. VEGF-B is dispensable for blood vessel growth but critical for their survival, and VEGF-B targeting inhibits pathological angiogenesis. Proc Natl Acad Sci U S A. 2009;106(15):6152-6157.

40. Li X, Lee C, Tang Z, et al. VEGF-B: A survival, or an angiogenic factor? Cell Adh Migr. 2009;3(4):322-327.

41. Cao Y, Chen H, Zhou L, et al. Heterodimers of placenta growth factor/vascular endothelial growth factor. Endothelial activity, tumor cell expression, and high affinity binding to flk-1/KDR. J Biol Chem. 1996;271(6):3154-3162.

42. Cao Y, Linden P, Shima D, Browne F, Folkman J. In vivo angiogenic activity and hypoxia induction of heterodimers of placenta growth factor/vascular endothelial growth factor. J Clin Invest. 1996;98(11):2507-2511.

43. Alitalo K, Carmeliet P. Molecular mechanisms of lymphangiogenesis in health and disease. Cancer Cell. 2002;1(3):219-227.

44. Chien MH, Ku CC, Johansson G, et al. Vascular endothelial growth factor-C (VEGF-C) promotes angiogenesis by induction of COX-2 in leukemic cells via the VEGF-R3/JNK/AP-1 pathway. Carcinogenesis. 2009;30(12):2005-2013.

45. Zhao B, Smith G, Cai J, Ma A, Boulton M. Vascular endothelial growth factor C promotes survival of retinal vascular endothelial cells via vascular endothelial growth factor receptor-2. Br J Ophthalmol. 2007;91(4):538-545.

46. Senger DR, Galli SJ, Dvorak AM, Perruzzi CA, Harvey VS, Dvorak HF. Tumor cells secrete a vascular permeability factor that promotes accumulation of ascites fluid. Science. 1983;219(4587):983-985.

47. Giannotta M, Trani M, Dejana E. VE-cadherin and endothelial adherens junctions: Active guardians of vascular integrity. Dev Cell. 2013;26(5):441-454.

48. Dejana E, Orsenigo F, Lampugnani MG. The role of adherens junctions and VE-cadherin in the control of vascular permeability. J Cell Sci. 2008;121(Pt 13):2115-2122.

49. Corada M, Mariotti M, Thurston G, et al. Vascular endothelial-cadherin is an important determinant of microvascular integrity in vivo. Proc Natl Acad Sci U S A. 1999;96(17):9815-9820.

50. Gavard J, Gutkind JS. VEGF controls endothelial-cell permeability by promoting the β-arrestin-dependent endocytosis of VE-cadherin. Nat Cell Biol. 2006;8(11):1223-1234.

51. Lampugnani MG, Orsenigo F, Gagliani MC, Tacchetti C, Dejana E. Vascular endothelial cadherin controls VEGFR-2 internalization and signaling from intracellular compartments. J Cell Biol. 2006;174(4):593-604.

52. Coon BG, Baeyens N, Han J, et al. Intramembrane binding of VE-cadherin to VEGFR2 and VEGFR3 assembles the endothelial mechanosensory complex. J Cell Biol. 2015;208(7):975-986.

53. Wennerberg K, Rossman KL, Der CJ. The ras superfamily at a glance. J Cell Sci. 2005;118(Pt 5):843-846.

54. Cherfils J, Zeghouf M. Regulation of small GTPases by GEFs, GAPs, and GDIs. Physiol Rev. 2013;93(1):269-309.

55. Pylayeva-Gupta Y, Grabocka E, Bar-Sagi D. RAS oncogenes: Weaving a tumorigenic web. Nat Rev Cancer. 2011;11(11):761-774.

56. Hobbs GA, Der CJ, Rossman KL. RAS isoforms and mutations in cancer at a glance. J Cell Sci. 2016;129(7):1287-1292.

57. Ehrhardt A, Ehrhardt GR, Guo X, Schrader JW. Ras and relatives--job sharing and networking keep an old family together. Exp Hematol. 2002;30(10):1089-1106.

58. Lowe DG, Capon DJ, Delwart E, Sakaguchi AY, Naylor SL, Goeddel DV. Structure of the human and murine R-ras genes, novel genes closely related to ras proto-oncogenes. Cell. 1987;48(1):137-146.

59. Self AJ, Caron E, Paterson HF, Hall A. Analysis of R-Ras signalling pathways. J Cell Sci. 2001;114(Pt 7):1357-1366.

60. Lowe DG, Goeddel DV. Heterologous expression and characterization of the human R-ras gene product. Mol Cell Biol. 1987;7(8):2845-2856.

61. Prior IA, Lewis PD, Mattos C. A comprehensive survey of ras mutations in cancer. Cancer Res. 2012;72(10):2457-2467.

62. Marte BM, Rodriguez-Viciana P, Wennstrom S, Warne PH, Downward J. R-Ras can activate the phosphoinositide 3-kinase but not the MAP kinase arm of the ras effector pathways. Curr Biol. 1997;7(1):63-70.

63. Liu WN, Yan M, Chan AM. A thirty-year quest for a role of R-Ras in cancer: From an oncogene to a multitasking GTPase. Cancer Lett. 2017;403:59-65.

64. Zhang Z, Vuori K, Wang H, Reed JC, Ruoslahti E. Integrin activation by R-ras. Cell. 1996;85(1):61-69.

65. Wang HG, Millan JA, Cox AD, et al. R-Ras promotes apoptosis caused by growth factor deprivation via a bcl-2 suppressible mechanism. J Cell Biol. 1995;129(4):1103-1114.

66. Singh G, Hashimoto D, Yan X, et al. R-Ras is required for murine dendritic cell maturation and CD4+ T-cell priming. Blood. 2012;119(7):1693-1701.

67. Yan X, Yan M, Guo Y, et al. R-Ras regulates murine T cell migration and intercellular adhesion molecule-1 binding. PLoS One. 2015;10(12):e0145218.

68. Sawada J, Urakami T, Li F, et al. Small GTPase R-Ras regulates integrity and functionality of tumor blood vessels. Cancer Cell. 2012;22(2):235-249.

69. Komatsu M, Ruoslahti E. R-Ras is a global regulator of vascular regeneration that suppresses intimal hyperplasia and tumor angiogenesis. Nat Med. 2005;11(12):1346-1350.

70. Sawada J, Li F, Komatsu M. R-Ras protein inhibits autophosphorylation of vascular endothelial growth factor receptor 2 in endothelial cells and suppresses receptor activation in tumor vasculature. J Biol Chem. 2015;290(13):8133-8145.

71. Ketomäki T, Vähätupa M, May U, et al. R-Ras regulates vascular permeability, but not overall healing in skin wounds. Exp Dermatol. 2019;28(2):202-206.

72. May U, Prince S, Vähätupa M, et al. Resistance of R-Ras knockout mice to skin tumour induction. Sci Rep. 2015;5:11663.

73. Swann JB, Vesely MD, Silva A, et al. Demonstration of inflammation-induced cancer and cancer immunoediting during primary tumorigenesis. Proc Natl Acad Sci U S A. 2008;105(2):652-656.

74. Ray A, Basu S, Miller NM, Chan AM, Dittel BN. An increase in tolerogenic dendritic cell and natural regulatory T cell numbers during experimental autoimmune encephalomyelitis in rras-/- mice results in attenuated disease. J Immunol. 2014;192(11):5109-5117.

75. Kummola L, Ortutay Z, Vähätupa M, et al. R-Ras deficiency does not affect papain-induced IgE production in mice. Immun Inflamm Dis. 2017;5(3):280-288.

76. Lopez-Otin C, Bond JS. Proteases: Multifunctional enzymes in life and disease. J Biol Chem. 2008;283(45):30433-30437.

77. Seidah NG, Chretien M, Day R. The family of subtilisin/kexin like pro-protein and pro-hormone convertases: Divergent or shared functions. Biochimie. 1994;76(3-4):197-209.

78. Turpeinen H, Ortutay Z, Pesu M. Genetics of the first seven proprotein convertase enzymes in health and disease. Curr Genomics. 2013;14(7):453-467.

79. Seidah NG, Mayer G, Zaid A, et al. The activation and physiological functions of the proprotein convertases. Int J Biochem Cell Biol. 2008;40(6-7):1111-1125.

80. Artenstein AW, Opal SM. Proprotein convertases in health and disease. N Engl J Med. 2011;365(26):2507-2518.

81. Siegfried G, Basak A, Cromlish JA, et al. The secretory proprotein convertases furin, PC5, and PC7 activate VEGF-C to induce tumorigenesis. J Clin Invest. 2003;111(11):1723-1732.

82. Khatib AM, Siegfried G, Chretien M, Metrakos P, Seidah NG. Proprotein convertases in tumor progression and malignancy: Novel targets in cancer therapy. Am J Pathol. 2002;160(6):1921-1935.

83. Oksanen A, Aittomäki S, Jankovic D, et al. Proprotein convertase FURIN constrains Th2 differentiation and is critical for host resistance against toxoplasma gondii. J Immunol. 2014;193(11):5470-5479.

84. Pesu M, Muul L, Kanno Y, O'Shea JJ. Proprotein convertase furin is preferentially expressed in T helper 1 cells and regulates interferon γ. Blood. 2006;108(3):983-985.

85. Vähätupa M, Aittomäki S, Martinez Cordova Z, et al. T-cell-expressed proprotein convertase FURIN inhibits DMBA/TPA-induced skin cancer development. Oncoimmunology. 2016;5(12):e1245266.

86. Bassi DE, Lopez De Cicco R, Mahloogi H, Zucker S, Thomas G, Klein-Szanto AJ. Furin inhibition results in absent or decreased invasiveness and tumorigenicity of human cancer cells. Proc Natl Acad Sci U S A. 2001;98(18):10326-10331.

87. Kanda A, Noda K, Saito W, Ishida S. (Pro)renin receptor is associated with angiogenic activity in proliferative diabetic retinopathy. Diabetologia. 2012;55(11):3104-3113.

88. Ma J, Evrard S, Badiola I, Siegfried G, Khatib AM. Regulation of the proprotein convertases expression and activity during regenerative angiogenesis: Role of hypoxia-inducible factor (HIF). Eur J Cell Biol. 2017;96(5):457-468.

89. McMahon S, Grondin F, McDonald PP, Richard DE, Dubois CM. Hypoxia-enhanced expression of the proprotein convertase furin is mediated by hypoxia-inducible factor-1: Impact on the bioactivation of proproteins. J Biol Chem. 2005;280(8):6561-6569.

90. Silvestri L, Pagani A, Camaschella C. Furin-mediated release of soluble hemojuvelin: A new link between hypoxia and iron homeostasis. Blood. 2008;111(2):924-931.

91. Siegfried G, Khatib AM, Benjannet S, Chretien M, Seidah NG. The proteolytic processing of pro-platelet-derived growth factor-A at RRKR(86) by members of the proprotein convertase family is functionally correlated to platelet-derived growth factor-A-induced functions and tumorigenicity. Cancer Res. 2003;63(7):1458-1463.

92. Siegfried G, Basak A, Prichett-Pejic W, et al. Regulation of the stepwise proteolytic cleavage and secretion of PDGF-B by the proprotein convertases. Oncogene. 2005;24(46):6925-6935.

93. Cui Y, Jean F, Thomas G, Christian JL. BMP-4 is proteolytically activated by furin and/or PC6 during vertebrate embryonic development. EMBO J. 1998;17(16):4735-4743.

94. Dubois CM, Blanchette F, Laprise MH, Leduc R, Grondin F, Seidah NG. Evidence that furin is an authentic transforming growth factor- β 1-converting enzyme. Am J Pathol. 2001;158(1):305-316.

95. Roebroek AJ, Umans L, Pauli IG, et al. Failure of ventral closure and axial rotation in embryos lacking the proprotein convertase furin. Development. 1998;125(24):4863-4876.

96. Scamuffa N, Calvo F, Chretien M, Seidah NG, Khatib AM. Proprotein convertases: Lessons from knockouts. FASEB J. 2006;20(12):1954-1963.

97. Kim W, Essalmani R, Szumska D, et al. Loss of endothelial furin leads to cardiac malformation and early postnatal death. Mol Cell Biol. 2012;32(17):3382-3391.

98. Yakala GK, Cabrera-Fuentes HA, Crespo-Avilan GE, et al. FURIN inhibition reduces vascular remodeling and atherosclerotic lesion progression in mice. Arterioscler Thromb Vasc Biol. 2019;39(3):387-401.

99. Xian X, Gopal S, Couchman JR. Syndecans as receptors and organizers of the extracellular matrix. Cell Tissue Res. 2010;339(1):31-46.

100. Couchman JR. Transmembrane signaling proteoglycans. Annu Rev Cell Dev Biol. 2010;26:89-114.

101. De Rossi G, Whiteford JR. Syndecans in angiogenesis and endothelial cell biology. Biochem Soc Trans. 2014;42(6):1643-1646.

102. Beauvais DM, Rapraeger AC. Syndecan-1-mediated cell spreading requires signaling by αvβ3 integrins in human breast carcinoma cells. Exp Cell Res. 2003;286(2):219-232.

103. Robinson CJ, Mulloy B, Gallagher JT, Stringer SE. VEGF165-binding sites within heparan sulfate encompass two highly sulfated domains and can be liberated by K5 lyase. J Biol Chem. 2006;281(3):1731-1740.

104. Ashikari-Hada S, Habuchi H, Kariya Y, Kimata K. Heparin regulates vascular endothelial growth factor165-dependent mitogenic activity, tube formation, and its receptor phosphorylation of human endothelial cells. Comparison of the effects of heparin and modified heparins. J Biol Chem. 2005;280(36):31508-31515.

105. Nishiguchi KM, Kataoka K, Kachi S, Komeima K, Terasaki H. Regulation of pathologic retinal angiogenesis in mice and inhibition of VEGF-VEGFR2 binding by soluble heparan sulfate. PLoS One. 2010;5(10):e13493.

106. Corti F, Wang Y, Rhodes JM, et al. N-terminal syndecan-2 domain selectively enhances 6-O heparan sulfate chains sulfation and promotes VEGFA165-dependent neovascularization. Nat Commun. 2019;10(1):1562-019-09605-z.

107. Echtermeyer F, Streit M, Wilcox-Adelman S, et al. Delayed wound repair and impaired angiogenesis in mice lacking syndecan-4. J Clin Invest. 2001;107(2):R9-R14.

108. Ishiguro K, Kadomatsu K, Kojima T, et al. Syndecan-4 deficiency impairs the fetal vessels in the placental labyrinth. Dev Dyn. 2000;219(4):539-544.

109. Vuong TT, Reine TM, Sudworth A, Jenssen TG, Kolset SO. Syndecan-4 is a major syndecan in primary human endothelial cells in vitro, modulated by inflammatory stimuli and involved in wound healing. J Histochem Cytochem. 2015;63(4):280-292.

110. Hoon M, Okawa H, Della Santina L, Wong RO. Functional architecture of the retina: Development and disease. Prog Retin Eye Res. 2014;42:44-84.

111. Masland RH. The neuronal organization of the retina. Neuron. 2012;76(2):266-280.

112. Curcio CA, Sloan KR, Kalina RE, Hendrickson AE. Human photoreceptor topography. J Comp Neurol. 1990;292(4):497-523.

113. Jeon CJ, Strettoi E, Masland RH. The major cell populations of the mouse retina. J Neurosci. 1998;18(21):8936-8946.

114. Mannu GS. Retinal phototransduction. Neurosciences (Riyadh). 2014;19(4):275-280.

115. Newman E, Reichenbach A. The muller cell: A functional element of the retina. Trends Neurosci. 1996;19(8):307-312.

116. Reichenbach A, Bringmann A. New functions of muller cells. Glia. 2013;61(5):651-678.

117. Brew H, Attwell D. Electrogenic glutamate uptake is a major current carrier in the membrane of axolotl retinal glial cells. Nature. 1987;327(6124):707-709.

118. Li X, Liu J, Hoh J, Liu J. Muller cells in pathological retinal angiogenesis. Transl Res. 2018.

119. Vecino E, Rodriguez FD, Ruzafa N, Pereiro X, Sharma SC. Glia-neuron interactions in the mammalian retina. Prog Retin Eye Res. 2016;51:1-40.

120. Tao C, Zhang X. Development of astrocytes in the vertebrate eye. Dev Dyn. 2014;243(12):1501-1510.

121. Sparrow JR, Hicks D, Hamel CP. The retinal pigment epithelium in health and disease. Curr Mol Med. 2010;10(9):802-823.

122. Kevany BM, Palczewski K. Phagocytosis of retinal rod and cone photoreceptors. Physiology (Bethesda). 2010;25(1):8-15.

123. Booij JC, Baas DC, Beisekeeva J, Gorgels TG, Bergen AA. The dynamic nature of bruch's membrane. Prog Retin Eye Res. 2010;29(1):1-18.

124. Chase J. The evolution of retinal vascularization in mammals. A comparison of vascular and avascular retinae. Ophthalmology. 1982;89(12):1518-1525.

125. Provis JM. Development of the primate retinal vasculature. Prog Retin Eye Res. 2001;20(6):799-821.

126. Hughes S, Yang H, Chan-Ling T. Vascularization of the human fetal retina: Roles of vasculogenesis and angiogenesis. Invest Ophthalmol Vis Sci. 2000;41(5):1217-1228.

127. Gariano RF, Gardner TW. Retinal angiogenesis in development and disease. Nature. 2005;438(7070):960-966.

128. Ito M, Yoshioka M. Regression of the hyaloid vessels and pupillary membrane of the mouse. Anat Embryol (Berl). 1999;200(4):403-411.

129. Stahl A, Connor KM, Sapieha P, et al. The mouse retina as an angiogenesis model. Invest Ophthalmol Vis Sci. 2010;51(6):2813-2826.

130. Selvam S, Kumar T, Fruttiger M. Retinal vasculature development in health and disease. Prog Retin Eye Res. 2018;63:1-19.

131. Korn C, Augustin HG. Mechanisms of vessel pruning and regression. Dev Cell. 2015;34(1):5-17.

132. Fruttiger M, Calver AR, Kruger WH, et al. PDGF mediates a neuron-astrocyte interaction in the developing retina. Neuron. 1996;17(6):1117-1131.

133. Stone J, Itin A, Alon T, et al. Development of retinal vasculature is mediated by hypoxia-induced vascular endothelial growth factor (VEGF) expression by neuroglia. J Neurosci. 1995;15(7 Pt 1):4738-4747.

134. Joyal JS, Nim S, Zhu T, et al. Subcellular localization of coagulation factor II receptor-like 1 in neurons governs angiogenesis. Nat Med. 2014;20(10):1165-1173.

135. Foulds WS, Kaur C, Luu CD, Kek WK. A role for photoreceptors in retinal oedema and angiogenesis: An additional explanation for laser treatment? Eye (Lond). 2010;24(5):918-926.

136. Fukushima Y, Okada M, Kataoka H, et al. Sema3E-PlexinD1 signaling selectively suppresses disoriented angiogenesis in ischemic retinopathy in mice. J Clin Invest. 2011;121(5):1974-1985.

137. Gerhardt H, Golding M, Fruttiger M, et al. VEGF guides angiogenic sprouting utilizing endothelial tip cell filopodia. J Cell Biol. 2003;161(6):1163-1177.

138. Jakobsson L, Franco CA, Bentley K, et al. Endothelial cells dynamically compete for the tip cell position during angiogenic sprouting. Nat Cell Biol. 2010;12(10):943-953.

139. Hellstrom M, Phng LK, Hofmann JJ, et al. Dll4 signalling through Notch1 regulates formation of tip cells during angiogenesis. Nature. 2007;445(7129):776-780.

140. Armulik A, Genove G, Betsholtz C. Pericytes: Developmental, physiological, and pathological perspectives, problems, and promises. Dev Cell. 2011;21(2):193-215.

141. Andrae J, Gallini R, Betsholtz C. Role of platelet-derived growth factors in physiology and medicine. Genes Dev. 2008;22(10):1276-1312.

142. Weidemann A, Krohne TU, Aguilar E, et al. Astrocyte hypoxic response is essential for pathological but not developmental angiogenesis of the retina. Glia. 2010;58(10):1177-1185.

143. Nakamura-Ishizu A, Kurihara T, Okuno Y, et al. The formation of an angiogenic astrocyte template is regulated by the neuroretina in a HIF-1-dependent manner. Dev Biol. 2012;363(1):106-114.

144. Eichler W, Yafai Y, Keller T, Wiedemann P, Reichenbach A. PEDF derived from glial muller cells: A possible regulator of retinal angiogenesis. Exp Cell Res. 2004;299(1):68-78.

145. Eichler W, Yafai Y, Wiedemann P, Reichenbach A. Angiogenesis-related factors derived from retinal glial (muller) cells in hypoxia. Neuroreport. 2004;15(10):1633-1637.

146. Behzadian MA, Wang XL, Windsor LJ, Ghaly N, Caldwell RB. TGF-β increases retinal endothelial cell permeability by increasing MMP-9: Possible role of glial cells in endothelial barrier function. Invest Ophthalmol Vis Sci. 2001;42(3):853-859.

147. Shen W, Fruttiger M, Zhu L, et al. Conditional mullercell ablation causes independent neuronal and vascular pathologies in a novel transgenic model. J Neurosci. 2012;32(45):15715-15727.

148. Rathnasamy G, Foulds WS, Ling EA, Kaur C. Retinal microglia - A key player in healthy and diseased retina. Prog Neurobiol. 2019;173:18-40.

149. Santos AM, Calvente R, Tassi M, et al. Embryonic and postnatal development of microglial cells in the mouse retina. J Comp Neurol. 2008;506(2):224-239.

150. Yang P, Das PK, Kijlstra A. Localization and characterization of immunocompetent cells in the human retina. Ocul Immunol Inflamm. 2000;8(3):149-157.

151. Silverman SM, Wong WT. Microglia in the retina: Roles in development, maturity, and disease. Annu Rev Vis Sci. 2018;4:45-77.

152. Checchin D, Sennlaub F, Levavasseur E, Leduc M, Chemtob S. Potential role of microglia in retinal blood vessel formation. Invest Ophthalmol Vis Sci. 2006;47(8):3595-3602.

153. Congdon NG, Friedman DS, Lietman T. Important causes of visual impairment in the world today. JAMA. 2003;290(15):2057-2060.

154. Fong DS, Aiello L, Gardner TW, et al. Retinopathy in diabetes. Diabetes Care. 2004;27 Suppl 1:S84-7.

155. Leasher JL, Bourne RR, Flaxman SR, et al. Global estimates on the number of people blind or visually impaired by diabetic retinopathy: A meta-analysis from 1990 to 2010. Diabetes Care. 2016;39(9):1643-1649.

156. Saaddine JB, Honeycutt AA, Narayan KM, Zhang X, Klein R, Boyle JP. Projection of diabetic retinopathy and other major eye diseases among people with diabetes mellitus: United states, 2005-2050. Arch Ophthalmol. 2008;126(12):1740-1747.

157. Yau JW, Rogers SL, Kawasaki R, et al. Global prevalence and major risk factors of diabetic retinopathy. Diabetes Care. 2012;35(3):556-564.

158. Wong TY, Klein R, Islam FM, et al. Diabetic retinopathy in a multi-ethnic cohort in the united states. Am J Ophthalmol. 2006;141(3):446-455.

159. Stitt AW, Curtis TM, Chen M, et al. The progress in understanding and treatment of diabetic retinopathy. Prog Retin Eye Res. 2016;51:156-186.

160. Aiello LP. The potential role of PKC β in diabetic retinopathy and macular edema. Surv Ophthalmol. 2002;47 Suppl 2:S263-9.

161. Caldwell RB, Bartoli M, Behzadian MA, et al. Vascular endothelial growth factor and diabetic retinopathy: Role of oxidative stress. Curr Drug Targets. 2005;6(4):511-524.

162. Beltramo E, Porta M. Pericyte loss in diabetic retinopathy: Mechanisms and consequences. Curr Med Chem. 2013;20(26):3218-3225.

163. Campochiaro PA. Ocular neovascularization. J Mol Med (Berl). 2013;91(3):311-321.

164. Iandiev I, Uckermann O, Pannicke T, et al. Glial cell reactivity in a porcine model of retinal detachment. Invest Ophthalmol Vis Sci. 2006;47(5):2161-2171.

165. Friedlander M. Fibrosis and diseases of the eye. J Clin Invest. 2007;117(3):576-586.

166. Gardner TW, Davila JR. The neurovascular unit and the pathophysiologic basis of diabetic retinopathy. Graefes Arch Clin Exp Ophthalmol. 2017;255(1):1-6.

167. Cheung N, Mitchell P, Wong TY. Diabetic retinopathy. Lancet. 2010;376(9735):124-136.

168. Antonetti DA, Barber AJ, Bronson SK, et al. Diabetic retinopathy: Seeing beyond glucose-induced microvascular disease. Diabetes. 2006;55(9):2401-2411.

169. Blencowe H, Lawn JE, Vazquez T, Fielder A, Gilbert C. Preterm-associated visual impairment and estimates of retinopathy of prematurity at regional and global levels for 2010. Pediatr Res. 2013;74 Suppl 1:35-49.

170. Ludwig CA, Chen TA, Hernandez-Boussard T, Moshfeghi AA, Moshfeghi DM. The epidemiology of retinopathy of prematurity in the united states. Ophthalmic Surg Lasers Imaging Retina. 2017;48(7):553-562.

171. Lee J, Dammann O. Perinatal infection, inflammation, and retinopathy of prematurity. Semin Fetal Neonatal Med. 2012;17(1):26-29.

172. Terry TL. Fibroblastic overgrowth of persistent tunica vasculosa lentis in infants born prematurely: II. report of cases-clinical aspects. Trans Am Ophthalmol Soc. 1942;40:262-284.

173. Jefferies AL, Canadian Paediatric Society, Fetus and Newborn Committee. Retinopathy of prematurity: An update on screening and management. Paediatr Child Health. 2016;21(2):101-108.

174. Shah PK, Prabhu V, Karandikar SS, Ranjan R, Narendran V, Kalpana N. Retinopathy of prematurity: Past, present and future. World J Clin Pediatr. 2016;5(1):35-46.

175. Rogers S, McIntosh RL, Cheung N, et al. The prevalence of retinal vein occlusion: Pooled data from population studies from the United States, Europe, Asia, and Australia. Ophthalmology. 2010;117(2):313-9.e1.

176. Hayreh SS, Zimmerman MB, Podhajsky P. Incidence of various types of retinal vein occlusion and their recurrence and demographic characteristics. Am J Ophthalmol. 1994;117(4):429-441.

177. Natural history and clinical management of central retinal vein occlusion. The central vein occlusion study group. Arch Ophthalmol. 1997;115(4):486-491.

178. Risk factors for branch retinal vein occlusion. The eye disease case-control study group. Am J Ophthalmol. 1993;116(3):286-296.

179. Ip M, Hendrick A. Retinal vein occlusion review. Asia Pac J Ophthalmol (Phila). 2018;7(1):40-45.

180. Smith W, Assink J, Klein R, et al. Risk factors for age-related macular degeneration: Pooled findings from three continents. Ophthalmology. 2001;108(4):697-704.

181. Al-Zamil WM, Yassin SA. Recent developments in age-related macular degeneration: A review. Clin Interv Aging. 2017;12:1313-1330.

182. Klein R, Klein BE, Linton KL, DeMets DL. The Beaver Dam Eye Study: The relation of age-related maculopathy to smoking. Am J Epidemiol. 1993;137(2):190-200.

183. Aiello LP, Avery RL, Arrigg PG, et al. Vascular endothelial growth factor in ocular fluid of patients with diabetic retinopathy and other retinal disorders. N Engl J Med. 1994;331(22):1480-1487.

184. Kliffen M, Sharma HS, Mooy CM, Kerkvliet S, de Jong PT. Increased expression of angiogenic growth factors in age-related maculopathy. Br J Ophthalmol. 1997;81(2):154-162.

185. Yoshimura T, Sonoda KH, Sugahara M, et al. Comprehensive analysis of inflammatory immune mediators in vitreoretinal diseases. PLoS One. 2009;4(12):e8158.

186. Khalaf N, Helmy H, Labib H, Fahmy I, El Hamid MA, Moemen L. Role of angiopoietins and tie-2 in diabetic retinopathy. Electron Physician. 2017;9(8):5031-5035.

187. Nguyen QD, De Falco S, Behar-Cohen F, et al. Placental growth factor and its potential role in diabetic retinopathy and other ocular neovascular diseases. Acta Ophthalmol. 2018;96(1):e1-e9.

188. Amin R, Puklin JE, Frank RN. Growth factor localization in choroidal neovascular membranes of age-related macular degeneration. Invest Ophthalmol Vis Sci. 1994;35(8):3178-3188.

189. Cabral T, Mello LGM, Lima LH, et al. Retinal and choroidal angiogenesis: A review of new targets. Int J Retina Vitreous. 2017;3:31-017-0084-9.

190. Fagiani E, Christofori G. Angiopoietins in angiogenesis. Cancer Lett. 2013;328(1):18-26.

191. Hakanpää L, Sipilä T, Leppänen VM, et al. Endothelial destabilization by angiopoietin-2 via integrin β1 activation. Nat Commun. 2015;6:5962.

192. Benest AV, Kruse K, Savant S, et al. Angiopoietin-2 is critical for cytokine-induced vascular leakage. PLoS One. 2013;8(8):e70459.

193. Ng DS, Yip YW, Bakthavatsalam M, et al. Elevated angiopoietin 2 in aqueous of patients with neovascular age related macular degeneration correlates with disease severity at presentation. Sci Rep. 2017;7:45081.

194. Sato T, Shima C, Kusaka S. Vitreous levels of angiopoietin-1 and angiopoietin-2 in eyes with retinopathy of prematurity. Am J Ophthalmol. 2011;151(2):353-7.e1.

195. Grigsby JG, Cardona SM, Pouw CE, et al. The role of microglia in diabetic retinopathy. J Ophthalmol. 2014;2014:705783.

196. Rungger-Brandle E, Dosso AA, Leuenberger PM. Glial reactivity, an early feature of diabetic retinopathy. Invest Ophthalmol Vis Sci. 2000;41(7):1971-1980.

197. Grunewald M, Avraham I, Dor Y, et al. VEGF-induced adult neovascularization: Recruitment, retention, and role of accessory cells. Cell. 2006;124(1):175-189.

198. Lobov IB, Rao S, Carroll TJ, et al. WNT7b mediates macrophage-induced programmed cell death in patterning of the vasculature. Nature. 2005;437(7057):417-421.

199. Apte RS, Richter J, Herndon J, Ferguson TA. Macrophages inhibit neovascularization in a murine model of age-related macular degeneration. PLoS Med. 2006;3(8):e310.

200. Lu P, Li L, Liu G, van Rooijen N, Mukaida N, Zhang X. Opposite roles of CCR2 and CX3CR1 macrophages in alkali-induced corneal neovascularization. Cornea. 2009;28(5):562-569.

201. Dong A, Xie B, Shen J, et al. Oxidative stress promotes ocular neovascularization. J Cell Physiol. 2009;219(3):544-552.

202. Kim LA, D'Amore PA. A brief history of anti-VEGF for the treatment of ocular angiogenesis. Am J Pathol. 2012;181(2):376-379.

203. Balaratnasingam C, Dhrami-Gavazi E, McCann JT, Ghadiali Q, Freund KB. Aflibercept: A review of its use in the treatment of choroidal neovascularization due to age-related macular degeneration. Clin Ophthalmol. 2015;9:2355-2371.

204. Chiang A, Regillo CD. Preferred therapies for neovascular age-related macular degeneration. Curr Opin Ophthalmol. 2011;22(3):199-204.

205. Avery RL, Pearlman J, Pieramici DJ, et al. Intravitreal bevacizumab (avastin) in the treatment of proliferative diabetic retinopathy. Ophthalmology. 2006;113(10):1695.e1-1695.15.

206. Rosenfeld PJ, Moshfeghi AA, Puliafito CA. Optical coherence tomography findings after an intravitreal injection of bevacizumab (avastin) for neovascular age-related macular degeneration. Ophthalmic Surg Lasers Imaging. 2005;36(4):331-335.

207. Gragoudas ES, Adamis AP, Cunningham ET,Jr, Feinsod M, Guyer DR, VEGF Inhibition Study in Ocular Neovascularization Clinical Trial Group. Pegaptanib for neovascular age-related macular degeneration. N Engl J Med. 2004;351(27):2805-2816.

208. Chen Y, Wiesmann C, Fuh G, et al. Selection and analysis of an optimized anti-VEGF antibody: Crystal structure of an affinity-matured fab in complex with antigen. J Mol Biol. 1999;293(4):865-881.

209. Heier JS, Brown DM, Chong V, et al. Intravitreal aflibercept (VEGF trap-eye) in wet age-related macular degeneration. Ophthalmology. 2012;119(12):2537-2548.

210. Sarwar S, Bakbak B, Sadiq MA, et al. Fusion proteins: Aflibercept (VEGF trap-eye). Dev Ophthalmol. 2016;55:282-294.

211. Papadopoulos N, Martin J, Ruan Q, et al. Binding and neutralization of vascular endothelial growth factor (VEGF) and related ligands by VEGF trap, ranibizumab and bevacizumab. Angiogenesis. 2012;15(2):171-185.

212. Van der Giet M, Henkel C, Schuchardt M, Tolle M. Anti-VEGF drugs in eye diseases: Local therapy with potential systemic effects. Curr Pharm Des. 2015;21(24):3548-3556.

213. Yang S, Zhao J, Sun X. Resistance to anti-VEGF therapy in neovascular age-related macular degeneration: A comprehensive review. Drug Des Devel Ther. 2016;10:1857-1867.

214. Miyamoto N, Mandai M, Kojima H, et al. Response of eyes with age-related macular degeneration to anti-VEGF drugs and implications for therapy planning. Clin Ophthalmol. 2017;11:809-816.

215. Lux A, Llacer H, Heussen FM, Joussen AM. Non-responders to bevacizumab (avastin) therapy of choroidal neovascular lesions. Br J Ophthalmol. 2007;91(10):1318-1322.

216. Dossarps D, Bron AM, Koehrer P, Aho-Glele LS, Creuzot-Garcher C, FRCR net (FRenCh Retina specialists net). Endophthalmitis after intravitreal injections: Incidence, presentation, management, and visual outcome. Am J Ophthalmol. 2015;160(1):17-25.e1.

217. Falavarjani KG, Nguyen QD. Adverse events and complications associated with intravitreal injection of anti-VEGF agents: A review of literature. Eye (Lond). 2013;27(7):787-794.

218. Zehetner C, Kirchmair R, Huber S, Kralinger MT, Kieselbach GF. Plasma levels of vascular endothelial growth factor before and after intravitreal injection of bevacizumab, ranibizumab and pegaptanib in patients with age-related macular degeneration, and in patients with diabetic macular oedema. Br J Ophthalmol. 2013;97(4):454-459.

219. Wang X, Sawada T, Sawada O, Saishin Y, Liu P, Ohji M. Serum and plasma vascular endothelial growth factor concentrations before and after intravitreal injection of aflibercept or ranibizumab for age-related macular degeneration. Am J Ophthalmol. 2014;158(4):738-744.e1.

220. Huang CY, Lien R, Wang NK, et al. Changes in systemic vascular endothelial growth factor levels after intravitreal injection of aflibercept in infants with retinopathy of prematurity. Graefes Arch Clin Exp Ophthalmol. 2018;256(3):479-487.

221. Meadows KL, Hurwitz HI. Anti-VEGF therapies in the clinic. Cold Spring Harb Perspect Med. 2012;2(10):10.1101/cshperspect.a006577.

222. Kurihara T, Westenskow PD, Bravo S, Aguilar E, Friedlander M. Targeted deletion of Vegfa in adult mice induces vision loss. J Clin Invest. 2012;122(11):4213-4217.

223. Stone J, Chan-Ling T, Pe'er J, Itin A, Gnessin H, Keshet E. Roles of vascular endothelial growth factor and astrocyte degeneration in the genesis of retinopathy of prematurity. Invest Ophthalmol Vis Sci. 1996;37(2):290-299.

224. Nishijima K, Ng YS, Zhong L, et al. Vascular endothelial growth factor-A is a survival factor for retinal neurons and a critical neuroprotectant during the adaptive response to ischemic injury. Am J Pathol. 2007;171(1):53-67.

225. Saint-Geniez M, Maharaj AS, Walshe TE, et al. Endogenous VEGF is required for visual function: Evidence for a survival role on muller cells and photoreceptors. PLoS One. 2008;3(11):e3554.

226. Ford KM, Saint-Geniez M, Walshe T, Zahr A, D'Amore PA. Expression and role of VEGF in the adult retinal pigment epithelium. Invest Ophthalmol Vis Sci. 2011;52(13):9478-9487.

227. Lohela M, Bry M, Tammela T, Alitalo K. VEGFs and receptors involved in angiogenesis versus lymphangiogenesis. Curr Opin Cell Biol. 2009;21(2):154-165.

228. Bogdanov P, Corraliza L, Villena JA, et al. The db/db mouse: A useful model for the study of diabetic retinal neurodegeneration. PLoS One. 2014;9(5):e97302.

229. Ward DT, Yau SK, Mee AP, et al. Functional, molecular, and biochemical characterization of streptozotocin-induced diabetes. J Am Soc Nephrol. 2001;12(4):779-790.

230. Patz A. The role of oxygen in retrolental fibroplasia. Albrecht Von Graefes Arch Klin Exp Ophthalmol. 1975;195(2):77-85.

231. Patz A. Current concepts of the effect of oxygen on the developing retina. Curr Eye Res. 1984;3(1):159-163.

232. Patz A, Eastham A, Higginbotham DH, Kleh T. Oxygen studies in retrolental fibroplasia. II. The production of the microscopic changes of retrolental fibroplasia in experimental animals. Am J Ophthalmol. 1953;36(11):1511-1522.

233. Smith LE, Wesolowski E, McLellan A, et al. Oxygen-induced retinopathy in the mouse. Invest Ophthalmol Vis Sci. 1994;35(1):101-111.

234. Scott A, Fruttiger M. Oxygen-induced retinopathy: A model for vascular pathology in the retina. Eye (Lond). 2010;24(3):416-421.

235. Kim CB, D'Amore PA, Connor KM. Revisiting the mouse model of oxygen-induced retinopathy. Eye Brain. 2016;8:67-79.

236. Benjamin LE, Hemo I, Keshet E. A plasticity window for blood vessel remodelling is defined by pericyte coverage of the preformed endothelial network and is regulated by PDGF-B and VEGF. Development. 1998;125(9):1591-1598.

237. Connor KM, Krah NM, Dennison RJ, et al. Quantification of oxygen-induced retinopathy in the mouse: A model of vessel loss, vessel regrowth and pathological angiogenesis. Nat Protoc. 2009;4(11):1565-1573.

238. Barnett JM, Yanni SE, Penn JS. The development of the rat model of retinopathy of prematurity. Doc Ophthalmol. 2010;120(1):3-12.

239. Ritter MR, Banin E, Moreno SK, Aguilar E, Dorrell MI, Friedlander M. Myeloid progenitors differentiate into microglia and promote vascular repair in a model of ischemic retinopathy. J Clin Invest. 2006;116(12):3266-3276.

240. Scott A, Powner MB, Fruttiger M. Quantification of vascular tortuosity as an early outcome measure in oxygen induced retinopathy (OIR). Exp Eye Res. 2014;120:55-60.

241. Tobe T, Ortega S, Luna JD, et al. Targeted disruption of the FGF2 gene does not prevent choroidal neovascularization in a murine model. Am J Pathol. 1998;153(5):1641-1646.

242. Rakic JM, Lambert V, Devy L, et al. Placental growth factor, a member of the VEGF family, contributes to the development of choroidal neovascularization. Invest Ophthalmol Vis Sci. 2003;44(7):3186-3193.

243. Lambert V, Wielockx B, Munaut C, et al. MMP-2 and MMP-9 synergize in promoting choroidal neovascularization. FASEB J. 2003;17(15):2290-2292.

244. Zhou J, Pham L, Zhang N, et al. Neutrophils promote experimental choroidal neovascularization. Mol Vis. 2005;11:414-424.

245. Ragauskas S, Kielczewski E, Vance J, Kaja S, Kalesnykas G. In vivo multimodal imaging and analysis of mouse laser-induced choroidal neovascularization model. J Vis Exp. 2018;(131). doi(131):10.3791/56173.

246. Giani A, Thanos A, Roh MI, et al. In vivo evaluation of laser-induced choroidal neovascularization using spectral-domain optical coherence tomography. Invest Ophthalmol Vis Sci. 2011;52(6):3880-3887.

247. Zambrowicz BP, Friedrich GA, Buxton EC, Lilleberg SL, Person C, Sands AT. Disruption and sequence identification of 2,000 genes in mouse embryonic stem cells. Nature. 1998;392(6676):608-611.

248. Ishiguro K, Kadomatsu K, Kojima T, et al. Syndecan-4 deficiency impairs focal adhesion formation only under restricted conditions. J Biol Chem. 2000;275(8):5249-5252.

249. Roebroek AJ, Taylor NA, Louagie E, et al. Limited redundancy of the proprotein convertase furin in mouse liver. J Biol Chem. 2004;279(51):53442-53450.

250. Cordova ZM, Gronholm A, Kytölä V, et al. Myeloid cell expressed proprotein convertase FURIN attenuates inflammation. Oncotarget. 2016;7(34):54392-54404.

251. Sauer B. Inducible gene targeting in mice using the cre/lox system. Methods. 1998;14(4):381-392.

252. DiGiovanni J. Multistage carcinogenesis in mouse skin. Pharmacol Ther. 1992;54(1):63-128.

253. Abel EL, Angel JM, Kiguchi K, DiGiovanni J. Multi-stage chemical carcinogenesis in mouse skin: Fundamentals and applications. Nat Protoc. 2009;4(9):1350-1362.

254. Perez-Losada J, Balmain A. Stem-cell hierarchy in skin cancer. Nat Rev Cancer. 2003;3(6):434-443.

255. Stahl A, Chen J, Sapieha P, et al. Postnatal weight gain modifies severity and functional outcome of oxygen-induced proliferative retinopathy. Am J Pathol. 2010;177(6):2715-2723.

256. Tahergorabi Z, Khazaei M. A review on angiogenesis and its assays. Iran J Basic Med Sci. 2012;15(6):1110-1126.

257. Nicosia RF. The aortic ring model of angiogenesis: A quarter century of search and discovery. J Cell Mol Med. 2009;13(10):4113-4136.

258. Shao Z, Friedlander M. Choroid sprouting assay: An ex vivo model of microvascular angiogenesis. 2013;8(7):e69552.

259. Livak KJ, Schmittgen TD. Analysis of relative gene expression data using real-time quantitative PCR and the $2^{-\Delta\Delta Ct}$ method. Methods. 2001;25(4):402-408.

260. Scheppke L, Aguilar E, Gariano RF, et al. Retinal vascular permeability suppression by topical application of a novel VEGFR2/src kinase inhibitor in mice and rabbits. J Clin Invest. 2008;118(6):2337-2346.

261. Xu Q, Qaum T, Adamis AP. Sensitive blood-retinal barrier breakdown quantitation using evans blue. Invest Ophthalmol Vis Sci. 2001;42(3):789-794.

262. Golias C, Charalabopoulos A, Stagikas D, Charalabopoulos K, Batistatou A. The kinin system--bradykinin: Biological effects and clinical implications. Multiple role of the kinin system--bradykinin. Hippokratia. 2007;11(3):124-128.

263. Cifani P, Kentsis A. Towards comprehensive and quantitative proteomics for diagnosis and therapy of human disease. Proteomics. 2017;17(1-2):10.1002/pmic.201600079. Epub 2016 Dec 21.

264. Gillet LC, Navarro P, Tate S, et al. Targeted data extraction of the MS/MS spectra generated by data-independent acquisition: A new concept for consistent and accurate proteome analysis. Mol Cell Proteomics. 2012;11(6):O111.016717.

265. Rost HL, Rosenberger G, Navarro P, et al. OpenSWATH enables automated, targeted analysis of data-independent acquisition MS data. Nat Biotechnol. 2014;32(3):219-223.

266. Jylhä A, Nättinen J, Aapola U, et al. Comparison of iTRAQ and SWATH in a clinical study with multiple time points. Clin Proteomics. 2018;15:24-018-9201-5. eCollection 2018.

267. Rosenberger G, Koh CC, Guo T, et al. A repository of assays to quantify 10,000 human proteins by SWATH-MS. Sci Data. 2014;1:140031.

268. Vessey KA, Wilkinson-Berka JL, Fletcher EL. Characterization of retinal function and glial cell response in a mouse model of oxygen-induced retinopathy. J Comp Neurol. 2011;519(3):506-527.

269. Mehdi MK, Sage-Ciocca D, Challet E, Malan A, Hicks D. Oxygen-induced retinopathy induces short-term glial stress and long-term impairment of

photoentrainment in mice. Graefes Arch Clin Exp Ophthalmol. 2014;252(4):595-608.

270. Kim SJ, Jin J, Kim YJ, Kim Y, Yu HG. Retinal proteome analysis in a mouse model of oxygen-induced retinopathy. J Proteome Res. 2012;11(11):5186-5203.

271. Tu C, Beharry KD, Shen X, et al. Proteomic profiling of the retinas in a neonatal rat model of oxygen-induced retinopathy with a reproducible ion-current-based MS1 approach. J Proteome Res. 2015;14(5):2109-2120.

272. Nättinen J, Jylhä A, Aapola U, et al. Topical fluorometholone treatment and desiccating stress change inflammatory protein expression in tears. Ocul Surf. 2018;16(1):84-92.

273. FANTOM Consortium and the RIKEN PMI and CLST (DGT), Forrest AR, Kawaji H, et al. A promoter-level mammalian expression atlas. Nature. 2014;507(7493):462-470.

274. Siegert S, Cabuy E, Scherf BG, et al. Transcriptional code and disease map for adult retinal cell types. Nat Neurosci. 2012;15(3):487-95, S1-2.

275. Barker H, Aaltonen M, Pan P, et al. Role of carbonic anhydrases in skin wound healing. Exp Mol Med. 2017;49(5):e334.

276. Zheng X, Zhou AX, Rouhi P, et al. Hypoxia-induced and calpain-dependent cleavage of filamin A regulates the hypoxic response. Proc Natl Acad Sci U S A. 2014;111(7):2560-2565.

277. Johns SC, Yin X, Jeltsch M, et al. Functional importance of a proteoglycan coreceptor in pathologic lymphangiogenesis. Circ Res. 2016;119(2):210-221.

278. Morgan MR, Hamidi H, Bass MD, Warwood S, Ballestrem C, Humphries MJ. Syndecan-4 phosphorylation is a control point for integrin recycling. Dev Cell. 2013;24(5):472-485.

279. Bertrand J, Stange R, Hidding H, et al. Syndecan 4 supports bone fracture repair, but not fetal skeletal development, in mice. Arthritis Rheum. 2013;65(3):743-752.

280. Sawada J, Komatsu M. Normalization of tumor vasculature by R-Ras. Cell Cycle. 2012;11(23):4285-4286.

281. Hellstrom M, Gerhardt H, Kalen M, et al. Lack of pericytes leads to endothelial hyperplasia and abnormal vascular morphogenesis. J Cell Biol. 2001;153(3):543-553.

282. Von Tell D, Armulik A, Betsholtz C. Pericytes and vascular stability. Exp Cell Res. 2006;312(5):623-629.

283. Jain RK, Booth MF. What brings pericytes to tumor vessels? J Clin Invest. 2003;112(8):1134-1136.

284. Gawecka JE, Griffiths GS, Ek-Rylander B, Ramos JW, Matter ML. R-ras regulates migration through an interaction with filamin A in melanoma cells. PLoS One. 2010;5(6):e11269.

285. Griffiths GS, Grundl M, Allen JS,3rd, Matter ML. R-Ras interacts with filamin a to maintain endothelial barrier function. J Cell Physiol. 2011;226(9):2287-2296.

286. Li F, Sawada J, Komatsu M. R-Ras-Akt axis induces endothelial lumenogenesis and regulates the patency of regenerating vasculature. Nat Commun. 2017;8(1):1720-017-01865-x.

287. Allingham MJ, van Buul JD, Burridge K. ICAM-1-mediated, src- and Pyk2-dependent vascular endothelial cadherin tyrosine phosphorylation is required for leukocyte transendothelial migration. J Immunol. 2007;179(6):4053-4064.

288. Weis SM, Cheresh DA. Pathophysiological consequences of VEGF-induced vascular permeability. Nature. 2005;437(7058):497-504.

289. Wallez Y, Cand F, Cruzalegui F, et al. Src kinase phosphorylates vascular endothelial-cadherin in response to vascular endothelial growth factor: Identification of tyrosine 685 as the unique target site. Oncogene. 2007;26(7):1067-1077.

290. Aragon-Sanabria V, Pohler SE, Eswar VJ, Bierowski M, Gomez EW, Dong C. VE-cadherin disassembly and cell contractility in the endothelium are necessary for barrier disruption induced by tumor cells. Sci Rep. 2017;7:45835.

291. Xiao K, Garner J, Buckley KM, et al. p120-catenin regulates clathrin-dependent endocytosis of VE-cadherin. Mol Biol Cell. 2005;16(11):5141-5151.

292. Ichimiya H, Maeda K, Enomoto A, Weng L, Takahashi M, Murohara T. Girdin/GIV regulates transendothelial permeability by controlling VE-cadherin trafficking through the small GTPase, R-ras. Biochem Biophys Res Commun. 2015;461(2):260-267.

293. Woods A, Couchman JR. Syndecan 4 heparan sulfate proteoglycan is a selectively enriched and widespread focal adhesion component. Mol Biol Cell. 1994;5(2):183-192.

294. Ting KK, Zhao Y, Shen W, et al. Therapeutic regulation of VE-cadherin with a novel oligonucleotide drug for diabetic eye complications using retinopathy mouse models. Diabetologia. 2019;62(2):322-334.

295. Davidson MK, Russ PK, Glick GG, Hoffman LH, Chang MS, Haselton FR. Reduced expression of the adherens junction protein cadherin-5 in a diabetic retina. Am J Ophthalmol. 2000;129(2):267-269.

296. Diokmetzidou A, Soumaka E, Kloukina I, et al. Desmin and αB-crystallin interplay in the maintenance of mitochondrial homeostasis and cardiomyocyte survival. J Cell Sci. 2016;129(20):3705-3720.

297. Kannan R, Sreekumar PG, Hinton DR. α crystallins in the retinal pigment epithelium and implications for the pathogenesis and treatment of age-related macular degeneration. Biochim Biophys Acta. 2016;1860(1):258-268.

298. Sinha D, Klise A, Sergeev Y, et al. βA3/A1-crystallin in astroglial cells regulates retinal vascular remodeling during development. Mol Cell Neurosci. 2008;37(1):85-95.

299. Zhang C, Gehlbach P, Gongora C, et al. A potential role for β- and γ-crystallins in the vascular remodeling of the eye. Dev Dyn. 2005;234(1):36-47.

300. Nagaraj RH, Nahomi RB, Mueller NH, Raghavan CT, Ammar DA, Petrash JM. Therapeutic potential of α-crystallin. Biochim Biophys Acta. 2016;1860(1 Pt B):252-257.

301. Kim YH, Park SY, Park J, et al. Reduction of experimental diabetic vascular leakage and pericyte apoptosis in mice by delivery of αA-crystallin with a recombinant adenovirus. Diabetologia. 2012;55(10):2835-2844.

302. Kase S, He S, Sonoda S, et al. αB-crystallin regulation of angiogenesis by modulation of VEGF. Blood. 2010;115(16):3398-3406.

303. Kannan R, Sreekumar PG, Hinton DR. Novel roles for α-crystallins in retinal function and disease. Prog Retin Eye Res. 2012;31(6):576-604.

304. Ishikawa K, Sreekumar PG, Spee C, et al. αB-crystallin regulates subretinal fibrosis by modulation of epithelial-mesenchymal transition. Am J Pathol. 2016;186(4):859-873.

305. Dimberg A, Rylova S, Dieterich LC, et al. αB-crystallin promotes tumor angiogenesis by increasing vascular survival during tube morphogenesis. Blood. 2008;111(4):2015-2023.

306. Shen M, Tao Y, Feng Y, Liu X, Yuan F, Zhou H. Quantitative proteomic analysis of mice corneal tissues reveals angiogenesis-related proteins involved in corneal neovascularization. Biochim Biophys Acta. 2016;1864(7):787-793.

307. Losiewicz MK, Fort PE. Diabetes impairs the neuroprotective properties of retinal α-crystallins. Invest Ophthalmol Vis Sci. 2011;52(9):5034-5042.

308. Kase S, Ishida S, Rao NA. Increased expression of αA-crystallin in human diabetic eye. Int J Mol Med. 2011;28(4):505-511.

309. Thanos S, Bohm MR, Meyer zu Horste M, et al. Role of crystallins in ocular neuroprotection and axonal regeneration. Prog Retin Eye Res. 2014;42:145-161.

310. Chen W, Lu Q, Lu L, Guan H. Increased levels of αB-crystallin in vitreous fluid of patients with proliferative diabetic retinopathy and correlation with vascular endothelial growth factor. Clin Exp Ophthalmol. 2017;45(4):379-384.

311. Delanghe JR, Speeckaert R, Speeckaert MM. Behind the scenes of vitamin D binding protein: More than vitamin D binding. Best Pract Res Clin Endocrinol Metab. 2015;29(5):773-786.

312. Albert DM, Scheef EA, Wang S, et al. Calcitriol is a potent inhibitor of retinal neovascularization. Invest Ophthalmol Vis Sci. 2007;48(5):2327-2334.

313. Merrigan SL, Kennedy BN. Vitamin D receptor agonists regulate ocular developmental angiogenesis and modulate expression of dre-miR-21 and VEGF. Br J Pharmacol. 2017;174(16):2636-2651.

314. Kisker O, Onizuka S, Becker CM, et al. Vitamin D binding protein-macrophage activating factor (DBP-maf) inhibits angiogenesis and tumor growth in mice. Neoplasia. 2003;5(1):32-40.

315. Kanda S, Mochizuki Y, Miyata Y, Kanetake H, Yamamoto N. Effects of vitamin D(3)-binding protein-derived macrophage activating factor (GcMAF) on angiogenesis. J Natl Cancer Inst. 2002;94(17):1311-1319.

316. Kalkunte S, Brard L, Granai CO, Swamy N. Inhibition of angiogenesis by vitamin D-binding protein: Characterization of anti-endothelial activity of DBP-maf. Angiogenesis. 2005;8(4):349-360.

317. Layana AG, Minnella AM, Garhofer G, et al. Vitamin D and age-related macular degeneration. Nutrients. 2017;9(10):10.3390/nu9101120.

318. Skowron K, Pawlicka I, Gil K. The role of vitamin D in the pathogenesis of ocular diseases. Folia Med Cracov. 2018;58(2):103-118.

319. Reins RY, McDermott AM. Vitamin D: Implications for ocular disease and therapeutic potential. Exp Eye Res. 2015;134:101-110.

320. Jamali N, Wang S, Darjatmoko SR, Sorenson CM, Sheibani N. Vitamin D receptor expression is essential during retinal vascular development and attenuation of neovascularization by 1, 25$(OH)_2D_3$. PLoS One. 2017;12(12):e0190131.

321. Sugioka K, Saito A, Kusaka S, Kuniyoshi K, Shimomura Y. Identification of vitreous proteins in retinopathy of prematurity. Biochem Biophys Res Commun. 2017;488(3):483-488.

322. Raymond MA, Desormeaux A, Labelle A, et al. Endothelial stress induces the release of vitamin D-binding protein, a novel growth factor. Biochem Biophys Res Commun. 2005;338(3):1374-1382.

323. Huang B, Deora AB, He KL, et al. Hypoxia-inducible factor-1 drives annexin A2 system-mediated perivascular fibrin clearance in oxygen-induced retinopathy in mice. Blood. 2011;118(10):2918-2929.

324. Sers C, Riethmuller G, Johnson JP. MUC18, a melanoma-progression associated molecule, and its potential role in tumor vascularization and hematogenous spread. Cancer Res. 1994;54(21):5689-5694.

325. Yan X, Lin Y, Yang D, et al. A novel anti-CD146 monoclonal antibody, AA98, inhibits angiogenesis and tumor growth. Blood. 2003;102(1):184-191.

326. Bardin N, Blot-Chabaud M, Despoix N, et al. CD146 and its soluble form regulate monocyte transendothelial migration. Arterioscler Thromb Vasc Biol. 2009;29(5):746-753.

327. Stalin J, Nollet M, Garigue P, et al. Targeting soluble CD146 with a neutralizing antibody inhibits vascularization, growth and survival of CD146-positive tumors. Oncogene. 2016;35(42):5489-5500.

328. Wragg JW, Finnity JP, Anderson JA, et al. MCAM and LAMA4 are highly enriched in tumor blood vessels of renal cell carcinoma and predict patient outcome. Cancer Res. 2016;76(8):2314-2326.

329. Jiang T, Zhuang J, Duan H, et al. CD146 is a coreceptor for VEGFR-2 in tumor angiogenesis. Blood. 2012;120(11):2330-2339.

330. Harhouri K, Kebir A, Guillet B, et al. Soluble CD146 displays angiogenic properties and promotes neovascularization in experimental hind-limb ischemia. Blood. 2010;115(18):3843-3851.

331. Pecci A, Ma X, Savoia A, Adelstein RS. MYH9: Structure, functions and role of non-muscle myosin IIA in human disease. Gene. 2018;664:152-167.

332. Irianto J, Pfeifer CR, Xia Y, Discher DE. SnapShot: Mechanosensing matrix. Cell. 2016;165(7):1820-1820.e1.

333. Bordeleau F, Mason BN, Lollis EM, et al. Matrix stiffening promotes a tumor vasculature phenotype. Proc Natl Acad Sci U S A. 2017;114(3):492-497.

334. Huynh J, Nishimura N, Rana K, et al. Age-related intimal stiffening enhances endothelial permeability and leukocyte transmigration. Sci Transl Med. 2011;3(112):112-122.

335. Lampi MC, Reinhart-King CA. Targeting extracellular matrix stiffness to attenuate disease: From molecular mechanisms to clinical trials. Sci Transl Med. 2018;10(422):10.1126/scitranslmed.aao0475.

336. Newell-Litwa KA, Horwitz R, Lamers ML. Non-muscle myosin II in disease: Mechanisms and therapeutic opportunities. Dis Model Mech. 2015;8(12):1495-1515.

337. Vicente-Manzanares M, Ma X, Adelstein RS, Horwitz AR. Non-muscle myosin II takes centre stage in cell adhesion and migration. Nat Rev Mol Cell Biol. 2009;10(11):778-790.

338. Morrison AR, Yarovinsky TO, Young BD, et al. Chemokine-coupled β2 integrin-induced macrophage Rac2-myosin IIA interaction regulates VEGF-A mRNA stability and arteriogenesis. J Exp Med. 2014;211(10):1957-1968.

339. Huang Y, Shi H, Zhou H, Song X, Yuan S, Luo Y. The angiogenic function of nucleolin is mediated by vascular endothelial growth factor and nonmuscle myosin. Blood. 2006;107(9):3564-3571.

340. Christian S, Pilch J, Akerman ME, Porkka K, Laakkonen P, Ruoslahti E. Nucleolin expressed at the cell surface is a marker of endothelial cells in angiogenic blood vessels. J Cell Biol. 2003;163(4):871-878.

341. Fogal V, Sugahara KN, Ruoslahti E, Christian S. Cell surface nucleolin antagonist causes endothelial cell apoptosis and normalization of tumor vasculature. Angiogenesis. 2009;12(1):91-100.

342. Garfias Y, Iturriaga-Goyon E, Castro I, et al. Characterization of retinal nucleolin expression in an oxygen-induced retinopathy model. Invest.Ophthalmol.Vis.Sci. Abstract Issue 2019.

343. Evrard SM, Lecce L, Michelis KC, et al. Endothelial to mesenchymal transition is common in atherosclerotic lesions and is associated with plaque instability. Nat Commun. 2016;7:11853.

344. Hong L, Du X, Li W, Mao Y, Sun L, Li X. EndMT: A promising and controversial field. Eur J Cell Biol. 2018;97(7):493-500.

345. Li J, Bowens N, Cheng L, et al. Myocardin-like protein 2 regulates TGFβ signaling in embryonic stem cells and the developing vasculature. Development. 2012;139(19):3531-3542.

346. Trembley MA, Velasquez LS, de Mesy Bentley KL, Small EM. Myocardin-related transcription factors control the motility of epicardium-derived cells and the maturation of coronary vessels. Development. 2015;142(1):21-30.

347. Menendez MT, Ong EC, Shepherd BT, et al. BRG1 (brahma-related gene 1) promotes endothelial mrtf transcription to establish embryonic capillary integrity. Arterioscler Thromb Vasc Biol. 2017;37(9):1674-1682.

348. Gasparics A, Sebe A. MRTFs- master regulators of EMT. Dev Dyn. 2018;247(3):396-404.

349. Crider BJ, Risinger GM,Jr, Haaksma CJ, Howard EW, Tomasek JJ. Myocardin-related transcription factors A and B are key regulators of TGF- β1-induced fibroblast to myofibroblast differentiation. J Invest Dermatol. 2011;131(12):2378-2385.

350. Dejana E, Hirschi KK, Simons M. The molecular basis of endothelial cell plasticity. Nat Commun. 2017;8:14361.

351. Schwartz MA, Vestweber D, Simons M. A unifying concept in vascular health and disease. Science. 2018;360(6386):270-271.

352. Cao Y, Feng B, Chen S, Chu Y, Chakrabarti S. Mechanisms of endothelial to mesenchymal transition in the retina in diabetes. Invest Ophthalmol Vis Sci. 2014;55(11):7321-7331.

353. Thomas AA, Biswas S, Feng B, Chen S, Gonder J, Chakrabarti S. lncRNA H19 prevents endothelial-mesenchymal transition in diabetic retinopathy. Diabetologia. 2019;62(3):517-530.

354. Zhan Y, Guo J, Yang W, et al. MNK1/2 inhibition limits oncogenicity and metastasis of KIT-mutant melanoma. J Clin Invest. 2017;127(11):4179-4192.

355. Liu Y, Sun L, Su X, Guo S. Inhibition of eukaryotic initiation factor 4E phosphorylation by cercosporamide selectively suppresses angiogenesis, growth and survival of human hepatocellular carcinoma. Biomed Pharmacother. 2016;84:237-243.

356. Schrufer TL, Antonetti DA, Sonenberg N, Kimball SR, Gardner TW, Jefferson LS. Ablation of 4E-BP1/2 prevents hyperglycemia-mediated induction of VEGF expression in the rodent retina and in muller cells in culture. Diabetes. 2010;59(9):2107-2116.

357. Miller WP, Mihailescu ML, Yang C, et al. The translational repressor 4E-BP1 contributes to diabetes-induced visual dysfunction. Invest Ophthalmol Vis Sci. 2016;57(3):1327-1337.

358. Wei J, Jiang H, Gao H, Wang G. Blocking mammalian target of rapamycin (mTOR) attenuates HIF-1α pathways engaged-vascular endothelial growth factor (VEGF) in diabetic retinopathy. Cell Physiol Biochem. 2016;40(6):1570-1577.

359. Dennis MD, Shenberger JS, Stanley BA, Kimball SR, Jefferson LS. Hyperglycemia mediates a shift from cap-dependent to cap-independent translation via a 4E-BP1-dependent mechanism. Diabetes. 2013;62(7):2204-2214.

360. Segura I, Lange C, Knevels E, et al. The oxygen sensor PHD2 controls dendritic spines and synapses via modification of filamin A. Cell Rep. 2016;14(11):2653-2667.

361. Nallapalli RK, Ibrahim MX, Zhou AX, et al. Targeting filamin A reduces K-RAS-induced lung adenocarcinomas and endothelial response to tumor growth in mice. Mol Cancer. 2012;11:50-4598-11-50.

362. Salimi R, Bandaru S, Devarakonda S, et al. Blocking the cleavage of filamin A by calpain inhibitor decreases tumor cell growth. Anticancer Res. 2018;38(4):2079-2085.

363. Feng Y, Chen MH, Moskowitz IP, et al. Filamin A (FLNA) is required for cell-cell contact in vascular development and cardiac morphogenesis. Proc Natl Acad Sci U S A. 2006;103(52):19836-19841.

364. Loy CJ, Sim KS, Yong EL. Filamin-A fragment localizes to the nucleus to regulate androgen receptor and coactivator functions. Proc Natl Acad Sci U S A. 2003;100(8):4562-4567.

365. Savoy RM, Ghosh PM. The dual role of filamin A in cancer: Can't live with (too much of) it, can't live without it. Endocr Relat Cancer. 2013;20(6):R341-56.

366. Del Valle-Perez B, Martinez VG, Lacasa-Salavert C, et al. Filamin B plays a key role in vascular endothelial growth factor-induced endothelial cell motility through its interaction with rac-1 and vav-2. J Biol Chem. 2010;285(14):10748-10760.

367. Zhou X, Tian F, Sandzen J, et al. Filamin B deficiency in mice results in skeletal malformations and impaired microvascular development. Proc Natl Acad Sci U S A. 2007;104(10):3919-3924.

368. Su YT, Gao C, Liu Y, et al. Monoubiquitination of filamin B regulates vascular endothelial growth factor-mediated trafficking of histone deacetylase 7. Mol Cell Biol. 2013;33(8):1546-1560.

369. Tokunaga CC, Mitton KP, Dailey W, et al. Effects of anti-VEGF treatment on the recovery of the developing retina following oxygen-induced retinopathy. Invest Ophthalmol Vis Sci. 2014;55(3):1884-1892.

370. Gao X, Wang YS, Li XQ, et al. Macrophages promote vasculogenesis of retinal neovascularization in an oxygen-induced retinopathy model in mice. Cell Tissue Res. 2016;364(3):599-610.

371. Kataoka K, Nishiguchi KM, Kaneko H, van Rooijen N, Kachi S, Terasaki H. The roles of vitreal macrophages and circulating leukocytes in retinal neovascularization. Invest Ophthalmol Vis Sci. 2011;52(3):1431-1438.

372. Zhou Y, Yoshida S, Nakao S, et al. M2 macrophages enhance pathological neovascularization in the mouse model of oxygen-induced retinopathy. Invest Ophthalmol Vis Sci. 2015;56(8):4767-4777.

373. Davies MH, Eubanks JP, Powers MR. Microglia and macrophages are increased in response to ischemia-induced retinopathy in the mouse retina. Mol Vis. 2006;12:467-477.

374. Tammela T, Zarkada G, Nurmi H, et al. VEGFR-3 controls tip to stalk conversion at vessel fusion sites by reinforcing notch signalling. Nat Cell Biol. 2011;13(10):1202-1213.

375. Liyanage SE, Fantin A, Villacampa P, et al. Myeloid-derived vascular endothelial growth factor and hypoxia-inducible factor are dispensable for ocular neovascularization--brief report. Arterioscler Thromb Vasc Biol. 2016;36(1):19-24.

376. Nurnberg C, Kociok N, Brockmann C, et al. Myeloid cells contribute indirectly to VEGF expression upon hypoxia via activation of muller cells. Exp Eye Res. 2018;166:56-69.

377. Khatib AM, Lahlil R, Scamuffa N, et al. Zebrafish ProVEGF-C expression, proteolytic processing and inhibitory effect of unprocessed ProVEGF-C during fin regeneration. PLoS One. 2010;5(7):e11438.

378. Lopez de Cicco R, Watson JC, Bassi DE, Litwin S, Klein-Szanto AJ. Simultaneous expression of furin and vascular endothelial growth factor in human oral tongue squamous cell carcinoma progression. Clin Cancer Res. 2004;10(13):4480-4488.

379. Jaaks P, D'Alessandro V, Grob N, et al. The proprotein convertase furin contributes to rhabdomyosarcoma malignancy by promoting vascularization, migration and invasion. PLoS One. 2016;11(8):e0161396.

380. Pesu M, Watford WT, Wei L, et al. T-cell-expressed proprotein convertase furin is essential for maintenance of peripheral immune tolerance. Nature. 2008;455(7210):246-250.

381. Thomas G. Furin at the cutting edge: From protein traffic to embryogenesis and disease. Nat Rev Mol Cell Biol. 2002;3(10):753-766.

382. Kusakabe M, Cheong PL, Nikfar R, McLennan IS, Koishi K. The structure of the TGF- β latency associated peptide region determines the ability of the proprotein convertase furin to cleave TGF-betas. J Cell Biochem. 2008;103(1):311-320.

383. Bai Y, Liang S, Yu W, et al. Semaphorin 3A blocks the formation of pathologic choroidal neovascularization induced by transforming growth factor β. Mol Vis. 2014;20:1258-1270.

384. Wang X, Ma W, Han S, et al. TGF-β participates choroid neovascularization through Smad2/3-VEGF/TNF-α signaling in mice with laser-induced wet age-related macular degeneration. Sci Rep. 2017;7(1):9672-017-10124-4.

385. Yingchuan F, Chuntao L, Hui C, Jianbin H. Increased expression of TGF-β1 and smad 4 on oxygen-induced retinopathy in neonatal mice. Adv Exp Med Biol. 2010;664:71-77.

386. Kim KS, Park JM, Kong T, et al. Retinal angiogenesis effects of TGF-β1 and paracrine factors secreted from human placental stem cells in response to a pathological environment. Cell Transplant. 2016;25(6):1145-1157.

387. Baumann J, Huang SF, Gassmann M, Tsao CC, Ogunshola OO. Furin inhibition prevents hypoxic and TGFβ-mediated blood-brain barrier disruption. Exp Cell Res. 2019; Jul 20:111503.

388. McColl BK, Paavonen K, Karnezis T, et al. Proprotein convertases promote processing of VEGF-D, a critical step for binding the angiogenic receptor VEGFR-2. FASEB J. 2007;21(4):1088-1098.

PUBLICATIONS

PUBLICATION I

Lack of R-Ras leads to increased vascular permeability in ischemic retinopathy

Maria Vähätupa, Stuart Prince, Suvi Vataja, Teija Mertimo, Marko Kataja, Kati Kinnunen, Varpu Marjomäki, Hannu Uusitalo, Masanobu Komatsu, Tero A.H. Järvinen, & Hannele Uusitalo Järvinen

Investigative Ophthalmology & Visual Science. 2016, 57:4898-4909
doi: 10.1167/iovs.16-19212

Lack of R-Ras Leads to Increased Vascular Permeability in Ischemic Retinopathy

Maria Vähätupa,[1,2] Stuart Prince,[2] Suvi Vataja,[1] Teija Mertimo,[1] Marko Kataja,[3] Kati Kinnunen,[4] Varpu Marjomäki,[5] Hannu Uusitalo,[1,3] Masanobu Komatsu,[6] Tero A.H. Järvinen,[2,7] and Hannele Uusitalo-Järvinen[1,3]

[1]Department of Ophthalmology, University of Tampere, Tampere, Finland
[2]Department of Anatomy, University of Tampere, Tampere, Finland
[3]Eye Centre, Tampere University Hospital, Tampere, Finland
[4]Department of Ophthalmology, Kuopio University Hospital, Kuopio, Finland
[5]Department of Biological and Environmental Science/Nanoscience Center, University of Jyväskylä, Jyväskylä, Finland
[6]Sanford Burnham Prebys Medical Discovery Institute at Lake Nona, Orlando, Florida, United States
[7]Department of Musculoskeletal Disorders, Tampere University Hospital, Tampere, Finland

Correspondence: Hannele Uusitalo-Järvinen, Department of Ophthalmology, School of Medicine, 33014 University of Tampere, Finland; llhauus@uta.fi.

Submitted: January 25, 2016
Accepted: July 14, 2016

Citation: Vähätupa M, Prince S, Vataja S, et al. Lack of R-Ras leads to increased vascular permeability in ischemic retinopathy. *Invest Ophthalmol Vis Sci*. 2016;57:4898–4909. DOI:10.1167/iovs.16-19212

Purpose. The role of R-Ras in retinal angiogenesis and vascular permeability was evaluated in an oxygen-induced retinopathy (OIR) model using R-Ras knockout (KO) mice and in human diabetic neovascular membranes.

Methods. Mice deficient for R-Ras and their wild-type (WT) littermates were subjected to 75% oxygen from postnatal day 7 (P7) to P12 and then returned to room air. At P17 retinal vascularization was examined from whole mounts, and retinal vascular permeability was studied using Miles assay. Real-time RT-PCR, Western blotting, and immunohistochemistry were used to assess the expression of R-Ras in retina during development or in the OIR model. The degree of pericyte coverage and vascular endothelial (VE)-cadherin expression on WT and R-Ras KO retinal blood vessels was quantified using confocal microscopy. The correlation of R-Ras with vascular endothelial growth factor receptor 2 (VEGFR2) and human serum albumin on human proliferative diabetic retinopathy membranes was assessed using immunohistochemistry.

Results. In retina, R-Ras expression was mostly restricted to the vasculature. Retinal vessels in the R-Ras KO mice were significantly more permeable than WT controls in the OIR model. A significant reduction in the direct physical contact between pericytes and blood vessel endothelium as well as reduced VE-cadherin immunostaining was found in R-Ras–deficient mice. In human proliferative diabetic retinopathy neovascular membranes, R-Ras expression negatively correlated with increased vascular leakage and expression of VEGFR2, a marker of blood vessel immaturity.

Conclusions. Our results suggest that R-Ras has a role in controlling retinal vessel maturation and stabilization in ischemic retinopathy and provides a potential target for pharmacologic manipulation to treat diabetic retinopathy.

Keywords: retina, diabetic retinopathy, neovascularization, retinal ischemia

Diabetic macular edema (DME) and proliferative diabetic retinopathy (PDR) are the two forms of diabetic retinopathy causing blindness. Vascular endothelial growth factor (VEGF) plays a crucial role in these diseases by causing vascular leakage and pathologic neovascularization.[1–3] Anti-VEGF drugs are regarded as the mainstay of treatment for patients affected by DME. However, VEGF inhibition fails to provide sufficient efficacy in all DME cases; only half of patients attain significant improvement in visual acuity.[4] Anti-VEGF therapy is also accompanied by rare, but severe, ocular and systemic side effects. In PDR, anti-VEGF may be associated with development of tractional retinal detachment[5,6] Furthermore, intravitreally administered anti-VEGF agents may cause sustained systemic VEGF inhibition[7,8] This is why they are relatively contraindicated in pregnant women[9] and patients with cardiovascular insufficiency.[10,11] Thus, alternative therapies are needed for more effective and safer treatment of diabetic retinopathy.[12,13]

R-Ras is a small GTPase of the Ras family of oncogenes.[14] Despite the close structural similarity to other members of the Ras family, the function of R-Ras is distinct from other Ras proteins.[15] Whereas all other members of the Ras family may cause malignant transformation, R-Ras has very little or no transforming activity.[16] Furthermore, the opposing functions of R-Ras and H-Ras extend to cell–extracellular matrix (ECM) adhesion,[17] cell differentiation,[18] and signaling.[19] These opposing functions have led to the suggestion that the balance between R-Ras and other Ras members acts as a switch that controls proliferation and invasion versus quiescence in cells.[15,20,21]

Recently, active Ras signaling has been implicated as a key driver of pathologic angiogenesis in neovascular diseases of the

retina.[22] Conversely, exactly the opposite role has recently been shown for R-Ras in the regulation of angiogenesis.[20] R-Ras function has been shown to be essential for the establishment of mature and functional blood vessels in tumors by stabilization of immature, leaky vessels, enhancing perfusion and ultimately reducing plasma leakage.[15,21] Based on these functions, R-Ras has been classified as an antiangiogenic molecule. However, R-Ras is functionally different from classic antiangiogenic agents as it does not induce endothelial cell apoptosis as do other antiangiogenic molecules, but actually promotes endothelial cell survival.[20] Thus, R-Ras could provide a potential agonistic therapeutic target for treatment of a variety of retinal diseases associated with ischemia, neovascularization, and vascular leakage. In the present study, the role of R-Ras in the retina was studied by analyzing expression of R-Ras in the retina and by analyzing the effect of R-Ras deficiency on the structural and functional integrity of retinal vasculature during development and ischemic retinopathy using an oxygen-induced retinopathy model (OIR). To address the role of R-Ras in PDR, association of its expression with vascular immaturity and leakiness was examined in human retinal neovascular membranes.

Methods

Mice

For the experiments, wild-type (WT) C57BL/6 mice from Harlan Sprague Dawley (Indianapolis, IN, USA) and homozygous R-Ras knockout (KO) mice were used. R-Ras KO mice with an insertion deleting R-Ras expression between exons 4 and 5 of *Rras* on chromosome 7 (R-Ras KO mice) have been described previously.[20] Before any experiments, R-Ras heterozygous mice were backcrossed eight times with the C57BL/6 strain to obtain homozygous KO and WT mice in the same genetic background. The mice were bred, and the genotype was determined by PCR. Mice were fed with standard laboratory pellets and water ad libitum. All animal experiments were performed according to the ARVO Statement for the Use of Animals in Ophthalmic and Vision Research in accordance with protocols approved by the National Animal Ethics Committee of Finland.

Oxygen-Induced Retinopathy Model

The experiments on the OIR model were carried out as described in detail previously.[23,24] Briefly, neonatal mice at postnatal day 7 (P7) were exposed to 75% oxygen for 5 days. At P12, they were returned to normal room air.[23] Animals were euthanized at P12 to assess the degree of vascular regression and at P17 to determine the rate of retinal revascularization and preretinal neovascularization. As postnatal weight gain has been shown to affect outcome in the OIR model,[25] only the pups weighing between 6.3 and 7.5 g at P17 were included in the study.

Immunohistochemistry (IHC) and Isolectin GS-IB_4 Staining

For the analysis of retinal vasculature, eyes were enucleated, fixed with 4% paraformaldehyde (PFA), and retinas dissected. Flat-mount retinas were blocked in 20% normal goat and 20% fetal bovine serums for 2 hours, incubated overnight Isolectin (Isolectin GS-IB_4, 1:200; Invitrogen, Carlsbad, CA, USA) and with anti-NG2 chondroitin sulfate proteoglycan antibody (1:80; Millipore, Billerica, MA), followed by Alexa Fluor-conjugated secondary antibody. Retinas were imaged via confocal microscope (LSM 700; Carl Zeiss, Oberkochen, Germany) and the rate of angiogenesis was determined during development (P0–P6) and in the OIR model as previously described.[24] Briefly, retinas were imaged using confocal microscopy (Carl Zeiss LSM 700) with 5× objective. By focusing just above the inner limiting membrane of the retina, the preretinal neovascular tufts were readily distinguished from the underlying superficial vascular plexus. Areas of vascular obliteration and pathologic neovascularization (meaning neovascular tufts) were quantified from these images using image editing software (Adobe Photoshop CS3; Adobe Systems, Inc., San Jose, CA, USA). The rate of developmental angiogenesis at P0 to P6 was determined by measuring the length of vasculature from the optic nerve to the tips of the blood vessels. Four measurements per retina were taken and an average was calculated.

For immunohistochemistry, the eyes were fixed with 4% PFA and embedded in paraffin or immediately frozen in ornithine carbamoyltransferase embedding compound in isopentane cooled with liquid nitrogen and later fixed with acetone. The IHC was carried out on 4- to 6-μm-thick tissue sections using the following primary antibodies: rabbit anti–R-Ras (1:50) and rabbit anti-VEGFR2 (1:100; both Cell Signaling Technology, Danvers, MA, USA), rabbit anti–R-Ras (1:750) and mouse anti-VEGFR2 (1:200, clone sc.6251; both Santa Cruz Biotechnology, Dallas, TX, USA), rat anti-mouse CD31 (1:50; BD Pharmingen, San Diego, CA, USA), guinea pig anti-NG2 antibody (1:100, gift from William Stallcup),[26] rabbit anti-Syndecan (1:500) and rabbit anti-human vascular endothelial (VE)-cadherin (1:500; both from Abcam, Cambridge, UK), and rabbit anti-human serum albumin (1:100; Lifespan Biosciences, Seattle, WA, USA), followed by horseradish peroxidase (HRP) or fluorescein-conjugated secondary antibodies. Hematoxylin staining was used as a counterstain. Samples were mounted with Vectashield mounting medium with 4′,6-diamidino-2-phenylindole (Vector Laboratories) and analyzed via confocal microscope. Each staining experiment included sections stained without primary antibody as negative controls. Percentage of R-Ras positive cells in preretinal neovessels were quantified manually by using the count tool in Adobe Photoshop (Adobe Systems, Inc.) ($n = 6$ mice, 4–6 sections/retina).

Quantification of Pericyte Coverage and VE-Cadherin Colocalization With CD31

Pericyte coverage of the blood vessels was quantified from WT and R-Ras KO P17 OIR model whole-mount retinas. Samples were imaged using confocal microscopy (Carl Zeiss LSM 700) with a 63× objective lens, and 3D pictures were made from Z-stacks. Pictures selected for the analysis were randomly taken from Isolectin IB_4 and NG2-stained flat-mounts from the most superficial vascular plexus at the tips of the blood vessels next to avascular area. This is a region of retina where the blood vessels are growing toward the optic nerve. Direct contact between pericytes (NG2) and endothelial cells (Isolectin B_4) were quantified by colocalization analysis with BioImageXD (provided in the public domain at http://www.bioimagexd.org).[27] The percentage of EC area colocalized with pericyte area was quantified in each image, and the result expressed as a mean of two different images for each retina. The intensity of VE-cadherin staining and colocalization of VE-cadherin and CD31 was quantified from frozen sections using BioImage XD.

Real-Time Quantitative PCR (qPCR)

Eyes were collected at P0, P4, P7, P12, P17, and P22 and placed immediately in cold RNA stabilization reagent (RNAlater; Sigma-Aldrich Corp., St. Louis, MO, USA) for the

Investigative Ophthalmology & Visual Science

duration of dissection of the retinas. RNA was extracted using RNA isolation kit (RNeasy Mini Kit; Qiagen, Hilden, Germany) following the manufacturer's instructions. The integrity of extracted RNA was verified on formaldehyde agarose gel. Reverse transcription of RNA was carried out using cDNA synthesis kit (Maxima First Strand cDNA Synthesis Kit; Thermo Fisher Scientific, Boston, MA, USA), according to the manufacturer's instructions. Real-time qPCR was done using the PCR dye (SYBR Green; Thermo Fisher Scientific) method according to the manufacturer's recommendations and performed in white 96-well plates (Multiply PCR plates; Sarstedt, Nümbrecht, Germany). The fluorescence signal was detected using a sequence detection system (ABI Prism 7000 Sequence Detection System 1.2; Applied Biosystems, Carlsbad, CA, USA). The following intron-spanning primers specific for exon 3 and 4 of *Rras* were used: 5′-ACAGGCA GAGTTTCAATGAG-3′ (forward), 5′-GTTCTCCAGATCTGCC TTG-3′ (reverse). *Ppia* was used as an endogenous control gene (5′-CACCGTGTTCTTCGACATC-3′ and 5′-ATTCTGTGA AAGGAGGAACC-3′), allowing the comparison of samples.[20] Two or three replicates were analyzed for each sample, and the results were expressed as a mean for each sample. Negative, no template (NTC) and no reverse transcriptase (no RT), controls were included in every qPCR analysis. A melting curve analysis was performed to check for unspecific PCR products (which didn't occur). Reaction efficiencies for both primer pairs were tested with standard curve analysis in different time points. Due to similar efficiencies for both primer pairs, the differences in gene expression levels were determined by the comparative Ct method (ΔΔCt method).[28]

Vascular Permeability Assay

Vascular permeability was quantified by Miles assay in retinas as described previously.[29] Briefly, the mice were injected with 2% Evans Blue ([EB], 150 μL/20g; Sigma-Aldrich Corp.) intraperitoneally, and the circulation time was 24 h for P16 or 1 hour for P17 injected mice. Phosphate-buffered saline–injected mice were used as a negative control. Animals were euthanized at P17, and blood was collected from the left ventricle. Retinas were dissected and weighed. Blood was centrifuged at 3,550*g* for 15 minutes, and plasma was diluted 1:100 and 1:1000 in N, N-dimethylformamide (Sigma-Aldrich Corp.). All samples were incubated in a shaker (100 rpm) in 200 μL N, N-dimethylformamide overnight at 78°C. Retinas were centrifuged at 17,000*g* for 45 minutes at 4°C, and the supernatants were collected. The EB absorbance of each sample was measured at 620 nm by spectrophotometer. EB concentration in the retina was proportioned and normalized by the weight of the retina and the amount of EB concentration in the plasma.[30]

Western Blotting

Retinas were lysed in 10 μL of cold RIPA buffer per 1 mg of tissue with added protease inhibitor (cOmplete; Roche, Basel, Switzerland) and phosphatase inhibitor (Halt; Thermo Fisher Scientific).

The tissues were homogenized using CK14 beads and a tissue homogenizer (Precellys; Bertin Technologies, Montigny-le-Bretonneux, France). From each sample, 40 μg of protein was loaded per well of a 4-12% gradient gel (NuPAGE; Invitrogen, Carlsbad, CA, USA) and electroblotted on polyvinylidene fluoride membranes (Immun-Blo; Bio-Rad Laboratories, Hercules, California). For detection of specific proteins by immunoblotting, the following primary antibodies were used: rabbit anti–R-Ras (1:500; Cell Signaling Technology), goat anti-GAPDH (1:500: AbCam) and horse anti-mouse IgG (1:2000; Cell Signaling Technology). Primary antibodies were detected by HRP-coupled antibodies. Western blot images were captured via software (ImageQuant; GE Healthcare, Chalfont St. Giles, UK) and quantified by densitometry using Adobe Photoshop CS3 software, where GAPDH was used to normalize for protein loading. A calibrator control sample was included in every membrane to enable sample comparison between different membranes.

Retinal and Neovascular Samples From Human Patients

Preretinal neovascular membranes were obtained from eight type I diabetic patients who were undergoing pars plana vitrectomy for the treatment of PDR. All patients were Caucasians, and altogether there were five females and three males. At the time of pars plana, vitrectomy patients' mean age was 33 years (range, 27–56 years) and mean duration of diabetes was 24 years (range, 16–32 years). Normal human retinas were obtained from patients whose eyes were enucleated due to choroidal melanoma. The protocol for collecting human tissue samples was approved by the institutional review boards of the Pirkanmaa Hospital District and the Kuopio University Hospital. The study was conducted in accordance with the Declaration of Helsinki. All patients gave written informed consent. During vitrectomy, the fibrovascular membranes were isolated, grasped with vitreous forceps, and pulled out through a sclerotomy. The sample was immediately fixed with 4% formaldehyde for 3 h, transferred to 70% ethanol, embedded in paraffin, and processed for immunohistochemistry. The number of R-Ras–positive neovessels was calculated from CD31 and R-Ras–double-stained tissue sections, and correlation between R-Ras and VEGFR2 was quantified from R-Ras and VEGFR2 double-stained sections. Immunohistochemistry against human serum albumin (HSA) was done to quantify the amount of vascular leakage outside the neovessels. Quantification was done using IHC Profiler plugin in ImageJ software (http://imagej.nih.gov/ij/; provided in the public domain by National Institutes of Health, Bethesda, MD, USA). The area of positive staining for HSA was compared to the total analyzed area, and correlation analysis between HSA and percentage of R-Ras–positive neovessels was performed for each sample.

Statistical Analysis

Student's *t*-test was conducted for normally distributed data and nonparametric Mann-Whitney *U* test using statistical software (GraphPad Prism 6.01; GraphPad Software, San Diego, CA, USA, and IBM SPSS Statistics; IBM, Amonk, NY, USA) for nonnormally distributed data to test the statistical significance of the results. Spearman's rank correlation test was conducted to test correlation between two variables. *P* values less than 0.05 were considered statistically significant.

Results

R-Ras Expression Peaks During Retinal Developmental Angiogenesis But Does Not Influence the Rate of Developmental Angiogenesis

R-Ras KO mice are fertile and show no obvious morphologic abnormalities,[20,31] and their eyes appear normal upon histologic examination. To address the role of R-Ras on retinal angiogenesis in vivo, the expression profile of R-Ras in the

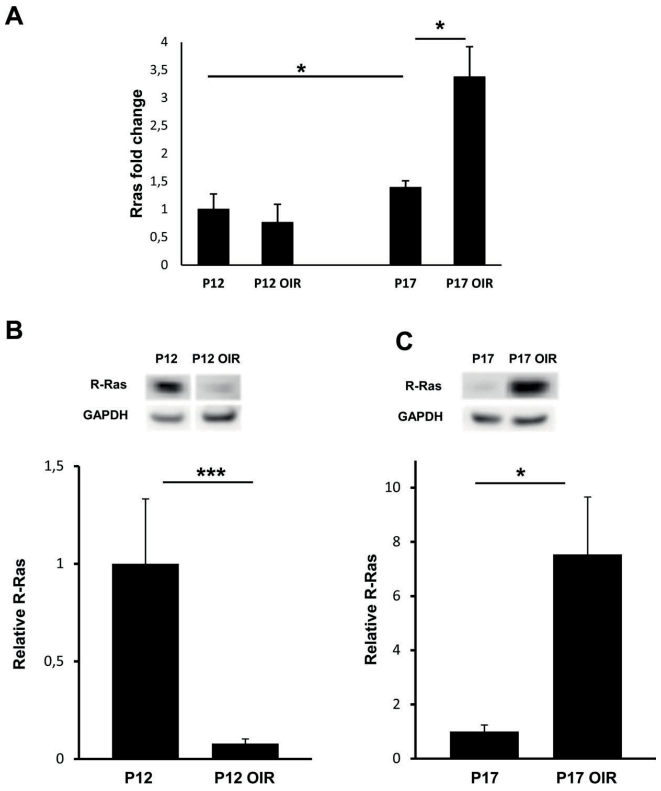

Figure 1. Hypoxia-driven R-Ras expression in the OIR model. Hypoxia-induced angiogenesis in retina was studied with the OIR model. Retinas were harvested immediately after the exposure to hyperoxia (P12) and after hypoxia-driven pathologic angiogenesis has reached its maximum at P17. Retinas from normal mice were harvested at corresponding time points. Retinas were subjected to either quantitative mRNA (real-time qPCR) analysis using SYBR Green method or protein (Western blotting) analysis. For immunoblotting, retinal protein supernatants were electrophoresed on gradient gels, standard Western blotting was carried out with R-Ras–specific antibody, and GAPDH detection was used as a loading control. (**A**) The graph represents fold changes ($2^{-\Delta\Delta Ct}$ method) in the *Rras* mRNA expression level relative to the *Rras* mRNA expression level of normal mice at P12. The level of *Rras* mRNA expression between normal and OIR model retinas is equal at P12, whereas at P17 hypoxia leads to 2.5-fold upregulation of *Rras* mRNA ($P = 0.016$, * nonparametric Mann-Whitney *U* test). *Error bars* represent the minimum and maximum of the fold change. (P12, P17 OIR: $n = 4$; P17, P12 OIR: $n = 5$.) (**B**, **C**) The level of R-Ras protein expression was quantified by densitometric analysis of immunoblotted protein. R-Ras protein level at P17 shows a 7.5-fold increase ($P = 0.016$) during hypoxia-induced angiogenesis. *Error bars* represent ± 95% confidence intervals. (P12: $n = 6$; P12 OIR: $n = 7$; P17: $n = 5$; P17: $n = 5$.) The results are analyzed with nonparametric Mann-Whitney *U* test. The samples presented above were run on the same gel. Representative samples were cropped and presented side-by-side.

developing mouse retina as well as the developmental rate of angiogenesis in WT and R-Ras KO mice were characterized.

To assess the temporal expression pattern of R-Ras during developmental retinal angiogenesis, qPCR and Western blot analysis were used. Quantitative PCR demonstrated that the *Rras* mRNA expression increased from P0 onward, peaked at P17, and started to decline from P17 until P22. Western blot analysis demonstrated a R-Ras protein expression profile similar to the mRNA profile: an increase in expression from P0 until P17 and a decline from P17 to P22 (Supplementary Fig. S1). The increase in *Rras* mRNA and protein levels from P0 to P17 correlates with the development of retinal vascular plexuses.[32] The R-Ras levels peaked at P17, when all three vascular plexuses are formed and vascular density peaks in the retina[33] (Supplementary Fig. S1). The findings are consistent with the notion that R-Ras appears in the blood vessels during their differentiation and is most strongly expressed in fully differentiated, quiescent blood vessels.[20] The reduction in *Rras* mRNA and protein expression levels from P17 to P22 can be explained by the remodeling of retinal vasculature (including vascular pruning), the outcome of which is decreased endothelial cell density at P28.[34] Consistent with this finding, the results show a similar decrease in the intensity of Isolectin IB_4 staining from P12 onward (Supplementary Fig. S2). No R-Ras protein or mRNA expression was detected in the retinas collected from R-Ras KO mice.

To explore whether the increase in R-Ras expression level seen during retinal development influences the rate of superficial vascular plexus formation (developmental angiogenesis), retinas from P0, P2, P4, and P6 WT and R-Ras KO mice were analyzed. In P0, P2, P4, and P6 neonatal mice, the diameter of retinal superficial vascular plexuses were similar both in R-Ras KO and WT mice, indicating that R-Ras expression is not necessary for in vivo angiogenesis during neonatal development (Supplementary Fig. S3). The lack of

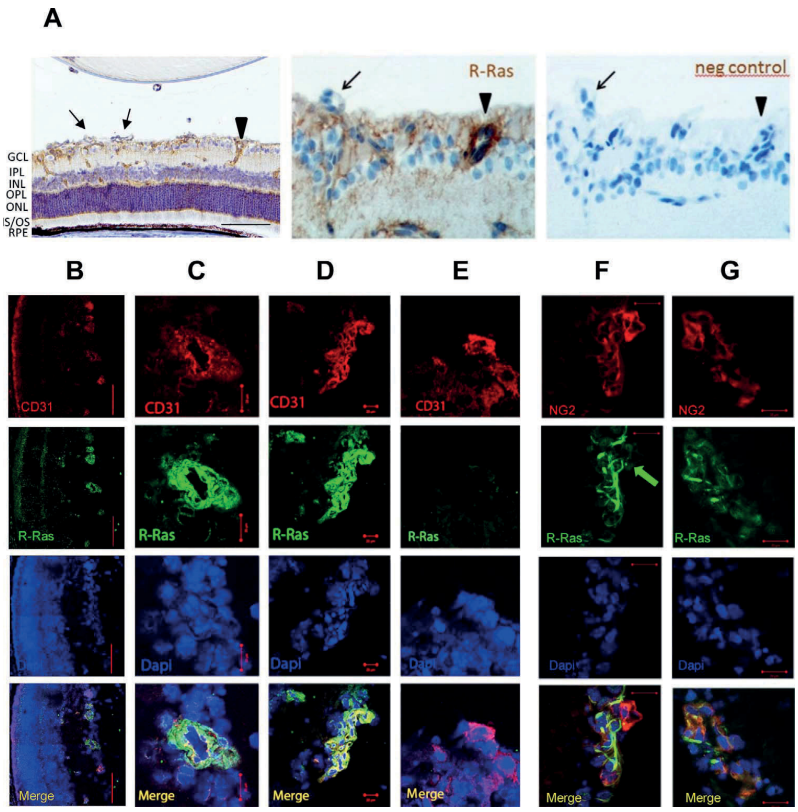

Figure 2. R-Ras is strongly, but selectively expressed in the endothelial cells and pericytes of blood vessels in retina. Oxygen-induced retinopathy was induced by exposing WT pups to 75% oxygen at P7 for 5 days and returning them to normal room air at P12. After 5 days in normoxia (at P17), the R-Ras expression was determined from the revascularized retinas by IHC and immunofluorescence (IF) using R-Ras–specific primary antibody. (**A**) Representative images of R-Ras expression in the OIR model. More than 30% of the preretinal blood vessels are negative for R-Ras (*arrow*), whereas blood vessels in retina are R-Ras positive (*arrowhead*). *Right*, negative control (no primary antibody). There is also faint R-Ras expression from other retinal cells, presumably from neural cells in the retina. GCL, ganglion cell layer; IPL, inner plexiform layer; INL, inner nuclear layer, OPL, outer plexiform layer; ONL, outer nuclear layer; IS/OS, photoreceptor inner/outer segments; RPE, retinal pigment epithelium. (**B–E**) Representative confocal images showing the colocalization of R-Ras (*green*) and CD31 (*red*) in the retina of frozen sections after immunofluorescence staining. (**C**) R-Ras is expressed in the endothelial cells in the retina and (**D**) also in the preretinal blood vessels. (**E**) Some of the preretinal blood vessels are negative for R-Ras. (**F**) R-Ras is expressed in the pericytes (NG2, *red*) in the retina. Some pericytes of preretinal blood vessels are negative for R-Ras in OIR (*arrow*), but (**G**) R-Ras is also expressed in the pericytes of preretinal neovessels. *Scale bars*: 100 μm (**A**, **B**), 20 μm (**C–G**).

influence on development of retinal vasculature by R-Ras is in line with the above-reported low expression of R-Ras at the early stages of retinal vascular development (Supplementary Fig. S1).

Induction and Selective Disappearance of R-Ras From the Pathologic Neovasculature in OIR

Next, the R-Ras expression profile in the OIR model was analyzed using WT mice. Using qPCR, a 2.5-fold increase of *Rras* mRNA from normal P17 to P17 OIR model retinas was detected. Using Western blot analysis, a 7.5-fold increase in R-Ras protein levels was seen in OIR P17 retinas compared to healthy P17 retinas. At P12, the expression of R-Ras was reduced in OIR. The amount of R-Ras expression is in line with regression of the vasculature at P12 and vessel regrowth at P17 in the OIR model (Fig. 1). Using R-Ras immunohistochemistry, R-Ras was found to be localized mainly to the blood vessels in OIR retinas (Fig. 2, Supplementary Fig. S4). A faint R-Ras expression was also detected outside of the retinal blood vessels in mouse retina (Fig. 2A). This immunohistochemical signal most probably represents low expressions from retinal neuronal cells, which are known to express R-Ras.[35] Using R-Ras and endothelial cell (CD31), as well as R-Ras and pericyte (NG2), double-staining, R-Ras expression was shown to be confined to endothelial cells and pericytes in retinal vessels (Fig. 2). It appeared that all of the retinal blood vessels expressed R-Ras, whereas only 68% of the preretinal neovessels had R-Ras expression at P17 in the OIR model (Fig. 2A, Supplementary Fig. S4). This finding was confirmed by double immunofluorescent imaging of the retina showing some preretinal neovessels devoid of R-Ras expression in OIR (Figs. 2E, 2F). By costaining the retinal tissue sections for R-Ras and endothelial cells, as well as for R-Ras and pericytes, the R-Ras expression was confirmed to be confined to both endothelial cells and pericytes (Figs. 2B–G).

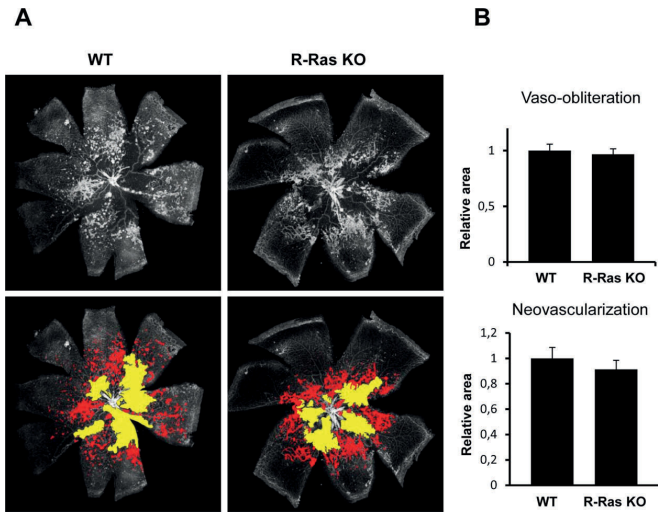

FIGURE 3. Neither revascularization nor pathologic neovascularization is affected by R-Ras deficiency in the OIR model. Wild-type and R-Ras KO mice pups were exposed to hyperoxia as previously described, and retinas were harvested at P17. Areas of vascular obliteration and pathologic neovascularization (meaning neovascular tufts) were quantified from Isolectin IB_4–stained whole mounts using Adobe Photoshop CS3. (**A**) Representative retinas of WT and R-Ras KO mice at P17. The revascularization rate was determined by quantifying the avascular areas (*yellow*) in retinal flat mounts. The amount of pathologic neovascularization (tufts, *red*) was also determined. (**B**) Summary of quantitative analysis of vascular obliteration (*yellow*) and neovascularization (*red*). The avascular and pathologic neovascularization areas were measured, and results are represented as an area relative to WT area. *Error bars* represent ± 95% confidence intervals. (WT: $n = 63$, KO: $n = 48$ retinas.)

R-Ras Does Not Change the Hypoxic Revascularization Rate of the Retina

As all of the antiangiogenic molecules used to treat neovascular retinal diseases have been shown to inhibit sprouting angiogenesis induced in the OIR model,[36–38] the role of R-Ras in hypoxia-driven neovascularization in the retina was explored next. First, we determined whether regression of vessels under hyperoxic conditions in the OIR model is comparable between R-Ras KO and WT mice. After exposure to 75% oxygen between P7 and P12, retinas were evaluated at P12. Typical for this model,[39] large areas of the central vascular network were obliterated, with only a few major vessels remaining centrally in both WT and R-Ras KO mice (Supplementary Fig. S5). Quantitative analysis of obliterated areas in retina confirmed that the retinal vasculature in R-Ras KO and WT mice are affected in a similar fashion by hyperoxic exposure (Supplementary Fig. S5). Taken together, these data suggest that deletion of R-Ras has no observable effect on vascular regression and remodeling in the retina in response to hyperoxic conditions.

On return to normoxia, the avascular and hypoxic central retina stimulates rapid regrowth of vessels.[24] The rate of retinal revascularization in WT and R-Ras KO retinas was determined by quantifying avascular retinal area 5 days after the mice were returned to normoxia. There was no significant difference in the avascular retinal area between the WT and R-Ras KO, indicating that the rate of retinal revascularization is similar between the WT and R-Ras KO mice at P17 (Fig. 3). In addition to revascularization of the retina, the strong hypoxic stimulus from the center of the retina also drives abnormal misdirected sprouting of blood vessels into the vitreous at the interface between the centrally obliterated and peripherally perfused retina.[24] Preretinal (i.e., pathologic) neovascularization reaches its maximum in WT mice 5 days after returning to normoxia (at P17).[24] No significant differences in the number of preretinal neovascular tufts and clusters were found between R-Ras KO mice and WT mice (Fig. 3). The results indicate that neither the hypoxia-induced revascularization rate of the obliterated areas in retina nor the rate of preretinal neovascularization is affected by R-Ras deletion.

R-Ras Deficient Retinal Blood Vessels Have Increased Permeability in OIR

It has been recently shown that loss of R-Ras worsens blood vessel structure and perfusion and the pathologic plasma leakage in tumor angiogenesis.[15,21] In order to assess the role of R-Ras in controlling the vascular permeability of the retinal vasculature, the OIR model was used. The vascular leakage was quantified by measuring EB dye extravasation from retinal vessels. The R-Ras KO retinas had approximately 100% increase in the retinal EB leakage compared with the WT retinas in OIR ($P = 0.0223$ at 1 hour and $P = 0.0006$ at 24 hours; Figs. 4A–C). No difference was detected in the amount of EB leakage when comparing normal WT and R-Ras KO retinas (Supplementary Fig. S6). To confirm the enhanced retinal leakage in R-Ras KO animals in OIR, we also measured the amount of IgG heavy chain molecule accumulation in the retina, as this antibody subclass is normally compartmentalized within the circulation.[40] We could not detect a difference in IgG leakage in the normal retinas between WT and R-Ras KO animals. A 4-fold increase in the amount of IgG was detected in the R-Ras KO retinas over the WT retinas in OIR as a sign of increased vascular permeability ($P = 0.0007$; Fig. 4D). To rule out the possibility that the increased levels of IgG in the R-Ras KO OIR retinas were due to plasma cells, immunohistologic staining of CD138/Syndecan-1 was performed. There was no increase in the number of plasma cells in KO retinas compared to WT in the OIR samples (Supplementary Fig. S7).

Investigative Ophthalmology & Visual Science

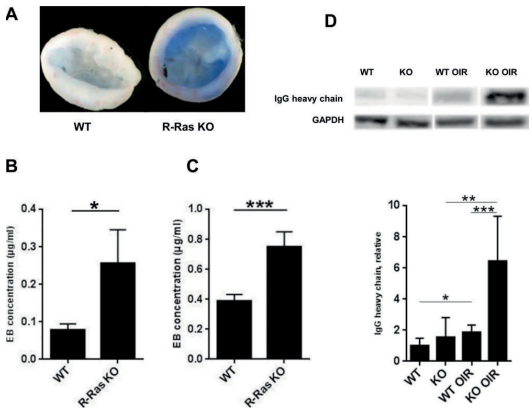

Figure 4. R-Ras deficiency increases vessel permeability in mouse OIR model. Wild-type and R-Ras KO mice pups were exposed to hyperoxia as described previously. The EB dye was injected IP, and retinas and blood samples were harvested after 1 hour and 24 hours at P17. Evans Blue concentrations were measured spectrophotometrically at 620 nm, and EB concentration for each sample was calculated from a standard curve. Results are expressed as relative to EB concentration in the plasma. (**A**) Representative R-Ras KO and WT OIR retinas after systemic injection of EB dye. In many of the R-Ras KO retinas, EB dye was visible, whereas most of the WT retinas were colorless. (**B**) Statistical analysis of a representative experiment shows a significant increase in vascular leakage in R-Ras KO OIR retinas compared to WT OIR retinas already at a 1-hour time point ($P = 0.0223$, *, nonparametric Mann-Whitney U test, WT $n = 6$, R-Ras KO $n = 8$). (**C**) There is a highly significant difference in vascular leakage between R-Ras KO and WT mice at the 24-hour time point ($P = 0.0006$, ***, nonparametric Mann-Whitney U test; WT $n = 20$, R-Ras KO $n = 18$). *Error bars* represent SEM. To assess the IgG protein accumulation, OIR retinas were harvested at P17, proteins were extracted and samples were electrophoresed on gradient gels, and Western blotting was done using anti-mouse IgG antibody. (**D**) Representative images of immunoblotting from where mouse IgG heavy chain densities were quantified and normalized against GAPDH. Relative comparison of IgG heavy chain protein from WT OIR and R-Ras KO OIR samples gives a 3.5-fold difference ($P = 0{,}0007$, ***, nonparametric Mann-Whitney U test). There is no difference in the IgG protein level between healthy WT and KO mice at P17 ($P = 0.7879$). *Error bars* represent ± 95% confidence intervals. (WT: $n = 6$, KO: $n = 6$, WT OIR: $n = 14$, KO OIR: $n = 16$.)

R-Ras Deficiency Severely Impairs Pericyte Coverage of Angiogenic Blood Vessels and Reduces VE-Cadherin Expression in OIR Model

Close interaction between sprouting endothelium and pericytes is crucial for vessel maturation and stability.[41,42] Pathologic, angiogenic vasculature in tumors is characterized by insufficient pericyte association around the blood vessels.[43] Consistent with this notion, a significant reduction in the direct physical contact between pericytes and the endothelium of blood vessels was found in R-Ras KO retinas in the OIR model at P17 (Figs. 5A–B). When the pericyte coverage around the tips of the sprouting angiogenic blood vessels was quantified, 40% reduction in the pericyte coverage was recorded in the R-Ras KO retinas over the WT retinas ($P = 0.033$; Fig. 5C).

Vascular endothelial-cadherin is a member of cadherin superfamily expressed exclusively on endothelial cells.[21] It is a crucial factor of adherens junctions between the endothelial cells.[15] R-Ras is known to stabilize adherens junctions by inhibiting VEGF-induced VE-cadherin internalization.[15] We studied the expression of VE-cadherin in OIR model, and we observed that both the intensity of the VE-cadherin immunostaining and colocalization of VE-cadherin with CD31 were significantly reduced in KO mice compared to WT mice (Fig. 5D). Colocalization analysis showed significant reduction in VE-cadherin and CD31 colocalization in R-Ras KO mice compared to WT mice (overlap coefficient according to Manders: $r = 0.51$ for WT, and $R = 0.43$ for KO ($P = 0.04$)). Our finding on VE-cadherin expression is in line what has been reported in tumor vasculature of R-Ras KO and WT mice.[21]

Reduced R–Ras Expression in the Neovessels of Human Diabetic Retinopathy Correlates With Increased Vascular Leakage and the Immature State of the Neovessels

R-Ras expression was restricted exclusively to blood vessels in normal human retina, and it was expressed in all blood vessels in normal human retinas (Supplementary Fig. S8). To address the relevance of our findings on the role of R-Ras in the OIR model to human ischemic retinopathies, the pathologic retinal neovascular membranes that develop in human diabetic retinopathy patients were studied. These neovascular membranes were collected from patients suffering from type I diabetes, who had already developed tractional retinal detachment due to fibrosis of neovascular membranes. Thus, the samples represent the end stage of the disease, where substantial amount of fibrosis is associated with neovessels, but they still contain regions with active pathologic angiogenesis. In the diabetic neovascular membranes, R-Ras expression was exclusively restricted to blood vessels (Fig. 6). Like pathologic preretinal neovessels in the OIR model, human diabetic neovascular membranes had varying expression of R-Ras (Fig. 6). Only approximately 80% of the blood vessels in the human neovascular membranes expressed any R-Ras protein at all (Fig. 6C). To explore whether R-Ras expression has any relation to the blood vessel maturity, the human tissue samples were double-stained for R-Ras and VEGFR2, a marker of blood vessel immaturity.[44,45] A strong inverse correlation between expression of the two proteins was identified (Spearman's $\rho = -0.821$, $P = 0.023$, $R^2 = 0.563$); the higher the percentage of immature blood vessels (VEGFR2+), the less R-Ras expression there was in the blood vessels (Fig. 6).

To address whether lack of R-Ras in immature blood vessels influences vascular permeability in human diabetic neovascular membranes, samples were stained for HSA. Samples with a low percentage of R-Ras–expressing blood vessels showed a strong accumulation of HSA outside the vessels, whereas samples with a high percentage of R-Ras–expressing blood vessels had HSA staining restricted mainly inside the vessels (Figs. 6A–B). There was a strong negative correlation between area of extravascular HSA and the number of R-Ras–positive vessels (Spearman's ρ: $r = -0.886$, $P = 0.019$, $R^2 = 0.835$); the more vascular leakage outside of the blood vessels, the less R-Ras expression was in the blood vessels. Furthermore, we could demonstrate that leaked, extravascular HSA was detected mainly around individual blood vessels that lack R-Ras (Fig. 7). This was especially evident in samples that had R-Ras in the majority of blood vessels as extravascular HSA mainly accumulated around those few blood vessels devoid of R-Ras expression (Fig. 7).

Discussion

The present study demonstrates that the small GTPase R-Ras regulates the pathologic permeability of blood vessels in hypoxia-driven angiogenesis without altering the rate of

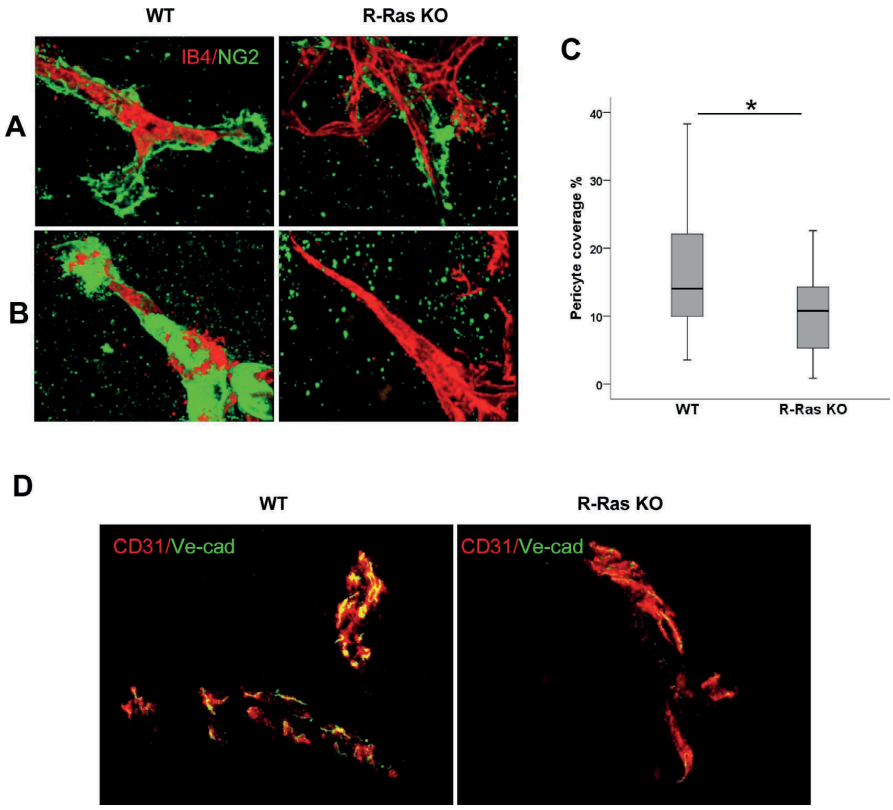

FIGURE 5. Pericyte coverage and VE-cadherin expression is reduced in R-Ras KO in the OIR model in angiogenic retinal blood vessels. Oxygen-induced retinopathy was induced in WT and R-Ras KO mice as described previously. Retinas were harvested at P17, and whole-mount retinas were double-stained with Alexa Fluor–conjugated Isolectin IB_4 and with an antibody against the pericyte marker NG2 proteoglycan. Three-dimensional images were taken from the most superficial vascular plexus at the tips of the blood vessels from the region where vessels grow toward the optic nerve. (**A**) Representative images of WT and R-Ras KO blood vessel endothelial cells (*red*) surrounded by pericytes (*green*). (**B**) The majority of images from WT mice retina had a lot of pericytes around the blood vessels, whereas the majority of pictures taken from the KO retinal blood vessels were lacking or had very few pericytes. (**C**) Direct contact between endothelial cells and pericytes was quantified by colocalization analysis. The result is shown as a percentage of endothelial cell area colocalized with pericytes in WT and R-Ras KO retinal blood vessel tips. The pericyte coverage is significantly reduced in R-Ras KO animals compared to WT by 40% ($P = 0.033$, *). *Error bars* represent ± 95% confidence intervals. (WT: $n = 15$; R-Ras KO: $n = 15$. Two pictures were taken from each retina, and an average was calculated). The expression of VE-cadherin was studied in the OIR model by staining frozen cross-sections of retina with antibodies against VE-cadherin and endothelial cells (CD31). The intensity as well as the colocalization of VE-cadherin staining with endothelial cells was quantified using BioImageXD. (**D**) Representative images of VE-cadherin (*green*) and CD31 (*red*) in P17 OIR model in WT and R-Ras KO are presented. Colocalization analysis showed significant reduction in VE-cadherin and CD31 colocalization in R-Ras KO mice compared to WT mice (overlap coefficient according to Manders: $r = 0.51$ for WT and $R = 0.43$ for KO [$P = 0.04$]), $n = 5$ mice for WT and $n = 5$ mice for KO.

revascularization of the hypoxic retina. Furthermore, by analyzing a set of preretinal vascular membranes obtained from diabetic retinopathy patients, we were able to demonstrate that neovascular membranes with reduced R-Ras expression in immature vessels display increased pathologic vascular leakage. Given that increased vascular leakage is the pathognomonic feature in human diabetic retinopathy, our study implicates that loss of R-Ras may have a pathologic role in this disease.

R-Ras reduced the pathologic vascular permeability in ischemia-induced retinopathy without inhibiting retinal angiogenesis, whether it was developmental or induced by hypoxia in OIR. This is a clear difference to all current available antiangiogenic therapies that have been shown to function in OIR by inhibiting sprouting angiogenesis.[36] Furthermore, the mechanism of resistance to the currently available antiangiogenic therapies both in tumors and retinopathy is actually related to the eradication of the neovessels, which, in turn, worsens the underlying ischemia and drives the formation of new, leaky blood vessels by alternative molecular mechanism.[13] Thus, the proposed molecular mechanism for future antiangiogenic therapies is one in which the angiogenic blood vessels are "normalized" to stable ones to alleviate the hypoxia and stop the detrimental aberrant vascular leakage.[46,47] Taken with earlier demonstrations of a causal relationship between R-Ras expression and vessel maturation,[15,20,48,49] our results suggest potential utility of R-Ras in treating retinopathies involving angiogenesis. Modulating R-Ras expression repre-

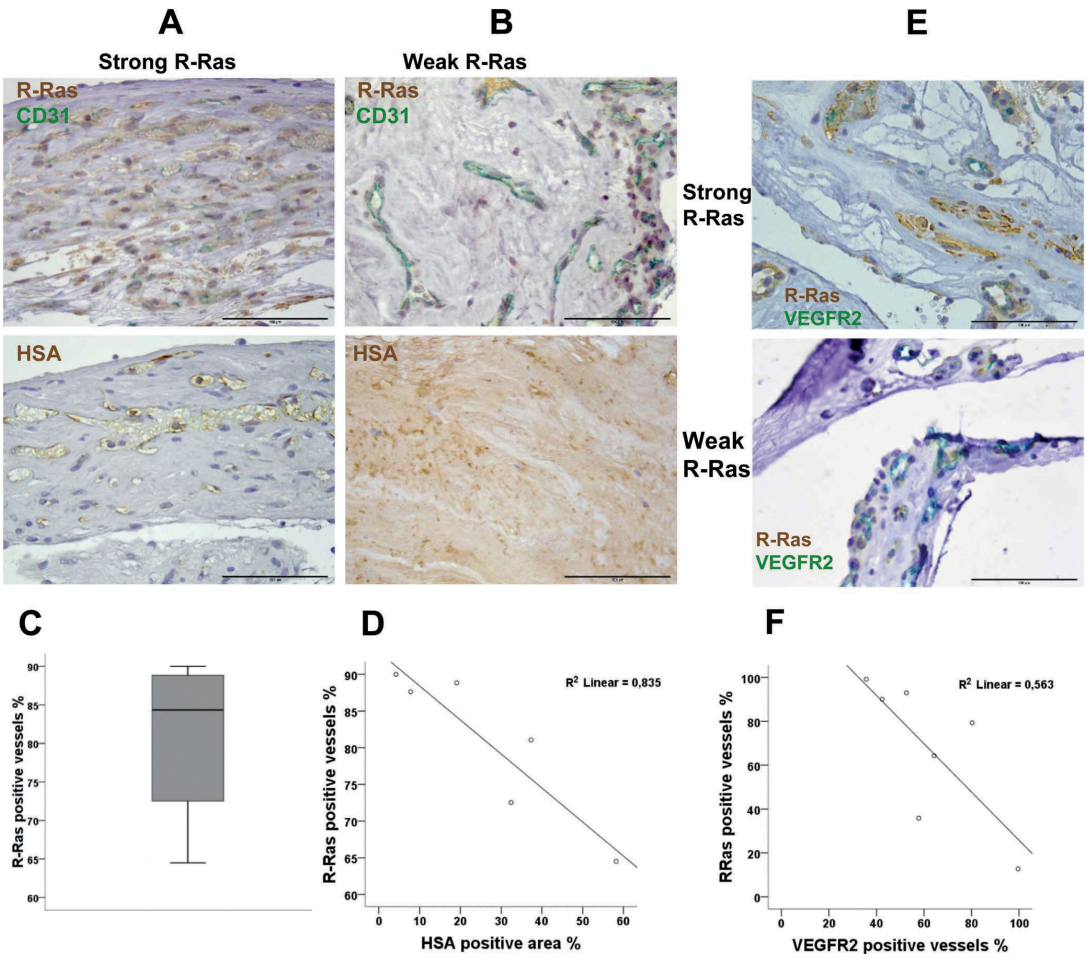

FIGURE 6. Reduced R-Ras expression correlates with leakage of human serum albumin in human diabetic retinopathy vasculature, and it is negatively correlated with VEGFR2 expression. Preretinal neovascular membranes obtained from vitrectomies from diabetic retinopathy patients were analyzed by immunohistochemistry for their protein expression. Immunohistochemical staining from adjacent sections was done with anti-CD31 + anti–R-Ras, anti-HSA, and anti–R-Ras + anti-VEGFR2 antibodies. The number of R-Ras–positive vessels was calculated from R-Ras and CD31 double-stained sections ($n = 7$; 5–9 different sections analyzed from each sample). Correlation analysis between R-Ras and VEGFR2 was done from R-Ras + VEGFR2 double-stained sections and compared to CD31 staining from adjacent sections ($n = 7$; 5–9 different sections analyzed from each sample). Vascular membranes with strong R-Ras expression show limited extravascular staining for HSA (**A**), whereas samples with weak R-Ras expression show strong staining for HSA outside the blood vessels (**B**). *Scale bars*: 100 μm. There is a strong inverse correlation between HSA-positive extravascular area and the percentage of R-Ras–positive neovessels (Spearman's ρ: $r = -0.886$, $P = 0.019$, *, $R^2 = 0.835$, $n = 6$ patients) (**D**). (**C**) Approximately 20% of the neovessels do not express any R-Ras at all (R-Ras–positive vessels 81 ± 10%, mean + SD, $n = 6$ patients). Data are shown as a box plot with median and 95% confidence interval. (**E**, **F**) Double-staining for R-Ras and VEGFR2 shows an inverse correlation (Spearman's ρ: $r = -0.821$, $P = 0.023$, $R^2 = 0.563$) between the number of R-Ras–expressing and VEGFR2-positive blood vessels. When a majority of blood vessels has R-Ras expression, a majority of blood vessels are negative for VEGFR2 expression, whereas the VEGFR2 expression is opposite when very few blood vessels express R-Ras. *Scale bars*: 200 μm.

sents a novel therapeutic approach that may be capable of addressing pathologic vascular permeability without simultaneously worsening the underlying pathobiology of the disease— hypoxia.

The differences between the mechanisms of R-Ras and other antiangiogenic therapies are evidenced by a recent report implicating activated Ras signaling as a key mediator of pathologic neovascularization induced by many cytokines and growth factors, including VEGF, in blinding neovascular eye diseases.[22] Westenskow et al.[22] reported that aberrant Ras signaling can be inhibited by a molecule called p120RasGAP. The inhibitory function of p120RasGAP on Ras-driven retinal neovascularization was shown to take place through the inhibition of sprouting angiogenesis.[22] In contrast, R-Ras functions in the retina primarily to stabilize vasculature and prevent leakage and does not inhibit sprouting angiogenesis in OIR. The mechanistic differences between R-Ras and p120Ras-

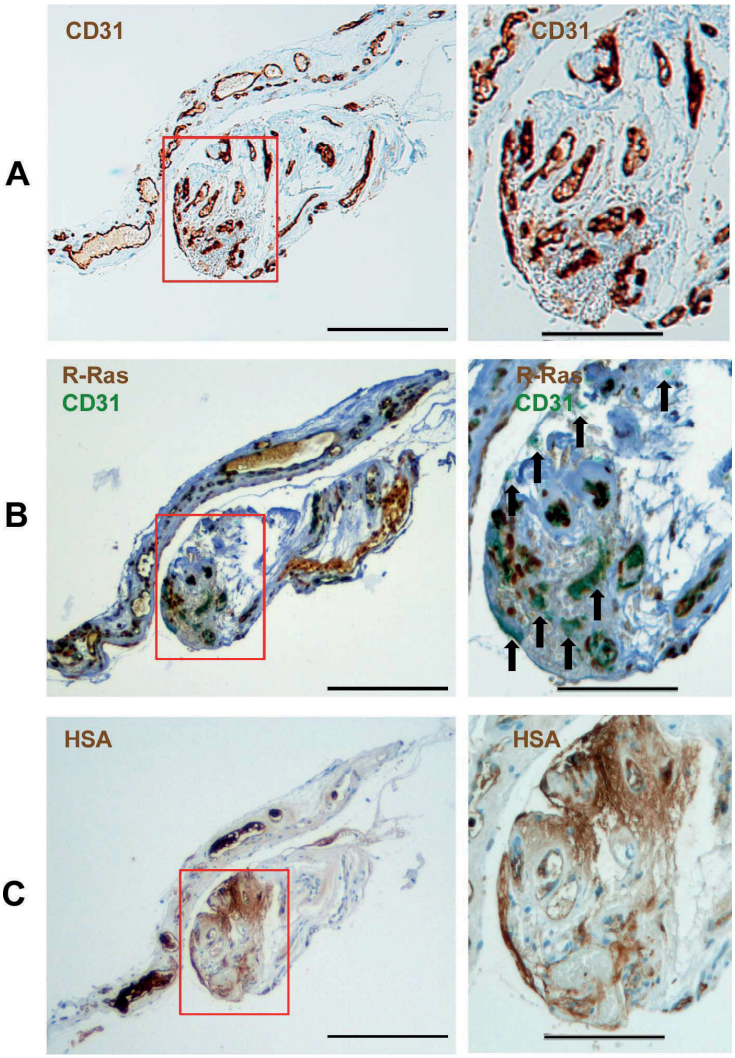

FIGURE 7. Vascular leakage is mainly from blood vessels that do not express R-Ras in human diabetic retinopathy. The preretinal membranes from human diabetic retinopathy patients were either stained for CD31, double-stained for CD31 (*green*) and R-Ras (*brown*) or stained for HSA (*brown*). (**A**) Blood vessels in preretinal membranes stained for endothelial cells (CD31, *brown*). (**B**) Double-staining of blood vessels (CD31, *green*) and R-Ras (*brown*) expression. (**C**) Vascular leakage was determined by using an antibody against HSA (*brown*). Red boxes on figures on the left are presented as high magnification pictures on the right. (**B** and **C**) No vascular leakage (restricted HSA staining only inside the neovessels) can be seen around neovessels with strong R-Ras expression. Conversely, the blood vessels that do not express any R-Ras show aberrant vascular permeability around them. *Arrows* represent R-Ras–negative blood vessels. *Scale bars* on the left represent 450 μm and 200 μm on the right.

GAP are further highlighted by the fact that p120RasGAP actually inhibits R-Ras.[50]

R-Ras has recently been proposed as a master regulator of transendothelial permeability in angiogenesis.[15,21,51] Our understanding of the molecular mechanisms by which R-Ras exerts its biological effects on endothelial cells has increased recently.[15,48] It has been demonstrated that R-Ras suppresses endothelial cells' response to VEGF by inhibiting internalization of VEGFR2 that is required for full activation of the receptor[49] as well as by inhibiting VEGFR2-p38MAPK-HSP27 signaling axis.[51] However, the biological effects of R-Ras in angiogenesis cannot be solely attributed to the inhibition of the VEGF signaling because VEGF inhibitors have been shown to function in OIR by inhibiting sprouting angiogenesis,[36,37] whereas R-Ras is known to promote endothelial cell survival.[20] In addition to the inhibition of VEGF, it has been demonstrated that R-Ras forms a complex with Rab interactor 2 protein and Rab5, and then this complex activate Rac1, which in turn activates integrins to promote endothelial cell adhesion to surrounding ECM.[52,53] R-Ras also interacts with filamin A,

which is crucial for maintaining of endothelial barrier function.[54] Furthermore, actin-binding protein Girdin/GIV regulates transendothelial permeability by controlling VE-cadherin trafficking through R-Ras.[48] In the present study, we confirmed a previous finding that R-Ras is required for recruitment of pericytes around endothelial cells,[21] which is crucial for blood vessel stabilization.[41] In accordance with previous studies on tumors, we demonstrated that R-Ras deficiency reduces VE-cadherin expression in endothelial cells, which may result in increased vessel leakiness in R-Ras–deficient mice.[21]

We demonstrate that angiogenic blood vessels, especially immature VEGFR2+ vessels, show reduced expression of R-Ras in human diabetic neovascular membranes, and the reduced R-Ras expression correlates with increased vascular leakage from the neovessels of human diabetic vasculature. We suggest that reduced vascular R-Ras expression is a critical feature in the pathogenesis of human diabetic retinopathy, especially in the accumulation of retinal edema. Thus, R-Ras represents a promising new therapeutic target to address angiogenesis-related pathologic vascular permeability.

Acknowledgments

The authors thank Anni Laitinen, Marianne Karlsberg, and Marja-Leena Koskinen for excellent technical assistance; Erkki Ruoslahti (Sanford Burnham Prebys Medical Discovery Institute, La Jolla, CA, USA) for providing the R-Ras knockout mice for the study and for his thoughtful comments on the manuscript; and William B. Stallcup (Sanford Burnham Prebys Medical Discovery Institute, La Jolla, CA, USA) for providing the NG2 antibody. The work was supported by the Sigrid Juselius Foundation, the Academy of Finland, Päivikki and Sakari Sohlberg Foundation, Instrumentarium Research Foundation, Finnish Medical Foundation, Pirkanmaa Hospital District Research Foundation, the Finnish Cultural Foundation, Finnish Diabetic Research Foundation, Diabetes Wellness Foundation, Tampere Tuberculosis Foundation, Finnish Eye Foundation, National Institute of Health Grant CA125255, National Science Foundation Grant CBET-1403535, and Florida Department of Health, Bankhead Coley Cancer Program Grant 4BB17, and the Mary and Georg Ehrnrooth Foundation.

Disclosure: **M. Vähätupa**, None; **S. Prince**, None; **S. Vataja**, None; **T. Mertimo**, None; **M. Kataja**, None; **K. Kinnunen**, None; **V. Marjomäki**, None; **H. Uusitalo**, None; **M. Komatsu**, None; **T.A.H. Järvinen**, None; **H. Uusitalo-Järvinen**, None

References

1. Ferrara N, Davis–Smyth T. The biology of vascular endothelial growth factor. *Endocr Rev*. 1997;18:4–25.
2. Keck PJ, Hauser SD, Krivi G, et al. Vascular permeability factor, an endothelial cell mitogen related to PDGF. *Science*. 1989; 246:1309–1312.
3. Vinores SA, Chan CC, Vinores MA, et al. Increased vascular endothelial growth factor (VEGF) and transforming growth factor beta (TGFbeta) in experimental autoimmune uveoretinitis: upregulation of VEGF without neovascularization. *J Neuroimmunol*. 1998;89:43–50.
4. Ford JA, Lois N, Royle P, Clar C, Shyangdan D, Waugh N. Current treatments in diabetic macular oedema: systematic review and meta-analysis. *BMJ Open*. 2013;3:e002269.
5. Arevalo JF, Maia M, Flynn HW Jr, et al. Tractional retinal detachment following intravitreal bevacizumab (Avastin) in patients with severe proliferative diabetic retinopathy. *Br J Ophthalmol*. 2008;92:213–216.
6. Moradian S, Ahmadieh H, Soheilian M, Dehghan MH, Azarmina M. Intravitreal bevacizumab in active progressive proliferative diabetic retinopathy. *Graefes Arch Clin Exp Ophthalmol*. 2008;246:1699–1705.
7. Chakravarthy U, Harding SP, Rogers CA, et al.; and the IVAN Study Investigators. Ranibizumab versus bevacizumab to treat neovascular age-related macular degeneration: one-year findings from the IVAN randomized trial. *Ophthalmology*. 2012; 119:1399–1411.
8. Matsuyama K, Ogata N, Matsuoka M, Wada M, Takahashi K, Nishimura T. Plasma levels of vascular endothelial growth factor and pigment epithelium-derived factor before and after intravitreal injection of bevacizumab. *Br J Ophthalmol*. 2010; 94:1215–1218.
9. Petrou P, Georgalas I, Giavaras G, Anastasiou E, Ntana Z, Petrou C. Early loss of pregnancy after intravitreal bevacizumab injection. *Acta Ophthalmol*. 2010;88(4):e136.
10. Chen HX, Cleck JN. Adverse effects of anticancer agents that target the VEGF pathway. *Nat Rev Clin Oncol*. 2009;6:465–477.
11. Nazer B, Humphreys BD, Moslehi J. Effects of novel angiogenesis inhibitors for the treatment of cancer on the cardiovascular system: focus on hypertension. *Circulation*. 2011;124:1687–1691.
12. Anderson OA, Bainbridge JW, Shima DT. Delivery of anti-angiogenic molecular therapies for retinal disease. *Drug Discov Today*. 2010;15:272–282.
13. Manousaridis K, Talks J. Macular ischaemia: a contraindication for anti-VEGF treatment in retinal vascular disease? *Br J Ophthalmol*. 2012;96:179–184.
14. Lowe DG, Capon DJ, Delwart E, Sakaquchi AY, Naylor SL, Goeddel DV. Structure of the human and murine R-ras genes, novel genes closely related to ras proto-oncogenes. *Cell*. 1987; 48:137–146.
15. Sawada J, Komatsu M. Normalization of tumor vasculature by R-Ras. *Cell Cycle*. 2012;11:4285–4286.
16. Lowe DG, Goeddel DV. Heterologous expression and characterization of the human R-ras gene product. *Mol Cell Biol*. 1987;7:2845–2856.
17. Zhang Z, Vuori K, Wang H, Reed JC, Ruoslahti E. Integrin activation by R-ras. *Cell*. 1996;85:61–69.
18. Suzuki J, Kaziro Y, Koide H. Positive regulation of skeletal myogenesis by R-Ras. *Oncogene*. 2000;19:1138–1146.
19. Ehrhardt A, Ehrhardt GR, Guo X, Schrader JW. Ras and relatives—job sharing and networking keep an old family together. *Exp Hematol*. 2002;30:1089–1106.
20. Komatsu M, Ruoslahti E. R-Ras is a global regulator of vascular regeneration that suppresses intimal hyperplasia and tumor angiogenesis. *Nat Med*. 2005;11:1346–1350.
21. Sawada J, Urakami T, Li F, et al. Small GTPase R-Ras regulates integrity and functionality of tumor blood vessels. *Cancer Cell*. 2012;22:235–249.
22. Westenskow PD, Kurihara T, Aquilar E, et al. Ras pathway inhibition prevents neovascularization by repressing endothelial cell sprouting. *J Clin Invest*. 2013;123:4900–4908.
23. Smith LE, Wesolowski E, McLellan A, et al. Oxygen-induced retinopathy in the mouse. *Invest Ophthalmol Vis Sci*. 1994;35: 101–111.
24. Uusitalo-Jarvinen H, Kurokawa T, Mueller BM, Andrade-Gordon P, Friedlander M, Ruf W. Role of protease activated receptor 1 and 2 signaling in hypoxia-induced angiogenesis. *Arterioscler Thromb Vasc Biol*. 2007;27:1456–1462.
25. Stahl A, Chen J, Sapieha P, et al. Postnatal weight gain modifies severity and functional outcome of oxygen-induced proliferative retinopathy. *Am J Pathol*. 2010;177:2715–2723.
26. Huang FJ, You WK, Bonaldo P, Seyfried TN, Pasquale EB, Stallcup WB. Pericyte deficiencies lead to aberrant tumor vascularizaton in the brain of the NG2 null mouse. *Dev Biol*. 2010;344:1035–1046.

27. Kankaanpaa P, Paavolainen L, Tiitta S, et al. BioImageXD: an open, general-purpose and high-throughput image-processing platform. *Nat Methods*. 2012;9:683–689.
28. Livak KJ, Schmittgen TD. Analysis of relative gene expression data using real-time quantitative PCR and the 2(-Delta C(T)) method. *Methods*. 2001;25:402–408.
29. Scheppke L, Aguilar E, Gariano RF, et al. Retinal vascular permeability suppression by topical application of a novel VEGFR2/Src kinase inhibitor in mice and rabbits. *J Clin Invest*. 2008;118:2337–2346.
30. Xu Q, Qaum T, Adamis AP. Sensitive blood-retinal barrier breakdown quantitation using Evans blue. *Invest Ophthalmol Vis Sci*. 2001;42:789–794.
31. May U, Prince S, Vahatupa M, et al. Resistance of R-Ras knockout mice to skin tumour induction. *Sci Rep*. 2015;5: 11663.
32. Fruttiger M. Development of the retinal vasculature. *Angiogenesis*. 2007;10:77–88.
33. Stahl A, Connor KM, Sapieha P, et al. The mouse retina as an angiogenesis model. *Invest Ophthalmol Vis Sci*. 2010;51: 2813–2826.
34. Ehling M, Adams S, Benedito R, Adams RH. Notch controls retinal blood vessel maturation and quiescence. *Development*. 2013;140:3051–3061.
35. Ivins JK, Yurchenco PD, Lander AD. Regulation of neurite outgrowth by integrin activation. *J Neurosci*. 2000;20:6551–6560.
36. Hollanders K, Van Bergen T, Van de Velde S, Stalmans I. Bevacizumab revisited: its use in different mouse models of ocular pathologies. *Curr Eye Res*. 2014;40:1–11.
37. Sone H, Kawakami Y, Segawa T, et al. Effects of intraocular or systemic administration of neutralizing antibody against vascular endothelial growth factor on the murine experimental model of retinopathy. *Life Sci*. 1999;65:2573–2580.
38. Tokunaga CC, Mitton KP, Dailey W, et al. Effects of anti-VEGF treatment on the recovery of the developing retina following oxygen-induced retinopathy. *Invest Ophthalmol Vis Sci*. 2014; 55:1884–1892.
39. Connor KM, Krah NM, Dennison RJ, et al. Quantification of oxygen-induced retinopathy in the mouse: a model of vessel loss, vessel regrowth and pathological angiogenesis. *Nat Protoc*. 2009;4:1565–1573.
40. Mayumi M, Kuritani T, Kubagawa H, Cooper MD. IgG subclass expression by human B lymphocytes and plasma cells: B lymphocytes precommitted to IgG subclass can be preferentially induced by polyclonal mitogens with T cell help. *J Immunol*. 1983;130:671–677.
41. Hellström M, Gerhardt H, Kalén M, et al. Lack of pericytes leads to endothelial hyperplasia and abnormal vascular morphogenesis. *J Cell Biol*. 2001;153:543–553.
42. Uemura A, Ogawa M, Hirashima M, et al. Recombinant angiopoietin-1 restores higher-order architecture of growing blood vessels in mice in the absence of mural cells. *J Clin Invest*. 2002;110:1619–1628.
43. Jain RK. Molecular regulation of vessel maturation. *Nat Med*. 2003;9:685–693.
44. Heidenreich R, Kappel A, Breier G. Tumor endothelium-specific transgene expression directed by vascular endothelial growth factor receptor-2 (Flk-1) promoter/enhancer sequences. *Cancer Res*. 2000;60:6142–6147.
45. Kappel A, Ronicke V, Damert A, Flamme I, Risau W, Breier G. Identification of vascular endothelial growth factor (VEGF) receptor-2 (Flk-1) promoter/enhancer sequences sufficient for angioblast and endothelial cell-specific transcription in transgenic mice. *Blood*. 1999;93:4284–4292.
46. Jain RK. Antiangiogenesis strategies revisited: from starving tumors to alleviating hypoxia. *Cancer Cell* 2014;26:605–622.
47. McIntyre A, Harris AL. Metabolic and hypoxic adaptation to anti-angiogenic therapy: a target for induced essentiality. *EMBO Mol Med*. 2015:7;368–379.
48. Ichimiya H, Maeda K, Enomoto A, Weng L, Takahashi M, Murohara T. Girdin/GIV regulates transendothelial permeability by controlling VE-cadherin trafficking through the small GTPase, R-Ras. *Biochem Biophys Res Commun*. 2015;461: 260–267.
49. Sawada J, Li F, Komatsu M. R-Ras protein inhibits autophosphorylation of vascular endothelial growth factor receptor 2 in endothelial cells and suppresses receptor activation in tumor vasculature. *J Biol Chem* 2015;290:8133–8145.
50. Dail M, Richter M, Godement P, Pasquale B. Eph receptors inactivate R-Ras through different mechanisms to achieve cell repulsion. *J Cell Sci*. 2006;119:1244–1254.
51. Sawada J, Li F, Komatsu M. R-Ras inhibits VEGF-induced p38MAPK activation and HSP27 phosphorylation in endothelial cells. *J Vasc Res*. 2015;52:347–359.
52. De Franceschi N, Hamidi H, Alanko J, Sahgal P, Ivaska J. Integrin traffic—the update. *J Cell Sci*. 2015;128;839–852.
53. Sandri C, Caccavari F, Valdembri D, et al. The R-Ras/RIN2/Rab5 complex controls endothelial cell adhesion and morphogenesis via active integrin endocytosis and Rac signaling. *Cell Res*. 2012;22:1479–1501.
54. Griffiths GS, Grundl M, Allen JS III, Matter ML. R-Ras interacts with filamin A to maintain endothelial barrier function. *J Cell Physiol*. 2011;226:2287–2296.

Investigative Ophthalmology & Visual Science

Supplementary information:

Lack of R-Ras Leads to Increased Vascular Permeability in Ischemic Retinopathy

Maria Vähätupa, Stuart Prince, Suvi Vataja, Teija Mertimo, Marko Kataja, Kati Kinnunen, Varpu Marjomäki, Hannu Uusitalo, Masanobu Komatsu, Tero AH Järvinen & Hannele Uusitalo-Järvinen

Supplementary Figure S1

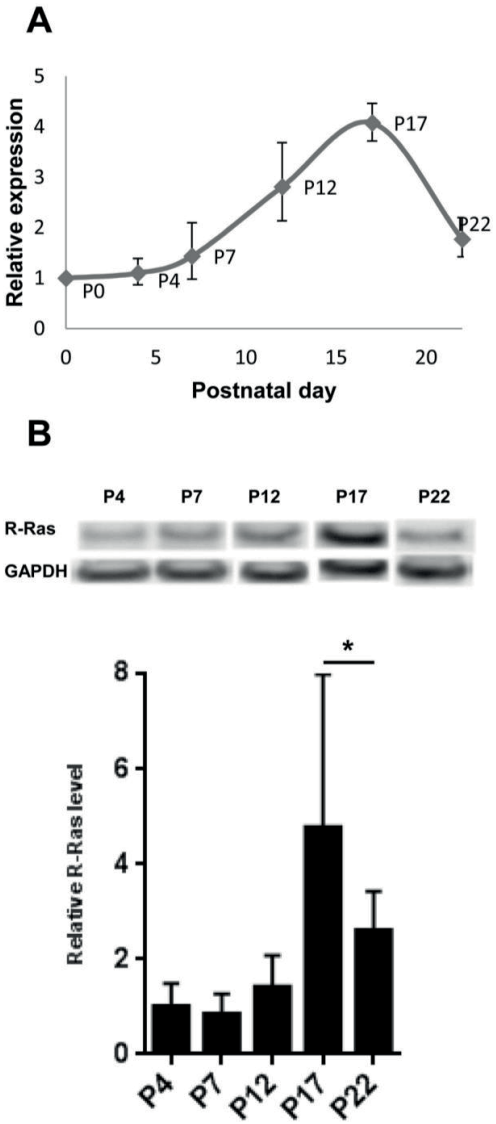

Supplementary Figure S1. ***Rras*** **mRNA expression increases along the maturation of retinal vasculature.** Retinal vasculogenesis was analyzed from normal mice at different time points (P0 – P22) during the development of retinal vasculature. Retinas were subjected to either quantitative mRNA (qPCR) or protein (western blotting) analysis as described in Figure 1. (**A**) The graph shows a pattern of relative *Rras* mRNA expression in the retina during development. The fold change in mRNA expression level is relative to P0 expression level ($2^{-\Delta\Delta Ct}$ method). On the X-axis is the postnatal day on which gene expression was measured. Error bars represent ± 95% confidence

intervals of the fold change (calculated from the ΔΔCt values and the limits has been anti-logged to get the confidence limits for the fold changes). (At P0 n=2, at other time points n=3 – 5.) (**B**) The R-Ras protein expression densitometry shows a similar pattern, where the expression peaks at P17 and drops thereafter. (p=0,016, *; P4, P7, P17 and P22 n=5, P12 n=4). The samples presented above were run on the same gel. Representative samples cropped and presented side-by-side.

Supplementary Figure S2

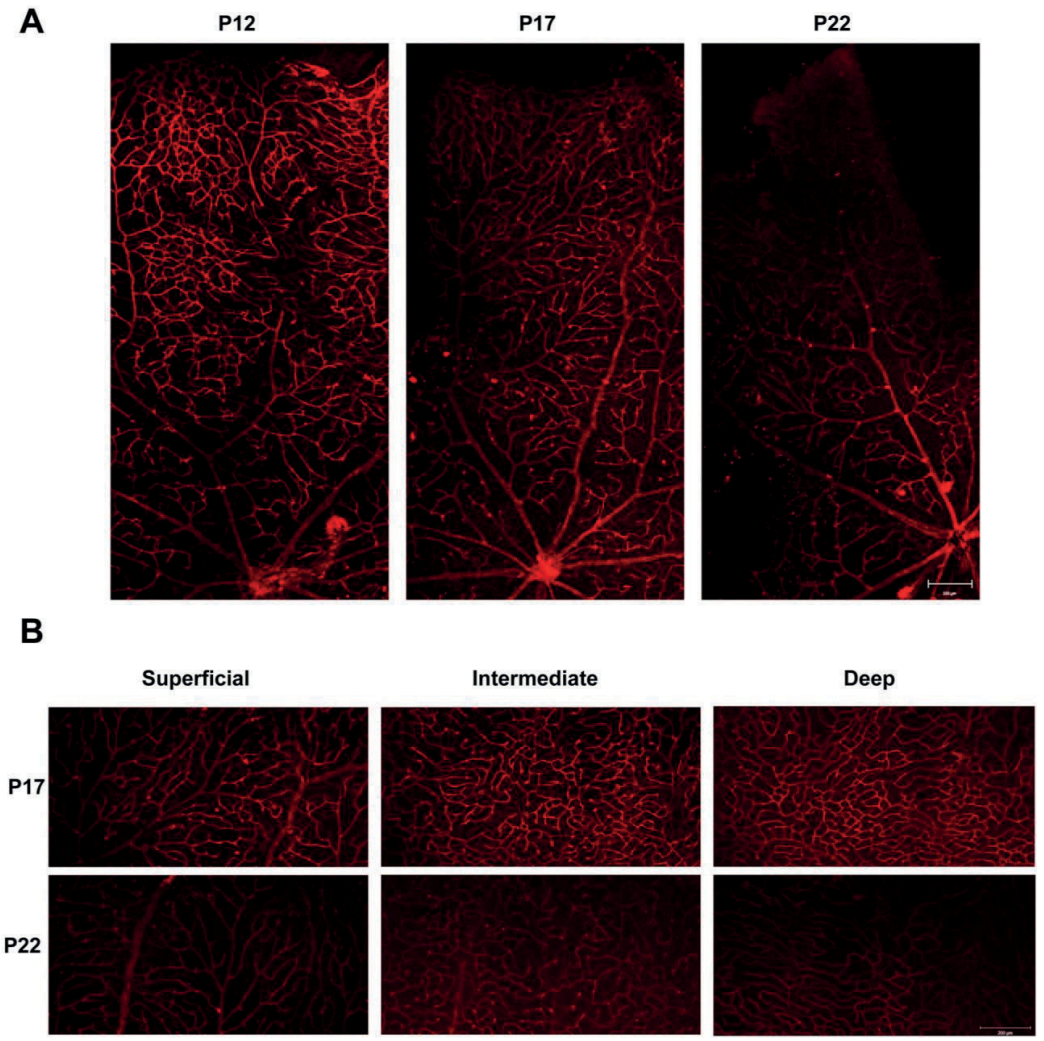

Supplementary Figure S2. Maturation and remodeling of the retinal vasculature. WT retinas from different time points (P12, P17 and P22) were dissected and fixed with 4% PFA. Retinas were stained with Alexa Fluor conjugated Isolectin IB_4 and imaged with confocal microscopy. (**A**) Representative images of sections of whole mounted retinas show a decrease in the intensity of the Isolectin IB_4 signals at P12 onwards. (**B**) All retinal vascular plexuses (superficial, intermediate and deep) show decreased intensity of Isolectin IB_4.

Supplementary Figure S3

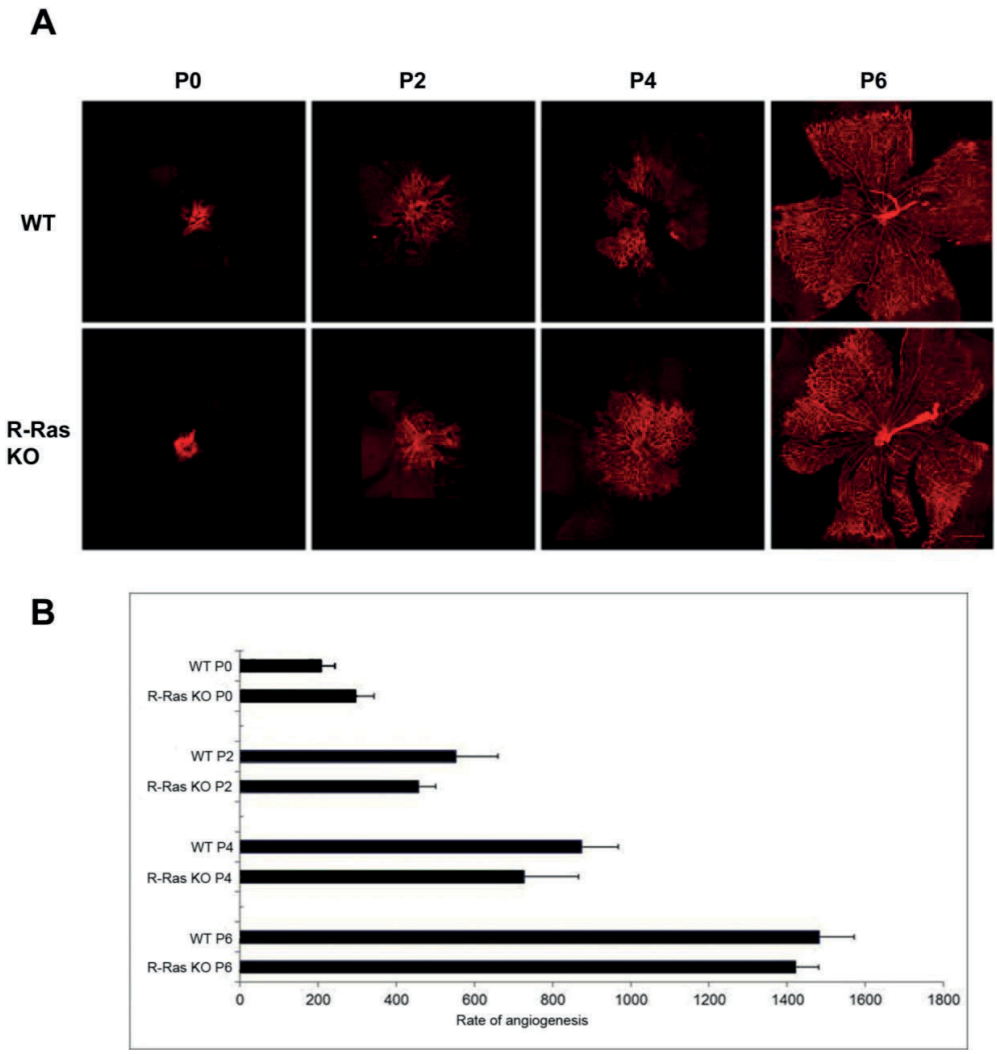

Supplementary Figure S3. The developmental rate of retinal angiogenesis is not affected by R-Ras deficiency. Eyes were harvested from healthy mice at P0-P6 when the development of the superficial vascular plexus occurs. Retinas were fixed with 4% PFA and stained with Alexa Fluor conjugated Isolectin IB_4. (**A**) The rate of early angiogenesis was quantified in retinal flat mounts by measuring the length of vasculature from the optic nerve to the tips of the blood vessels. Four measurements per retina were taken and an average was calculated. The length of angiogenic vasculature of superficial vascular plexus is the same in WT and R-Ras KO retinas at all analyzed

time points. Scale bar represents 500 μm. (**B**) There is no significant difference in the length of vasculature in superficial vascular plexus between WT and R-Ras KO mice during development (NS, student´s t-test). Error bars represent SDs. (WT n=41, R-Ras KO n=33)

Supplementary Figure S4

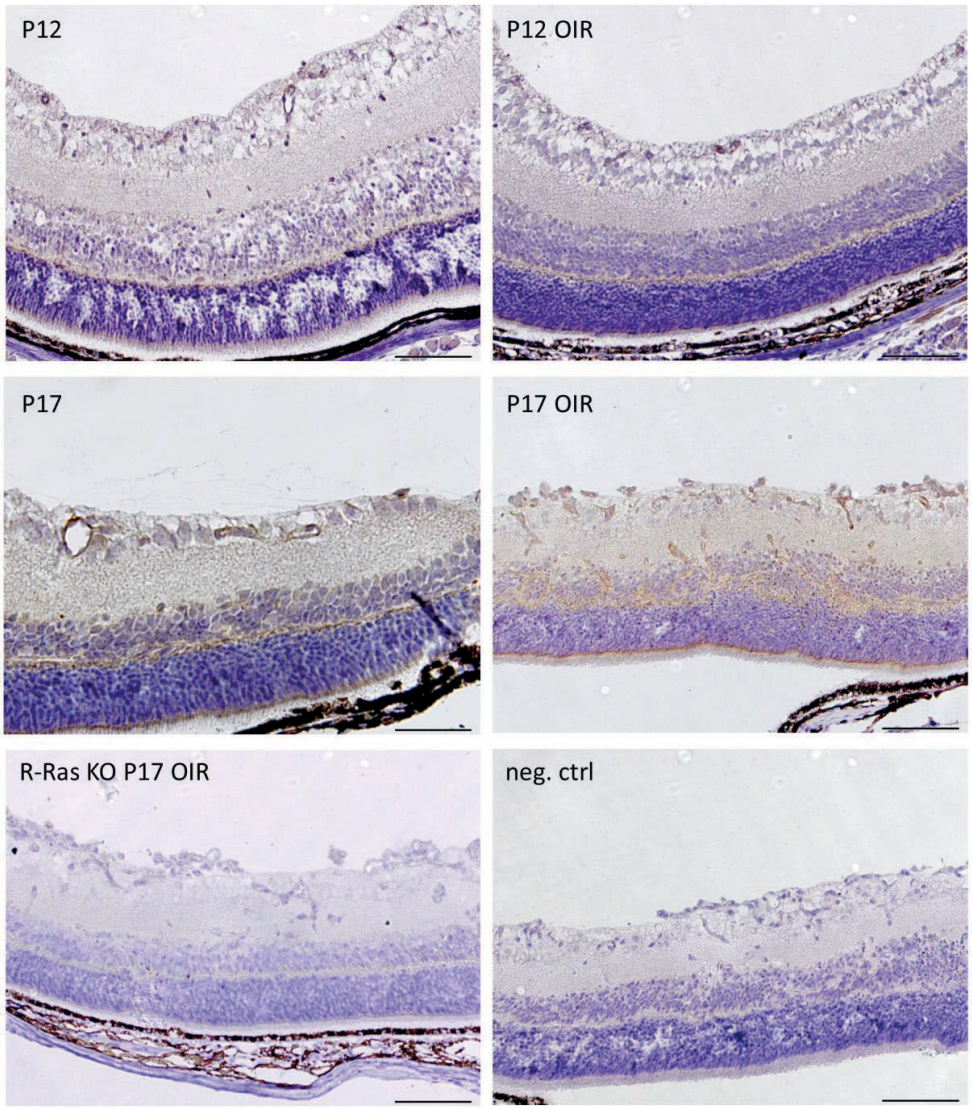

Supplementary Figure S4. R-Ras expression in retina during development and oxygen induced retinopathy (OIR). Strong R-Ras expression can be seen from the retinal blood vessels, while a faint expression is seen from neurons during normal development at P12 and P17. R-Ras expression decreases from the retina after 5 days exposure to 75 % oxygen (P12 OIR). On return to normoxia, strong R-Ras expression can be seen in the blood vessels that re-vascularize the retina,

whereas some of the preretinal neovessels are negative for R-Ras expression in OIR mouse model (P17 OIR). Both R-Ras KO retinas (R-Ras KO P17 OIR) and negative immunohistochemical control show no R-Ras staining at P17 in OIR model. Eyes were harvested at P12 and P17 during normal development and in OIR model.

Supplementary Figure S5

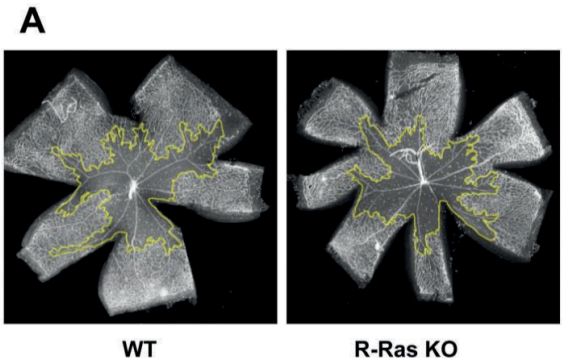

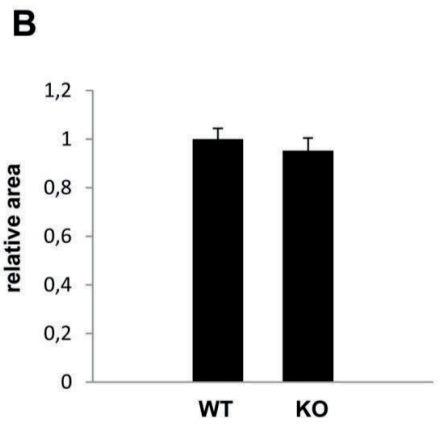

Supplementary Figure S5. R-Ras deficiency doesn't affect vascular regression in OIR model. WT and R-Ras KO mice pups were exposed to 75% hyperoxia for 5 days. Retinas were harvested right after the return to normoxia to quantify the degree of vascular regression. (**A-B**) Quantitative analysis of avascular areas (inside the line) at P12 shows that the vascular regression is similar in WT and KO animals. Error bars represents SDs. (WT n=10, KO n=8.)

Supplementary Figure S6

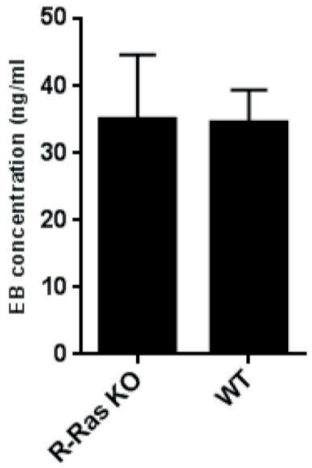

Supplementary Figure S6. There is no difference in vessel permeability in the retinas of healthy WT and R-Ras KO mice. To see whether there is vascular leakage in healthy R-Ras KO animals the Evans Blue dye was injected to WT and R-Ras KO animals and let circulate for 24 hours. Retinas were harvested and plasma samples taken and all samples were incubated in N, N-Dimethylformamide overnight at 78 °C. Evans Blue dye concentration depicting the leakage was measured spectrophotometrically at 620 nm and EB concentration in the retina relative to EB concentration in the plasma was calculated. Graph shows that there is no difference in the vascular permeability between healthy WT and R-Ras KO animals. Error bars represent SEM. (p=0.2398, WT n=7, KO n=8 retinas)

Supplementary Figure S7

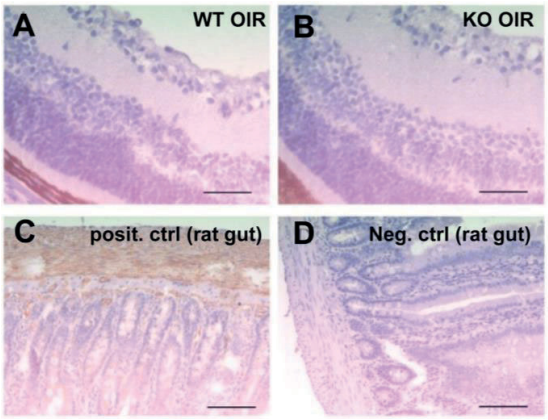

Supplementary Figure S7. **The number of plasma cells is not increased in the R-Ras KO mice retina in oxygen-induced retinopathy.** Plasma cell marker CD138 (1:500) and hematoxylin IHC stainings were done for P17 harvested OIR model retinas. (**A-B**) Representative images of WT and R-Ras KO mice retinas at P17 in the OIR model. Absence of plasma cells both in WT and KO retinas rules out the possibility that the increased levels of IgGs in the R-Ras KO OIR retinas are due to increased levels of plasma cells. (**C**) Positive control (gut) for CD138 (1:500) showing strong signal (brown) and (**D**) negative control (no primary antibody). Scale bars represent 50 μm.

Supplementary Figure S8

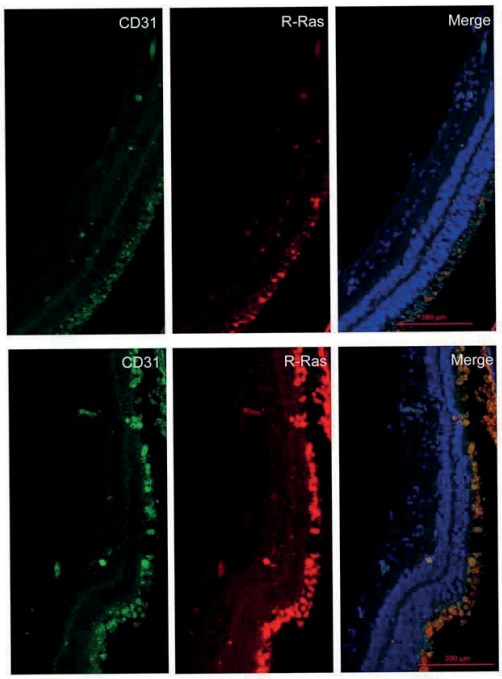

Supplementary Figure 8. R-Ras is expressed by all blood vessels in normal human retina. Normal retinas were collected from two patients whose eyes were enucleated due to choroidal melanoma. The R-Ras expression and blood vessels were determined from the retinas by double-immunofluorescence using R-Ras (green) and CD31 (red) specific primary antibodies and then studied by confocal microscope. (**A**) Representative image of R-Ras expression in normal human retina. R-Ras is restricted exclusively to blood vessels and all of the blood vessels are positive for R-Ras (**B**) Representative confocal image showing the expression of R-Ras (green) and blood vessels (red) in another normal retina. All of the blood vessels express R-Ras also in this sample. Scale bars represent 200 μm.

PUBLICATION II

Furin deficiency in myeloid cells leads to attenuated revascularization in a mouse-model of oxygen-induced retinopathy

Maria Vähätupa, Zuzet Martinez Cordova, Harlan Barker, Saara Aittomäki, Hannu Uusitalo, Tero A.H. Järvinen, Marko Pesu, & Hannele Uusitalo-Järvinen

Experimental Eye Research. 2018, 166:160-167
doi: 10.1016/j.exer.2017.10.013

Experimental Eye Research 166 (2018) 160–167

Contents lists available at ScienceDirect

Experimental Eye Research

journal homepage: www.elsevier.com/locate/yexer

Furin deficiency in myeloid cells leads to attenuated revascularization in a mouse-model of oxygen-induced retinopathy

Maria Vähätupa[a], Zuzet Martinez Cordova[a,b], Harlan Barker[a], Saara Aittomäki[a,b], Hannu Uusitalo[a,c], Tero A.H. Järvinen[a,d], Marko Pesu[a,b,e], Hannele Uusitalo-Järvinen[a,c,*]

[a] Faculty of Medicine & Life Sciences, University of Tampere, Tampere, Finland
[b] Immunoregulation, Institute of Biosciences and Medical Technology (BioMediTech), University of Tampere, Tampere, Finland
[c] Eye Centre, Tampere University Hospital, Tampere, Finland
[d] Departments of Musculoskeletal Disorders, Tampere University Hospital, Tampere, Finland
[e] Departments of Dermatology, Tampere University Hospital, Tampere, Finland

ARTICLE INFO

Keywords:
Angiogenesis
Furin
Macrophage
Oxygen-induced retinopathy model
Hypoxia

ABSTRACT

Ischemic retinopathy is a vision-threatening disease associated with chronic retinal inflammation and hypoxia leading to abnormal angiogenesis. Furin, a member of the proprotein convertase family of proteins, has been implicated in the regulation of angiogenesis due to its essential role in the activation of several angiogenic growth factors, including vascular endothelial growth factor-C (VEGF-C), VEGF-D and transforming growth factor - β (TGF- β). In the present study, we evaluated expression of furin in the retina and its role in retinal angiogenesis. As both inflammation and hypoxia contribute to angiogenesis, the role of furin was evaluated using myeloid-cell specific furin knockout (KO) mice (designated LysMCre-fur$^{(fl/fl)}$) both in developmental retinal angiogenesis as well as in hypoxia-driven angiogenesis using the oxygen-induced retinopathy (OIR) model. In the retina, furin expression was detected in endothelial cells, macrophages and, to some extent, in neurons. The rate of angiogenesis was not different in LysMCre-fur$^{(fl/fl)}$ mice when compared to their wild-type littermates during development. In the OIR model, the revascularization of retina was significantly delayed in LysMCre-fur$^{(fl/fl)}$ mice compared to their wild-type littermates, while there was no compensatory increase in the preretinal neovascularization in LysMCre-fur$^{(fl/fl)}$ mice. These results demonstrate that furin expression in myeloid cells plays a significant role in hypoxia-induced angiogenesis in retina.

1. Introduction

Ischemic retinopathies, such as retinopathy of prematurity (ROP), proliferative diabetic retinopathy (PDR), and retinal vein occlusion (RVO) are major causes of visual impairment and blindness in industrialized countries (Fong et al., 2004; Jonas et al., 2017; Reynolds, 2014). Retinal ischemia induces the stabilization of a transcription factor hypoxia inducible factor-1α (HIF-1α), which turns on the expression of a large number of angiogenic genes such as vascular endothelial growth factor (VEGF) (Campochiaro, 2015). This leads to retinal neovascularization associated with vitreous hemorrhages and fibrosis of neovascular membranes causing tractional retinal detachment and, ultimately, blindness (Campochiaro, 2015).

Retinal ischemia is also associated with inflammatory manifestations. Hypoxia attracts macrophages into hypoxic areas (Mitamura et al., 2005; Tsutsumi et al., 2003) where the hypoxia-activated macrophages and microglia, the immune cells of the retina, release not only proinflammatory but also angiogenic cytokines. In diabetic retinopathy (DR), both invading macrophages and resident microglia have been implicated in the pathogenesis of the retinopathy retinopathy (Abcouwer, 2012). Of note, macrophages have been shown to be the main source of VEGF-C in the retina. In the retina, VEGF-C signaling pathway regulates the branching of blood vessels (Tammela et al., 2011). VEGF-C is initially synthesized as an inactive precursor and requires activation by a proprotein convertase subtilisin/kexin (PCSK) family member furin to become biologically active (Siegfried et al., 2003b).

Proprotein convertase subtilisin/kexin (PCSK) family enzymes are a family of nine proteases (PCSK1-2, furin, PCSK4-7, MBTPS1, PCSK9) that cleave and convert their immature target proteins into biologically active forms by catalyzing endoproteolytic cleavage at a target site typically made up of the basic amino acids arginine and lysine (Turpeinen et al., 2013). Accordingly, PCSK enzymes play a key regulatory role in a multitude of biological events governed by the growth

* Corresponding author. Faculty of Medicine & Life Sciences, 33014, University of Tampere, Finland.
E-mail address: llhauus@uta.fi (H. Uusitalo-Järvinen).

https://doi.org/10.1016/j.exer.2017.10.013
Received 4 January 2017; Received in revised form 1 September 2017; Accepted 11 October 2017
Available online 13 October 2017

factors (Turpeinen et al., 2013). Among the PCSK family members, furin is a ubiquitously expressed prototypical serine endoprotease recently implicated to play a key role in various biological processes such autoimmunity and inflammation, and various human diseases (Oksanen et al., 2014; Pesu et al., 2008; Turpeinen et al., 2013; Vähätupa et al., 2016a). In fibrovascular tissue from PDR patients, furin expression was shown to co-localize with one of its cleavage targets, a (pro)-renin receptor protein, whose expression level is elevated in PDR and associated with angiogenic activity, suggesting that furin cleavage has a role in DR (Kanda et al., 2012).

In addition to VEGF-C (Khatib et al., 2010; Siegfried et al., 2003a), furin is also required for the activation of a large number of other proangiogenic growth factors, such as VEGF-D (McColl et al., 2007), platelet derived growth factors A and B (PDGF-A and –B) (Siegfried et al., 2003b, 2005), bone morphogenetic protein-4 (BMP-4) (Cui et al., 1998) and transforming growth factor-β (TGF-β) (Dubois et al., 2001). On the other hand, the expression of furin itself can be induced by hypoxia, as it is one of the target genes of HIF-1α (Ma et al., 2017; McMahon et al., 2005; Silvestri et al., 2008). Despite being linked to angiogenesis, the functions of furin in these processes are still poorly known, but the phenotype of the total furin knockout (KO) mice, lethality during embryonal development due to cardiovascular defects, suggested blood vessel specific functions (Roebroek et al., 1998; Scamuffa et al., 2006). This notion was confirmed by endothelial specific furin KO that also led to embryonal death due to vascular defects, and by the endothelial cells lacking furin that were unable to grow *ex vivo* (Kim et al., 2012).

As endothelial cells lacking furin cannot grow at all (Kim et al., 2012), we decided to elucidate the role of furin on retinal angiogenesis by addressing the expression of furin in the retina and by assessing the effect of myeloid cell-derived furin on retinal angiogenesis using furin conditional KO mice (myeloid cell-specific furin KO; LysMCre-fur$^{(fl/fl)}$). The effect of myeloid cells-derived furin on angiogenesis was studied in developmental retinal angiogenesis, as well as in hypoxia-induced angiogenesis in a mouse-model for oxygen-induced retinopathy (OIR), which is the most widely used model for ischemic retinopathies (Connor et al., 2009; Smith et al., 1994). In the OIR model, both recruited, blood-derived macrophages as well as the resident macrophages of the retina, microglia, have been shown to participate in the regulation of angiogenesis (Checchin et al., 2006; Gao et al., 2016; Kataoka et al., 2011; Zhou et al., 2015).

2. Results

2.1. Furin is expressed in macrophages and retinal microglia

Using data from published genome-wide expression studies, the retinal-cell specific E-GEOD-33089 experiment and the much wider searching FANTOM project, we extracted expression data for furin in cells related to retina. In the larger, but far less specific, FANTOM project cDNA analysis of furin expression showed the highest values in monocyte derived macrophages (Fig. 1A). In the retinal cell-specific experiment, based on 155 samples analyzed by microarray, the highest furin expression was found in microglia (Fig. 1B).

2.2. Furin is expressed in the retina during development and in the OIR model

To further study the role of furin on retinal angiogenesis *in vivo*, we first determined a temporal and spatial expression profile of furin in WT mice during development and in the OIR model. Immunohistochemistry showed a few cells with weak expression of furin in retina at P4 (postnatal day 4), and thereafter the expression of furin was substantially stronger from P7 onwards at all studied time points during development (Fig. 1C). In the OIR model, strong expression of furin was detected in the vascular layers of the retina at P14 and P17 (Fig. 1D). Using double-immunohistochemistry for furin and for endothelial cells marker CD31 as well as for furin and macrophage marker F4/80, furin expression was localized to endothelial cells (Fig. 1E–F) in the retina and in the preretinal vascular tufts as well as to macrophages surrounding blood vessels (Fig. 1G–H) in OIR retinas. In addition to these cells, furin immunoreactivity was also detected in neurons in the retina (Fig. 1).

2.3. Lack of furin in myeloid cells does not influence the rate of developmental angiogenesis

To investigate the role of furin in angiogenesis, we studied mice deficient for *furin* gene expression in myeloid cells (LysMCre-fur$^{(fl/fl)}$) and their respective wild-type littermates (LysM WT) during developmental retinal angiogenesis and during ischemia induced retinal angiogenesis using oxygen-induced retinopathy model (OIR). LysMCre-fur$^{(fl/fl)}$ mice are fertile without no obvious morphological abnormalities (Cordova et al., 2016), and their eyes appear normal upon histological examination. As total depletion of resident retinal macrophages has been shown to slow down the rate of developmental retinal angiogenesis (Checchin et al., 2006), we first explored whether myeloid cell derived furin influences the rate of superficial vascular plexus formation (developmental angiogenesis) in retinas from P6 LysM WT and LysMCre-fur$^{(fl/fl)}$. In P6 neonatal mice, the diameters of retinal superficial vascular plexuses were similar and no differences in either the number of branching points or filopodia count were detected between LysMCre-fur$^{(fl/fl)}$ and LysM WT mice, indicating that furin expression by myeloid cells does not have a major influence on *in vivo* angiogenesis during neonatal development (Fig. 2A–E). This finding is in line with the above reported appearance of furin at the late stages of retinal vascular development (Fig. 1C).

2.4. Mice deficient for furin expression in myeloid cells show reduced hypoxic revascularization rate of the retina

The role of myeloid cell derived furin in hypoxia-driven neovascularization in the retina was explored next. First, we determined whether regression of vessels under hyperoxic conditions in the OIR model is comparable between LysMCre-fur$^{(fl/fl)}$ and LysM WT mice. After exposure to 75% oxygen between P7 and P12, retinas were evaluated at P12. Typical for this model (Smith et al., 1994; Uusitalo-Järvinen et al., 2007; Vähätupa et al., 2016b), large areas of the central vascular network were regressed with only a few major vessels remaining centrally in both LysM WT and LysMCre-fur$^{(fl/fl)}$ mice (Fig. 2F). Quantitative analysis of vaso-obliterated areas in retina confirmed that the retinal vasculature in LysMCre-fur$^{(fl/fl)}$ and LysM WT mice was similarly affected by hyperoxic exposure (Fig. 2G). Taken together, these data suggest that deletion of furin from myeloid cells has not a significant effect on vascular regression in OIR model.

On return to normoxia, the avascular central retina becomes hypoxic and stimulates rapid regrowth of vessels (Smith et al., 1994; Uusitalo-Järvinen et al., 2007). The rate of retinal revascularization in LysM WT and LysMCre-fur$^{(fl/fl)}$ retinas was determined by quantifying the avascular retinal area 5 days after the mice were returned to normoxia. There was a statistically significant difference in the avascular retinal area between the LysM WT and LysMCre-fur$^{(fl/fl)}$ mice at P17 showing that the rate of retinal revascularization is substantially (30%) reduced in mice where furin is depleted from myeloid cells (Fig. 2J). In addition to revascularization of the retina, the strong hypoxic stimulus from the center of the retina also drives abnormal misdirected sprouting of blood vessels towards the vitreous at the interface between the centrally obliterated and peripherally perfused retina (Smith et al., 1994; Uusitalo-Järvinen et al., 2007). This pathological, preretinal neovascularization reaches its maximum 5 days after return to normoxia (at P17). There was no statistically significant difference in the amount of preretinal neovascularization between LysM WT and

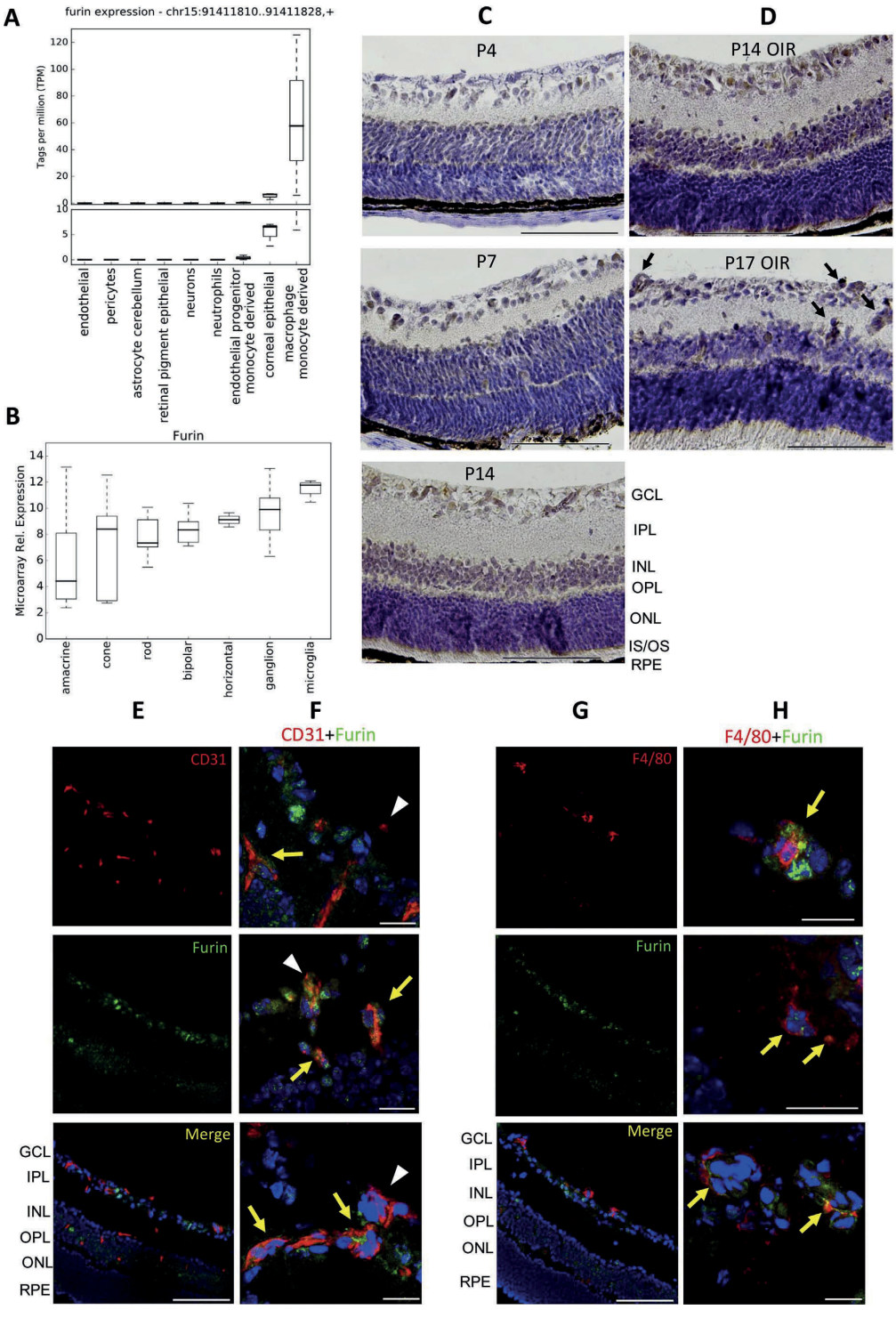

(caption on next page)

Fig. 1. Furin is expressed by the endothelial cells and macrophages in retina. Using expression data from the FANTOM 5 project, cDNA expression data was extracted for the primary furin CAGE for relevant cell types (A). Expression data for furin in different retinal cell types was extracted from previously performed microarray expression analysis (B). In panels A–B the cell types are sorted by increasing average expression from left to right. Furin expression from retina was determined during developmental angiogenesis at P4, P7 and P14 and in OIR model at P14 and P17 from the revascularized retinas by IHC and IF using furin specific antibody. Representative images of furin expression during development (C) and in the OIR model (D). Arrows are pointing furin specific staining at P17 OIR. Scale bars represents 100 μm. Representative confocal images showing CD31 positive endothelial cells (red) and furin (green) (E–F) and F4/80 positive macrophages (red) and furin (green) (G–H) in the retina of frozen sections after immunofluorescence staining. Panels E and G are showing stainings at 20× magnification and panels F and H at 63× magnification. Arrows are pointing the endothelial cells or macrophages that are expressing furin. Arrowheads are pointing neovascular tufts. GCL, ganglion cell layer; IPL, inner plexiform layer; INL, inner nuclear layer; OPL, outer plexiform layer; ONL, outer nuclear layer; IS/OS, photoreceptor inner/outer segments; RPE, retinal pigment epithelium. Scale bars represents 100 μm in E and G and 20 μm in F and H.

LysMCre-fur$^{(fl/fl)}$ retinas (Fig. 2K). The results indicate that myeloid cell expressed furin has a role in hypoxia-induced revascularization in retina, but does not influence the pathological preretinal neovascularization.

3. Discussion

The present study demonstrates that macrophages associated with retinal blood vessels express furin and the lack of furin in myeloid cells delays hypoxia-driven angiogenesis in retina. It has previously been shown that the endothelial specific deficiency of furin leads to embryonal death due to vascular defects (Roebroek et al., 1998), and the cultured endothelial cells lacking furin cannot grow (Kim et al., 2012). Our results confirm an important role for furin in angiogenesis as we show for the first time that furin deficiency in myeloid cells leads to impaired angiogenesis in hypoxia-induced retinal angiogenesis.

Previous studies have shown that resident macrophages, microglia, are needed for proper angiogenesis in retina during both developmental and hypoxia-induced angiogenesis (Checchin et al., 2006). In this study, we demonstrate that myeloid-cell specific deletion of proprotein convertase furin leads to the attenuation of angiogenesis and reduced vascularization rate in OIR model. Among furin's target proteins are several proangiogenic growth factors, including VEGF-C which is expressed in macrophages and has a role in controlling the branching of blood vessels in the retina (Siegfried et al., 2003a; Tammela et al., 2011). VEGF-A, in turn, does not require activating cleavage by furin. Interestingly, a myeloid-cell specific ablation of VEGF-A expression does not change the VEGF levels in the OIR and does not have any influence on angiogenesis in the OIR model (Liyanage et al., 2016). Although further studies concerning the role of furin in retinal angiogenesis are required, our results suggest that the expression of furin in macrophages may be related to activation of proangiogenic growth factors by furin in the retina. This is in line with previous studies showing simultaneous induction of VEGF-C and furin expression in different disease models (Khatib et al., 2010; Lopez de Cicco et al., 2004; Siegfried et al., 2003a).

A major function of furin is to control the bioavailability of anti-inflammatory TGF-β1 (Pesu et al., 2008). As a matter of fact, both furin and TGF-β are involved in the regulation of each other's activity; furin is needed for the activation of different TGF-β isoforms from inactive precursor molecules to active, mature forms (Pesu et al., 2008; Ventura et al., 2017). The active TGF-β2, in turn, induces furin expression (Ventura et al., 2017). Thus, together they generate a self-sustaining loop for high TGF-β activity (Ventura et al., 2017). TGF-β signaling is associated with neovascularization in many diseases, including neovascular ocular diseases (Amin et al., 1994; Bai et al., 2014; Wang et al., 2017). The expression of TGF-β is elevated in the OIR model, suggesting that TGF-β signaling contributes to retinal revascularization (Yingchuan et al., 2010). A previous study has shown that the TGF-β1 bioactivity is reduced in mice deficient in furin expression in myeloid cells (Cordova et al., 2016). Thus, another plausible explanation for the reduction of revascularization in the retina of LysMCre-fur$^{(fl/fl)}$ mice could be the reduced bioavailability of TGF-β due to lack of activating furin.

Although retinal revascularization rate and the formation of pathological preretinal tufts are inter-related in the OIR model, we identified a delayed revascularization rate in retina without a subsequent increase of pathological preretinal tuft formation in LysMCre-fur$^{(fl/fl)}$ mice in the OIR model. One explanation is that resident macrophages, microglia, persist in the retina in response to five-day long hyperoxia despite blood vessels disappearing completely from retina (Davies et al., 2006). Once the revascularization is initiated upon return to normoxia, i.e. induction of hypoxia in retina, resident microglial cells respond to hypoxia by secreting proangiogenic growth factors and direct the revascularization, but selectively only in retina, where they are located. This notion is supported by the facts that the microglia are mainly located in the avascular areas after the hyperoxia-period and the function of macrophage-derived VEGF-C is to convert the tip cells to stalk cells during retinal angiogenesis (Tammela et al., 2011). The lack of influence on preretinal pathological revascularization in the LysMCre-fur$^{(fl/fl)}$ mice is rather striking because we observed significantly larger avascular areas in LysMCre-fur$^{(fl/fl)}$ mice than in WT mice. This, in turn, should theoretically induce more pronounced compensatory preretinal pathological tuft formation, but we could not demonstrate that. An explanation why larger avascular retinal area does not translate into enhanced preretinal neovascularization, may be impaired proangiogenic growth factor activation in LysMCre-fur$^{(fl/fl)}$ mice.

Taken together our study demonstrates that the lack of furin in myeloid cells delays hypoxia-driven angiogenesis in retina and implicates furin expressed outside of the endothelial cells to the regulation of hypoxia-induced angiogenesis.

4. Methods

4.1. Mice

Monocyte/Macrophage-specific furin conditional knockout LysMCre-fur$^{(fl/fl)}$ was generated as described previously (Cordova et al., 2016). Briefly, mice bearing floxed *fur* alleles were backcrossed six times with C57BL/6 mice. LysMCre mice on C57BL/6 background were purchased from Taconic. LysMCre mice were bred with *fur*$^{(fl/fl)}$ animals to generate myeloid-specific furin knockout mice LysMCre-*fur*$^{(fl/fl)}$. Mice were housed under pathogen-free standard conditions, bred and the genotype was determined by PCR. Mice were fed with standard laboratory pellets and water *ad libitum*. All animal experiments were performed according to the ARVO statement for the use of animals in ophthalmic and vision research in accordance with protocols approved by the National Animal Ethics Committee of Finland.

4.2. Oxygen-induced retinopathy (OIR) model

The experiments on OIR model were carried out as described in detail previously (Smith et al., 1994; Stahl et al., 2010b; Uusitalo-Järvinen et al., 2007; Vähätupa et al., 2016b). Briefly, neonatal mice at P7 and their nursing mother were exposed to 75% oxygen for 5 days. At P12, the mice were returned to normal room air. Animals were euthanized at P12 to assess the degree of vascular regression and at P17 to determine the rate of retinal revascularization and preretinal neovascularization. As postnatal weight gain has been shown to affect outcome in the OIR model, the pups included in the study were weight-matched (Stahl et al., 2010a).

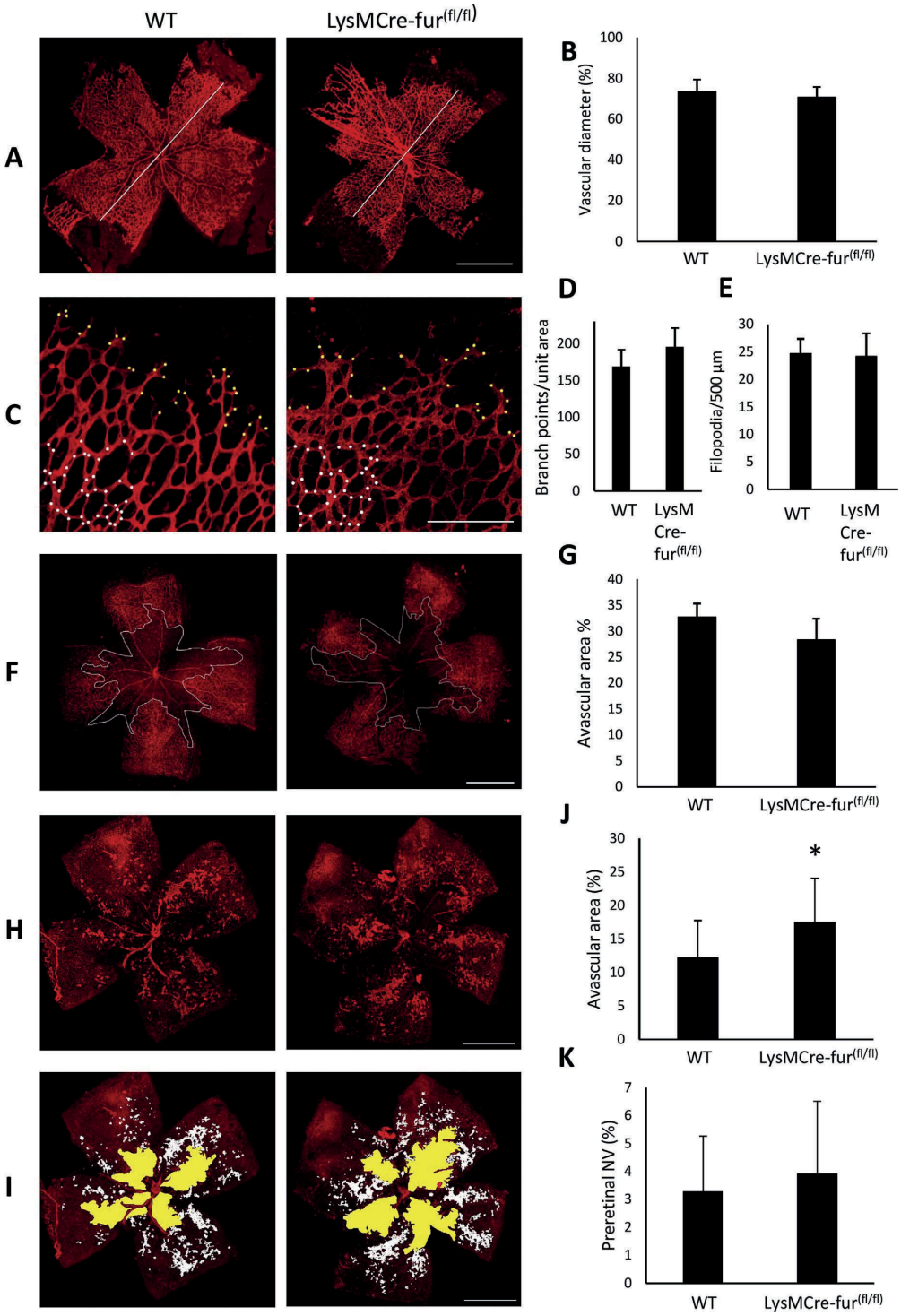

(caption on next page)

Fig. 2. Furin deficiency in myeloid cells inhibits revascularization rate in the retina during the OIR model. Eyes were harvested from healthy and LysMCre-fur($^{fl/fl}$) mice at P6 when the development of the superficial vascular plexus has occurred and in the OIR model at P12 and P17. Retinas were fixed with 4% PFA, flat mounted and stained with Alexa Fluor conjugated Isolectin IB_4. (A) The rate of early angiogenesis was quantified in retinal flat mounts by measuring the length of vasculature via the optic nerve. (B) There was no difference in the length of angiogenic vasculature of superficial vascular plexus between WT and LysMCre-fur($^{fl/fl}$) retinas at P6. (C) The number of branch points (white dots) in retinal vascular plexus and filopodia protrusions (yellow dots) from tip cells were counted from P6 retinas. The results are expressed as the number of branch points per unit area (D) and filopodia per 500 μm of vascular front (E). Both outcomes were similar between genotypes. WT n = 7 and KO n = 6. (F) Representative images of retinas right after the hyperoxic phase of OIR at P12. (G) Quantitative analysis of the avascular areas (inside the white line) shows that the vascular regression is similar in WT and LysMCre-fur($^{fl/fl}$) animals. (WT n = 4, KO n = 7 retinas.) (H) Representative OIR model retinas of WT and LysMCre-fur($^{fl/fl}$) mice at P17. (I) The avascular areas (yellow) and preretinal pathological neovascularization (tufts, white) were quantified. (J) Revascularization rate of retina is reduced by 30% ($p = 0.012$) in the LysMCre-fur($^{fl/fl}$) mice, while no differences were detected in the pathological revascularization, i.e. in the preretinal tufts (K). (WT n = 26 and KO n = 19 retinas.) Scale bar represents 1 mm in A, F, H and I and 200 μm in C. Error bars represent SDs.

4.3. FANTOM analysis of retinal cell types

The FANTOM project has performed expression analysis on 1839 samples from 573 primary cells, 152 tissues, and 250 cell lines in human. Specifically, the data comes from cap analysis gene expression (CAGE) sequencing of cDNA (FANTOM Consortium et al., 2014). Expression data was extracted for the primary furin CAGE for relevant cell types: endothelial cells, pericytes, astrocytes, retinal pigment epithelium cells, neurons, neutrophils, endothelial progenitor cells, corneal epithelial cells and monocyte derived macrophages.

4.4. Microarray analysis of retinal cell types

A microarray expression analysis of mouse genes in various retinal cell type groups was performed previously and is stored as accession E-GEOD-33089 on the ArrayExpress database (https://www.ebi.ac.uk/arrayexpress/experiments/E-GEOD-33089). From the data we extracted furin gene expression values for 155 samples across 7 cell type groups: amacrine, cone, rod, bipolar, horizontal, ganglion, and microglia (Siegert et al., 2012). Both FANTOM and microarray analyses were performed utilizing supercomputer resources provided by CSC–IT Center for Science of the Finnish Ministry of Education and Culture and the raw data was processed as previously described in detail elsewhere (Barker et al., 2017).

4.5. Immunohistochemistry (IHC) and isolectin GS-IB_4 staining

For immunohistochemistry, the eyes were fixed with 4% PFA and embedded in paraffin (for IHC), or freshly frozen in OCT embedding compound in liquid nitrogen cooled isopentane and later fixed with methanol (for immunofluorescence). The IHC stainings were carried out on 4–6 μm thick tissue sections using the following primary antibodies: rabbit anti-furin, (H-220), (Santa Cruz Biotechnology, Dallas, TX), rat anti-CD31 (BD Pharmingen, San Diego, CA) and rat anti-F4/80 (Life Technologies, Paisley, UK) followed by horseradish peroxidase (HRP) or fluorescein-conjugated secondary antibodies. Hematoxylin staining was used as a counterstain. IF samples were mounted with Vectashield mounting medium with DAPI (Vector Laboratories, Burlingame, CA) and images were taken with confocal microscope (Carl Zeiss LSM 700). As a negative control, each staining included sections stained without primary antibody.

4.6. Quantitative analysis of angiogenesis

For the analysis of retinal vasculature, eyes were enucleated, fixed with 4% PFA and retinas dissected. Flat mount retinas were blocked in 10% normal goat serum for 2 h, incubated overnight with Isolectin GS-IB_4 (1:200, Invitrogen, Carlsbad, CA) Retinas were imaged via confocal microscope (Carl Zeiss LSM 700) and the rate of angiogenesis was determined during development (P6) and in the OIR model as previously described (Connor et al., 2009; Stahl et al., 2010b). Briefly, retinas were imaged using confocal microscopy (Carl Zeiss LSM 700) with 10 × objective by focusing on the preretinal neovascular tufts and the underlying superficial vascular plexus. Areas of vascular obliteration and pathological neovascularization (neovascular tufts) were computed, in pixels, and divided by the total retinal area using Adobe Photoshop CS3. The rate of developmental angiogenesis at P6 was determined by measuring the diameter of vasculature via the optic nerve to the tips of the blood vessels. Analysis of vessel branching and number of filopodia sprouts were quantified as previously described (Lobov et al., 2007). Each point where three capillary segments met was counted as one junction. Branch points from the capillary plexus from two areas (370 μm × 550 μm) per retina were counted and results are shown by the average count per unit area. The number of filopodia protrusions from the tip cells were counted from the length of 500 μm of the sprouting vascular front (two measures per retina).

4.7. Statistical analysis

Student's t-test was conducted for normally distributed data and nonparametric Mann-Whitney *U* test (GraphPad Prism 6.01 and IBM SPSS statistics) for non-normally distributed data to test the statistical significance of the results. *P*-values less than 0.05 were considered statistically significant.

5. Statement of author contributions

M.V, T.J and H. U-J designed the research. M.V and H.B. performed the research. M.V, H.B, T.J and H. U-J analyzed the data. M.P, S.A and Z.M.C provided LysMCre-fur($^{fl/fl}$) mice for the study. M.V contributed the genotyped mice littermates. M.V, Z.M.C, H.B, T.J and H. U-J wrote the manuscript. M.V made the figures. All authors reviewed the paper.

Conflict of interest statement

The authors declare no conflict of interest.

Acknowledgements

We thank Marianne Karlsberg for excellent technical assistance. The work was supported by the Sigrid Juselius Foundation, the Academy of Finland, Päivikki and Sakari Sohlberg Foundation, Instrumentarium Research Foundation, Finnish Medical Foundation, Pirkanmaa Hospital District Research Foundation and the Finnish Cultural Foundation, Finnish Diabetic Research Foundation, Finnish Eye Foundation.

References

Abcouwer, S.F., 2012. Neural inflammation and the microglial response in diabetic retinopathy. J. Ocul. Biol. Dis. Infor 4, 25–33.

Amin, R., Puklin, J.E., Frank, R.N., 1994. Growth factor localization in choroidal neovascular membranes of age-related macular degeneration. Invest. Ophthalmol. Vis. Sci. 35, 3178–3188.

Bai, Y., Liang, S., Yu, W., Zhao, M., Huang, L., Zhao, M., Li, X., 2014. Semaphorin 3A blocks the formation of pathologic choroidal neovascularization induced by transforming growth factor β Mol. Vis. 20, 1258–1270.

Barker, H., Aaltonen, M., Pan, P., Vähätupa, M., Kaipiainen, P., May, U., Prince, S., Uusitalo-Järvinen, H., Waheed, A., Pastorekova, S., Sly, W.S., Parkkila, S., Järvinen, T.A., 2017. Role of carbonic anhydrases in skin wound healing. Exp. Mol. Med. 49, e334.

Campochiaro, P.A., 2015. Molecular pathogenesis of retinal and choroidal vascular diseases. Prog. Retin. Eye Res. 49, 67–81.

Checchin, D., Sennlaub, F., Levavasseur, E., Leduc, M., Chemtob, S., 2006. Potential role of microglia in retinal blood vessel formation. Invest. Ophthalmol. Vis. Sci. 47,

3595–3602.
Connor, K.M., Krah, N.M., Dennison, R.J., Aderman, C.M., Chen, J., Guerin, K.I., Sapieha, P., Stahl, A., Willett, K.L., Smith, L.E., 2009. Quantification of oxygen-induced retinopathy in the mouse: a model of vessel loss, vessel regrowth and pathological angiogenesis. Nat. Protoc. 4, 1565–1573.
Cordova, Z.M., Gronholm, A., Kytola, V., Taverniti, V., Hamalainen, S., Aittomäki, S., Niininen, W., Junttila, I., Ylipaa, A., Nykter, M., Pesu, M., 2016. Myeloid cell expressed proprotein convertase FURIN attenuates inflammation. Oncotarget 23 7(34):54392–54404.
Cui, Y., Jean, F., Thomas, G., Christian, J.L., 1998. BMP-4 is proteolytically activated by furin and/or PC6 during vertebrate embryonic development. EMBO J. 17, 4735–4743.
Davies, M.H., Eubanks, J.P., Powers, M.R., 2006. Microglia and macrophages are increased in response to ischemia-induced retinopathy in the mouse retina. Mol. Vis. 12, 467–477.
Dubois, C.M., Blanchette, F., Laprise, M.H., Leduc, R., Grondin, F., Seidah, N.G., 2001. Evidence that furin is an authentic transforming growth factor-β1-converting enzyme. Am. J. Pathol. 158, 305–316.
FANTOM Consortium, the RIKEN PMI, CLST (DGT),Forrest, A.R., Kawaji, H., Rehli, M., Baillie, J.K., de Hoon, M.J., Haberle, V., Lassmann, T., Kulakovskiy, I.V., Lizio, M., Itoh, M., Andersson, R., Mungall, C.J., Meehan, T.F., Schmeier, S., Bertin, N., Jorgensen, M., Dimont, E., Arner, E., Schmidl, C., Schaefer, U., Medvedeva, Y.A., Plessy, C., Vitezic, M., Severin, J., Semple, C., Ishizu, Y., Young, R.S., Francescatto, M., Alam, I., Albanese, D., Altschuler, G.M., Arakawa, T., Archer, J.A., Arner, P., Babina, M., Rennie, S., Balwierz, P.J., Beckhouse, A.G., Pradhan-Bhatt, S., Blake, J.A., Blumenthal, A., Bodega, B., Bonetti, A., Briggs, J., Brombacher, F., Burroughs, A.M., Califano, A., Cannistraci, C.V., Carbajo, D., Chen, Y., Chierici, M., Ciani, Y., Clevers, H.C., Dalla, E., Davis, C.A., Detmar, M., Diehl, A.D., Dohi, T., Drablos, F., Edge, A.S., Edinger, M., Ekwall, K., Endoh, M., Enomoto, H., Fagiolini, M., Fairbairn, L., Fang, H., Farach-Carson, M.C., Faulkner, G.J., Favorov, A.V., Fisher, M.E., Frith, M.C., Fujita, R., Fukuda, S., Furlanello, C., Furino, M., Furusawa, J., Geijtenbeek, T.B., Gibson, A.P., Gingeras, T., Goldowitz, D., Gough, J., Guhl, S., Guler, R., Gustincich, S., Ha, T.J., Hamaguchi, M., Hara, M., Harbers, M., Harshbarger, J., Hasegawa, A., Hasegawa, Y., Hashimoto, T., Herlyn, M., Hitchens, K.J., Ho Sui, S.J., Hofmann, O.M., Hoof, I., Hori, F., Huminiecki, L., Iida, K., Ikawa, T., Jankovic, B.R., Jia, H., Joshi, A., Jurman, G., Kaczkowski, B., Kai, C., Kaida, K., Kaiho, A., Kajiyama, K., Kanamori-Katayama, M., Kasianov, A.S., Kasukawa, T., Katayama, S., Kato, S., Kawaguchi, S., Kawamoto, H., Kawamura, Y.I., Kawashima, T., Kempfle, J.S., Kenna, T.J., Kere, J., Khachigian, L.M., Kitamura, T., Klinken, S.P., Knox, A.J., Kojima, M., Kojima, S., Kondo, N., Koseki, H., Koyasu, S., Krampitz, S., Kubosaki, A., Kwon, A.T., Laros, J.F., Lee, W., Lennartsson, A., Li, K., Lilje, B., Lipovich, L., Mackay-Sim, A., Manabe, R., Mar, J.C., Marchand, B., Mathelier, A., Mejhert, N., Meynert, A., Mizuno, Y., de Lima Morais, D.A., Morikawa, H., Morimoto, M., Moro, K., Motakis, E., Motohashi, H., Mummery, C.L., Murata, M., Nagao-Sato, S., Nakachi, Y., Nakahara, F., Nakamura, T., Nakamura, Y., Nakazato, K., van Nimwegen, E., Ninomiya, N., Nishiyori, H., Noma, S., Noma, S., Noazaki, T., Ogishima, S., Ohkura, N., Ohimiya, H., Ohno, H., Ohshima, M., Okada-Hatakeyama, M., Okazaki, Y., Orlando, V., Ovchinnikov, D.A., Pain, A., Passier, R., Patrikakis, M., Persson, H., Piazza, S., Prendergast, J.G., Rackham, O.J., Ramilowski, J.A., Rashid, M., Ravasi, T., Rizzu, P., Roncador, M., Roy, S., Rye, M.B., Saijyo, E., Sajantila, A., Saka, A., Sakaguchi, S., Sakai, M., Sato, H., Savvi, S., Saxena, A., Schneider, C., Schultes, E.A., Schulze-Tanzil, G.G., Schwegmann, A., Sengstag, T., Sheng, G., Shimoji, H., Shimoni, Y., Shin, J.W., Simon, C., Sugiyama, D., Sugiyama, T., Suzuki, M., Suzuki, N., Swoboda, R.K., t Hoen, P.A., Tagami, M., Takahashi, N., Takai, J., Tanaka, H., Tatsukawa, H., Tatum, Z., Thompson, M., Toyodo, H., Toyoda, T., Valen, E., van de Wetering, M., van den Berg, L.M., Verado, R., Vijayan, D., Vorontsov, I.E., Wasserman, W.W., Watanabe, S., Wells, C.A., Winteringham, L.N., Wolvetang, E., Wood, E.J., Yamaguchi, Y., Yamamoto, M., Yoneda, M., Yonekura, Y., Yoshida, S., Zabierowski, S.E., Zhang, P.G., Zhao, X., Zucchelli, S., Summers, K.M., Suzuki, H., Daub, C.O., Kawai, J., Heutink, P., Hide, W., Freeman, T.C., Lenhard, B., Bajic, V.B., Taylor, M.S., Makeev, V.J., Sandelin, A., Hume, D.A., Carninci, P., Hayashizaki, Y., 2014. A promoter-level mammalian expression atlas. Nature 507, 462–470.
Fong, D.S., Aiello, L., Gardner, T.W., King, G.L., Blankenship, G., Cavallerano, J.D., Ferris 3rd, F.L., Klein, R., American Diabetes Association, 2004. Retinopathy in diabetes. Diabetes Care 27 (Suppl. 1), S84–S87.
Gao, X., Wang, Y.S., Li, X.Q., Hou, H.Y., Su, J.B., Yao, L.B., Zhang, J., 2016. Macrophages promote vasculogenesis of retinal neovascularization in an oxygen-induced retinopathy model in mice. Cell Tissue Res. 364, 599–610.
Jonas, J.B., Mones, J., Glacet-Bernard, A., Coscas, G., 2017. Retinal vein occlusions. Dev. Ophthalmol. 58, 139–167.
Kanda, A., Noda, K., Saito, W., Ishida, S., 2012. (Pro)renin receptor is associated with angiogenic activity in proliferative diabetic retinopathy. Diabetologia 55, 3104–3113.
Kataoka, K., Nishiguchi, K.M., Kaneko, H., van Rooijen, N., Kachi, S., Terasaki, H., 2011. The roles of vitreal macrophages and circulating leukocytes in retinal neovascularization. Invest. Ophthalmol. Vis. Sci. 52, 1431–1438.
Khatib, A.M., Lahlil, R., Scamuffa, N., Akimenko, M.A., Ernest, S., Lomri, A., Lalou, C., Seidah, N.G., Villoutreix, B.O., Calvo, F., Siegfried, G., 2010. Zebrafish ProVEGF-C expression, proteolytic processing and inhibitory effect of unprocessed ProVEGF-C during fin regeneration. PLoS One 5, e11438.
Kim, W., Essalmani, R., Szumska, D., Creemers, J.W., Roebroek, A.J., D'Orleans-Juste, P., Bhattacharya, S., Seidah, N.G., Prat, A., 2012. Loss of endothelial furin leads to cardiac malformation and early postnatal death. Mol. Cell. Biol. 32, 3382–3391.
Liyanage, S.E., Fantin, A., Villacampa, P., Lange, C.A., Denti, L., Cristante, E., Smith, A.J., Ali, R.R., Luhmann, U.F., Bainbridge, J.W., Ruhrberg, C., 2016. Myeloid-derived vascular endothelial growth factor and hypoxia-inducible factor are dispensable for ocular neovascularization–brief report. Arterioscler. Thromb. Vasc. Biol. 36, 19–24.
Lobov, I.B., Renard, R.A., Papadopoulos, N., Gale, N.W., Thurston, G., Yancopoulos, G.D., Wiegand, S.J., 2007. Delta-like ligand 4 (Dll4) is induced by VEGF as a negative regulator of angiogenic sprouting. Proc. Natl. Acad. Sci. U. S. A. 104, 3219–3224.
Lopez de Cicco, R., Watson, J.C., Bassi, D.E., Litwin, S., Klein-Szanto, A.J., 2004. Simultaneous expression of furin and vascular endothelial growth factor in human oral tongue squamous cell carcinoma progression. Clin. Cancer Res. 10, 4480–4488.
Ma, J., Evrard, S., Badiola, I., Siegfried, G., Khatib, A.M., 2017. Regulation of the proprotein convertases expression and activity during regenerative angiogenesis: role of hypoxia-inducible factor (HIF). Eur. J. Cell Biol. 96, 457–468.
McColl, B.K., Paavonen, K., Karnezis, T., Harris, N.C., Davydova, N., Rothacker, J., Nice, E.C., Harder, K.W., Roufail, S., Hibbs, M.L., Rogers, P.A., Alitalo, K., Stacker, S.A., Achen, M.G., 2007. Proprotein convertases promote processing of VEGF-D, a critical step for binding the angiogenic receptor VEGFR-2. FASEB J. 21, 1088–1098.
McMahon, S., Grondin, F., McDonald, P.P., Richard, D.E., Dubois, C.M., 2005. Hypoxia-enhanced expression of the proprotein convertase furin is mediated by hypoxia-inducible factor-1: impact on the bioactivation of proproteins. J. Biol. Chem. 280, 6561–6569.
Mitamura, Y., Harada, C., Harada, T., 2005. Role of cytokines and trophic factors in the pathogenesis of diabetic retinopathy. Curr. Diabetes Rev. 1, 73–81.
Oksanen, A., Aittomäki, S., Jankovic, D., Ortutay, Z., Pulkkinen, K., Hamalainen, S., Rokka, A., Corthals, G.L., Watford, W.T., Junttila, I., O'Shea, J.J., Pesu, M., 2014. Proprotein convertase FURIN constrain Th2 differentiation and is critical for host resistance against Toxoplasma gondii. J. Immunol. 193, 5470–5479.
Pesu, M., Watford, W.T., Wei, L., Xu, L., Fuss, I., Strober, W., Andersson, J., Shevach, E.M., Quezado, M., Bouladoux, N., Roebroek, A., Belkaid, Y., Creemers, J., O'Shea, J.J., 2008. T-cell-expressed proprotein convertase furin is essential for maintenance of peripheral immune tolerance. Nature 455, 246–250.
Reynolds, J.D., 2014. Insights in ROP. Am. Orthopt. J. 64, 43–53.
Roebroek, A.J., Umans, L., Pauli, I.G., Robertson, E.J., van Leuven, F., Van de Ven, W.J., Constam, D.B., 1998. Failure of ventral closure and axial rotation in embryos lacking the proprotein convertase Furin. Development 125, 4863–4876.
Scamuffa, N., Calvo, F., Chretien, M., Seidah, N.G., Khatib, A.M., 2006. Proprotein convertases: lessons from knockouts. FASEB J. 20, 1954–1963.
Siegert, S., Cabuy, E., Scherf, B.G., Kohler, H., Panda, S., Le, Y.Z., Fehling, H.J., Gaidatzis, D., Stadler, M.B., Roska, B., 2012. Transcriptional code and disease map for adult retinal cell types. Nat. Neurosci. 15 487–495, S1-2.
Siegfried, G., Basak, A., Cromlish, J.A., Benjannet, S., Marcinkiewicz, J., Chretien, M., Seidah, N.G., Khatib, A.M., 2003Aa. The secretory proprotein convertases furin, PC5, and PC7 activate VEGF-C to induce tumorigenesis. J. Clin. Invest. 111, 1723–1732.
Siegfried, G., Khatib, A.M., Benjannet, S., Chretien, M., Seidah, N.G., 2003Ab. The proteolytic processing of pro-platelet-derived growth factor-A at RRKR(86) by members of the proprotein convertase family is functionally correlated to platelet-derived growth factor-A-induced functions and tumorigenicity. Cancer Res. 63, 1458–1463.
Siegfried, G., Basak, A., Prichett-Pejic, W., Scamuffa, N., Ma, L., Benjannet, S., Veinot, J.P., Calvo, F., Seidah, N., Khatib, A.M., 2005. Regulation of the stepwise proteolytic cleavage and secretion of PDGF-B by the proprotein convertases. Oncogene 24, 6925–6935.
Silvestri, L., Pagani, A., Camaschella, C., 2008. Furin-mediated release of soluble hemojuvelin: a new link between hypoxia and iron homeostasis. Blood 111, 924–931.
Smith, L.E., Wesolowski, E., McLellan, A., Kostyk, S.K., D'Amato, R., Sullivan, R., D'Amore, P.A., 1994. Oxygen-induced retinopathy in the mouse. Invest. Ophthalmol. Vis. Sci. 35, 101–111.
Stahl, A., Chen, J., Sapieha, P., Seaward, M.R., Krah, N.M., Dennison, R.J., Favazza, T., Bucher, F., Lofqvist, C., Ong, H., Hellstrom, A., Chemtob, S., Akula, J.D., Smith, L.E., 2010Aa. Postnatal weight gain modifies severity and functional outcome of oxygen-induced proliferative retinopathy. Am. J. Pathol. 177, 2715–2723.
Stahl, A., Connor, K.M., Sapieha, P., Chen, J., Dennison, R.J., Krah, N.M., Seaward, M.R., Willett, K.L., Aderman, C.M., Guerin, K.I., Hua, J., Lofqvist, C., Hellstrom, A., Smith, L.E., 2010Ab. The mouse retina as an angiogenesis model. Invest. Ophthalmol. Vis. Sci. 51, 2813–2826.
Tammela, T., Zarkada, G., Nurmi, H., Jakobsson, L., Heinolainen, K., Tvorogov, D., Zheng, W., Franco, C.A., Murtomaki, A., Aranda, E., Miura, N., Yla-Herttuala, S., Fruttiger, M., Makinen, T., Eichmann, A., Pollard, J.W., Gerhardt, H., Alitalo, K., 2011. VEGFR-3 controls tip to stalk conversion at vessel fusion sites by reinforcing Notch signalling. Nat. Cell Biol. 13, 1202–1213.
Tsutsumi, C., Sonoda, K.H., Egashira, K., Qiao, H., Hisatomi, T., Nakao, S., Ishibashi, M., Charo, I.F., Sakamoto, T., Murata, T., Ishibashi, T., 2003. The critical role of ocular-infiltrating macrophages in the development of choroidal neovascularization. J. Leukoc. Biol. 74, 25–32.
Turpeinen, H., Ortutay, Z., Pesu, M., 2013. Genetics of the first seven proprotein convertase enzymes in health and disease. Curr. Genomics 14, 453–467.
Uusitalo-Järvinen, H., Kurokawa, T., Mueller, B.M., Andrade-Gordon, P., Friedlander, M., Ruf, W., 2007. Role of protease activated receptor 1 and 2 signaling in hypoxia-induced angiogenesis. Arterioscler. Thromb. Vasc. Biol. 27, 1456–1462.
Vähätupa, M., Aittomäki, S., Martinez Cordova, Z., May, U., Prince, S., Uusitalo-Järvinen, H., Järvinen, T.A., Pesu, M., 2016EEAa. T-cell-expressed proprotein convertase FURIN inhibits DMBA/TPA-induced skin cancer development. Oncoimmunology 5, e1245266.
Vähätupa, M., Prince, S., Vataja, S., Mertimo, T., Kataja, M., Kinnunen, K., Marjomaki, V., Uusitalo, H., Komatsu, M., Järvinen, T.A., Uusitalo-Järvinen, H., 2016EEAb. Lack of r-ras leads to increased vascular permeability in ischemic retinopathy. Invest. Ophthalmol. Vis. Sci. 57, 4898–4909.
Ventura, E., Weller, M., Burghardt, I., 2017. Cutting edge: ERK1 mediates the autocrine positive feedback loop of TGFβ and furin in glioma-initiating cells. J. Immunol. 198, 4569–4574.

Wang, X., Ma, W., Han, S., Meng, Z., Zhao, L., Yin, Y., Wang, Y., Li, J., 2017. TGFβ participates choroid neovascularization through Smad2/3-VEGF/TNF-α signaling in mice with Laser-induced wet age-related macular degeneration. Sci. Rep. 7 9672–017-10124-4.

Yingchuan, F., Chuntao, L., Hui, C., Jianbin, H., 2010. Increased expression of TGF-β1 and Smad 4 on oxygen-induced retinopathy in neonatal mice. Adv. Exp. Med. Biol. 664, 71–77.

Zhou, Y., Yoshida, S., Nakao, S., Yoshimura, T., Kobayashi, Y., Nakama, T., Kubo, Y., Miyawaki, K., Yamaguchi, M., Ishikawa, K., Oshima, Y., Akashi, K., Ishibashi, T., 2015. M2 macrophages enhance pathological neovascularization in the mouse model of oxygen-induced retinopathy. Invest. Ophthalmol. Vis. Sci. 56, 4767–4777.

PUBLICATION III

SWATH-MS proteomic analysis of oxygen-induced retinopathy reveals novel potential therapeutic targets

Maria Vähätupa, Janika Nättinen, Antti Jylhä, Ulla Aapola, Marko Kataja, Peeter Kööbi, Tero A.H. Järvinen, Hannu Uusitalo, & Hannele Uusitalo-Järvinen

Investigative Ophthalmology & Visual Science. 2018, 59:3294-3306
doi: 10.1167/iovs.18-23831

SWATH-MS Proteomic Analysis of Oxygen-Induced Retinopathy Reveals Novel Potential Therapeutic Targets

Maria Vähätupa,[1] Janika Nättinen,[1,2] Antti Jylhä,[1,2] Ulla Aapola,[1,2] Marko Kataja,[3] Peeter Kööbi,[1,3] Tero A. H. Järvinen,[1,4] Hannu Uusitalo,[1–3] and Hannele Uusitalo-Järvinen[1,3]

[1]Faculty of Medicine & Life Sciences, University of Tampere, Tampere, Finland
[2]The Center for Proteomics and Personalized Medicine, Tampere, Finland
[3]Eye Centre, Tampere University Hospital, Tampere, Finland
[4]Department of Musculoskeletal Disorders, Tampere University Hospital, Tampere, Finland

Correspondence: Hannele Uusitalo-Järvinen, Faculty of Medicine and Life Sciences, 33014 University of Tampere, Finland; llhauus@uta.fi.

HU and HU-J contributed equally to the work presented here and should therefore be regarded as equivalent authors.

Submitted: January 9, 2018
Accepted: May 9, 2018

Citation: Vähätupa M, Nättinen J, Jylhä A, et al. SWATH-MS proteomic analysis of oxygen-induced retinopathy reveals novel potential therapeutic targets. *Invest Ophthalmol Vis Sci*. 2018;59:3294–3306. https://doi.org/10.1167/iovs.18-23831

Purpose. Oxygen-induced retinopathy (OIR) is the most widely used model for ischemic retinopathies such as retinopathy of prematurity (ROP), proliferative diabetic retinopathy (PDR), and retinal vein occlusion (RVO). The purpose of this study was to perform the most comprehensive characterization of OIR by a recently developed technique, sequential window acquisition of all theoretical mass spectra (SWATH-MS) proteomics.

Methods. Control and OIR retina samples collected from various time points were subjected to SWATH-MS and detailed data analysis. Immunohistochemistry from mouse retinas as well as neovascular membranes from human PDR and RVO patients were used for the detection of the localization of the proteins showing altered expression in the retina and to address their relevance to human ischemic retinopathies.

Results. We report the most extensive proteomic profiling of OIR to date by quantifying almost 3000 unique proteins and their expression differences between control and OIR retinas. Crystallins were the most prominent proteins induced by hypoxia in the retina, while angiogenesis related proteins such as Filamin A and nonmuscle myosin IIA stand out at the peak of angiogenesis. Majority of the changes in protein expression return to normal at P42, but there is evidence to suggest that proteins involved in neurotransmission remain at reduced level.

Conclusions. The results reveal new potential therapeutic targets to address hypoxia-induced pathological angiogenesis taking place in number of retinal diseases. The extensive proteomic profiling combined with pathway analysis also identifies novel molecular networks that could contribute to the pathogenesis of retinal diseases.

Keywords: proteomics, mass spectrometry, oxygen induced retinopathy, angiogenesis, hypoxia

Retinal ischemic diseases, such as retinopathy of prematurity (ROP), diabetic retinopathy (DR), and retinal vein occlusion (RVO) are major causes of visual impairment and blindness in industrialized countries.[1–5] The most prominent pathological features of these diseases are abnormal angiogenesis and enhanced vascular permeability, which leads to vision loss. However, inflammation, oxidative stress, and neuronal dysfunction are also contributing to the pathogenesis of ischemic retinal diseases.

The mouse oxygen-induced retinopathy (OIR) model[6] is a well-established animal model of ROP, which shares many hallmarks with human proliferative diabetic retinopathy (PDR) as well as neovascular RVO. Thus, it is the most widely used model to study retinal ischemic diseases.[7] OIR is characterized by hyperoxia-induced vessel loss from retina followed by regrowth of vasculature and formation of preretinal neovascularization upon return to normoxia. It is considered mainly as an angiogenesis model, but neuronal damage and pathological effects on retinal glia have also been reported in OIR.[8]

Due to complex interactions between vascular, neuronal, glial, and immune cells in retinal vascular disorders, it is important to study changes in whole retinal tissue simultaneously to gain more information about the pathogenesis of retinal disease. Mass spectrometry (MS)-based proteomic profiling has become a widely-used approach to assess the development and the progression of diseases.[9] Full proteome-based approach provides an unbiased method to study changes in proteins involved in any given tissue, organ, or disease. As the OIR model is considered as the most representative model for a large number of neovascular human retinal diseases, there has been considerable interest to characterize OIR with MS-based approaches. Previous studies on rodent OIR proteome have been done with Isobaric Tags for Relative and Absolute Quantitation (iTRAQ) MS approach,[10,11] and with ion-current-based MS1 quantification approach (ICB) from rat retinas.[12] With these methods, it has been possible to quantify almost 300[10,11] and 1300 proteins from retinas,[12] respectively. In this study, a recently developed technique,[13] sequential window acquisition of all theoretical mass spectra (SWATH)-MS proteomics, was used to compare proteomes of mouse OIR model with control retina. SWATH-MS is an MS method that combines data-independent acquisition (DIA) and data-dependent acqui-

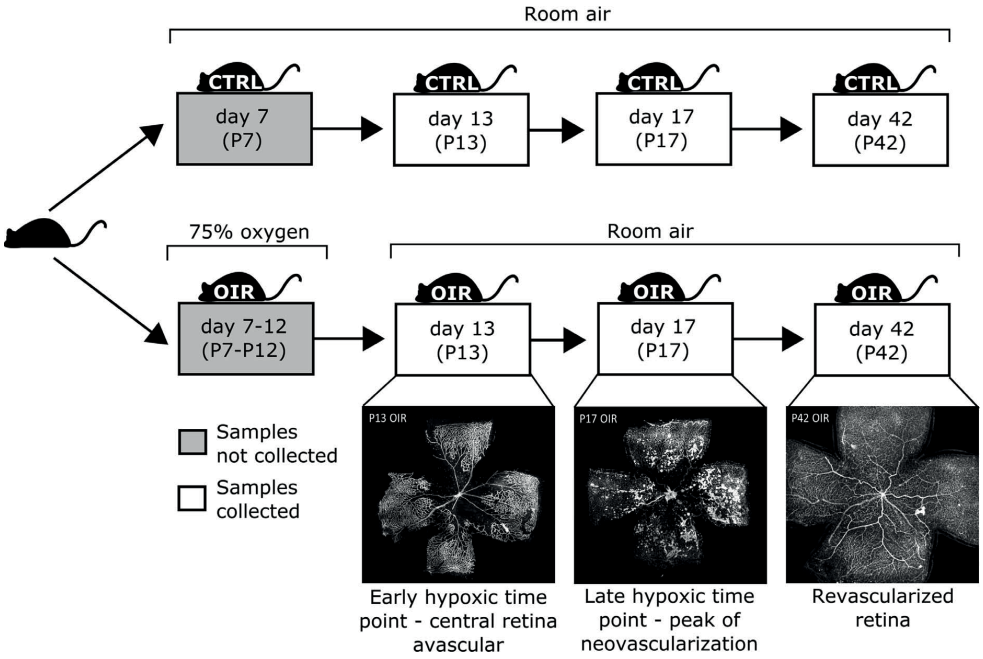

Figure 1. Outline of the study. OIR was generated by exposing the mice pups for 75% oxygen for 5 days from P7 to P12. Control and OIR retinas were collected to SWATH-MS analysis, while some retinas from each litter were used for histological examination to confirm the changes in the vasculature in OIR. Retinal vasculature was stained with Isolectin GS-IB_4. OIR samples were collected during hypoxia at P13 when central retina is avascular, at P17 when retina is partially revascularized and the neovascularization (preretinal tufts) peaks, and at P42 when retina is completely revascularized and neovascularization is regressed. Age-matching control samples were collected from mice housed in normal room air. P13 $n = 5$; P17 $n = 9$; P42 $n = 6$; P13 OIR $n = 5$; P17 OIR $n = 6$; P42 OIR $n = 7$.

sition (DDA), which iTRAQ and targeted data analysis uses, extending the throughput of proteins and data completeness.[14] Here we report the most extensive proteomic profiling of OIR to date by relatively quantifying almost 3000 unique proteins. The novel methodology used in the present study also allowed the temporal profiling of OIR proteome for the first time, while in the previous studies, it has been possible to compare the protein levels in a single time point. Immunohistochemistry was used to study the localization of differently expressed proteins in control and OIR retinas, as well as in neovascular membranes obtained from PDR and RVO patients to address the relevance of these findings to human ischemic retinopathies.

Materials and Methods

Mouse OIR Model

WT C57BL/6 mice were used for the study. Mice were housed under standard conditions with 12-hour dark/12-hour light cycle and fed with standard laboratory pellets and water ad libitum. The OIR model was generated as described in detail previously.[6,15–17] Briefly, to induce OIR, the pups at postnatal day 7 (P7) and their nursing mothers were exposed to 75% oxygen (ProOx P110 oxygen controller; Biospherix Ltd., Parish, NY, USA) for 5 days until P12 when they were returned to normal room air. Mice were sacrificed and retinas collected at P13 (early hypoxic phase), at P17 (late hypoxic phase and the peak of neovascularization), and at P42 (after vascular recovery) to assess the effect of OIR on retinal proteome. Control animals were housed under normal room air conditions and retinas were harvested at corresponding days. The study design is illustrated in Figure 1. As postnatal weight gain has been shown to affect outcome in the OIR model,[7] only the pups weighing between 6.3 and 7.5 g at P17 were included in the study. All animal experiments were conducted under ARVO Statement for the Use of Animals in Ophthalmic and Vision Research guidelines in accordance with protocols approved by the National Animal Ethics Committee of Finland.

For the proteomic analysis, eye balls were harvested into cold PBS and retinas were dissected immediately under the dissection microscope, and retinas were snap frozen with liquid nitrogen. Samples were stored in −70°C until sample preparation.

Proteomics

Chemicals and Materials. Acetonitrile (ACN), formic acid (FA), water (UHPLC-MS grade), triethylammonium bicarbonate buffer 1M (TEAB), sodium dodecyl sulfate (SDS), iodoacetamide (IAA), trifluoroacetic acid (TFA), ammonium bicarbonate (ABC), and urea were all purchased from Sigma Aldrich Corp. (St. Louis, MO, USA). Radioimmunoprecipitation assay (RIPA) cell lysis buffer, a cocktail (Halt Protease Inhibitor Cocktail), and sample clean up tips (C18) were from Thermo Fisher Scientific (San Jose, CA, USA). A kit (Bio-Rad DC) and bovine serum albumin standard were purchased from Bio-Rad (Hercules, CA, USA), and 30 kDa molecular weight cut off (MWCO) centrifugal devices were from PALL (Port Washington, NY, USA).

Sample Preparation and Analysis. Proteins were extracted by submerging tissues to 300 µL RIPA cell lysis buffer in ice and homogenized using plastic pestles and centrifuged (2400*g*/min, 5 minutes). After centrifugation, tissue samples were set in cold ultrasonic bath for 5 minutes and incubated on ice for 25 minutes. After incubation, samples were centrifuged at 21,000*g* for 20 minutes and the supernatant containing the proteins were transferred to new tube. Protein concentration was measured using Bio-Rad DC protein quantification kit. Average amount of protein recovered per sample was 253.8 ± 32.9 µg (± SD). Fifty micrograms of total protein was taken from each sample to tryptic digestion.

Samples were then subjected to reduction, alkylation, and tryptic digestion. These steps were performed as described in detail in the Supplementary Methods. For MS analysis, the samples were eluted to the same concentration and 4 µg sample was injected into NanoLC-TripleTOF (Sciex 5600+). Two replicate MS analyses were produced from each sample. Analysis of the samples was done by NanoLC-TripleTOF MS using SWATH acquisition as described in the Supplementary Methods.

Protein Identification and Quantification. As part of the SWATH analysis method, a relative protein quantification library, consisting of >3500 retinal proteins, was created using retina samples from this study. Overall library consisted of 32 different samples and 45 data-dependent analysis (DDA) runs with same LC gradient and instrument settings that were used for SWATH analyses. Library was created using Protein Pilot 4.7 (Sciex, Redwood City, CA, USA) and all DDA runs spectra were identified against Mouse UniprotKB/SwissProt protein library. Quantification was done by Peak Viewer and Marker Viewer (Sciex). False discovery rate (FDR) 1% was used in the library creation and only distinctive peptides were used in the quantification. Retention time calibration was done for all samples using 15 representative peptides from two different proteins, α-enolase (ENO1) and albumin (ALB). Five transitions per peptide and 1 to 15 peptides were used for protein quantification calculations. All statistically significant (adjusted $P < 0.05$) and other interesting proteins discussed further were subjected to manual inspection of peptides. This consisted of checking correct peak selection in the chromatogram (FDR 1%, 99% peptide confidence level), sufficient signal to noise ratio inspection (>7), and chromatogram inspection in relation to library chromatogram. Also, variation of replicate MS analysis results was calculated as means to all samples/protein. All peptides were eliminated from results processing if manual inspection requirements were not fulfilled. Proteins with missing values were excluded from consideration. Checked proteins whose quantification was based on only one specific peptide are marked with †-symbol to the graphs and tables. Most of these proteins were small proteins, meaning a small likelihood of having more than one specific peptide identified for quantification.

Western Blotting. Retinal protein lysates were run into SDS PAGE gels, transferred to polyvinylidene diflouride (PVDF) membranes, and immunoblotted with anti-Flna, anti-Myh9, and anti-glyceraldehyde-3-phosphate dehydrogenase (GAPDH) antibodies, as described in the Supplementary Methods.

Immunohistochemistry. For the retinal flat mount analysis, the eye balls were harvested at P13, P17, and P42. Eye balls were fixed with 4% paraformaldehyde (PFA) for 1 hour where after retinas were dissected, stained with isolectin (Isolectin GS-IB_4; Invitrogen, Carlsbad, CA, USA), flat mounted, and imaged via confocal microscope (LSM 700; Carl Zeiss, Oberkochen, Germany).

For immunohistochemistry, the eye balls were harvested, fixed with 4% PFA for 4 hours, and processed for paraffin embedding. Five-micrometer thick sections were subjected to antigen retrieval (Tris-EDTA, pH9), blocked and incubated either with anti-Filamin-A antibody (Cat#ab76289; Abcam, Cambridge, UK) or anti-Myh9 antibody (Cat#11128-1-AP; Proteintech, Rosemont, IL, USA) followed by horseradish peroxidase (HRP) conjugated secondary antibodies. For immunofluorescence (IF) double-staining, sections were pretreated with trypsin and incubated with anti-Myh9 antibody (Proteintech) and anti-CD31 (Cat#550274; BD BioSciences, San Jose, CA, USA) or anti-Myh9 and anti-NG2 (provided by W. Stallcup, Sanford Burnham Prebys Medical Discovery Institute, La Jolla, CA, USA),[18] followed by appropriate Alexa Fluor dye conjugated secondary antibodies (Invitrogen). Samples were imaged via confocal microscope (LSM700; Carl Zeiss).

Neovascular membranes were obtained from nine PDR and one RVO patients, who were undergoing pars plana vitrectomy. At the time of surgery, patients' mean age was 37 years (range, 27–56 years) and mean duration of diabetes was 26 years (range, 21–32 years). The protocol for collecting human tissue samples was approved by the institutional review boards of the Pirkanmaa Hospital District, and the study was conducted in accordance with the Declaration of Helsinki. All patients gave written informed consent. The fibrovascular membranes were isolated, grasped with vitreous forceps, and pulled out through a sclerotomy. Samples were immediately fixed with 10% formalin for 3 hours, transferred to 70% ethanol, and processed for paraffin embedding and immunohistochemistry. Samples were stained with anti-Myh9 antibody (Proteintech) and anti-HSA (cat #LS-B6178; LSBio, Seattle, WA, USA) followed by HRP conjugated secondary antibodies.

Statistical Analysis. Proteins were quantified and $\log_2$-transformation was applied to the data, and in addition, geometric means of replicate MS analyses were taken. No further normalization was deemed necessary. The quality of the replicate MS analyses was analyzed by analyzing the intraclass correlation (ICC), and Spearman's rank correlation was used to generate *P* values in permutation tests ($n = 1000$ permutations / replicate MS analyses).

Principal component analysis (PCA) was used to cluster the samples based on full proteomic profiles. Two-sample *t*-test was used to analyze differences between the relative protein expression levels of control and OIR retinas. Levene's test was performed for the statistically significant proteins (after *P* value adjustment), and two proteins had a *P* value < 0.05. For these proteins, the statistical significance was checked with Wilcoxon rank sum test.

Benjamini-Hochberg adjustment was used to account for multiple testing, and the significance threshold, α, was set at 0.05. All statistical analyses for the proteomics data were performed using R software version 3.2.3 (R Core Team, Foundation for Statistical Computing, Vienna, Austria) and IPA software (IPA; QIAGEN, Redwood City, CA, USA).

Results

Protein Profiles Are Associated With the Developmental Stage of the Retina

To study the protein profiles of control and OIR retinas, we first confirmed the development of OIR by staining the vasculature from retinal flat mounts at different time points (Fig. 1). With SWATH-MS quantification, we then used a library of 121,145 peptides from 32 samples, corresponding to 1,576,233 identified spectra in an assembly of 3316 protein groups using FDR of 1.0%. From this library, 2944 proteins had distinct peptides sequences with matching spectra to SWATH-MS analysis, and these proteins were quantified in all samples. Out of 2944 relatively quantified proteins, the quantification

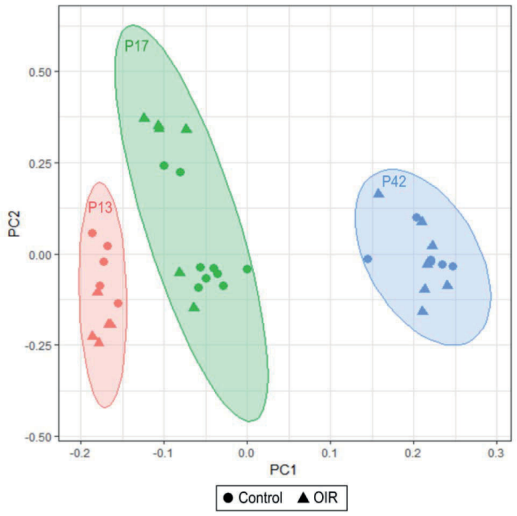

FIGURE 2. PCA shows distinct clustering of retinal proteins based on the developmental stage of the retina. The protein profiles obtained from control and OIR retinas are clearly different at P13 (*red*), P17 (*green*), and P42 (*blue*). Control (●) and OIR (▲) samples are also separated quite distinctively within the clusters at P13 and P17, but no more at P42.

was based on more than one peptide in 2177 proteins. Proteins quantified using a single peptide are marked in the figure legends. The replicate MS analysis quality checks showed that the ICC coefficient was 0.99 between the replicates. Permutation tests using Spearman's correlation showed that 94.4% of the replicate MS analyses had a $P < 0.05$, which suggests that they were of excellent quality.

For the proteomic data, we first wanted to evaluate the underlying patterns and differences between time points. PCA was performed for the whole data, and the plotting results based on the first two components suggested that there was a clear division between different time points of both control and OIR retina samples (Fig. 2). In addition, some separation was seen between control and OIR retinas at P13 and P17. At P42, the two groups were overlapping and there was no longer detectable division between control and OIR protein profiles. Taken together, the strongest cause for the differences in protein expression levels based on the first component appears to be the developmental stage of mouse retina.

Differential Expression Analysis of OIR and Control Retinas: The Induction of Crystallins by Hypoxia at P13 and Angiogenesis-Related Proteins at P17

Next, we performed differential expression analysis in order to identify proteins, which differed between control and OIR samples in specific time points. Comparison of control and OIR samples resulted in 364 differentially expressed proteins at P13, 387 at P17, and 104 at P42 ($P < 0.05$) prior to further P value adjustments. These proteins are listed in Supplementary Table S1 for P13, Supplementary Table S2 for P17, and Supplementary Table S3 for P42.

P value adjustments to account for the multiple hypotheses testing reduced the number of statistically significant results and led to 17 differentially expressed proteins at P13, 22 at P17, and none at P42. To visualize the differential expression in response to hypoxia at P13, P17, and P42, volcano plots are shown (Figs. 3A–C). In addition to visualizing the statistically significant (adjusted $P < 0.05$) proteins and their associated up- or downregulation, the plots revealed a highly upregulated group of proteins in response to hypoxia at P13 OIR (Fig. 3A). These proteins are crystallins, including members of α-, β-, and γ-crystallins. The expression levels of individual crystallins did not reach statistically significant difference after P value adjustment, but they are the most upregulated proteins in the whole data according to fold change (FC) ($\log_2$ FC 2.67–4.32) (Supplementary Fig. S1 and Supplementary Table S1). It is also noteworthy that based on FC alone, the most upregulated ($\log_2$ FC > 2) proteins at the peak of the

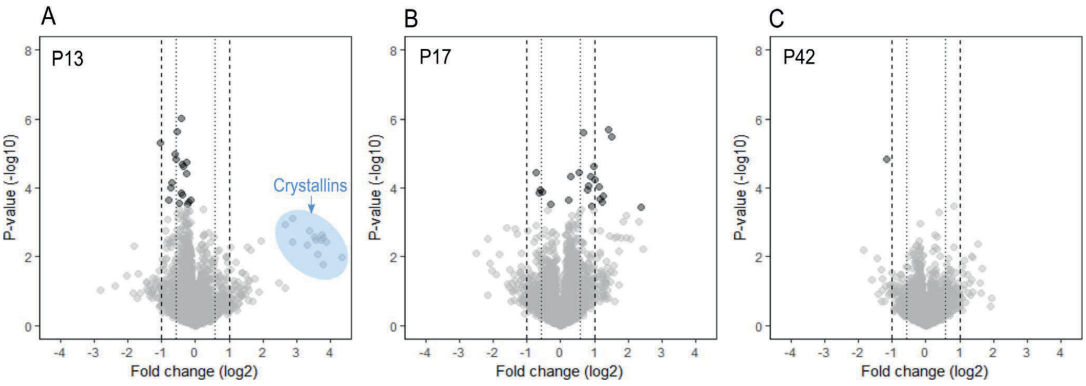

FIGURE 3. Volcano plots of the differential expression analysis. The $\log_2$ FC is displayed in the *x*-axis and the P value ($-\log_{10}$) is shown in the *y*-axis and hence, proteins in the *top right* and *left* corners are the most interesting ones as they represent the most heavily upregulated or downregulated proteins in OIR. Points with *darker gray* are proteins with an adjusted P value < 0.05. (**A**) At P13, there were 17 proteins with adjusted $P < 0.05$ and these were all downregulated in OIR samples. The blue cluster (**A**) shows the crystallins, which were noticeably upregulated although most members of the crystallin family did not reach threshold for statistical significance. (**B**) Altogether 22 proteins showed differential expression based on their adjusted $P < 0.05$ in OIR at P17. In general, more proteins were upregulated in OIR samples compared to control retinas at P17 than at other studied time points. (**C**) One protein (Cartpt) was deemed statistically significant (based on the adjusted P value) at P42, but was discarded from the results during the manual peak evaluation.

Investigative Ophthalmology & Visual Science

angiogenesis (at P17), were vitamin D-binding protein (Gc), α-2-HS-glycoprotein/fetuin-A (Ahsg), α-1-antitrypsin 1-4 (Serpina1d), and carboxylesterase 1C (Ces1c) (nonadjusted $P < 0.05$) (Supplementary Table S2). Of the aforementioned proteins, one (Ahsg) was also statistically significant (Fig. 3B). At P42, cocaine- and amphetamine-regulated transcript protein (Cartpt) was initially found to be statistically significant after the P value adjustment (Fig. 3C). However, this change was deemed unreliable after manual peak checking.

The heat maps of the statistically significant results at P13 and P17 show the relative expression of the proteins and the differences between control and OIR samples (Figs. 4A, 4B). Four proteins had statistically significant difference at P13 (absolute $\log_2$ FC > 0.585; i.e., FC above 1.5: abs($\log_2$(1.5)): glutamine synthetase (Glul), guanylyl cyclase GC-E (Gucy2e), cGMP-gated cation channel α-1 (Cnga1) and rod outer segment membrane protein 1 (Rom1) (Fig. 4). Substantially more proteins showed similar difference ($\log_2$ FC $>$ abs(log2(1.5)) in the expression levels between OIR and control at P17: Ahsg, annexin A2 (Anxa2), transgelin-2 (Tagln2), cell surface glycoprotein MUC18 (Mcam), tropomyosin α-4 chain (Tpm4), filamin-B (Flnb), protein SON (Son), Gpx1, vinculin (Vcl), myosin-9 (Myh9), serpin H1 (Serpinh1), filamin-A (Flna), moesin (Msn), and annexin A6 (Anxa6) (Figs. 4B, 5). Similarly, downregulated proteins at P17 OIR were Glul, prosaposin receptor GPR37 (Gpr37), sideroflexin-5 (Sfxn5), and synaptic vesicle glycoprotein 2A (Sv2a) (Fig. 4B). Significantly downregulated proteins both at P13 OIR and P17 OIR were Glul and retinaldehyde-binding protein-1 (Rlbp1). The mean expression values are illustrated in Figure 5 and in Supplementary Figure S2 for all of the statistical significant proteins (adjusted P value < 0.05). There were no proteins with altered expression level at P42 OIR after P value adjustment.

Hypoxia Induces Filamin-A Cleavage at P17 OIR

In order to validate the results from proteomic analysis of OIR, Flna and Myh9 were selected for immunoblotting. Immunoblotting with C-terminal anti-Flna antibody confirmed increased Flna expression at P17 OIR (4.6-fold compared to P17 control). In hypoxia, Flna is cleaved by calpain-proteases to generate 90 kDa C-terminal fragment that interacts with hypoxia-inducible factor-1α (HIF-1α) and promotes angiogenesis.[43] The expression of C-terminal fragment of Flna ($Flna^{CT}$) generated in the presence of hypoxia was increased 14-fold in OIR at P17 OIR (Figs. 5C, 5D). Next, the expression of Myh9 was studied in OIR by immunoblotting. A 9.6-fold increase in the expression of the Myh9 was seen at P17 OIR when compared to the expression at P17 controls (Figs. 5E, 5F).

Filamin-A and Myh9 Expression Is Increased in the Angiogenic Blood Vessels in OIR Retinas

While proteomic analysis and immunoblotting revealed an increased expression of Flna and Myh9 at P17 OIR, immunohistochemical stainings confirmed substantially stronger expression of these proteins from P17 OIR retinas than from control retinas (Fig. 5G). We observed marked increase in Flna expression in preretinal tufts and blood vessels of inner retina in the OIR retinas in comparison to controls. Also, a faint staining is seen in others cell types, presumably retinal neurons, but the expression level in neurons looks identical in control and OIR retinas. Thus, the induction of Flna expression seen in OIR at P17 is clearly from the angiogenic blood vessels.

Myh9 expression in OIR retinas was studied in detail by performing double-immunofluorescent stainings for Myh9 and endothelial cell (CD31), and pericyte (NG2) markers. Strong Myh9 expression was localized to endothelial cells and pericytes in OIR at the peak of the angiogenesis at P17. All endothelial cells expressed Myh9, while there were some pericytes negative for Myh9 at P17 OIR (Fig. 6).

Abundant Expression of Myh9 on Neovascular Membranes From Human PDR Patients

Generally, the expression levels of Myh9 reflect the overall stiffness of the tissue.[19–21] The increased matrix stiffness destabilizing endothelial cell–cell junctions impairs the endothelial barrier function and leads to enhanced endothelial permeability.[22] We next studied Myh9 and human serum albumin (HSA; i.e., marker of vascular leakage) expression on human fibrovascular membranes (using adjacent tissue sections) from vitrectomized patients with PDR and RVO. Strong fibrosis formation leads to retinal traction and ultimately to retinal detachment in RVO. The samples represent the end stage of these diseases, where substantial amount of fibrosis has been formed, but the samples still contain also regions with active pathologic angiogenesis. When only a faint expression of Myh9 is seen outside of the blood vessels, the intensity of Myh9 staining in blood vessels is also faint one (Fig. 7). Strong Myh9 expression was seen both in the blood vessels and in the matrix in some samples and then HSA starts to accumulate in the tissue. Particularly strong Myh9 expression was seen all over the fibrotic membrane in the RVO sample that contains blood vessels and massive scarring (Fig. 7). Comparison of Myh9 expression to HSA expression showed a strong positive correlation between the two; more Myh9 expressing cells (increased matrix stiffness) outside the blood vessels, more Myh9 expression (contractility and destabilization of cell–cell junctions) in the blood vessels and the more abundant vascular leakage outside the blood vessels (Fig. 7).

Ingenuity Pathway Analysis (IPA) Identifies Angiogenesis and Transforming Growth Factor-β1 (TGF-β1) Pathway As the Most Prominent Features of OIR at P17. In order to connect the differentially expressed proteins to specific pathways and biological functions, pathway analysis was performed using IPA on the proteins showing statistically significant differences in their expression between control and OIR retinas (adjusted $P < 0.05$) in each time point. The top canonical pathways connected to the 17 proteins at P13 (Fig. 4A) were phototransduction pathway (P = 4.95e-10) (Supplementary Fig. S3), protein kinase A signaling (P = 2.29e-04), and glutamine biosynthesis I (P = 8.05e-04). There were no unbiased activation scores < -2 or > 2 for disease and biological functions or for upstream regulators.

For the 22 proteins identified in differential expression analysis at P17 (Fig. 4B), the top canonical pathways were actin cytoskeleton signaling (activation score = 2.1, P = 3.18e-06), ILK signaling (activation score = −1, P = 4.61e-05), and glutamine biosynthesis I (P = 1.04e-03). We then performed the disease and biological function enrichments analyses, which showed both necrosis and cell death reduced (P = 7.25e-04 and P = 6.94e-05, both with activation score ≤ -2), while angiogenesis was increased (P = 2.53e-04, activation score ≥ 2). According to IPA, the increase in angiogenesis was due to the upregulation of Anxa2, Flna, Flnb, Gpx1, Mcam, Myh9, and Serpinh1. For further classification, upregulated proteins Tagln2, Vcl, Mcam, Flnb, ATP-dependent 6-phosphofructokinase (Pfkp), Myh9, and Flna are proteins involved in cell–cell adhesion (Amigo2). In addition, the upstream regulator analysis identified TGF-β1 (Tgfb1), MAP kinase-interacting serine/threonine-protein kinase 1 (Mknk1), and

A P13

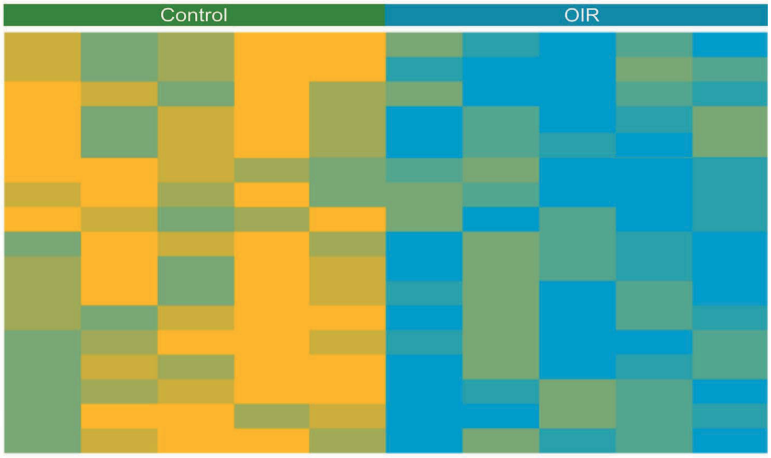

Symbol	Log2 fold change	P-value (adj.)
Cnga1	-0.7	0.02
Dnm1	-0.26	0.009
Rbbp9	-0.49	0.05
Rtcb	-0.13	0.04
Sptbn1	-0.24	0.05
Atp1b1	-0.37	0.009
Grk1	-0.58	0.009
Dusp3	-0.41	0.03
Rom1	-0.6	0.008
Nsf	-0.27	0.01
Gucy2e	-0.74	0.03
Rlbp1	-0.21	0.05
Glul	-1.05	0.005
Slc2a1	-0.4	0.04
Bsg	-0.54	0.003
Rcvrn	-0.42	0.003
Gnb1	-0.39	0.009

B P17

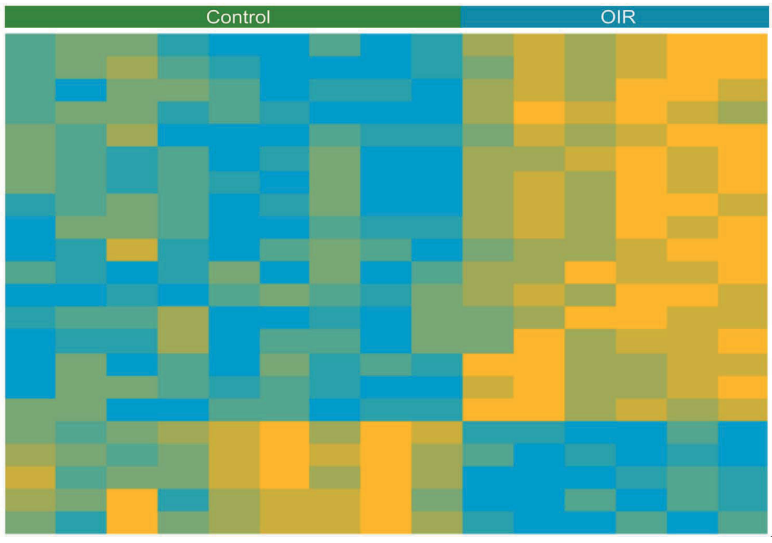

Symbol	Log2 fold change	P-value (adj.)
Pfn1	0.31	0.02
Flna	0.84	0.03
Tagln2	1.4	0.003
Flnb	1.15	0.04‡
Tpm4	1.24	0.04
Mcam	1.25	0.03
Ahsg	2.38	0.05
Vcl	0.97	0.02
Serpinh1	0.88	0.02‡
Crym	0.22	0.04
Gpx1	1.01	0.02†
Pfkp	0.54	0.02
Myh9	0.92	0.05
Msn	0.81	0.03
Son	1.12	0.03
Anxa2	1.51	0.003
Anxa6	0.68	0.003
Sv2a	-0.54	0.03
Glul	-0.74	0.02
Rlbp1	-0.3	0.04
Gpr37	-0.64	0.03
Sfxn5	-0.61	0.03

Figure 4. Heat maps of differentially expressed proteins between control and OIR retinas. Retinas from control and OIR mice were harvested at P13, P17, and P42 and processed to MS-SWATH analysis. The colors display discretized values of the relative protein expression levels as described in the color key legend. (**A**) Seventeen proteins downregulated during hypoxia at P13 OIR retinas compared to control retinas at P13 (adjusted P value < 0.05). (**B**) Twenty-two proteins up- or downregulated at P17 (neovascularization) OIR compared to control retinas at P17 (adjusted P value < 0.05). † = protein quantification based on only one specific peptide. ‡ = proteins that had significant Levene's test results (P value < 0.05), suggesting potential issues with t-test assumptions. For these proteins, the statistical significance was checked also with Wilcoxon rank sum test and results were deemed statistically significant.

MKL/myocardin-like protein 2 (Mkl2) as potential upregulated enhancers of angiogenesis (for all $P < 0.001$ and activation score ≥ 2), while brain-derived neurotrophic factor (Bdnf), Krueppel-like factor 3 (Klf3), and Myc proto-oncogene protein (Myc) were inhibited (for all $P < 0.001$ and activation score ≤ -2) (Supplementary Table S4).

Marginal Long-Term Changes in the Protein Expression Persist in OIR Retina

There were no proteins with statistically significant difference in the expression levels between OIR and control retina after P value adjustment at P42. We then performed the IPA analysis

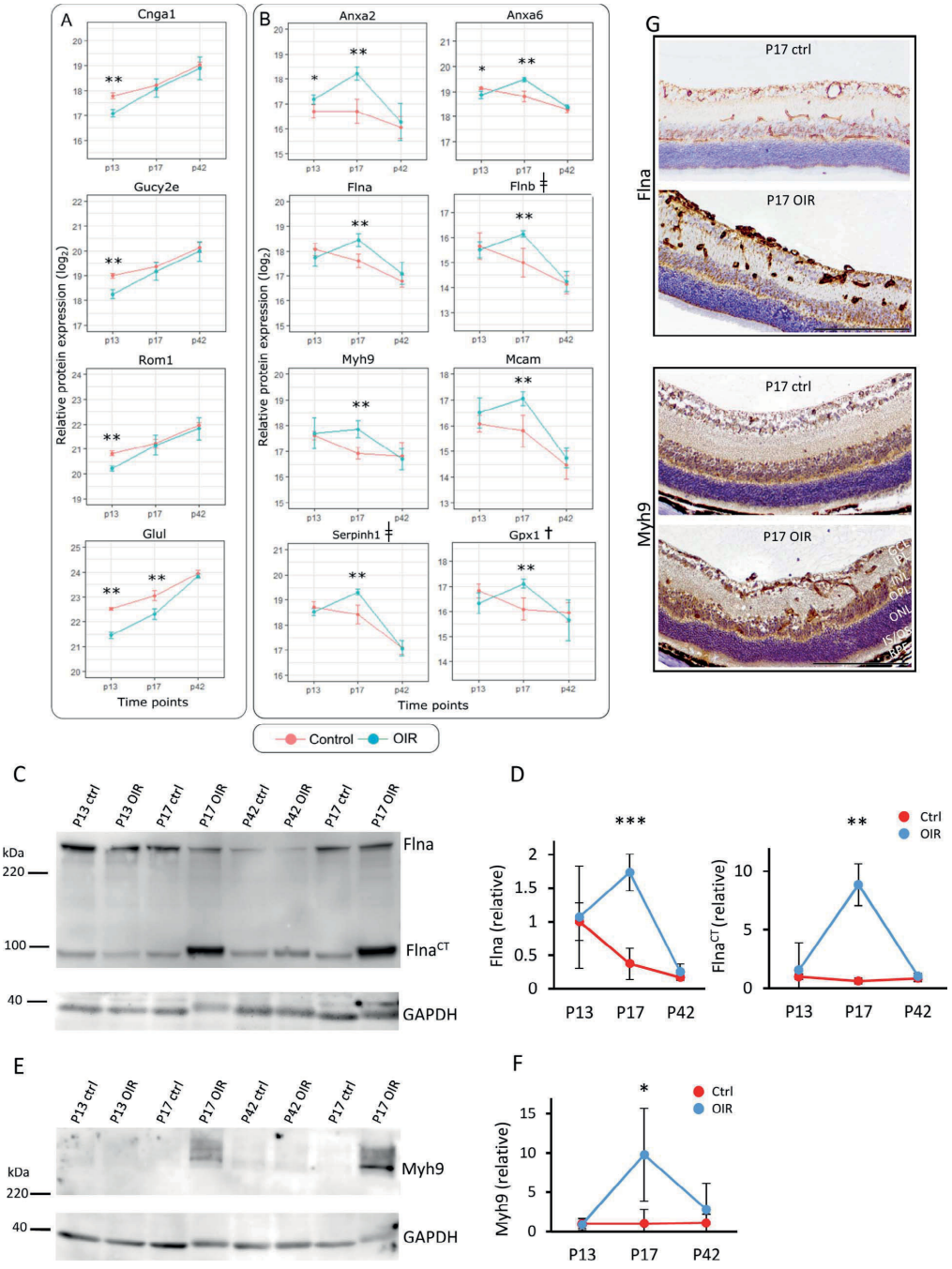

Figure 5. Differentially expressed proteins in OIR during hypoxia and angiogenesis. Mice pups were exposed to hyperoxia-induced OIR, and retinas were harvested at P13, P17, and P42. All retina samples were analyzed by MS-SWATH and the data underwent statistical analysis to compare control and OIR samples in each time point. The means and standard error bars are shown for control (*red*) and OIR (*blue*) samples for chosen proteins during hypoxia at P13 (**A**) and at the peak of neovascularization at P17 (**B**). The *asterisks* identify statistically significant differences between the two groups before *P* value adjustment (*), and after *P* value (**) adjustment. Note that Glul (**A**) is different both at P13 and at P17. (**C**) Western blot membrane immunoblotted with anti-Flna antibody shows increased Flna expression at P17 OIR and hypoxia-induced cleavage of C-

terminal fragment of Flna (Flna^{CT}). (**D**) Densitometric quantification revealed 4.6-fold induction in total Flna protein levels, while Flna^{CT} levels were increased 14-fold at P17 OIR compared to P17 control samples. (**E**, **F**) Western blotting against Myh9 and densitometric quantification showed 9.6-fold induction at P17 OIR compared to P17 control samples. (*$P < 0.05$; **$P < 0.01$; ***$P < 0.001$) (**G**) Control and OIR retinas collected at P17 were processed for immunohistochemical analysis and stained for Flna and Myh9 as described in the Materials and Methods section. Both Flna and Myh9 expression is increased in OIR retinas compared to controls. Strong expression of Flna and Myh9 can be seen from preretinal tufts (*arrows*) and from the blood vessels in inner retina in OIR. GCL, ganglion cell layer; IPL, inner plexiform layer; INL, inner nuclear layer, OPL, outer plexiform layer; ONL, outer nuclear layer; IS/OS, photoreceptor inner/outer segments; RPE, retinal pigment epithelium. *Scale bars* represent 200 μm. † = protein quantification based on only one specific peptide. ‡ = statistical significance was checked also with Wilcoxon rank sum test due to positive Levene's test results.

for proteins with nonadjusted *P* value ($P < 0.05$) as statistically significant (Supplementary Table S3). IPA analysis revealed decreased neurotransmission ($P = 6.56E\text{-}05$, activation score = −2) at P42 OIR compared to control retinas as the only significant difference between the groups. Altogether, 11 proteins in neurotransmission were involved (Supplementary Fig. S4A) and further examination revealed changes in the synaptic vesicle cycle pathway (KEGG) (Supplementary Fig. S4B). Selection of proteins upregulated at P42 OIR are illustrated in Figure 8. These are proteins associated at least with cell migration and adhesion, and retinal glial cells (Fig. 8).

Discussion

We have carried out the most comprehensive proteomics analysis of the commonly used experimental retinal angiogenesis model, OIR. The results reveal that in addition to the changes detected on proteins responding to hypoxia and those regulating angiogenesis, some changes in protein expression take place in the neuronal tissue of the retina. This is in accordance with the fact that human retinal vascular diseases are associated with neuropathy and gliopathy. Furthermore, the dysregulation of the cross talk between vasculature and retinal neuroglia and neuronal cells has been shown to contribute to the pathogenesis of DR.[23–25]

During the hypoxic phase, the most upregulated proteins were crystallins, which are small heat shock proteins that act as molecular chaperones by binding misfolded proteins to prevent their denaturation and aggregation.[26,27] They protect cells from hypoxia and maintain mitochondrial integrity.[26,28] In addition to their neuroprotective role, crystallins also have other roles in vascular biology.[29,30] αB-crystallin functions as a chaperone for VEGFA and is crucial for its proper secretion, which in turn, is crucial for endothelial cell survival in hypoxia.[28,31,32] Thus, αB-crystallin knockout mice had less VEGFA and neovascularization than WT in OIR.[31] In the eye, crystallins were originally characterized as abundant lens proteins, but they are also expressed in developing and mature retina.[28,32–34] Their expression is dramatically upregulated in numerous retinal diseases, such as mechanical injury, ischemic insults, age-related macular degeneration (AMD), uveoretinitis, and DR.[28] Concerning the potential therapeutic value of crystallins in retinal diseases, their exact functions are emerging.[27,35] Namely, the recently discovered roles for αB–crystallin in mediating TGF-β induced epithelial-mesenchymal transformation (EMT) and subretinal fibrosis in AMD,[27] while αA–crystallin providing neuroprotection for retina in DR,[35] point out the opposite therapeutic values for these crystallin-family members.[27,36]

A large number of proteins was also downregulated in response to hypoxia in retina. Among these proteins were Cnga1, Gucy2e, Rom1, and Grk1, proteins associated with phototransduction. Since rod photoreceptors are the most oxygen-dependent cells in the retina,[37] the downregulation of proteins associated with rod function is a plausible outcome in hypoxia.

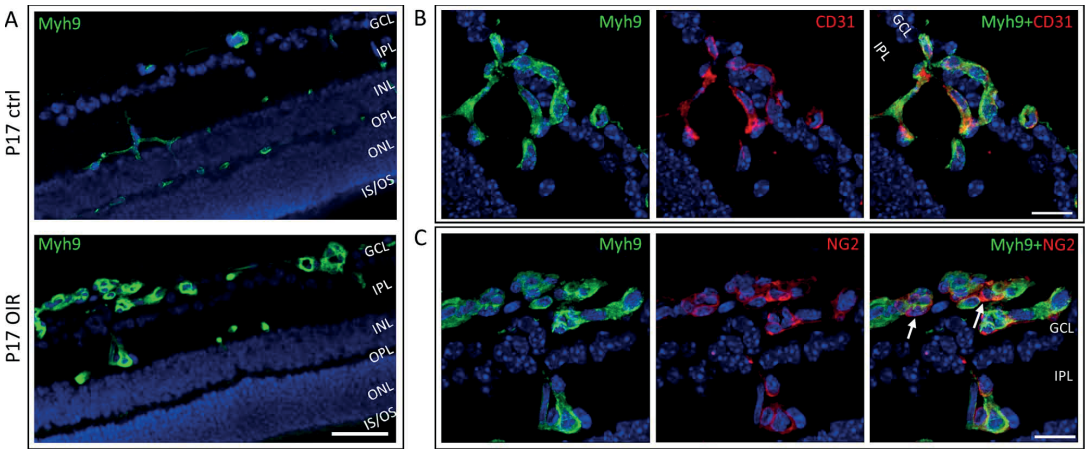

Figure 6. Myh9 is expressed in retinal blood vessels and induced by angiogenesis during OIR. (**A**) Control and OIR retinas were processed for IHC and stained for nonmuscle myosin IIA (Myh9) as described in the Materials and Methods section. Myh9 expression is confined to blood vessels in normal retina at P17. Strong Myh9 is induced in the angiogenic blood vessels at the peak of angiogenesis in OIR retina at P17. (**B**) Double-IF stainings for Myh9 and endothelial cells (CD31) (**B**) and Myh9 and pericytes (NG2) (**C**) confirmed that the Myh9 expression comes from endothelial cells and from some of the pericytes in OIR retina at P17. *Arrows* (**C**) are pointing to pericytes that do not express Myh9. GCL, ganglion cell layer; IPL, inner plexiform layer; INL, inner nuclear layer, OPL, outer plexiform layer; ONL, outer nuclear layer; IS/OS, photoreceptor inner/outer segments. *Scale bars* represent 50 μm in panel **A** and 20 μm in panels **B** and **C**.

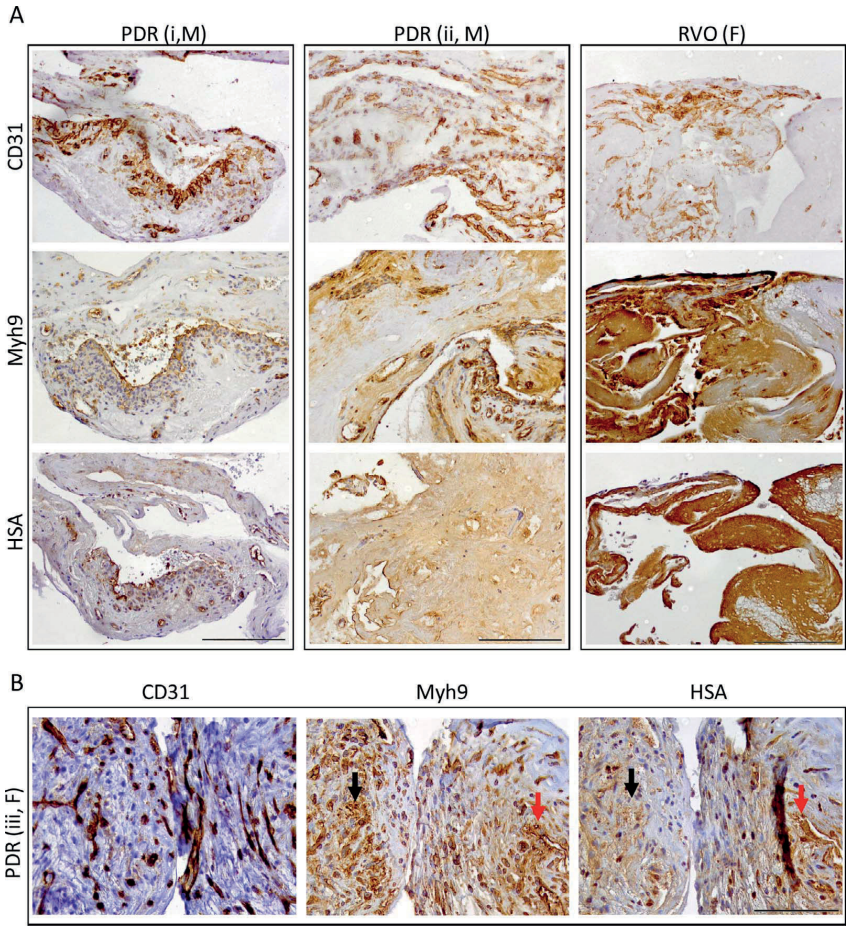

FIGURE 7. Myh9 is strongly expressed in human PDR and RVO fibrovascular membranes. Adjacent sections of fibrovascular membranes obtained from *pars plana* vitrectomies from PDR and RVO patients were stained for blood vessels (CD31), Myh9, and HSA. (**A**) Rather faint Myh9 expression was restricted to the blood vessels while almost no HSA accumulation was seen outside of the blood vessels in some PDR samples [PDR (i)]. Strong Myh9 expression was seen not only in the blood vessels, but also in the cells outside of the blood vessels and HSA had accumulated into the fibrovascular membrane's extracellular matrix in some PDR cases [PDR (ii)] as a sign of prominent vascular leakage. Especially strong Myh9 expression as well as substantial HSA accumulation were seen throughout the RVO sample, where strong fibrosis formation has taken place. (**B**) High magnification images from PDR patient (iii) show strong Myh9 expression in the highly vascularized area where HSA has leaked into the extracellular matrix (*arrows*). *Scale bars* represent 200 μm in panel **A** and 100 μm in panel **B**. M, male; F, female.

The most abundant changes in the retinal protein expression in OIR were seen at the peak of neovascularization at P17. Among the most upregulated proteins were plasma proteins Ahsg, Gc, Apoa1, Alb, and Tf (Supplementary Table S2). This is most probably due to increased permeability of the angiogenic blood vessels, which leads to the accumulation of plasma proteins in retinal tissue by leakage. However, some of these proteins could also have relevant biological functions, not just be bystanders by leakage, in OIR. Fetuin-A (Ahsg) as well as its cellular receptors, Anxa2 and -6, were highly upregulated in OIR. Fetuin-A is an adhesive glycoprotein that binds to Anxa2 and -6 and induces cell proliferation in its target cells.[38] Anxa2, in turn, drives angiogenesis in OIR.[38] Gc is a multifunctional glycoprotein that acts as a carrier protein for vitamin D but can also modulate certain immune and inflammatory responses.[39] Vitamin D, in turn, is known to inhibit retinal neovascularization in OIR,[40] and vitamin D receptor agonists inhibit developmental retinal angiogenesis.[41] Thus, the accumulation of Gc by the leakage from the angiogenic blood vessels could be a natural, endogenous signal to suppress angiogenesis at the time angiogenesis reaches its peak in OIR.

In line with the extensive angiogenesis taking place in retina at P17, IPA analysis revealed proteins "related to angiogenesis" being the most significantly upregulated proteins. Among these proteins were Filamins, Flna and Flnb. In hypoxia, oxygen-sensing prolyl hydroxylase domain protein 2 (PHD2) inactivation rapidly upregulates Flna expression.[42] Flna, in turn, interacts physically with HIF-1α and promotes angiogenesis.[43] Hypoxia induces calpain-dependent cleavage of Flna, and its C-terminal fragment ($Flna^{CT}$) accumulates in the nucleus and facilitates the nuclear localization of HIF-1α.[43] Our study shows that hypoxia induces Flna cleavage, that is, $Flna^{CT}$

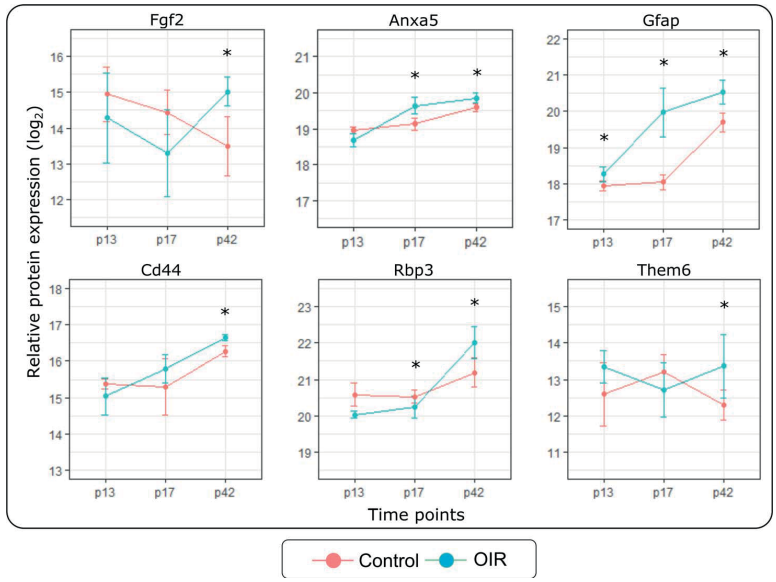

FIGURE 8. Selection of upregulated proteins at P42 OIR. Mice were exposed to OIR, and control and OIR retinas were harvested at P13, P17, and P42. Samples were analyzed by MS-SWATH, and the data underwent statistical analysis to compare control and OIR samples. The means and standard error bars are shown for control (*red*) and OIR (*blue*) samples for chosen proteins involved in cell migration and adhesion (Fgf2, Anxa5, CD44) and retinal glial cells (Gfap). Rbp3 has a critical role in visual cycle. The *asterisks* identify statistically significant differences between the two groups before *P* value adjustment (*P* value < 0.05).

generation in OIR. Very recently it was shown that blocking the calpain-dependent cleavage of Flna impairs tumor cell proliferation and migration.[44] Furthermore, it is worth noting that Flna also interacts with small GTPase, R-Ras,[45,46] the master regulator of vascular permeability in angiogenesis[46–50] and the gene needed for proper endothelial lumenogenesis.[51] The interaction between Flna and R-Ras is crucial for controlling vascular permeability in angiogenesis.[45,46] R-Ras, in turn, regulates vascular permeability in OIR and the reduced expression of R-Ras is associated with vascular leakage in PDR.[16] The interaction between R-Ras and Flna takes place with the N-terminal part of Flna.[45] Thus, selective blocking of the C-terminal cleavage of Flna ($Flna^{CT}$) could potentially be therapeutic in ischemic retinal diseases with pathological angiogenesis.

Another angiogenesis-related protein that stands out is Myh9. Myh9 gene encodes for Myosin 9, a heavy chain of Myosin IIA, a cytoskeletal contractile protein.[52] In general, the expression levels of Myh9 reflect the stiffness of the tissue; cells in stiff tissues express plenty of Myh9, while the cells in nonstiff tissues express low levels of Myh9.[19–21] In addition to the stiffness of the tissue, cell migration induces high mechanical strains on the cells as their "pierce" through extracellular matrix. Thus, the migrating cells upregulate the expression of Myh9 to make themselves more rigid to withstand the mechanical forces placed on them during the migratory process,[19–21] but their enhanced contractility destabilizes endothelial cell–cell junctions and impairs endothelial barrier function, resulting in increased vascular permeability.[22,53,54] Angiogenesis is essentially a cell migratory process and as shown in this study, the upregulation of the Myh9 takes place in the angiogenic endothelial cells in the retina. Thus, the induction of Myh9 during the peak of angiogenesis in OIR is plausible phenomenon, but could also be highly relevant as the increased vascular leakage is a hallmark in OIR. We also studied samples obtained from human PDR and RVO patients and showed that the vascular leakage in these diseases correlates with the amount of Myh9 expression in this area. Endothelial cell contractility (i.e., enhanced Myh9 expression) increases not only with cell migration, but also with the increased matrix stiffness resulting in increased endothelial permeability due to impaired endothelial barrier function.[22,53–55] Thus, the changes in matrix stiffness and the resultant endothelial cell contractility could be highly relevant for large number of neovascular retinal diseases associated with pathological leakage from the blood vessels.

Myh9 also regulates angiogenesis via controlling the production of VEGFA in ischemia-driven arteriogenesis[56] as well as controlling nucleolin translocalization.[57] Nucleolin is primarily a nuclear protein that translocates to cell surface in angiogenesis.[57–59] The different antagonists of nucleolin, among them Myh9 antibodies, have been shown to inhibit tumor angiogenesis by stabilizing the pathological vasculature,[57,59] which enhances tissue oxygenation.[59] The modest increase (log_2 FC 0.23) in nucleolin expression seen by MS in OIR at P17 suggests that the effects of nucleolin in angiogenesis is merely related to its translocation from nucleus to cell surface than increase in its expression level.

The present proteomics approach quantifies complete expression pattern of almost 3000 proteins and thus provides strong value to identify pathways involved in OIR. Using the upstream regulator analysis with IPA, the most potential and activated upstream regulator driving angiogenesis was TGF-β1. This is in accordance with previous studies showing TGF-β1 upregulation in OIR.[60] Interestingly, conditional ocular deletions of TGF-β signaling results in pronounced structural changes of retinal capillaries and a phenotype similar to human DR.[61,62] The upstream regulator analysis identified Mkl2 and

Mknk1 as enhancers of angiogenesis in OIR. Mkl2, a transcriptional coactivator, regulates conserved TGF-β signaling pathway.[63] Mice deficient for Mkl2 die at the early embryonic state, and Mkl2$^{-/-}$ ECs have defects in cytoskeletal organization and cell adhesion.[63] Mkl2/TGF-β pathway is required for the maturation and stabilization of embryonic vasculature,[63–65] but also for the myofibroblast transformation and EMT induction.[66,67] The enhanced TGF-β signaling taking place in vasculature leads to the endothelial-mesenchymal transition (EndMT), a process that has many similarities with EMT.[68,69] The transformed endothelial cells have high vascular permeability, further driving inflammation and by thus perpetuating the incomplete repair state.[69] This inflammation–TGF-β circuit in vasculature also promotes fibrosis in the surrounding tissue, and it is largely irreversible.[68,69] The recently identified association between TGF-β signaling and αβ-crystallin in the EMT and subretinal scarring,[27] the massive induction of crystallins by hypoxia and the subsequent activation of TGF-β/Mkl2-signaling pathways in OIR provide clues about the potential interplay that leads to retinal fibrosis in the human neovascular diseases of retina.

Another upstream regulator potentially enhancing angiogenesis in OIR is Mknk1/MNK1. Mknk1 is a kinase that exclusively phosphorylates a cap-binding subunit of the eIF4F translation initiation complex, eIF4E, and selectively facilitating translation of proliferation, migration, and survival promoting mRNAs, among them VEGFA.[70] Inhibition of eIF4E phosphorylation, in turn, suppressed angiogenesis.[71] In retina, eIF4E interacts with 4E-bp1, which expression is enhanced in retina by diabetes-induced hyperglycemia and necessary for VEGFA expression.[72,73] Our results suggest that blocking MNK-eIF4E pathway could be a potential target for blocking pathological angiogenesis in retinal diseases.

We included the late OIR-time point, P42, in our study to assess whether hypoxic exposure and subsequent neovascularization cause permanent changes in the protein expression in the retina. Very little is known about the long-term effects of OIR on retina, although the information could be useful to understand the prognosis of ROP. The disruption of the retinal morphology as well as decrease in neuronal function have been reported after OIR.[74] Our IPA analysis revealed decreased neurotransmission at P42 OIR retinas. Further examination revealed changes in the synaptic vesicle cycle pathway (KEGG) (Supplementary Fig. S4).

The present proteomics analysis revealed novel pathways that might contribute to the development of pathological angiogenesis in OIR. Furthermore, we were able to identify molecular interplay between the proteins induced by hypoxia and then by subsequent angiogenesis in OIR. They could be potential druggable targets of retinal diseases inflected with hypoxia and neovascularization.

Acknowledgments

The authors thank Saara Lähdekorpi and Marianne Karlsberg for excellent technical assistance; William B. Stallcup (Sanford Burnham Prebys Medical Discovery Institute, La Jolla, CA, USA) for providing the NG2 antibody. The imaging of the IF samples was done with a confocal microscope provided by Tampere Imaging Facility, BioMediTech, and Faculty of Medicine and Life Sciences, University of Tampere.

Supported by Academy of Finland, Finnish Diabetic Research Foundation, Diabetes Wellness Foundation, Tampere Tuberculosis Foundation, Pirkanmaa Hospital District Research Foundation, Finnish Eye Foundation, Finnish Cultural Foundation, Mary and Georg C. Ehrnrooth's Foundation, Päivikki and Sakari Sohlberg Foundation, Elsemay Björn Fund, and TEKES.

Disclosure: **M. Vähätupa**, None; **J. Nättinen**, None; **A. Jylhä**, None; **U. Aapola**, None; **M. Kataja**, None; **P. Kööbi**, None; **T.A.H. Järvinen**, None; **H. Uusitalo**, None; **H. Uusitalo-Järvinen**, None

References

1. Reynolds JD. Insights in ROP. *Am Orthopt J*. 2014;64:43–53.
2. Fong DS, Aiello LP, Ferris FL III, Klein R. Diabetic retinopathy. *Diabetes Care*. 2004;27:2540–2553.
3. Laouri M, Chen E, Looman M, Gallagher M. The burden of disease of retinal vein occlusion: review of the literature. *Eye (Lond)*. 2011;25:981–988.
4. Laatikainen L, Ojamo M, Rudanko SL, et al. Improving visual prognosis of the diabetic patients during the past 30 years based on the data of the Finnish Register of Visual Impairment. *Acta Ophthalmol*. 2016;94:226–231.
5. Gissler M, Ojamo M, Ritvanen A, Uusitalo H. Pediatric ocular disorders and visual handicap in Finland—what do the registers tell? *Duodecim*. 2017;133:159–166.
6. Smith LE, Wesolowski E, McLellan A, et al. Oxygen-induced retinopathy in the mouse. *Invest Ophthalmol Vis Sci*. 1994;35:101–111.
7. Stahl A, Connor KM, Sapieha P, et al. The mouse retina as an angiogenesis model. *Invest Ophthalmol Vis Sci*. 2010;51:2813–2826.
8. Vessey KA, Wilkinson-Berka JL, Fletcher EL. Characterization of retinal function and glial cell response in a mouse model of oxygen-induced retinopathy. *J Comp Neurol*. 2011;519:506–527.
9. Cifani P, Kentsis A. Toward comprehensive and quantitative proteomics for diagnosis and therapy of human disease. *Proteomics*. 2017;17:1600079.
10. Kim SJ, Jin J, Kim YJ, Kim Y, Yu HG. Retinal proteome analysis in a mouse model of oxygen-induced retinopathy. *J Proteome Res*. 2012;11:5186–5203.
11. Zhou L, Xinling L, Koh SK, Xiaorong L, Beuerman RW. Quantitative proteomic analysis of retina in oxygen-induced retinopathy mice using iTRAQ with 2D NanoLC-nanoESI-MS/MS. *Jiomics*. 2011;1:226–235.
12. Tu C, Beharry KD, Shen X, et al. Proteomic profiling of the retinas in a neonatal rat model of oxygen-induced retinopathy with a reproducible ion-current-based MS1 approach. *J Proteome Res*. 2015;14:2109–2120.
13. Gillet LC, Navarro P, Tate S, et al. Targeted data extraction of the MS/MS spectra generated by data-independent acquisition: a new concept for consistent and accurate proteome analysis. *Mol Cell Proteomics*. 2012;11:O111.016717.
14. Rosenberger G, Koh CC, Guo T, et al. A repository of assays to quantify 10,000 human proteins by SWATH-MS. *Sci Data*. 2014;1:140031.
15. Uusitalo-Järvinen H, Kurokawa T, Mueller BM, Andrade-Gordon P, Friedlander M, Ruf W. Role of protease activated receptor 1 and 2 signaling in hypoxia-induced angiogenesis. *Arterioscler Thromb Vasc Biol*. 2007;27:1456–1462.
16. Vähätupa M, Prince S, Vataja S, et al. Lack of R-Ras leads to increased vascular permeability in ischemic retinopathy. *Invest Ophthalmol Vis Sci*. 2016;57:4898–4909.
17. Vähätupa M, Cordova ZM, Aittomäki S, et al. Furin deficiency in myeloid cells leads to attenuated revascularization in a mouse-model of oxygen-induced retinopathy. *Exp Eye Res*. 2018;166:160–167.
18. Huang FJ, You WK, Bonaldo P, Seyfried TN, Pasquale EB, Stallcup WB. Pericyte deficiencies lead to aberrant tumor vascularization in the brain of the NG2 null mouse. *Dev Biol*. 2010;344:1035–1046.

19. Cho S, Irianto J, Discher DE. Mechanosensing by the nucleus: from pathways to scaling relationships. *J Cell Biol*. 2017;216:305–315.
20. Discher DE, Smith L, Cho S, Colasurdo M, Garcia AJ, Safran S. Matrix mechanosensing: from scaling concepts in 'omics data to mechanisms in the nucleus, regeneration, and cancer. *Annu Rev Biophys*. 2017;46:295–315.
21. Irianto J, Pfeifer CR, Xia Y, Discher DE. SnapShot: mechanosensing matrix. *Cell*. 2016;165:1820–1820.e1.
22. Bordeleau F, Mason BN, Lollis EM, et al. Matrix stiffening promotes a tumor vasculature phenotype. *Proc Natl Acad Sci U S A*. 2017;114:492–497.
23. Barber AJ. A new view of diabetic retinopathy: a neurodegenerative disease of the eye. *Prog Neuropsychopharmacol Biol Psychiatry*. 2003;27:283–290.
24. Kern TS. Interrelationships between the retinal neuroglia and vasculature in diabetes. *Diabetes Metab J*. 2014;38:163–170.
25. Nakahara T, Mori A, Kurauchi Y, Sakamoto K, Ishii K. Neurovascular interactions in the retina: physiological and pathological roles. *J Pharmacol Sci*. 2013;123:79–84.
26. Diokmetzidou A, Soumaka E, Kloukina I, et al. Desmin and αB-crystallin interplay in the maintenance of mitochondrial homeostasis and cardiomyocyte survival. *J Cell Sci*. 2016;129:3705–3720.
27. Ishikawa K, Sreekumar PG, Spee C, et al. αB-Crystallin regulates subretinal fibrosis by modulation of epithelial-mesenchymal transition. *Am J Pathol*. 2016;186:859–873.
28. Kannan R, Sreekumar PG, Hinton DR. Alpha crystallins in the retinal pigment epithelium and implications for the pathogenesis and treatment of age-related macular degeneration. *Biochim Biophys Acta*. 2016;1860:258–268.
29. Sinha D, Klise A, Sergeev Y, et al. βA3/A1-crystallin in astroglial cells regulates retinal vascular remodeling during development. *Mol Cell Neurosci*. 2008;37:85–95.
30. Zhang C, Gehlbach P, Gongora C, et al. A potential role for β- and γ-crystallins in the vascular remodeling of the eye. *Dev Dyn*. 2005;234:36–47.
31. Kase S, He S, Sonoda S, et al. αB-crystallin regulation of angiogenesis by modulation of VEGF. *Blood*. 2010;115:3398–3406.
32. Kannan R, Sreekumar PG, Hinton DR. Novel roles for α-crystallins in retinal function and disease. *Prog Retin Eye Res*. 2012;31:576–604.
33. Vazquez-Chona F, Song BK, Geisert EE Jr. Temporal changes in gene expression after injury in the rat retina. *Invest Ophthalmol Vis Sci*. 2004;45:2737–2746.
34. Smolich BD, Tarkington SK, Saha MS, Grainger RM. Xenopus γ-crystallin gene expression: evidence that the γ-crystallin gene family is transcribed in lens and nonlens tissues. *Mol Cell Biol*. 1994;14:1355–1363.
35. Ruebsam A, Dulle JE, Myers AM, et al. A specific phosphorylation regulates the protective role of αA-crystallin in diabetes. *JCI Insight*. 2018;3:e97919.
36. Nagaraj RH, Nahomi RB, Mueller NH, Raghavan CT, Ammar DA, Petrash JM. Therapeutic potential of α-crystallin. *Biochim Biophys Acta*. 2016;1860:252–257.
37. Cringle SJ, Yu DY, Alder VA. Intraretinal oxygen tension in the rat eye. *Graefes Arch Clin Exp Ophthalmol*. 1991;229:574–577.
38. Huang B, Deora AB, He KL, et al. Hypoxia-inducible factor-1 drives annexin A2 system-mediated perivascular fibrin clearance in oxygen-induced retinopathy in mice. *Blood*. 2011;118:2918–2929.
39. Delanghe JR, Speeckaert R, Speeckaert MM. Behind the scenes of vitamin D binding protein: more than vitamin D binding. *Best Pract Res Clin Endocrinol Metab*. 2015;29:773–786.
40. Albert DM, Scheef EA, Wang S, et al. Calcitriol is a potent inhibitor of retinal neovascularization. *Invest Ophthalmol Vis Sci*. 2007;48:2327–2334.
41. Merrigan SL, Kennedy BN. Vitamin D receptor agonists regulate ocular developmental angiogenesis and modulate expression of dre-miR-21 and VEGF. *Br J Pharmacol*. 2017;174:2636–2651.
42. Segura I, Lange C, Knevels E, et al. The oxygen sensor PHD2 controls dendritic spines and synapses via modification of filamin A. *Cell Rep*. 2016;14:2653–2667.
43. Zheng X, Zhou AX, Rouhi P, et al. Hypoxia-induced and calpain-dependent cleavage of filamin A regulates the hypoxic response. *Proc Natl Acad Sci U S A*. 2014;111:2560–2565.
44. Salimi R, Bandaru S, Devarakonda S, et al. Blocking the cleavage of filamin A by calpain inhibitor decreases tumor cell growth. *Anticancer Res*. 2018;38:2079–2085.
45. Griffiths GS, Grundl M, Allen JS III, Matter ML. R-Ras interacts with filamin A to maintain endothelial barrier function. *J Cell Physiol*. 2011;226:2287–2296.
46. Sawada J, Urakami T, Li F, et al. Small GTPase R-Ras regulates integrity and functionality of tumor blood vessels. *Cancer Cell*. 2012;22:235–249.
47. Sawada J, Komatsu M. Normalization of tumor vasculature by R-Ras. *Cell Cycle*. 2012;11:4285–4286.
48. Ichimiya H, Maeda K, Enomoto A, Weng L, Takahashi M, Murohara T. Girdin/GIV regulates transendothelial permeability by controlling VE-cadherin trafficking through the small GTPase, R-Ras. *Biochem Biophys Res Commun*. 2015;461:260–267.
49. Komatsu M, Ruoslahti E. R-Ras is a global regulator of vascular regeneration that suppresses intimal hyperplasia and tumor angiogenesis. *Nat Med*. 2005;11:1346–1350.
50. Zhao K, Li X, Lin B, et al. Oroxyloside inhibits angiogenesis through suppressing internalization of VEGFR2/Flk-1 in endothelial cells. *J Cell Physiol*. 2018;233:3454–3464.
51. Li F, Sawada J, Komatsu M. R-Ras-Akt axis induces endothelial lumenogenesis and regulates the patency of regenerating vasculature. *Nat Commun*. 2017;8:1720.
52. Pecci A, Ma X, Savoia A, Adelstein RS. MYH9: structure, functions and role of non-muscle myosin IIA in human disease. *Gene*. 2018;664:152–167.
53. Huynh J, Nishimura N, Rana K, et al. Age-related intimal stiffening enhances endothelial permeability and leukocyte transmigration. *Sci Transl Med*. 2011;3:112–122.
54. Lampi MC, Reinhart-King CA. Targeting extracellular matrix stiffness to attenuate disease: from molecular mechanisms to clinical trials. *Sci Transl Med*. 2018;10:eaao0475.
55. Kohn JC, Lampi MC, Reinhart-King CA. Age-related vascular stiffening: causes and consequences. *Front Genet*. 2015;6:112.
56. Morrison AR, Yarovinsky TO, Young BD, et al. Chemokine-coupled β2 integrin-induced macrophage Rac2-Myosin IIA interaction regulates VEGF-A mRNA stability and arteriogenesis. *J Exp Med*. 2014;211:1957–1968.
57. Huang Y, Shi H, Zhou H, Song X, Yuan S, Luo Y. The angiogenic function of nucleolin is mediated by vascular endothelial growth factor and nonmuscle myosin. *Blood*. 2006;107:3564–3571.
58. Christian S, Pilch J, Akerman ME, Porkka K, Laakkonen P, Ruoslahti E. Nucleolin expressed at the cell surface is a marker of endothelial cells in angiogenic blood vessels. *J Cell Biol*. 2003;163:871–878.
59. Fogal V, Sugahara KN, Ruoslahti E, Christian S. Cell surface nucleolin antagonist causes endothelial cell apoptosis and normalization of tumor vasculature. *Angiogenesis*. 2009;12:91–100.

Investigative Ophthalmology & Visual Science

60. Yingchuan F, Chuntao L, Hui C, Jianbin H. Increased expression of TGF-β1 and Smad 4 on oxygen-induced retinopathy in neonatal mice. *Adv Exp Med Biol*. 2010;664: 71–77.
61. Braunger BM, Leimbeck SV, Schlecht A, Volz C, Jagle H, Tamm ER. Deletion of ocular transforming growth factor β signaling mimics essential characteristics of diabetic retinopathy. *Am J Pathol*. 2015;185:1749–1768.
62. Schlecht A, Leimbeck SV, Jagle H, Feuchtinger A, Tamm ER, Braunger BM. Deletion of endothelial transforming growth factor-β signaling leads to choroidal neovascularization. *Am J Pathol*. 2017;187:2570–2589.
63. Li J, Bowens N, Cheng L, et al. Myocardin-like protein 2 regulates TGFβ signaling in embryonic stem cells and the developing vasculature. *Development*. 2012;139:3531–3542.
64. Trembley MA, Velasquez LS, de Mesy Bentley KL, Small EM. Myocardin-related transcription factors control the motility of epicardium-derived cells and the maturation of coronary vessels. *Development*. 2015;142:21–30.
65. Menendez MT, Ong EC, Shepherd BT, et al. BRG1 (Brahma-Related Gene 1) promotes endothelial Mrtf transcription to establish embryonic capillary integrity. *Arterioscler Thromb Vasc Biol*. 2017;37:1674–1682.
66. Crider BJ, Risinger GM Jr, Haaksma CJ, Howard EW, Tomasek JJ. Myocardin-related transcription factors A and B are key regulators of TGF-β1-induced fibroblast to myofibroblast differentiation. *J Invest Dermatol*. 2011;131:2378–2385.
67. Gasparics A, Sebe A. MRTFs- master regulators of EMT. *Dev Dyn*. 2017;247:396–404.
68. Dejana E, Hirschi KK, Simons M. The molecular basis of endothelial cell plasticity. *Nat Commun*. 2017;8:14361.
69. Schwartz MA, Vestweber D, Simons M. A unifying concept in vascular health and disease. *Science*. 2018;360:270–271.
70. Zhan Y, Guo J, Yang W, et al. MNK1/2 inhibition limits oncogenicity and metastasis of KIT-mutant melanoma. *J Clin Invest*. 2017;127:4179–4192.
71. Liu Y, Sun L, Su X, Guo S. Inhibition of eukaryotic initiation factor 4E phosphorylation by cercosporamide selectively suppresses angiogenesis, growth and survival of human hepatocellular carcinoma. *Biomed Pharmacother*. 2016;84: 237–243.
72. Dennis MD, Kimball SR, Fort PE, Jefferson LS. Regulated in development and DNA damage 1 is necessary for hyperglycemia-induced vascular endothelial growth factor expression in the retina of diabetic rodents. *J Biol Chem*. 2015;290: 3865–3874.
73. Miller WP, Mihailescu ML, Yang C, et al. The translational repressor 4E-BP1 contributes to diabetes-induced visual dysfunction. *Invest Ophthalmol Vis Sci*. 2016;57:1327–1337.
74. Tokunaga CC, Mitton KP, Dailey W, et al. Effects of anti-VEGF treatment on the recovery of the developing retina following oxygen-induced retinopathy. *Invest Ophthalmol Vis Sci*. 2014;55:1884–1892.

Investigative Ophthalmology & Visual Science

Supplementary method information

Denaturation, alkylation, reduction and tryptic digestion

Same protocol has been used before. [1] After the proteins were extracted from tissue samples and proteins concentration was measured 0.05 M ABC, denatured with 2 % SDS and reduced with 50 mM Tris- (2-carboxyethyl) phosphine. After 60 min of incubation at + 60 °C samples were centrifuged and transferred into Pall Nanosep® 30 kDa MWCO centrifugal devices with low protein binding membrane and flushed two times with 200 µl of 8 M urea solution followed by iodoacetamide alkylation for 20 min in dark at RT. Samples were flushed three times with 8 M urea solution and 50 mM ABC before starting the enzymatic digestion with trypsin for 16 h at + 37 °C. Ratio of trypsin to protein in enzymatic digestion was 1:25. The following day samples were flushed twice with 40 µl 0.1M TEAB and once 50 µl 0.5 M NaCl to collect peptides from the filter and dried in speed vacuum. Samples were solubilized to 0.1 % TFA and desalted with C18 tips. The tips were conditioned with 50 % ACN and equilibrated with sample solvent. The clean-up was performed by aspirating and dispensing samples for 10 cycles. Tips were then rinsed with 2.5 % ACN in 0.1 % TFA. Finally, peptides were eluted with 80 % ACN in 0.1 % FA. Samples were dried in speed vacuum concentrator and stored at -20 °C until reconstituted to loading solution (5 % ACN, 0.1 % FA and HMR calibration peptides according to manufacturer guidelines) NanoRPLC-TripleTOF SWATH analysis. SWATH analysis samples were diluted to equal concentrations before injection to the instrument.

NanoRPLC-TripleTOF

Retinal proteins were analyzed by Nano-RPLC- TripleTOF instrumentation using Eksigent 425 NanoLC coupled to high speed TripleTOF™ 5600+ mass spectometer (Sciex, Concord, Canada). A microcapillary RP-LC column (cHiPLC® ChromXP C18-CL, 3 µm particle size, 120 Å, 75 µm i.d × 15 cm, Eksigent Concord, Canada) was used for LC separation of peptides. Samples were first loaded into trap column (cHiPLC® ChromXP C18-CL, 3 µm particle size, 120 Å, 75 µm i.d × 5 mm) from autosampler and flushed for 10 min at 2 µl/min (2 % ACN, 0.1 % FA). The flush system was

then switched to line with analytical column. Tear samples were analyzed with 120 min 6 step gradient using eluent A: 0.1 % FA in 1 % ACN and eluent B: 0.1 % FA in ACN (eluent B from 5 % to 7 % over 2 min, 7 % to 24 % over 55 min, 24 % to 40 % over 29 min, 40 % to 60 % over 6 min, 60 % to 90 % over 2 min and kept at 90 % for 15 min, 90 % to 5 % over 0.1 min and kept at 5 % for 13 min) at 300 nl/min.

Key parameters for TripleTOF mass spectrometer in SWATH ID library analysis were: ion spray voltage floating (ISVF) 2300 V, curtain gas (CUR) 30, interface heater temperature (IHT) +125°C, ion source gas 1 13, declustering potential (DP) 100 V. Library for SWATH analysis was created from the same samples by information dependent-aquisition (IDA) method and relative quantitation analysis was done by SWATH method. All methods were run by Analyst TF 1.5 software (Sciex, Redwood City, USA). For IDA parameters, 0.25 s MS survey scan in the mass range 350-1250 mz were followed by 60 MS/MS scans in the mass range of 100-1500 Da (total cycle time 3.302 s). Switching criteria were set to ions greater than mass to charge ratio (m/z) 350 and smaller than 1250 (m/z) with charge state 2-5 and an abundance threshold of more than 120 counts. Former target ions were excluded for 12 s. IDA rolling collision energy (CE) parameters script was used for automatically controlling CE. SWATH quantification analysis parameters were the same as for SWATH ID, with the following exceptions: cycle time 3.332 s and MS parameters set to 15 Da windows with 1 Da overlap between mass range 350-1250 Da followed by 40 MS/MS scans in the mass range of 350-1250 Da. SWATH analysis method has been published in Nättinen et al 2018. [2]

Immunoblotting

17 µg of protein from retinal lysates was loaded and run into 4-12% gradient gel (NuPAGE; Invitrogen, Carlsbad, CA, USA) and transferred on polyvinylidene fluoride membranes (Amersham Biosciences, Little Chalfont, UK). Membranes were blocked with 5 % NFM/TBST and specific proteins were detected by immunoblotting with following primary antibodies: rabbit anti-Flna

(Cat#ab76289, Abcam, Cambridge, UK), rabbit anti-Myh (Cat#11128-1-AP, Proteintech, Rosemont, IL, USA), and goat anti-GAPDH (Cat#ab9483, Abcam) followed by appropriate HRP-coupled secondary antibodies. Clarity Western ECL Substrates (Bio-Rad, Hercules, CA, USA) were used for enhanced chemiluminescence and Western blot images were captured via ImageQuant LAS 4000 software (ImageQuant; GE Healthcare, Chalfont St. Giles, UK). Proteins levels for Myh9, total Flna and $Flna^{CT}$ were quantified by densitometry using Adobe Photoshop CS3 software, and GAPDH was used to normalize for protein loading. A calibration protein samples was included in every membrane to enable combined results from several membranes. Two sample t-test was used to analyze differences between the relative protein expression levels of control and OIR retinas.

References

1. Hongisto H, Jylhä A, Nättinen J, et al. Comparative proteomic analysis of human embryonic stem cell-derived and primary human retinal pigment epithelium. Sci Rep. 2017;7:6016-017-06233-9.

2. Nättinen J, Jylhä A, Aapola U, et al. Topical fluorometholone treatment and desiccating stress change inflammatory protein expression in tears. Ocul Surf. 2018;16:84-92.

Supplementary Figures

SWATH-MS proteomic analysis of oxygen-induced retinopathy reveals novel potential therapeutic targets

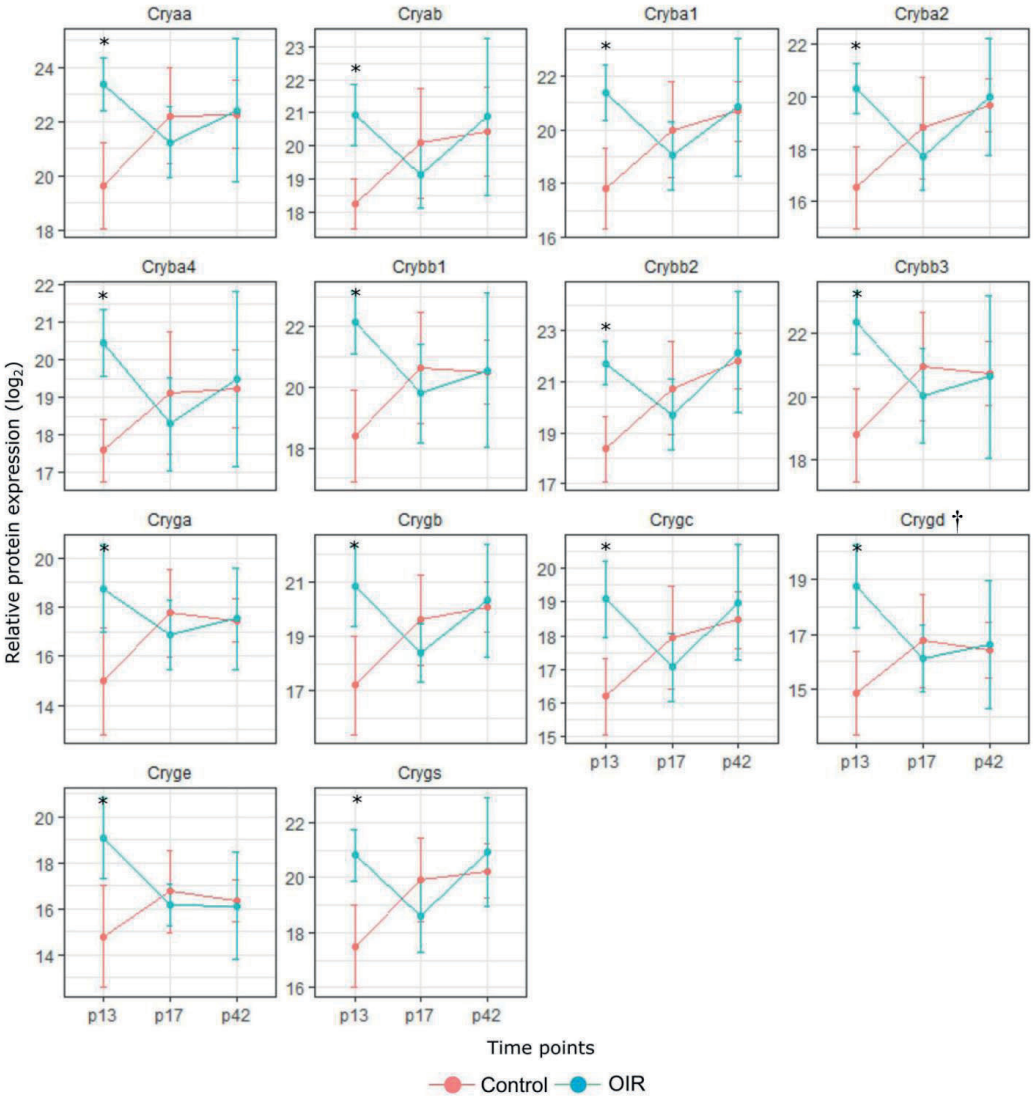

Supplementary Figure 1. Graphs illustrating the expression of crystallins during OIR. Retinas were harvested from OIR and control retinas at P13, P17 and P42 and samples were analyzed by MS-SWATH proteomics. The means with standard error bars are shown for control (red) and OIR (blue) samples for crystallins, which were most upregulated group of proteins at P13 OIR compared to room

air controls. Asterisks identifies statistically significant differences between the two groups before P value adjustement (P value <0.05). † = protein quantification based on only one specific peptide.

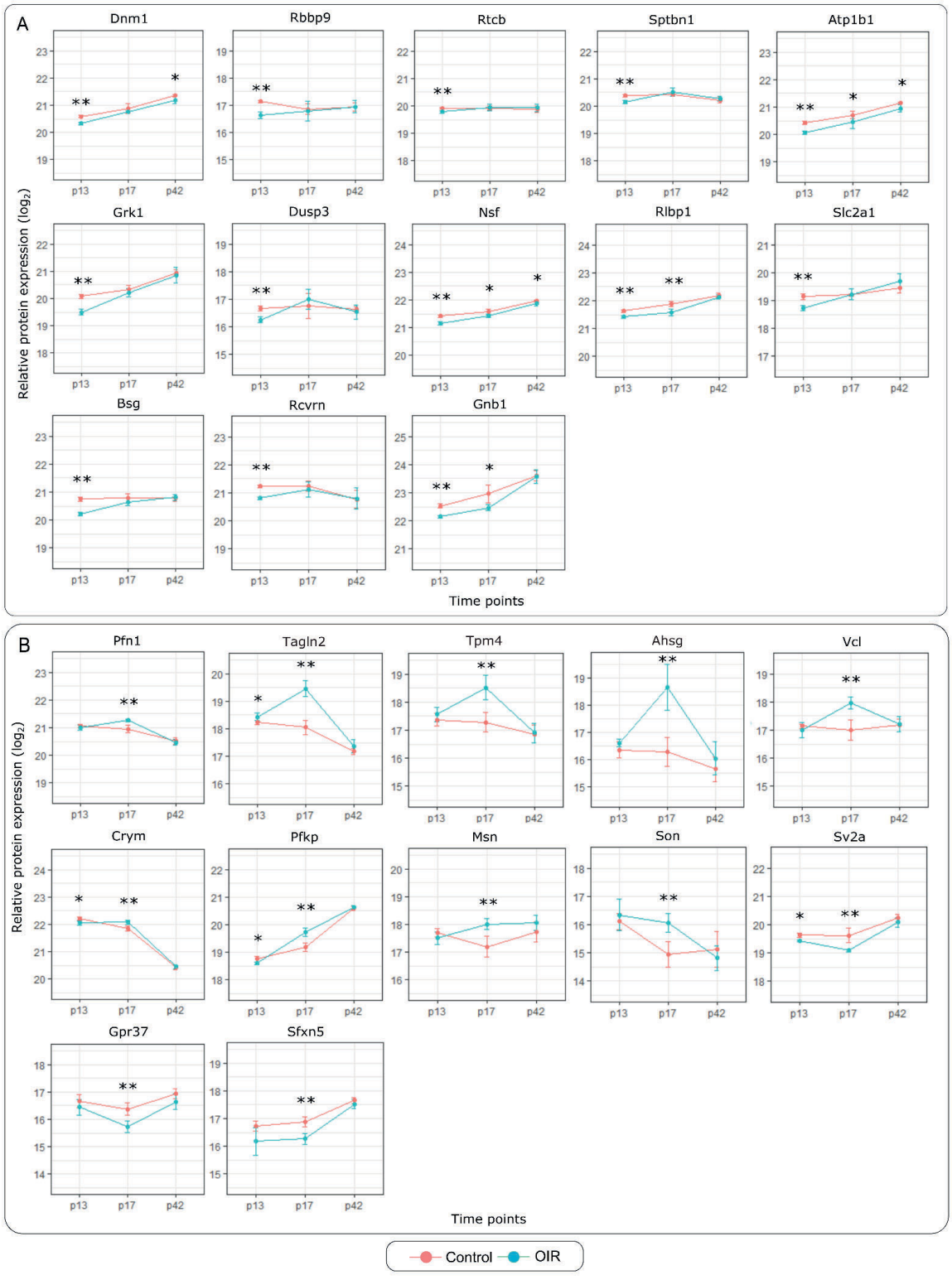
A
Dnm1
Rbbp9
Rtcb
Sptbn1
Atp1b1
Grk1
Dusp3
Nsf
Rlbp1
Slc2a1
Bsg
Rcvrn
Gnb1
Relative protein expression (log2)
Time points
p13
p17
p42
B
Pfn1
Tagln2
Tpm4
Ahsg
Vcl
Crym
Pfkp
Msn
Son
Sv2a
Gpr37
Sfxn5
Relative protein expression (log2)
Time points
Control
OIR

Supplementary Figure 2. Differentially expressed proteins in OIR. Mice pups were exposed to hyperoxia-induced OIR, and retinas were harvested at P13, P17 and P42. All retina samples were analyzed by MS-SWATH and the data underwent statistical analysis to compare control and OIR samples in each time point. The means and standard error bars are shown for control (red) and OIR (blue) samples for some of the proteins during hypoxia at P13 (A) and at the peak of neovascularization at P17 (B). Asterisks identifies statistically significant differences between the two groups before P value adjustment (*), and after P value (**) adjustment. Note that some of the differently expressed proteins were illustrated in Figure 5.

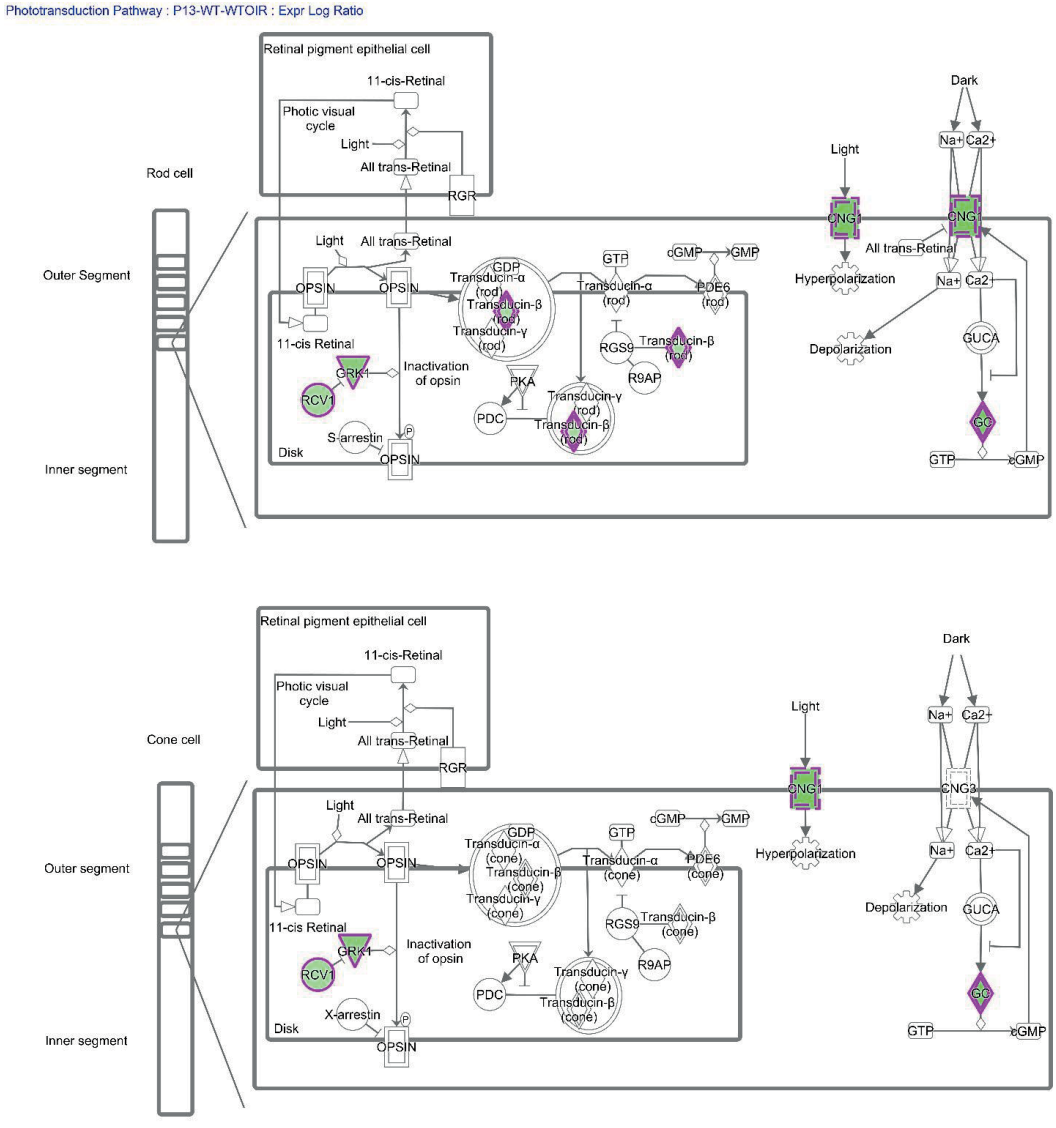

Supplementary Figure 3. Illustration from canonical pathway analysis from Ingenuity Pathway Analysis (IPA) showing phototransduction pathway with proteins downregulated in OIR retinas (colored) compared to controls at P13.

A

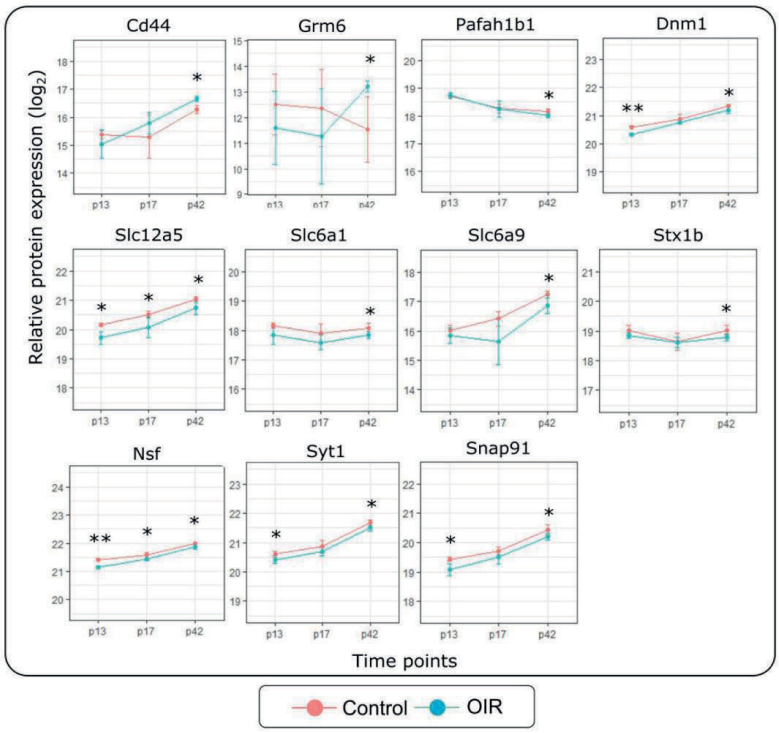

B

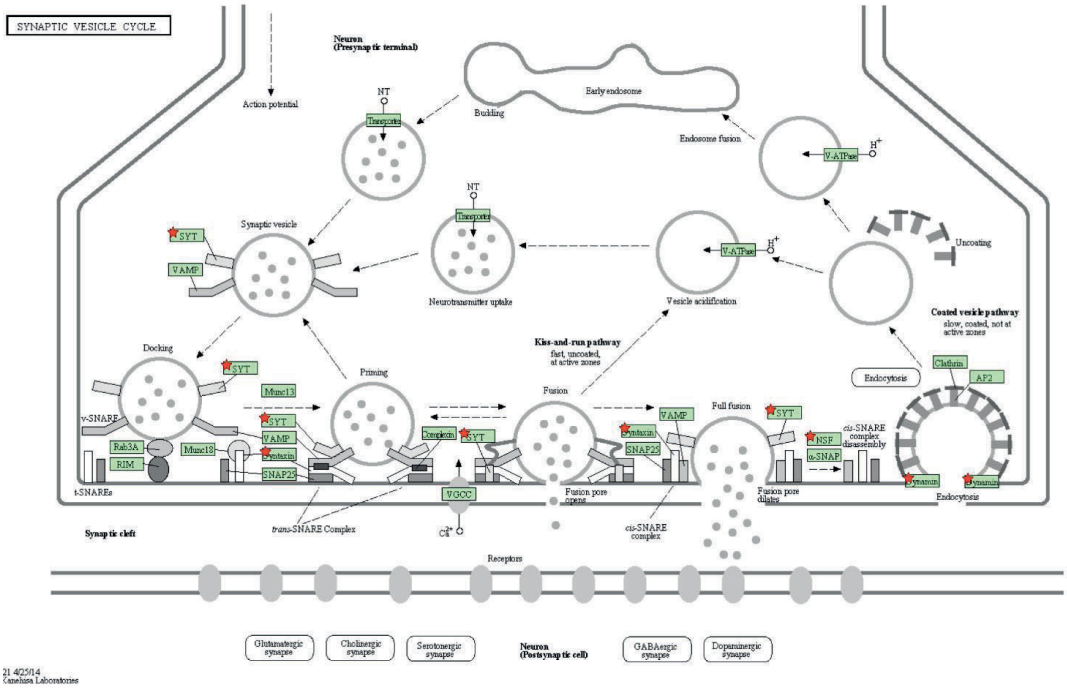

Supplementary Figure 4. Proteins involved in neurotransmission remained at reduced level at P42 OIR. (A) IPA analysis at P42 revealed decreased neurotransmission at P42 OIR compared to controls. Protein expression levels of neurotransmission proteins during OIR are visualized. Asterisks identifies statistically significant differences between the two groups before P value adjustement (P value <0.05). (B) KEGG pathway analysis revealed that some of these proteins (red star) are part of synaptic vesicle cycle.

PUBLICATION IV

Syndecan-4 is required for efficient VE-Cadherin trafficking during pathological angiogenesis

Giulia De Rossi, Maria Vähätupa, Enrico Cristante, Sidath E. Liyanage, Ulrike May, Laura Pellinen, Saara Aittomäki, Zuzet Martinez Cordova, Marko Pesu, Hannele Uusitalo-Järvinen, James W. Bainbridge, Tero A.H. Järvinen and James R. Whiteford

Submitted